

Collaborative action of molecular chaperones, ubiquitin E3 ligases and signaling molecules in the reversal of glioblastoma and other brain tumors

THESIS

Submitted to the Delhi Technological University for the
award of the degree of

DOCTOR OF PHILOSOPHY

Submitted by

**Sudhanshu Sharma (DST-INSPIRE SRF)
(2K19/PHDBT/04)**

Under the Supervision of
Prof. Pravir Kumar, PhD
Professor and Head, Dean (International affairs)
Department of Biotechnology
Delhi Technological University, Delhi



Faculty of Department of Biotechnology
Delhi Technological University
(Formerly Delhi College of Engineering)
Shahbad Daultpur, Main Bawana Road, Delhi-110042, INDIA

SEPTEMBER, 2023

**Copyright ©Delhi Technological University-2023
All rights reserved.**

***Dedicated to
My Father***

DECLARATION

I hereby declare that the thesis entitled “**Collaborative action of molecular chaperones, ubiquitin E3 ligases and signaling molecules in the reversal of glioblastoma and other brain tumors**” submitted by me, for the award of the degree of *Doctor of Philosophy* to **Delhi Technological University (Formerly DCE)** is a record of *bona fide* work carried out by me under the guidance of Prof. Pravir Kumar.

I further declare that the work reported in this thesis has not been submitted and will not be submitted, either in part or in full, for the award of any other degree or diploma in this Institution or any other Institute or University.

Name: Sudhanshu Sharma
Reg No: 2K19/PHDBT/04
Department of Biotechnology
Delhi Technological University (DTU)
Shahbad Daulatpur, Bawana Road, Delhi-
110042
Place: New Delhi
Date:

CERTIFICATE

This is to certify that the thesis entitled “**Collaborative action of molecular chaperones, ubiquitin E3 ligases and signaling molecules in the reversal of glioblastoma and other brain tumors**” submitted by **Mr. Sudhanshu Sharma** to **Delhi Technological University (Formerly DCE)**, for the award of the degree of “Doctor of Philosophy” in Biotechnology is a record of *bona fide* work carried out by him. Sudhanshu Sharma has worked under my guidance and supervision and has fulfilled the requirements for the submission of this thesis, which to our knowledge has reached requisite standards.

The results contained in this thesis are original and have not been submitted to any other university or institute for the award of any degree or diploma.

Prof. Pravir Kumar, PhD
Head (BT) and Dean (IA)
Department of Biotechnology
Delhi Technological University (DTU)
Shahbad Daulatpur, Bawana Road, Delhi-
110042
Place: New Delhi
Date:

ACKNOWLEDGEMENT

*First and above all, I bow down to the **GOD, the ALMIGHTY** for his grace, blessings and countless love from the very inception to the completion of this research work. During the complete course of this work, I have felt the grace of God which enlighten my knowledge and thoughts. This thesis appears in its current form due to the motivation and guidance of many people. I would therefore like to acknowledge all of them.*

*I would like to express my gratitude to **Prof. Jai Prakash Saini**, Vice chancellor, Delhi Technological University, Delhi for providing me the opportunity to carry out this work in this prestigious institute. Further, I express my gratitude to **Prof. Yogesh Singh**, former Vice chancellor Delhi Technological University, Delhi for providing me opportunity and infrastructure to complete this work.*

*It is a great pleasure to express my sincere gratitude to my thesis supervisor **Prof. Pravir Kumar**, Professor, DRC chairman and Head, Department of Biotechnology, Delhi Technological University for his invaluable advice, constant support and patience during my PhD study. His immense knowledge and plentiful experience have encouraged me in all the time of my research period. I am very happy to inscribe this page, and I owe a warm thanks to you sir. Here, I would also like to thanks **Prof. Jai Gopal Sharma**, Former Head of the Department, department of Biotechnology, for providing me the infrastructure and smooth functioning of official work.*

*I would like to thanks to **Dr. Rashmi Ambasta**, CSIR Scientist, Delhi Technological University, Delhi, for her support and motivation in the planning and execution of the experimentations.*

*Immeasurable appreciation to my colleagues **Dr. Dia Advani, Dr. Rohan Gupta, Rahul Tripathi** and **Smita Kumari** for their precious support and a cherished time spent together in the lab. I also want to thank my juniors **Neetu Rani, Mehar Sahu, Shefali Kardam** and **Shruitkirti Vashishth** for their support.*

*Special appreciation and thanks to **Dr. Dia Advani and Rahul Tripathi** who have provided their valuable support and guidance throughout the journey.*

I gratefully acknowledge the fellowship received for my research work from the department of Science and Technology (DST), Govt. of India. I wish to acknowledge the Senior Management and technical staff of DTU, for providing support to my work.

*Most importantly, credit is due to my parents and family members, who were always there to bring positivity and hope. This PhD study would not have been possible without the corporation of my mother **Smt. Madhuri Sharma** and brother **Mr. Kushagra Sharma**. I am profoundly grateful to them for their extended love and patience during the difficult times.*

*At last, I want to dedicate my thesis to my father **Late Dr. S.K. Sharma** who dreamt for me and blessed me to cherish my dreams. Words run less to express my gratitude to my dear father. I know today he will be the happiest for me in the heavenly kingdom.*

ABSTRACT

Brain tumors represents a class of tumors that arises from the malignant transformation of the astrocytes and glial cells. Despite various advancements, treatment options remain limited to chemotherapy and radiotherapy followed by surgery giving an overall survival of 14~15 months. These therapies are somewhere restricted in giving a better survival and cure. There is a need for new therapeutics that could potentially target various brain tumors based on molecular pathways and pathology. Here ubiquitin E3 ligases and heat shock proteins can be used as targets as they bind a wide array of substrates and therefore, can be attractive targets for new inhibitors. Through our study, we have tried to sort various ubiquitin E3 ligases based on their expression, pathways to which these ligases are associated, and mutational frequencies, and then we tried to screen potent inhibitors against the most favorable E3 ligase and heat shock proteins as very few studies are available concerning inhibition of E3 ligase and heat shock proteins in GBM and ependymomas.

We performed an integrated omics analysis to predict the mutual regulatory differential HSP signatures that were associated with both glioblastoma and ependymomas. Further, we explored the various common dysregulated biological processes operating in both the tumors, and were analyzed using functional enrichment, gene ontology along with the pathway analysis of the predicted HSPs. We established an interactome network of protein-protein interaction (PPIN) to identify the hub HSPs that were commonly associated with GBMs and ependymoma. To understand the mutual molecular mechanism of the HSPs in both malignancies, transcription factors, and miRNAs overlapping with both diseases were explored. Moreover, a transcription factor-miRNAs-HSPs coregulatory network was constructed along with the prediction of potential candidate drugs that were based on perturbation-induced gene expression analysis. Finally, the ranking of the drugs was arranged based on various drug scores. In conclusion, this study gave a spotlight on the mutual targetable HSPs, biological pathways, and regulatory

signatures associated with GBMs and ependymoma with an improved understanding of crosstalk involved. Additionally, the role of therapeutics was also explored against HSP90AB1. These findings could potentially be able to explain the interplay of HSP90AB1 and other HSPs within these two malignancies.

TABLE OF CONTENTS

<i>Declaration</i>		iv
<i>Certificate</i>		v
<i>Acknowledgement</i>		vi-vii
<i>Abstract</i>		xii-xi
<i>Contents</i>		x-xiii
<i>List of Figures</i>		xiv-xvi
<i>List of Tables</i>		xvii-xvii
<i>List of Graphs</i>		xix
<i>Abbreviations</i>		xx-xxii
CHAPTER I	INTRODUCTION	1-4
1.1	Overview	2
1.2	Rationale of the study	3
1.3	Aim and Objectives	3
1.3.1	Aim	3
1.3.2	Objectives	3
1.4.	Summary of Thesis	3-4
CHAPTER II	REVIEW OF LITERATURE	5-31
2.1	Introduction	6
2.1.1	E3 ligases: putative grenade to eradicate glioblastoma progression	6-9
2.1.2	HDM2 E3 ligase as drug targets	9-10
2.1.3	SCF (SKP1-CULLIN-F BOX) e3 ligases	10-12
2.1.4	APC/C ubiquitin e3 ligase	12-13
2.1.5	Other ubiquitin E3 ligases	13-14
2.2	Heat shock proteins (hsps) as molecular chaperones	15-17
2.2.1	Deregulated HSPs in glioblastoma environment	17-19
2.2.2	HSP27 as molecular targets	19-20
2.2.3	HSP40 as molecular targets	20-21
2.2.4	HSP60 as molecular targets	21-22
2.2.5	HSP70 as molecular targets	22-23
2.2.6	HSP90 as molecular targets	23-24
2.3	Cell cycle, CDKs and regulatory proteins as therapeutic targets	24-31

CHAPTER III	DECODING THE ROLE OF UBIQUITIN E3 LIGASES AND THE THERAPEUTIC TARGETING OF UBIQUITIN E3 LIGASES	32-64
3.1	Introduction	33-37
3.2	Material and Methodology	38-43
3.2.1	Collection of raw data	38
3.2.2	DEGs identification	38
3.2.3	E3 ligase screening and Venn analysis	38
3.2.4	Functional enrichment analysis of predicted E3 ligase	39
3.2.5	Mutational analysis and expressional analysis	39
3.2.6	Compound library screening	39
3.2.7	ADMET and BBB permeability analysis of candidate drugs	39
3.2.8	Molecular docking analysis	40
3.2.9	Molecular dynamic simulation studies	40-43
3.3	Results	43-71
3.3.1	Raw data collection and screening of DEGs	43
3.3.2	Ubiquitin E3 ligase identification and Venn analysis	44-46
3.3.3	Expression profiling and mutational analysis	46
3.3.4	Functional enrichment and pathway analysis	46-51
3.3.5	Compound prediction, BBB and ADMET parameters	51
3.3.6	MDM2-Alkaloids interacting profiling	51-55
3.3.7	MDM2-Alkaloids complexes dynamic stability	55-60
3.4	Discussion	60-63
3.5	Key highlights of the study	64
CHAPTER IV	DISSECTING THE FUNCTIONAL SIGNIFICANCE OF HEAT SHOCK PROTEINS IN GLIOBLASTOMA AND EPENDYMOMAS USING OMICS ANALYSIS AND DRUG PREDICTION USING VIRTUAL SCREENING	65-107
4.1	Introduction	66-68
4.2	Methodology	69-74
4.2.1	Retrieval of raw data	69
4.2.2	Data processing, analysis of DEGs and prediction of HSPs	69

4.2.3	Protein-protein functional interaction and network analysis	70
4.2.4	Functional enrichment and pathway analysis	70-71
4.2.5	Identification of common regulatory transcriptomes	71
4.2.6	Transcriptional and post transcriptional regulations of TF-HSPs, TF-miRNAs, miRNAs-HSPs and HSPs-TF	71-72
4.2.7	Drug screening and Target HSP confirmation	72
4.2.8	Ranking and scoring of predicted drugs	72
4.2.9	Molecular docking, ADMET and BBB analysis	72-73
4.2.10	Molecular dynamic simulation studies	73-74
4.3	Results	74
4.3.1	Collection of raw data	74-75
4.3.2	Differential expression of HSPs in GBMs and ependymoma	75-77
4.3.3	Construction of HSP PPIN in ependymoma and glioblastoma	77-78
4.3.4	Functional enrichment and pathway analysis of predicted HSPs	79-85
4.3.5	Identification of mutual regulatory transcriptomes linking HSPs in GBMs and ependymomas	85-88
4.3.6	Establishment of miRNA-TFs-HSPs coregulatory network	88-91
4.3.7	Prediction of potential drug candidates and putative targetable HSP validation	91-92
4.3.8	Drug prioritization based on ranking scores using CODRES	92-96
4.3.9	Docking, ADMET and BBB analysis HSP90AB1	96-100
4.3.10	MD simulation studies	100-102
4.4	Discussion	102-110
4.5	Conclusion	111
CHAPTER V	<i>IN-SILICO</i> MOLECULAR DOCKING AND SIMULATION ANALYSIS TO IDENTIFY NATURAL COMPOUNDS TARGETING HEAT SHOCK PROTEINS IN BRAIN TUMORS	112-129
5.1	Introduction	113
5.2	Computational methods and methodology	114
5.2.1	Data source	114
5.2.2	DEGs screening and HSP prediction	114
5.2.3	Enrichment and pathway analysis	114
5.2.4	Mutational analysis of predicted HSPs	114
5.2.5	Compound screening, ADMET analysis and BBB permeability check	114
5.2.6	Molecular docking analysis	115
5.2.7	Molecular dynamic simulation studies	115
5.3	Results	116
5.3.1	Data collection and identification of DEGs	116

5.3.2	Functional enrichment and pathway analysis of identified HSPs	116
5.3.3	Mutational analysis	117-118
5.3.4	Compound selection, BBB check and ADMET analysis	118
5.3.5	Molecular docking analysis and interpretation	119-120
5.3.6	MD simulation analysis and interpretation	120-122
5.4	Discussion	123
5.5	Conclusion and future prospects	124
CHAPTER VII	DISCUSSION, LIMITATIONS OF THE STUDY AND FUTURE PROSPECTS	123-162
6.1	Discussion	125-128
6.2	Limitations of the study	129
6.3	Future prospects	130
	Annexures	131-146
Annexure 1	Annexure 1: Representation of various ubiquitin E3 ligases present in datasets GSE4290, GSE50161, and GSE 104291	131
Annexure 2	Annexure 2: Tabular representation of common interacting ubiquitin E3 ligases filtered using Venn analysis	132
Annexure 3	Tabular representation of various alkaloids with their BBB scores and ADMET profiling	132-139
Annexure 4	Representation of various HSPs in different tumors from GSE50161	139
Annexure 5	Representation of TFs interacting with HSPs with their degree and betweenness	140-146
	References	147-194
	List of publications	195-197
	Biosketch	198-202

LIST OF FIGURES

Figure number	Title of the figure	Page number
CHAPTER II		
Figure 2.1	Ubiquitin E3 ligases and inhibitors targeting glioblastoma	8
Figure 2.2	Distribution of heat shock proteins and molecular chaperones in various organelles and associated inhibitors	18
Figure 2.3	Cell cycle, CDKs and their inhibitors targeting glioblastoma	25
Figure 2.4	Cell cycle regulatory proteins, checkpoints and associated inhibitors	29
CHAPTER III		
Figure 3.1	Flow chart of the methodology adopted in E3 ligases and therapeutics	42
Figure 3.2	Representation of the Venn analysis, mutational analysis and expression analysis of ubiquitin E3 ligases	45
Figure 3.3	Functional enrichment and pathway analysis	50
Figure 3.4	Molecular docking confirmation in 2D and 3D	54
Figure 3.5	Plots showing RMSD and RMSF of protein alone, protein-ligand and ligand complex	57
Figure 3.6	Plots showing Rg, interaction energy and radius of gyration of protein alone, protein-ligand and ligand complex	59
Figure 3.7	Proposed mechanism of evodiamine and sanguinarine in MDM2 inhibition	63
CHAPTER IV		
Figure 4.1	Workflow pipeline	74
Figure 4.2	Venn analysis of heat shock proteins	76

Figure 4.3	GO functional enrichment analysis and pathway analysis	78
Figure 4.4	Transcription factors-Heat shock proteins network	86
Figure 4.5	miRNA-hub heat shock proteins network shows the interaction between the hub HSPs and associated transcription factors (TFs).	90
Figure 4.6	Graphical representation of the scores of candidate drugs obtained using CoDReS.	93
Figure 4.7	Molecular docking confirmations in 2D and 3D representation	97
Figure 4.8	Molecular dynamic simulation analysis till 50ns	102
Figure 4.9	Inferred mechanism of action of mechanism of HSP inhibitors in HSP pathways	110

CHAPTER V

Figure 5.1	Functional enrichment analysis of the predicted heat shock proteins	117
Figure 5.2	Mutational analysis of the predicted HSPs	118
Figure 5.3	Docking analysis of the alkaloids	120
Figure 5.4	Molecular dynamics simulation (RMSD, RMSF, Rg) analysis of the selected compounds	121

CHAPTER VI

Figure 6.1	Summary of various signaling targets associated with glioblastoma and ependymoma.	129
------------	---	-----

LIST OF TABLES

Table number	Title of the table	Page number
CHAPTER II		
Table 2.1	List of molecular chaperones with their implicative role in normal cellular homeostasis, altered function in GBMs	16-17
Table 2.2	CDKs along with their cyclins and their functions in GBMs	27-28
CHAPTER III		
Table 3.1	Representation of the functionally enriched ubiquitin E3 ligases with associated biological pathways	48
Table 3.2	KEGG pathway analysis of predicted E3 ligases	49
Table 3.3	Docking analysis, ADMET parameters and BBB analysis	52
Table 3.4	Binding energies and the number of interactions of evodiamine and sanguinarine with reference compounds	55
CHAPTER IV		
Table 4.1	Representation of the functionally enriched heat shock proteins with associated biological pathways in glioblastoma and ependymomas	80-83
Table 4.2	KEGG pathway analysis of the identified heat shock proteins in glioblastoma and ependymoma	84
Table 4.3	Top transcription factors and associated heat shock proteins	87
Table 4.4	Representation of the common regulatory miRNAs targeting heat shock proteins	88

Table 4.5	Comparative scores of different drug targeting heat shock proteins	96
-----------	--	----

Table 4.6	Binding affinity, ADMET and BBB permeability analysis	100
-----------	---	-----

CHAPTER V

Table 5.1	Docking scores and summary of the interactions of various alkaloids with HSP90AB1	119
-----------	---	-----

LIST OF GRAPHS

Graph number	Title of the graph	Page number
CHAPTER V		
Graph 4.6	Graphical representation of the scores of various drugs for drug ranking and CoDReS	93

ABBREVIATIONS

Abbreviation	Definition
PPIN	Protein-Protein interaction network
ABCG1	ATP binding cassette sub-family G member 1
ADMET	Absorption, distribution, metabolism, excretion and toxicity.
RMSF	Root means square fluctuation
GEO	Gene expression omnibus
ns	Nanoseconds
ApoE	Apolipoprotein E
RING	Really interesting new gene
WNT	Wingless-type murine mammary tumor virus integration sites
PDB	Protein databank
BBB	Blood brain barrier
BDNF	Brain-derived neurotrophic factor
TFs	Transcription factors
BRCA	Breast cancer
Rg	Radius of gyration
CDKs	Cyclin-dependent kinases
RMSD	Root means square deviations
CREEDS	Crowd extracted expressions of differential signatures
Cmap	Connectivity map
KEGG	Kyoto encyclopedia of genes and genomics
CoDReS	Computational drug repurposing score
RTKs	Receptor tyrosine kinases
GO	Gene ontology
IDH1	Isocitrate dehydrogenase 1
PDGFR- β	: Platelet derived growth factor receptors β
EMT	Epithelial-to-mesenchymal transitions
EGFR	Epidermal growth factor receptor
USF2	Upstream transcription factor 2
FOXC1	Fork head box C1
GATA2	GATA-binding factor 2
GEO	Gene expression
TRANSFAC	Transcription factor database
GREIN	GEO RNA-seq Experiments Interactive Navigator
GBM	Glioblastoma
GEPAL2	Gene expression profiling interactive analysis 2
HSPMdb	Heat shock protein modulatory database
HSP	Heat shock proteins

BAX: Bcl2	Bcl2 associated protein
NPT	Constant temperature constant pressure
NVT	Constant temperature, constant volume
GADD45	GADD45, and DNA-damage inducible gene
IL-1 β	Interleukin-1 beta
iLINCS	Integrative LINCS
JNK	c-Jun N-terminal kinase
ARF	Alternate reading frame
LRRK2	Leucine rich repeat kinase 2
LXR	Liver X receptor
mAb	Monoclonal antibody
MAO	Monoamine oxidases
MAPKs	Mitogen-activated protein kinases
MAPT	Microtubule-associated protein tau
MCS	Maximum common substructure
MDM2	Mouse double minute 2 homolog
mHtt	Mutant huntingtin
MIST	Molecular Interaction Search Tool
MM-PBSA	Molecular Mechanics Poisson-Boltzmann surface area
MPTP	1-methyl-4-phenyl-1,2,3,6-tetrahydropyridine
MDR	Multiple drug resistance
MD	Molecular dynamic
NDDs	Neurodegenerative
NEDD4	Neural precursor cell expressed developmentally Down-regulated 4
NIH	National Institutes of Health
PDB	Protein data bank
Pgp	P glycoprotein
PI3K-PKB/Akt	Phosphoinositide-3-kinase-protein kinase B/Akt
PINK1	PTEN-induced kinase 1
PPAR γ	Peroxisome proliferator-activated receptor gamma
PS	Presenilin
QSAR	Quantitative structure-activity relationship
ROS	Reactive oxygen species
RRMS	Relapsing-remitting MS
RT-PCR	Reverse transcriptase-polymerase chain reaction
RXR	Retinoid X Receptor
SNCA	Synuclein alpha
SNP	Single nucleotide polymorphism
SOD1	Superoxide dismutase

SPCE	Simple point charge
SRC	Src proto-oncogene
TGF β	Transforming growth factor-beta
TNF α	Tumor necrosis factor-alpha
TRIM 21	Tripartite motif-containing 21
TTD	Therapeutic Target Database
UniProtKB	UniProt Knowledgebase
UPR	Unfolded protein response
UPS	Ubiquitin proteasome system
VEGF	Vascular endothelial growth factor
WHO	World Health Organization

CHAPTER I

INTRODUCTION

CHAPTER I: INTRODUCTION

1.1 OVERVIEW

Protein folding, aggregation and transport is an important post-translational modification required for fundamental processing and to maintain cellular homeostasis. Improper protein folding is a hallmark in cancer development and progression. For this machinery to be efficient two important protective strategies follow. First strategy brings molecular chaperones into action that stabilizes the conformation and promotes folding of non-native proteins whenever required. Proteins if found misfolded, are then removed by degradation using the ubiquitin-proteasome system. Glioblastoma multiforme (GBM) a tumor derived from glial cells in human brain are the most malignant and aggressive among all other gliomas [1]. GBMs are located within the cerebral cortex and are more prominent in adults within the age scale of 40 - 60 years [2]. For several years the treatment regime for GBMs includes surgical resections followed by high doses of postoperative radiotherapy, promising a poor survival outcome of just 10-12 months [3,4] Further administration of temozolomide (TMZ) orally as a chemotherapeutic agent in addition to surgery and radiotherapy only prolongs the survival by 2-3 months [3] . Despite various advancements in FDA - approved drugs as chemotherapeutic agents there are still very limited therapies that give poor outcome in GBMs. To improve the tumor control rate, use of combinatorial therapies that can halt or reduce the tumorigenic functions like cellular proliferation, proteostasis, vascularization and other signaling events like apoptosis and autophagy can be promising therapeutic approach. Evident studies have also shown that several molecular chaperones (such as members of heat shock proteins (HSPs) families -70 and 90) can form symbiotic association with the ubiquitin-proteasome system. Dual inhibition of ubiquitin ligases and molecular chaperones can therefore, be an effective therapeutic approach and can give better survival outcomes.

1.2. RATIONALE OF THE STUDY

- Achieving inhibition using either small molecule, peptide, siRNA and targeting the enzyme-substrate complex could be favourable.
- Few or no approved drugs for E3 ligases and molecular chaperones in brain tumors. Chances of toxicity is minimal.
- Heat shock proteins can be more promising targets as cancerous cell take up their machinery to increase their number, in invasion and metastasis.
- Tumor cells are more HSP chaperonage-dependent than normal cells
- Few inhibitors for glioblastoma and no inhibitors for ependymoma. Chemotherapy and radiotherapy only give symptomatic relief

1.3. AIMS AND OBJECTIVES

1.3.1. AIM

Reversal of brain tumor symptoms by targeting the ubiquitin E3 ligases and the molecular chaperones

1.3.2. OBJECTIVE

1. To identify the various ubiquitin E3 ligases that can be targeted in glioblastomas and to predict compounds targeting the identified ubiquitin E3 ligase.
2. To understand the role of heat shock proteins in brain tumors and to screen putative inhibitors targeting these HSPs.
3. To identify natural compounds targeting the predicted heat shock proteins in glioblastoma.

1.4. SUMMARY OF THE THESIS

The current thesis is designed and divided into six different chapters. Chapter 1 focusses on

giving an introduction of brain tumors and the role of ubiquitination and molecular chaperones in these brain tumors. The future perspectives and limitations of our study were also delineated with potential contributions to the science. Chapter 2 of the thesis focusses on the review of the literature and the current knowledge of the studies conducted in glioblastoma and ependymomas. Chapter 3 focusses on the identification of potential ubiquitin E3 ligases that could be actually targeted using various natural inhibitors, leading to glioblastoma suppression. Various pathways that were deregulated in GBMs that were associated with ubiquitin E3 ligases were also explored. Chapter 4 describes the role of various heat shock protein and their mutualistic role in both glioblastoma and ependymomas. The chapter also defines the various regulatory transcriptomes in both of these tumors that could act as potential biomarkers. Finally, the identification of potent inhibitors has been done using drug ranking, molecular docking and molecular dynamic simulations studies. Chapter 5 predict the role of various natural alkaloids in the therapeutic targeting of the predicted heat shock protein HSP90AB1 using bioinformatic analysis and simulation studies till 100ns. Chapter 6 describes the discussion of the overall findings of the thesis, along with the limitations of the study and the associated future prospects and contribution to the science.

CHAPTER II

REVIEW OF LITERATURE

CHAPTER II: REVIEW OF LITERATURE

2.1 INTRODUCTION

For the cell cycle to work efficiently there is need for timely synthesis and degradation of cell cycle regulatory proteins. Major regulatory pathway to eliminate these proteins involves the ubiquitin proteasome system. This pathway requires various catalytic enzymes to function, including the ubiquitin – activating enzymes (E1), ubiquitin - conjugating enzyme (E2) and the most important E3 ubiquitin ligases. Activation of ubiquitin by E1 activating enzyme, then entering into thioester linkage with catalytic cysteine residue; further transferred to E2 conjugating part. After that an E3 ligase behaving as “bona fide” enzyme or matchmaker (RING E3), transfers the ubiquitin from charged E2 [5,6] to substrate. This leads to the formation of an isopeptide bond between C-terminal glycine residue of ubiquitin and lysine residue of substrate [7]. Though E3 ligases are the determinants of target of the ubiquitination system, they are very prominent in regulating the cell cycle. As E3 ubiquitin ligases binds to specific protein substrates and promotes their transfer controlling various key molecules involved in apoptosis (caspases), cellular senescence like the p53, p21, hippo), hedgehog signaling, inflammation (Necrotic factor- κ B), metastasis and therefore, can be an effective intruder in GBMs progression and metastatic invasion.

2.1.1. E3 LIGASES: PUTATIVE GRENADE TO ERADICATE GBMS PROGRESSION

Bortezomib (Velcade or PS-341) which is a proteasome inhibitor is the first and only drug approved by the FDA for the treatment of refractory multiple myeloma and mantle cell lymphoma [8]. It causes an overall inhibition of wide range of cellular proteins, which also blocks necessary protein to function. To prevent such a chaos, specific E3 ligase inhibitors can stabilize a particular set of cellular E3 proteins, thus avoiding any undesirable effects on other cellular proteins [9,10]. With this approach high rate of selectivity can be achieved with less

associated cytotoxicity. E3 ligases can work either as simple peptides (PARKIN), more complex (like MDM2/MDMX, homo or heterodimers) and even larger complexes like the anaphase promoting complexes (APCs) / cyclosome or Cullin-RING ligases (Including RING and RING-like ligases) and the HECT ligase (NEDD4 and HERC family) along with accessory proteins [11]. HECT ligases consist of C-terminus domain; accepting the ubiquitin molecule from E2 enzyme before transferring to the substrate molecule [12] while the RING ligases contain a zinc finger domain, allowing the E2 enzymes to directly transfer ubiquitin to the substrate molecule [13]. E3 ligases are an important regulator of key oncogenes like epidermal growth factor receptors (EGFR) or the tumor suppression genes (like the TP53) [14]. Unregulated functions or mutations in these E3 ligases are a causative factor for oncogenic overexpression or tumor suppressor gene down-regulation that elevates glioblastoma progression. Understanding these molecular targets and functioning of various E3 ligases can be fruitful therapeutic venue in treating such aggressive malignancies like GBMs. Representation of various ubiquitin E3 ligases along with associated inhibitors targeting glioblastoma is shown in **Figure 2.1**.

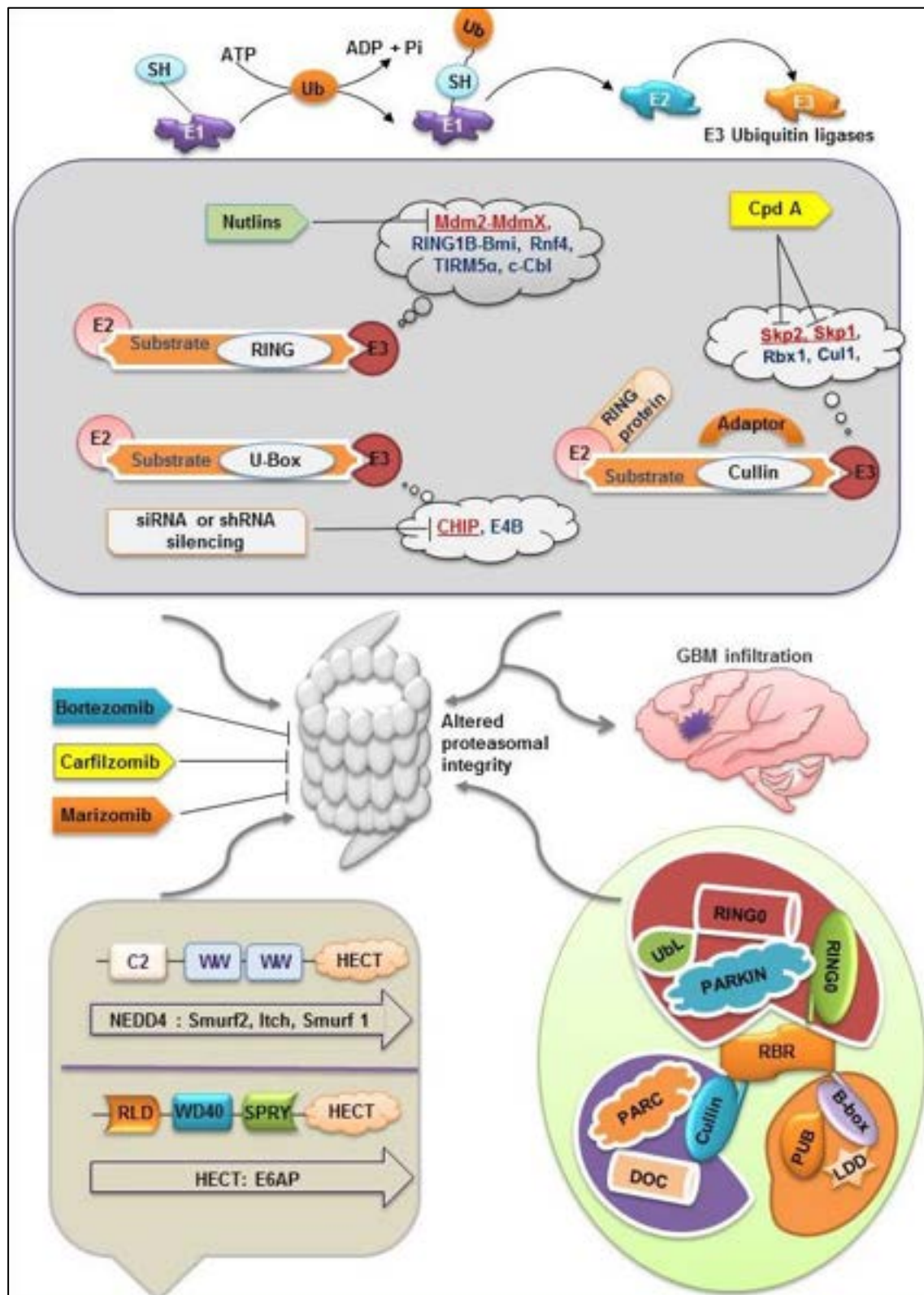


Figure 2.1: Ubiquitin E3 ligases and proteasome inhibitors targeting glioblastoma (GBMs): Ubiquitin E3 ligases classes of enzymes are classified according to the presence of characteristic domains and on how the ubiquitin is transferred to the substrate protein. This class of enzymes includes RING (Really interesting new gene) family, HECT (homologous to E6-AP carboxyl terminus) E3 ligases and RBR (RING-between RING) E3 ligase. Inhibitor that targets the proteasomal machinery includes Bortezomib, carfilzomib and marizomib that halts

proteostasis and prevents the accumulation of abnormal proteins required by GBM in their functioning. Inhibitors such as nutlins binds, Cpd A and si-RNA or sh-RNA mediated silencing binds various members of RING E3 ligases. Silencing other members like HECT and RBR E3 family using small interfering RNAs (siRNA) or shRNA mediates the subsequent reduction in GBM subpopulation.

E6AP (Ube3a) is a HECT domain ligase that mediates the interaction between human papillomavirus protein E6 and P53 (acts as a proto-oncogene) [14] and this E6/E6AP complex is responsible for binding to p53; causing the targeted degradation of ubiquitinated p53 by E6AP [15]. This E6/E6AP multi-complex also promotes ubiquitination of various apoptosis-inducing proteins like Bcl-2 homologous antagonist killer (BAK) [16] and Bcl-2 associated X protein (BAX), various cell cycle regulators like Cdk1, Cdk4 [17], proliferation regulators such as Mitogen-associated protein kinases-1 (MAPK-1) [18].

2.1.2. HDM2 E3 LIGASES AS DRUG TARGETS

Mouse double minute-2 (MDM2) and MDMX (also called HDMX and MDM4) are the proteins whose oncogenic activity is to inhibit the activity of p53 tumor suppressor gene [19]. MDM2 encodes a 90-kDa protein that was found to be responsible for the spontaneous transformation of murine cell line BALB/c3TC [20]. MDM2 is a member of RING family of E3 ligases [21] that heterodimers with MDM4 using the RING domains[22]. MDM2 is overexpressed in GBMs and therefore exerts their effect by causing the loss of p53 activity [23–25]. Activity of p53 is either regulated by binding of MDM2 with N-terminal transactivation domain [26] or by modulation of p53 levels by monoubiquitinating at or near the C-terminus [27]. CREB-binding protein (CBP) and p300 then, catalyzes the degradation of p53 by polyubiquitination [28,29]. Hdm2 is also identified as a major target of the RAS (acts as an oncogene and a suppressor of GBM phenotype) and RAF kinase pathway [23]. As high expression levels of Hdm2 are indicative of poor prognosis and depleted overall survival of glioblastoma patients; therefore, it can be valuable asset for targeting in GBMs by reactivating p53 that induces apoptosis in glioblastoma cancer cells harboring wild type p53. Due to lack of specific inhibitors of Hdm2 ligases, target validation remains a crucial step in case of GBMs. Therefore, it is preferable to

break the p53-Hdm2 interactions rather than focusing on breaking the activity of E3 ligases [24,30].

2.1.3. SCF (SKP1-CULLIN-F BOX) E3 LIGASES

The SCF complex is the largest family of E3 ubiquitin ligases composed of Skp1, Cullin, F-box proteins and the ROC/SAG/RBX RING finger proteins [31,32]. These are responsible for the clearance of most of the proteins that are regulated by Ubiquitin-proteasome system (UPS) [33]. Proteins that are removed are composed of cell cycle regulatory proteins, onco-proteins and various tumor suppressor proteins [34–37]. Studies have shown that the crystal structure of SCF-RBX complex is made up of Cul-1 that acts as a protein scaffold and binds at the N-terminus of the Skp1-F box^{Skp2} which acts a protein substrate-recognition complex and the C-terminus (RBX1) that is responsible for the recruitment of E2 conjugating enzyme [38,39]. There is around 69 F-box proteins in human genome including seven cullins (Cul-1, 2, 3, 4A, 4B, 5, 7) and RING proteins namely RBX1/ROC1 and RBX2/ROC2 (also called sensitive to apoptosis gene (SAG)) [40–43]. Skp2 which is a F box protein, also acting as an oncogene and targets p27 for degradation and is also found to be overexpressed in variety of cancer including gliomas. It has been seen that a deletion or mutation in the tumor suppressor FBW7, then it caused the accumulation of oncogenic protein substrates including c-Jun, c-Myc, Cyclin E, mammalian target of rapamycin (mTOR), that increased the cell proliferation and hence, tumorigenesis [44,45]. Majority of SCF E3 ligase substrates are required during cell cycle, transcription of gene, signal transduction pathways and during replication of DNA [35,46,47]. Both members of the RING family contain a functional RING domain at the C-terminus that is conserved evolutionally [32]. When there is an overexpression RBX1 and RBX2 then binds to any member of Cullin family and can shows an in-vitro ubiquitin E3 ligase activity [48,49]. The major difference between these two ligases is that RBX1 is constitutively expressed and binds with Cul2/VHL whereas RBX2/SAG/ROC2 is induced during the conditions of stress and they binds to Cul5 or to suppressor of cytokine signaling [50] (SOCS). A study showed the

small interfering RNA (siRNA) mediated silencing of ROC1 triggered a response for DNA damage and cell cycle arrest through G2/M checkpoint, activated apoptosis in p53-independent manner causing suppression of glioblastoma cell growth [51]. Silencing of RBX1 induced senescence that further caused the accumulation of licensing proteins such as Orc1 and Cdt1, released during replication of DNA and were known to be SCF ligase substrates [52–55]. Another known protein called sensitive to apoptosis gene (SAG) which showed the property of a redox-inducible protein (RIP), later found to be the second member of RBX/ROC of SCF E3 ubiquitin ligase [32,40,56]. SAG functions as an antioxidant by suppressing the apoptotic mechanism induced by stimuli such as ischemia, activity of nitric oxide (NO), exposure to UV radiations or due to neurotoxic activity [57–59]. Studies have shown that glioblastoma patients with high expression levels of SAG show a poor prognosis and reduced overall survival [60,61]. SAG exerts its E3 ubiquitin ligase activity when they form complex with other components of SCF family thus, promoting the removal or degradation of procaspases-3, Hypoxia inducible factor-1 alpha (HIF-1 α), c-Jun that plays important role in apoptosis, carcinogenesis and during cellular proliferation [62–65]. SiRNA silencing of these proteins showed negligible impact on the growth of normal cell but was able to reduce the tumorigenic efficiency both in-vitro and in-vivo in lung cancer and in U87MG human glioblastoma cell lines [65]. These findings suggest that both RBX1 and RBX2 can act as a potential anti-neoplastic target. F box proteins of the SCF complex controls various biological sequences like the targeted degradation of substrates as they can recognize and target multiple substrates (Skp2 targeting p57, p21) [66]. Among ~ 69 proteins of F box family, tumor suppressive β -TrCP and oncogenic Skp2 and Fbxw7 are known to act as potential targets in GBMs [44,67]. Skp2 functions by recognizing and causing the degradation of various negative regulators of cell cycle (p21, p130, p57) [35,46,47]. Down-regulation of Skp2 by using siRNA silencing or by using antisense oligonucleotides showed a pattern of tumor cells inhibition in various cancers such as oral cancer, lung cancer and in GBMs [68,69]. β -transducing repeat-containing E3 ligase (β -TrCP)

which is also a substrate recognition component of SCF E3 complex promotes the targeted degradation of various tumor suppressors like I κ B which acts a negative regulator of Necrotic factor- κ B [70,71], Programmed cell death protein-4 (PDCD4) acting as translational suppressor by inhibiting the eIF4A and BIMeL1, which are known to be pro-apoptotic proteins [72]. Expression levels of β -TrCP is found to be high in case of human breast cancer cell lines and various primary tumors, but recent data suggest that the expression of β -TrCP is lower in low-grade (I and II) as compared to normal brain tissue samples and further studies also revealed that is even lower in high grade gliomas (III and IV) than lower grade gliomas. These findings suggest that β -TrCP could be an inhibitor in gliomas targeting therapy.

2.1.4. APC/C UBIQUITIN E3 LIGASES

Compared to SCF complex the architecture of APC/C is more sophisticated due to larger complex [73–75]. APC/C ubiquitin E3 ligases functions by acting as a cell cycle regulator and a mediator of mitosis. APC/C in vertebrates acts as a holoenzyme and is composed of fifteen different proteins and various co-activator subunits (Cdc20/cdh1) [76–78]. Cdc20 or cdh1 is coded by FRZ1 gene and are required for binding of APC/C to the substrate followed by its degradation [79]. It is made up of three sub complexes namely scaffolding sub-complex platform, a tetratricopeptide repeat arm (TPR) and the substrate identification and a catalytic core [78]. E2 enzymes such as UBCH10 and UBE2S controls the K11 chain functions like initiation and elongation as predicted by studies suggesting the regulatory role of controlling cell division and acting as degraders of APC/C complex. Various pathological studies identified a chain of mutations in ANAPC6/Apc6, ANAPC8/Apc8 and ANAPC3/Apc3 in case of gliomas, neuroblastoma and in various chorio-carcinoma tissues [80]. Studies have been to validate the role of APC/C^{CDH1} as a tumor suppressor in normal brain tissue while deregulating the APC/C^{CDH1} showed glioblastoma progression [74]. APC/C^{CDH1} also acts as an attenuator in GBM cancer stem cells (CSCs) during the G1 phase of cell cycle progression, leading to an elevation in levels of APC/C^{CDH1} substrates like CDC20 [81]. Using RNA mediated interference

(RNA-i) in silencing the CDC20 reduced the proliferation, invasion and auto-generation capacity of population of CSCs in GBMs [82,83]. These overall findings suggest that targeting the APC/C complex may act as a trigger to halt the GBMs survival efficiency.

2.1.5. OTHER E3 UBIQUITIN LIGASES: SIDE VILLAINS IN GBMS ASSASSINATION

Inhibitor of apoptosis proteins (IAP) are the class of E3 ligases that are characterized by the presence of one or more baculoviral IAP repeats (BIR) required during the suppression of apoptosis. This family of ligases constitutes a council of eight human members including Cellular inhibitor of apoptosis-1 (cIAP-1), cIAP-2, Ts-IAP, NAIP (NLR family apoptosis inhibitory protein), Survivin, Livin/ML-IAP and the Apollon/Bruce. Among these members the X-linked inhibitors of apoptosis (XIAP) holds a novel position[84–86]. These XIAPs shows the most conspicuous activity as an anti-apoptotic element by binding and inhibiting the various caspases (-3, -9 and -7). They also work by disabling the induction of cell death using their RING domain which shows the E3 ligase activity, responsible for degrading the apoptotic-regulatory factors using the proteasome machinery[87]. E3 ligases activity of IAP also modulates the nuclear factor–kappa B (NF-κB) activation combining with cIAP. IAPs in addition to controlling apoptosis also controls necroptosis (non-apoptotic programmed cell death) by preventing the assembly of cytosolic multi-protein complex, containing RIP1 and stimulates the NF-κB activation followed by NF-κB-dependent up-regulation of cytokines that are cytotoxic in nature[87]. Various mitochondrial proteins like as second mitochondrial-derived activator of caspases (Smac/DIABLO) negatively regulates the caspases inhibition by IAPs by binding to multiple IAPs and removing their inhibitory effects on various caspases (-3, -7, -9). Mitochondrial Smac consisting of four residues on their N-terminal (AVPI) binds to the groove on the surface of BIR3 domain of IAP proteins including XIAP, cIAP1 and cIAP2[88,89]. IAP proteins can show radio resistance during radiation therapy by tampering the cell death pathways at various cellular levels and are found to be highly expressed in various

brain malignancies like GBMs and in neuroblastoma[90]. Various therapeutic strategies have been developed to counter the direct induction of cell death by IAPs. One such approach focuses on the development of miniature molecular inhibitors that can mimic the endogenous IAP protein antagonist such Smac that are released from the inter-membrane space within the mitochondria into the cytosol, when apoptosis comes under play[87,91]. Smac mediated neutralization of XIAP causes an increased caspase activation further promoting caspase-mediated apoptosis. Inhibition if done for cIAP proteins then it leads to cell death via autocrine/paracrine signaling looped with Tumor necrotic factor- α (TNF- α) signaling[91]. Death receptor-5 also acts as an important mediator during Smac induced apoptosis. Other approach that makes cancer cells radio sensitive is by neutralizing the anti-apoptotic function of IAP is by the ectopic expression of Smac. By increasing the expression levels of mature form of Smac protein, caused an enhancement in gamma irradiation promoted apoptosis in GBM cancer cells and also in neuroblastoma thus, affected the cloning efficiency and long term survival capacity of these mutated cells[92]. Apart from activity in GBM cell lines, IAP inhibitors also showed sensitized the primary cultured glioblastoma cells obtained from GBM patients, as well as the Gliomas stem like cancer cells (GSCs) promising it as a therapeutic target.

PARKIN (Park 2) which is well conserved under RING between RING-RING family of E3 ligases, shares common characteristics of HECT and RING ligases and are found to be deleted or under expressed in case of GBMs[93,94]. Park2 plays an important role in regulating mitophagy[95] therefore, affecting the cellular proliferation, the cellular redox potential and ultimately metastasis[96,97]. Mutation in Park2 leads to stabilization of G1/S cyclins thus, increasing the number of cells in Synthetic and G2/M phase and also increases cellular proliferation[98–100]. Park2 is also acts a regulator during mitotic spindle and cytokine bridging and also leads to ubiquitination and degradation of HIF-1 α that promotes cellular migration[101]. Studies have also shown that a loss in Park2 caused tumor metastasis in mouse

models[102].

2.2. HEAT SHOCK PROTEINS (HSPs) AS MOLECULAR CHAPERONES

Heat shock proteins (HSPs) are the polypeptides that are highly conserved and are ubiquitously expressed within all living organisms[103,104]. These proteins are not only induced in conditions of stress but also are highly expressed in various high-grade gliomas. Their chaperonage function is to serve as molecular chaperones by assisting in protein folding and maintaining the activity of their client proteins[105,106]. On the basis of the molecular weight, HSPs are categorized into six families containing small HSPs like HSP27, HSP40, HSP60, HSP70 and HSP90, the larger family of HSPs containing HSP 110 and the GRP170 (Glucose related protein 170)[103,107,108]. Smaller HSPs are encoded by HSPB gene and function in an ATP-independent manner whereas high molecular weight HSPs are ATP-dependent and also show ATPase activity[109]. These chaperones are highly expressed in GBMs[110] and are responsive to death stimulus[111]. Multiple stress factors also known as heat shock response (HSR) are involved in the induction of HSP expression[112] under various conditions of stress. These HSR are regulated at various transcription levels by a class known as heat shock factors (HSF) that are known to be upstream transcriptional regulators of HSPs[113]. Vertebral HSFs include HSF1, 2, 3, 4 and HSFY that show structure similarity with highly conserved N-terminal-turn-helix DNA binding domain and C-terminal by binding with cis-acting sequence which is upstream of HSP genes collectively known as heat shock elements (HSEs)[114]. HSC70, GRP78, MTP70 and HSP90 β are some other known HSPs that are not induced under the conditions of stress and are expressed only in normal conditions[115,116]. In **Table 2.1** we have tried to elaborate the role of various HSPs in GBM.

S.no	Molecular HSPs Community	HSP classification within the community	Associated Co-chaperones	Implicative functions during normal cellular homeostasis	Impaired Molecular functions/expression in GBMs	Known therapeutic blockers	References
1	DNAJ	HSP40	Not defined	Acts as molecular chaperones, Enhancers of HSP70 ATPase activity	Promotes GBM invasion and metastasis; Alters the apoptotic machinery	Quercetin, si-RNA mediated knockdown	[117,118]
2	HSP60	HSP60	HSP 10	Interacts with HSP70 and HSP10, Assist in folding and translocation of cargo proteins	Expression rates higher in high grade gliomas, Interaction with HSP 90 and cyclophilin D, shows modulated tumor environment and halts apoptotic signaling	Down-regulation via si-RNA mediated knockdown	[119–121]
3	HSP70	HSP70, GRP75 (Mortalin), GRP78, HSPA1, HSPA8, HSPA9	CHIP, HSP40, BAG1, BAG3, HIP, HOP, GRPE	Promotes cell survival during stress, Assists during protein folding,	mHSP70 along with lipid globyltriaosylceramide (GBM3) defines tunneling nanotubes (TNT) clusters in GBM cells	GX15070 (BAG3), Gamintrinib	[122–125]
4	HSP90	GRP94, TRAP1, HSP90A, HSP90B	CYP40, HOP, FKBP51, FKBP52, CDC37	Signaling protein stabilizers, assist in folding and unfolding of guided proteins, Peptides loader of Class I MHC molecules.	Facilitates GBM cells migration by increasing cytosolic Ca ²⁺ via EGFR in ATP-dependent manner, Interaction with heparan sulfate proteoglycans (HSPGs) also promotes GBM invasion.	Geldanamycin, NVP-AUY922, IPI-504, Emodin, Radicol, 17-AAG, BIB021, Onalespib, 17-DMAG	[126–133]

5	Smaller HSPs	HSP27, HSP10, HSPB5	Not defined	Aggregate protein disassembly and their stabilization	HSP27 and HSB5 shows inclined expressions in GBMs, implies resistance to cytarabine and β -lapachone treatment, Increased expression leads to apoptotic resistance in GBMs.	Resveratrol, Rosmeric acid, Quercitin+Te mozolomide (TMZ),	[107,134–137]
6	Larger HSPs	HSP110, GRP170	Not defined	Dampers protein aggregation, Co-workers of HSP70 and assist in protein folding	Overexpression leads to reduced HSP70 interaction, Promoter of angiogenesis and increased metastasis.	Not reported	[138–140]

Table 2.1: List of molecular chaperones with their implicative role in normal cellular homeostasis, altered function in GBMs and their associated molecular chaperones.

2.2.1. DEREGULATED HSPTS IN GBMS ENVIRONMENT

High levels of HSPs are an indicative of poor prognosis and show increased resistance to radiotherapies with poor survival outcomes. GBMs show an increased level of HSP expression combined with hyper-activation of HSF1 that promotes invasion leading to metastasis. Studies have shown that HSP27, HSP70 and HSP90 are the most documented stress inducible HSPs in GBMs proliferation, progression and shows resistance to various treatment options. Various onco-proteomics studies have also identified these HSPs as majorly expressed in high grade gliomas as compared to the expression levels in normal cells[140]. Some of these major HSPs have been discussed to show the potential role and whether their chaperonin activity can be controlled by the inhibitors or through their knockdown to suppress GBMs progression. **Figure 2.2** has tried to showing the various inhibitors that potentially target invasive glioblastoma.

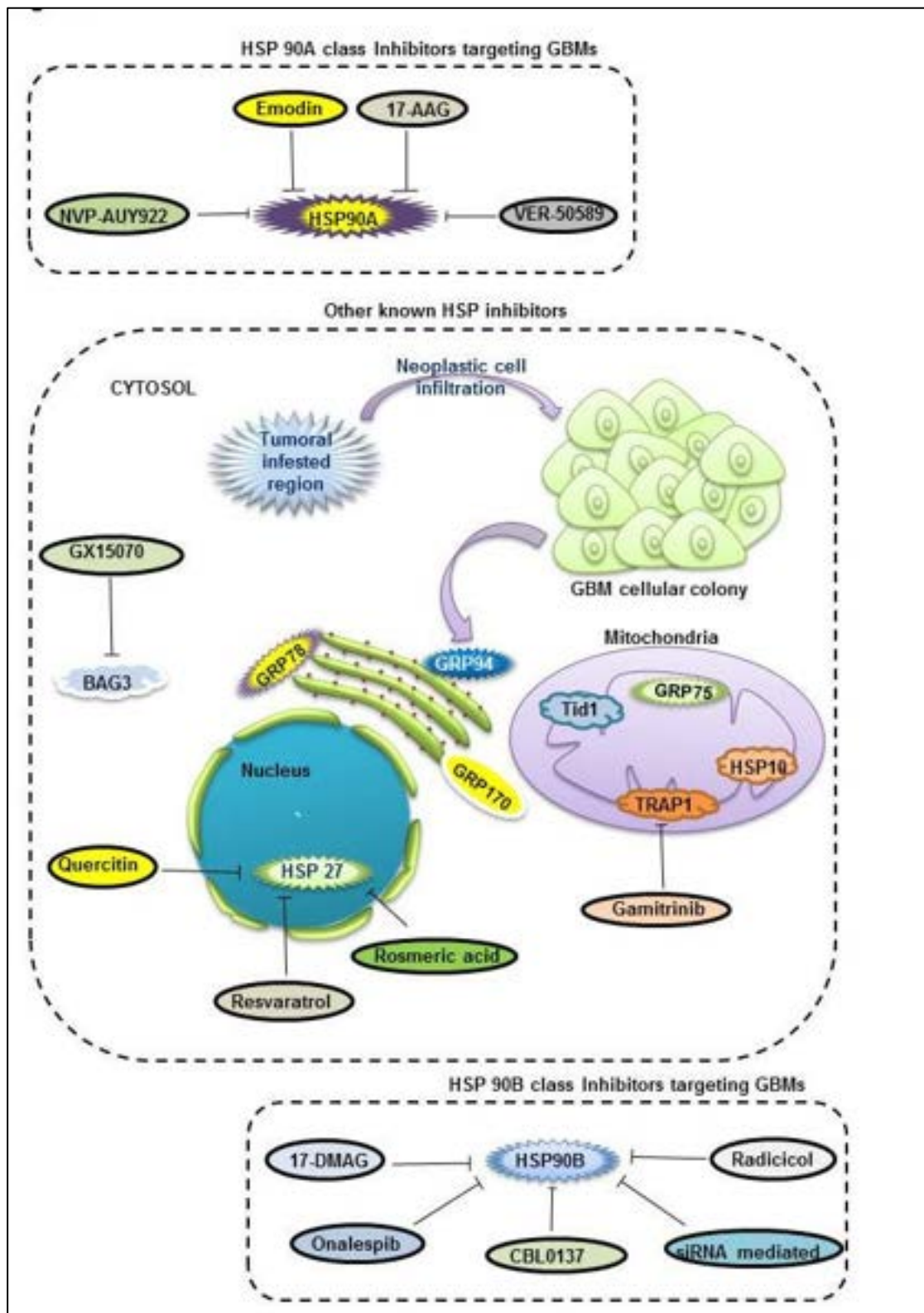


Figure 2.2: Distribution of various heat shock proteins (HSPs), molecular chaperons in various organelles and associated inhibitors targeting GBMs: HSPs are the modulators in various mechanisms such as proteostasis, which are highly relative in brain tumors such as gliomas. Class of HSPs such as HSP90 binds mutated proteins and causes stabilization of these molecules leading to mutagenesis. HSP90 also promotes resistance to cell death by preventing

the activation of procaspase-9. HSP27 inhibits procaspase-9 activation. Selective inhibition of HSP90 class (HSP 90A and HSP90B) using inhibitors emodin, 17-AAG, onalespib binds and inhibit the activity. Other HSPs such as HSP10, BAG3 and HSP27 are strongly modulated by inhibitors such as Rosmeric acid, resveratrol and quercetin binds HSPs and causes sensitization of GBMs to conventional therapies.

2.2.2. HSP27 AS MOLECULAR TARGET

HSP27 or HSPB1 belong to the class of small heat shock proteins (sHSP). These families of heat shock proteins are expressed in all human tissues, including neuronal cells (primary), in astrocytes but show high expression in skeletal and cardiac muscles and also show the ability to get phosphorylated and to get oligomerized. They can form oligomers of around 1,000 kDa and plays a central role in regulating the chaperone activity. These can be phosphorylated on three serine residues like 15th residue, 78th residue and the 82nd residue by a large number of kinases like the MAPKAP kinase, PKG and PKC. Protein partners that interacts with these HSPs includes histone deacetylase6 (HDAC-6), β -catenin, procaspase-3 and signal transducers and activators of transcription-2 (STAT2)[141]. They are overexpressed in a variety of cancers including high grade astrocytoma, intraepithelial neoplasia[108,142], in endometrial cancer but an opposite behavior of low expressivity is seen in case of neuroblastomas[143]. They are very crucial in promoting the proliferation and metastasis of gliomas cells. This property of HSP27 makes the cancer cells resistant to radiotherapy and adjuvant therapies. HSP27 shows a protective potential for cancer cells, acting as regulator of apoptosis by blocking different steps in this pathway. They bind with caspase-3 and cytochrome-c that are released from mitochondria and causes their inactivation[144,145] thus, causing this caspase cascade coming to an end. Studies have shown that HSP27 promotes neo-vascularization and promotes cell migration in peripheral blood by up-regulation of the vascular endothelial growth factors (VEGF) and activation of VEGF receptor type-2[146]. HSP27 have been shown to inhibit the p53 mediated transcription (p21), which ultimately targets p53 signaling[147]. HSP27 is known to be a modulator of the anti-apoptotic activity by degrading the apoptosome development as

cytochrome c released from the mitochondria bounded to HSP27, is unable to interact with procaspase9 and apoptotic protease activating factor1 (APAF1) thus, inactivating the caspases[148]. Inhibition of HSP27 can activate apoptosis under hypoxic condition and can cause depletion of CD133⁺ subpopulation in the blood serum[149]. Therefore, inactivating HSP27 using targeted therapies or siRNA mediated knockdown can be a possible therapeutic intervention against GBMs.

2.2.3. HSP40 AS MOLECULAR TARGETS

HSP40 proteins come under a class that consists of J-domain called DNAJ family. These HSPs mediates the ATPase activity of HSP70 by interacting with J-domain and therefore called as co-chaperones[150]. They are further categorized into three subclasses namely DNAJA, DNAJB and DNAJC. These chaperones assist HSP70 in various activities such as protein folding, unfolding, protein translation and their translocation finally leading to their degradation[151,152]. Studies have identified over-expressivity of HSP40 in various malignancies and shows potential role in glioblastoma progression[153]. Various members of HSP40 family shows tumor suppressive role like Tid1 also known as DNAJA3. Tid1 is a member of subclass A and is a regulator of apoptosis mediated by p53 signaling. Their overexpression caused apoptosis activation[154] in head carcinomas and therefore decreased proliferation, invasiveness and depleted cell growth in in-vitro conditions. HSP70 activity is regulated by two isoform of Tid1: hTid1 and hTid2 of which larger hTid1 is responsible for inducing apoptosis whereas hTid2 suppresses their activity[155,156]. Tid1 is also able to inhibit avian erythroblastosis viral oncogene homolog 2 (v-erb-B2) by inhibiting the extracellular signal-regulated kinases (ERK 1/2) and mitogen activated protein kinases (MAPK) therefore, switching apoptosis in abnormal cells[156,157]. Tid1 shows a contributive role in Wnt signaling by acting as a ligand against adenomatous polyposis coli (APC) which acts as a tumor suppressor[158].

DNA-like heat shock proteins (HJL1) or DNAJB4 a member of subclass B is also tumor

suppressive in nature[159]. HLJ1 is activated by YY 1 (Transcription factor) and activator protein 1 (AP1)[159]. Studies have identified that HJL1 can slow the cell cycle progression via p53/interferon independent STAT1/p21 (WAF1) in companion with reduced level of Cyclin D1 expression[160]. Curcumin found in turmeric increased HJL1 expression that reduced the invasiveness and metastasis in cells through E-cadherin expressional modulation[159]. Other members that can act as a possible therapeutic target includes ERDJ3 (DNAJB11)[161], MRJ (DNAJB6)[162], DNAJB8 and DNAJC6[163] however, no studies have been done yet to show their therapeutic role in case of GBMs and still needs a detailed examination.

2.2.4. HSP60 AS MOLECULAR TARGETS

HSP60 are the protein of chaperonin family that are induced during stress conditions and consists of fourteen members[150]. They are expressed in almost all the cellular compartments predominant being the eukaryotic mitochondria and are known as mitochondrial chaperones[164,165]. These HSP60s are encoded by HSPE, CCT, HSPD and various other genes[150]. They play an interactive role with HSP10 and acts as a co-chaperone for mitochondrial HSP70 also called mortalin[104,105,166]. HSP60 are found to be highly expressed in many cancer[104,166] types including high grade gliomas[167]. The structural morphology of this protein consists of three domains (apical, intermediate and equatorial)[168] and these domains are responsible for binding with Y-box binding protein1[169]. These proteins are also responsible for regulating the immune response by acting as an antigen for both B and T-lymphocytes[170]. They induce their anti-apoptotic effects on cancer cells by regulating the activities like angiogenesis, transformation efficiency and their ability to metastasize[171].

Studies have shown that HSP60 binds with cyclophilin D (CYPD) which is a component of mitochondrial permeability transition pore and other cofactors containing tumor necrosis factor receptor associated protein-1 (TRAP1) and HSP90[172]. They act as a modulator in tumor proliferation and prevent growth suppression. In vivo studies have shown that gene silencing

of HSP60 induces caspase dependent apoptosis by CYPD dependent mitochondrial permeability transitions[173]. These studies show that HSP60 are master regulators of cytoprotective chaperone network thus, preventing CYPD dependent cancer cell death. In case of neuroblastoma, HSP60 forms an interaction with intracellular protein clusterin (or SGP-2, Apo-lipoproteins J and TRPM-2)[174] and promotes cell survival by amplifying their survival and proliferative abilities. Evident studies have identified some of the compounds such as myrtucommulone (MC) an acyl-phloroglucinol found in leaves of a plant called myrtle, Sinularin present in corals *Sinularia flexibilis* that inhibited HSP60 in melanoma cells. HSP60 are known to be an important mediator in controlling drug resistance and therefore, can be a fruitful candidate in GBM therapies however, no such HSP60 inhibitor is used in treating GBMs.

2.2.5. HSP70 AS MOLECULAR TARGETS

HSP70 family of chaperones is composed of thirteen members of specialized proteins, some of which shows a positive correlation with the progression and proliferation of malignant cells[171,175]. These include the chaperoneic proteins induced during stress such as HSPA1, HSPA2, HSPA6 like HSP70B and cytosolic HSC70 (HSPA8), GRP78 (HSPA5) and mortalin HSPA9 that are constitutively expressed. HSP70 are localized in different cellular compartments that causes a surfeit of conditions induced during stress such as resistance to various therapeutic regime and apoptosis deregulation thus, halting cellular death[176,177]. Studies identified that not only cytosolic HSP70 are overexpressed in case of GBMs but also the membrane (mHSP70) and secreted forms of HSPs are also highly expressed in primary GBMs[178]. HSP70 interacts with other class of chaperones such as HSP90 and other co-chaperones like BAG3 to facilitate their proper functioning[179]. Malignant cells require the chaperone activity of HSP70 so that they are able to bypass the defensive mechanism such as apoptosis and autophagy that are carried by normal cells[124]. HSP70 implements their tumor protective role by suppressing both the extrinsic and intrinsic pathway of apoptosis mediated

cell death. HSP70 halts the intrinsic apoptotic machinery by binding with BAX (a member of Bcl-2 family) thus, blocking the mitochondrial translocation, also inhibits the apoptosome assembly by preventing Apaf-1 and procaspase9 from being oligomerized[180,181]. HSP70 is also known to inhibit the MAPK kinase signaling by interfering with c-Jun N-terminal kinase, p38 and Extracellular signal regulated kinases (ERK)[182]. Using C6 glioblastoma cell line (rat model) researchers identified that HSP70 was able to interact with inactive and oxidized form of GAPDH thus preventing their aggregation via the chaperone activity of HSP70. This showed the protective mechanism of HSP70 in oxidative stress induced in GBM cell line thus, rescuing the GAPDH activity that further elevated the survival in glioblastoma cells. By binding with apoptosis-inducing factors (AIF)[183], HSP70 also interacts with caspase-dependent pathway thus preventing chromatin condensation induced by AIF. An HSP70 molecular chaperone also prolongs survival in GBM cell by binding with endo-lysosomal bis-phosphate, which acts a positive regulator in catabolism of lysosomal sphingolipids[184]. This further stabilizes the lysosomal machinery thus inhibiting the process of membrane permeabilization and promotes survival of cancer cells[185].

2.2.6. HSP90 AS MOLECULAR TARGETS

Members of this chaperone family are the most studied among all other molecular chaperones and are supposed to be high conservative in nature. These molecular chaperones are involved in commanding a variety of cellular processes including angiogenesis, proliferation of cells, aggregation, stabilization and proteolytic degradation of various oncoproteins (client proteins) and also in cell cycle progression[186]. These chaperones are identified to be the key workers during invasion and in malignant transformation of GBM cells. HSP90s are encoded by family of five genes namely HSPC1 to HSPC5[178] and also exist in two isoform configurations, HSP90-alpha and HSP90-beta[187]. These chaperones form large protein complexes by binding to various co-chaperones that assist in maturation and degradation of various oncoproteins[188]. These chaperone proteins are found to be buttoned onto the plasma

membrane and are also found in the extracellular environment (eHSP90 or extracellular HSP90)[189]. These eHSP90 modulates AKT signaling by binding with low density lipoprotein receptor related protein-1 (LRP1) and thus, phosphorylates AKT on S897 residue of ephrin-A2 (p-Eph-A2S897). These HSPs are also involved in lamellipodia formation; a factor required by glioblastoma cells in migration and invasion to surrounding tissues during oxidative stress or hypoxia[189]. Extracellular HSP90 promotes GBM progression by increasing the levels of epidermal growth factor receptors (EGFR) cellular response or by activation of Toll-like receptors-4 (TLR-4)[190].

2.3. CELL CYCLE, CDKS AND REGULATORY PROTEINS AS THERAPEUTIC TARGETS

Cell cycle appears to be the soul of the cell as it is the only process through which a normal cell starts its journey to form a progeny of cells. Cell enters the cell cycle in G1 (Gap1) phase and commands themselves for DNA replication via mitogenic signals originating in S (synthesis) phase. Cell then enters the G2 (Gap2) phase (road to mitosis) further leading to M (Mitotic) phase[191,192]. The precision and orderly progression of cell cycle is guided by regulators such as cyclin-dependent kinases (CDKs) that forms functional complex network with another class known as cyclins[193–195]. Activity of CDKs is strongly governed during different phases of cell cycle, and after progression through the restriction point at G1 phase, cells become strongly committed to DNA replication and therefore, no further requirement of mitogenic signal to complete the cellular activity. Complex surveillance mechanism holds to check the cell cycle progression and if any abnormality in the machinery is detected then a sudden halt is initiated which triggers a cell cycle arrest[196]. Any mutation in the genes coding for these regulators (positive and negative) causes genomic instability, thereby promoting uncontrolled cellular proliferation leading to cancer or metastasis. **Figure 2.3** gives the overall representation of various inhibitors available till date targeting various CDKs that are involved in aberrant cell cycle progression leading to glioblastoma invasion and metastasis

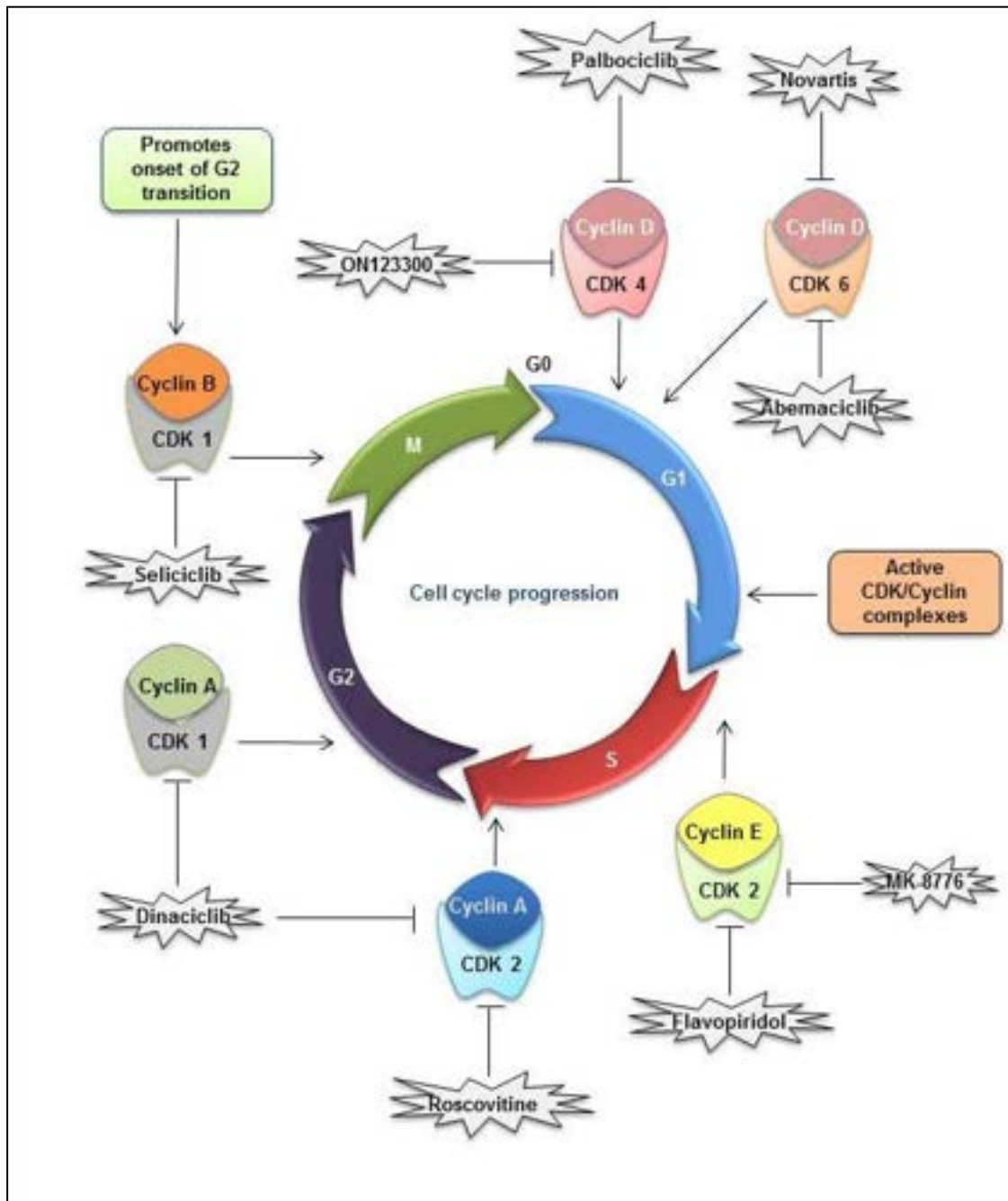


Figure 2.3: Cell cycle, cyclin-dependent kinase (CDKs) and their inhibitors targeting glioblastoma (GBMs): CDKs and cyclin are the key regulatory components in defining the progression of cell cycle. Cyclin B/CDK1 involved in M-phase defines the replicative machinery in DNA. During tumor invasion and proliferation function of these CDKs are distorted that leads to uncontrolled cell growth and increases the tumor load. Pharmacological inhibitors targeting these very complexes (Cyclin/CDK) causes sensitization of glioblastoma to conventional therapeutic regime such as chemotherapy and radiotherapy. Dinaciclib a potent inhibitor binding to cyclin A/CDk1 and Cyclin A/CDK2. Seliciclib binds Cyclin B/CDK1 complex targeting the M-phase of cell cycle. Inhibitors such as ON123300 and Palbociclib bind Cyclin D/CDK4. Novartis and abemaciclib binds G1 phase of cell cycle thereby preventing initiation of DNA replication in very early stage preventing progression of GBMs.

Discernment into the cells and mutations that drives to the development of gliomas has been seen in various studies concerning human clinical studies and data. Still, it remains controversial that whether gliomas have originated from neural stem cells (NSCs) or progenitor cells. Two major hypotheses govern the concept of glioma genesis involves cancer stem cell hypotheses and clonal hypotheses. Studies conducted using gliomas models suggest that NSCs are the actual cells of origin although some studies shows the defined ability of differentiated cells in tumor initiation[197]. Deregulation of cell cycle and its various regulators shows critical complex in the progression and development of GBMs, leading to resistance from therapeutic regime[198]. As GBMs tumor cells are dependent on the activity of CDKs and checkpoint kinases for their survival and proliferation therefore CDKs appears to be the prime target in combating GBMs. Proteasomal inhibition also leads to accumulation of various non-degrading proteins that involves cell cycle proteins and cyclins leading to proteotoxic stress ultimately causing cell death[199]. As CDKs are the master kinases in cell cycle therefore selection of CDK inhibitors requires specificity against CDKs either they target a specific CDK or are nonspecific pan inhibitors. Compounds such as flavopiridol (synthetic flavone) exhibits pro-apoptotic and anti-proliferative activity when tested in GBM cell lines. Purine-based analogs like roscovitine performs cell cycle arrest in G2/M transition and increased level of apoptosis in glioblastoma cells[200]. Protein such as cyclin D/CDK 4/6 retinoblastoma (Rb) are highly deregulated in GBMs and are critical mediators in cell cycle entry therefore, designing inhibitors targeting the functional domains of CDK4 and CDK6 could actually lead to phosphorylation of Rb protein thereby causing cell cycle arrest[191]. Other CDK 4/6 includes abemaciclib and ribociclib that are employed as single agents or given in combination with TMZ, showing inclined survival stats in xenograft GBM rodents[201]. Treatment strategy in using these CDK 4/6 inhibitors for invasive GBMs relies on their ability to cross the BBB[201]. Researchers have shown that CDK1 knockdown in GBMs showed inhibition in the proliferation potential, increased cellular apoptosis and made these abnormal cells sensitive to chemo-

radiotherapy[202]. Role of various CDK inhibitors that are still in clinical assessment along with inhibitory effect is described in **Table 2.2**.

S.no	Selective CDKs targets in GBM	Known CDK inhibitors	Associated Cyclins units	Functional importance of associated cyclins within the cell	Effect induced by CDKs inhibitors on GBMs	References
1	CDK 4/6	Ibrance (or Palbociclib)	Cyclin D	Guards the G1 phase of cell cycle and also maintains the E2F/Rb transition	Shows suppressive tumor growth; Extended rate of survival in mice model in combination with radiotherapy; Caused G1 arrest and showed senescence in GBM cells	[203–206]
2	CDK 1/2	Selicilib (or roscovitine)	Cyclin A, B1, E1, E2	Maintains DNA integrity at G2 transition and during mitosis controls spindle synthesis and assembly	Showed pro-apoptotic effects along with anti-proliferative activity when induced in GBM cell lines; Induced G2/M arrest	[207–209]
3	CDK 4/6	Abemaciclib (or LY2835219)	Cyclin D	Guards the G1 phase of cell cycle and also maintains the E2F/Rb transition	Prolonged survival in intracranial xenograft models; Increased synergistic effects when combined with Temozolomide (TMZ)	[201,203,210]
4	CDK2	MK-8776	Cyclin A, B1, E1, E2	Important mediators during G1-S transition	Reduced cellular activity in GBM cell lines when combined with gemcitabine;	[211]
5	CDK 1/2	Alvocidib (or flavopiridol)	Cyclin A, E1, E2	Maintains DNA integrity at G2 transition and during mitosis controls spindle synthesis and assembly	Delayed tumor load in intracranial and subcutaneous gliomas xenograft models; Increased re-sensitization of TMZ-resistant cells to TMZ.	[212–214]
6	CDK 4/6	Novartis (or Ribociclib)	Cyclin D	Checks G1 phase of cell cycle and also maintains the E2F/Rb transition	Unknown	[215–217]

7	CDK 4	ON123300	Cyclin D	Commands the RB/E2F transition in cell cycle	Increased synergistic activity when combined with gefitinib;	[218]
8	CDK 1/2	Dinaciclib	Cyclin A, E1, E2	Maintains DNA integrity at G2 transition and during mitosis controls spindle synthesis and assembly	Induced lateral G2 arrest and decreased the anti-proliferative activity	[219–221]

Table 2.2: Cyclin dependent kinases (CDKs) along with their cyclins depicting their altered functions in GBMs and known selective inhibitors

Apart from CDKs and cyclins various cell cycle proteins such as ataxia telangiectasia mutated (ATM), checkpoint kinase 1 (Chk1), wee1, polo-like kinase, aurora A can also be seen as therapeutic targets in handling GBMs. ATM which is a DNA damage checkpoint kinase is an important predictable targets, and ATM inhibitors such as KU-55933 (morpholinyl thianthrenyl-pyranone) and KU-60019 when administrated increased the sensitization of GBM cells to concurrent radiotherapy, suggesting its potential as a TMZ-sensitizing agents[222–224]. Wee1 seems to be the negative regulator of Cyclin B/CDK1 complex and can be seen as pharmacological targets in GBMs inhibition. NCT02207010 is an ongoing phase 0 clinical trial that is using Wee1 inhibitor AZD1775 in treating patients with recurrent GBMs[225,226]. Another class of cell cycle regulatory proteins PLK1 plays regulatory role in centrosome maturation, activation of Cyclin B/CDK1 and entry to mitosis[227]. **Figure 2.4** shows the targeted inhibitors that bind various cell cycle regulatory proteins involved in cell cycle. These proteins are highly expressed in GBMs, indicating poor prognosis and survival stats. An example of this class of inhibitors includes BI6727, BI2536 and GSK461364 that triggers apoptosis and prevents proliferation of GBM sub-population[228,229]. However, these compounds are still under clinical investigation and still needed to be tested further. Despite development of a number of small molecular as therapeutic blockers, targeting the various phases of cell cycle still a deep understanding of mechanism underlying cell cycle machinery

is required to trace the death pattern in GBMs, so that the survival is somewhere improved from current stats.

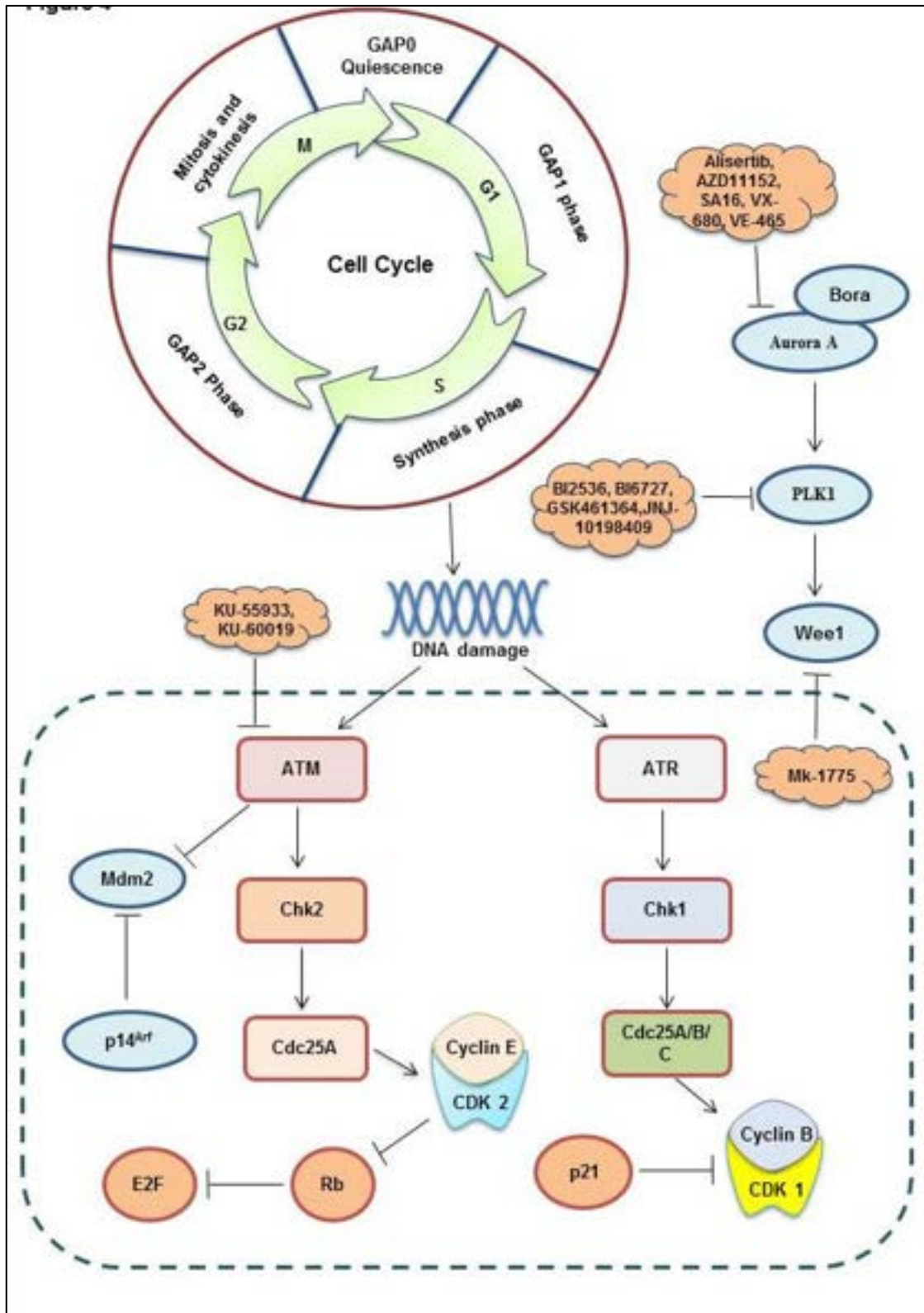


Figure 2.4: Cell cycle regulatory proteins, checkpoints and their associated inhibitors targeting glioblastoma: DNA damage checkpoints are the prime regulators in maintaining the integrity of DNA. Replication error if detected then these checkpoints cause inactivation of Cyclin/CDK1 and

Cyclin/CDK2 complexes. Checkpoint transducer kinases such as ataxia telangiectasia mutated (ATM) and ATM and Rad3-related (ATR) leads to the phosphorylation of Checkpoint kinases (Chk1 and Chk2) which appears to be the positive regulators in Cyclin/CDK complex. Tumor suppressor p53 causes activation of CDK inhibitor p21. During DNA damage p53 is unable to get degraded by proteasomal machinery due to binding of mouse-double minute2 (mdm2). Therapeutic regime targeting various proteins such as ATM, Wee1 and checkpoint kinases evade the DNA damage checkpoints and thus, sensitizes cancer cells to therapies targeting DNA damage. Selective inhibitors such as KU-5593 and KU-60019 targeting ATM, AZD11152 targeting aurora A and inhibitors such as Mk-1776 binds Wee1 and inhibits their activity. Various inhibitors targeting these regulatory proteins are hereby represented.

GBMs being the most lethal form of brain malignancies characterized with increased rate of invasiveness and aggressiveness shows poor prognosis in patients and reduced overall survival in patients. As these cells are highly resistant to conventional chemotherapy and radiotherapy therefore every aspect of treatment should be considered in treating these malignancies. Post translational modification, proteostasis and cell cycle are increasing becoming as the study of interest in handling these tumors. Inclusion of high-throughput screening in the identification of various ubiquitin E3 ligases as inhibitors using structure analysis of the E3 ligase binding pockets can be a fruitful aspect in pharmacological development of novel inhibitors that can reduce the proliferation and metastasis in GBMs. Molecular HSPs on the other hand can appear to be the game changers when talking about the therapeutic options in GBMs. As these classes of proteins are divine rulers in handling GBM cellular proliferation, migration, metastasis and survival therefore targeting members of this family such as HSP60, HSP90, HSP70 and HSP100, will be unraveling the various therapeutic potentials when dealing with GBMs.

From the therapeutic aspects, targeting the aberrant cell cycle is also considered to be a promising approach in combating GBMs. Inhibitors that potentially targets the cell cycle are characterized based on their efficiency to bind selective phases or checkpoints, and are known as CDK inhibitors and checkpoint kinase inhibitors. Using specific modulators of cell cycle either alone or in combination with other regimes such as chemotherapy, HSP inhibitors or ubiquitin E3 ligase inhibitors can help to eradicate GBMs and can somewhere will be improving

the standard of life in patients diagnosed with these aggressive tumors. In order to improve the efficiency of these inhibitors and to make them more effective there is a need to ideally screen the affected patient population, use of appropriate biomarkers, making sure that the therapeutic dosage should cross the BBB permeability and hit the target and last but not least, using drug combinations to avoid resistance from therapy. If these parameters can be possibly rectified in future and using the concept of trio inhibition (E3 ligases, molecular chaperones and cell cycle inhibitors) then there is a possibility that we will be able to successfully eradicate this very sarcastic tumor population known to be GBMs.

**DECODING THE ROLE OF UBIQUITIN E3 LIGASES
AND THE THERAPEUTIC TARGETING OF
UBIQUITIN E3 LIGASES**

CHAPTER III: DECODING THE ROLE OF UBIQUITIN E3 LIGASES AND THE THERAPEUTIC TARGETING OF UBIQUITIN E3 LIGASES

3.1 INTRODUCTION

Gliomas represent the most frequently occurring primary brain tumors that arise due to the abnormality in the glial cells such as ependymal cells, oligodendrocytes, astrocytes, etc. [230]. Based on the cells of origin these gliomas are classified as anaplastic astrocytoma, oligodendrogliomas, and glioblastoma[231]. Glioblastoma represents the most lethal and malignant form of brain tumor and accounts for 80 percent of the cases as recognized by the World Health Organization (WHO) [232]. However, the overall median survival of the patient remains only 9-15 months following the standard therapeutic regimes such as surgery, radiotherapy, and chemotherapy [233,234]. This lack in the precise therapeutic targeting of these tumors is due to the undefined etiology and incomplete knowledge of the underlying mechanism behind this disease. Recent data published concedes that there is 91% involvement of p53 pathway downregulation in a variety of carcinomas[235]. As the treatment options are very limited there is an urgent need to explore more options[236]. In that case, ubiquitin E3 ligase remains an untouched area of discussion as the inhibitors targeting these ligases are very few in the count. Ubiquitylation represents a reversible post-translational modification that is regulated by ubiquitin E3 ligases[237]. Ubiquitin E3 ligases are known to target a broad spectrum of substrates that are involved in processes like DNA repair, apoptosis, and metabolism[238]. Ubiquitin E3 ligases are the pinnacle of ubiquitination with a high frequency of selectivity against the substrate, therefore, making them an attractive drug target[239].

Various ubiquitin E3 ligases are known to play an important role in commanding several activities of cells. Ubiquitin E3 ligases such as MDM2 (Mouse double minute 2)[240], BRCA1 (Breast and ovarian cancer susceptibility protein 1)[241], Neural precursor cell expressed

developmentally Down-regulated 4 (NEDD4)[242], Tripartite motif-containing 21 (TRIM21)[243], Ring finger41 (RNF41)[244], Ubiquitin protein E3 ligase (UBE3A)[245] and various other E3 ligases impart an important role. Although very few inhibitors are currently available that can target these ligases and can cause suppression in GBM proliferation[246–248]. Our study aimed to identify a ubiquitin E3 ligase whose expression was higher in glioblastoma and plays a prominent role in GBM signaling. For that, we performed expressional and mutational studies to predict the most suitable E3 ligase for therapeutics. Through our observations, MDM2 was found to be the most suitable ubiquitin E3 ligase as it shows higher mutational frequencies in GBM and is also involved in the activation of p53[249]. MDM2 acts as a ubiquitin E3 ligase and functions by binding to p53 (Tumor suppressor protein)[250]. The binding of MDM2 to p53 causes the inactivation of p53, leading to the functional loss in p53 activity[251]. The functions mediated by p53 are DNA repair, senescence, apoptosis, arrest in cellular growth, and cell growth[252]. Whenever there is cellular stress like genotoxicity, damage to the DNA, oncogene activation, and hyperproliferative stress there is upregulation of an enzyme p14 alternate reading frame protein (ARF)[253]. This enzyme remains upstream to MDM2, promotes escape of p53 from MDM2 degradation and therefore, the tumor-suppressing functions of p53 are not lost[254]. Researchers have shown that mutation in MDM2 during cancerous conditions causes gene amplification in glioblastomas and on the side p53 remains wild-type[255]. This amplification causes an overexpression in MDM2 that causes the p53 inactivation and increased cancer progression. Hence, breaking the MDM2-p53 interactions seems to be a promising therapeutic approach to treating glioblastomas[256]. Studies have been done to identify inhibitors that can potentially target MDM2 but are still in pipeline. Inhibitors such as RG7112 (analogous to nutlin) causes MDM2 inactivation leading to increased cellular apoptosis, and cell cycle arrest, and showed a reduction in tumor growth in xenografts[257]. Nutlin-3a is known to inhibit the MDM2-p53 interactions and enhance p53-mediated apoptosis

in osteosarcoma[258]. Other inhibitors of MDM2 such as CGM097, MK8242, MI77301, and RG7388 are known to be used in various cancer although only a few are known to play an important role in the therapeutics of GBM[259–262]. Studies have also shown that inhibiting MDM2 can also be a therapeutic option in treating GBMs possessing p53 wild type[263,264]. These studies prove that MDM2 can be an effective target in tumorigenicity and breaking the p53-MDM2 interactions can be significant in GBM treatment. However, computational and *in-silico* analysis by inculcating a combined approach of docking at a molecular level and dynamic simulation studies at the initial screening and analysis can help us to identify potential inhibitors against these ligases as they are very limited in count[265,266].

Researchers have focused on identifying synthetic inhibitors as therapeutic options but these chemical inhibitors possess enhanced cytotoxicity. Studies concerning the use of natural alkaloids in GBM therapeutics are very few in number[267]. Natural alkaloids can be of great value as they show very less or no side effects. Alkaloids represent an important class of natural compounds and are shown to induce cell death in GBM as they are potent antioxidants[268]. Alkaloids such as melatonin (monoamine alkaloid) were able to inhibit MDM2 in the MCF7 breast cancer cell line[269]. Melatonin is also known to inhibit phosphorylation of MDM2, enhancing acetylation of p53 thereby leading to p53-MDM2 disruption and gain of functions of p53[270]. Another study found papaverine (non-narcotic opium alkaloid) was able to induce suppression in GBM activity[271]. Evodiamine is a natural alkaloid derived from the fruit of *Evodia rutaecarpa* (medicinal plant) mostly used by the Chinese in medicine[272]. This alkaloid is known to exhibit the property of anti-inflammation and is known to be reported in reducing the proliferation of cancerous cells by the process of apoptosis and cell cycle arrest[273]. Evodiamine was found to induce calcium/JNK mediated autophagy mitochondrial-mediated apoptosis in GBM[274,275]. However, the role of evodiamine in targeting MDM2 as ubiquitin E3 ligase remains unclear. Another alkaloid sanguinarine which is a benzo

phenanthridine alkaloid was able to induce apoptosis in human breast carcinoma cells[276]. A recent study shows that evodiamine can inhibit liver carcinoma via Met/EGFR signaling[277]. Evodiamine was found to induce apoptosis in lung carcinoma[278]. Evodiamine has been shown to target the cancer stem-like cells through the p53-p21-Rb pathway in breast cancer[279]. Sanguinarine a benzophenanthridine and is a nitrogen containing alkaloid, isolated from the roots of *Sanguinaria canadensis*[280]. This alkaloid is known to possess antibacterial and anti-inflammatory properties. Sanguinarine is found to induce apoptosis in p53 dependent manner in hepatocellular carcinoma[281]. Sanguinarine was also able to induce apoptosis in C6 rat glioblastoma cells[282]. Sanguinarine was also able to induce metastasis in breast cancer[283]. Sanguinarine is known to induce ROS-dependent activation of autophagy and possessed anti-glioma effect[284].

However, the role of sanguinarine in targeting MDM2 is not understood and how these alkaloids can be the potential inhibitors of ubiquitin E3 ligase is also unknown. [285]. Studies have shown that alkaloids can induce self-ubiquitination and degradation in MDM2 by targeting the MDM2-DAXX-HAUSP interactions [286]. Alkaloids such as berberine, matrine, and melatonin are reported to be effective in reducing the expression of MDM2 or decreasing the stability in acute lymphoblastic leukemia, liver carcinoma, and breast cancer [270,287]. Other studies in which alkaloids can be seen in altering the MDM2-p53 signaling are indole-3-carbinol [288] and fluspirilene[289] targeting breast and colon cancer. Since alkaloids can target a variety of cancers very few or no studies are available on the therapeutic targeting of GBM using alkaloids. In our study, we screened two natural alkaloids i.e., evodiamine and sanguinarine based on the literature, docking, and simulation studies. Also, we checked how these compounds are interacting with MDM2 and used nutlin-3a as the reference against MDM2[265].

Our study was focused on the identification of a potent ubiquitin E3 ligase and how these

ubiquitin E3 ligases can be targeted by using natural inhibitors. Our approach was based on using mutational analysis, pathway studies, and expressional analysis to explore the role of various ubiquitin E3 ligases in GBM. In the end, we were able to identify MDM2 as a targetable E3 ligase and we also tried to target this ligase with evodiamine and sanguinarine. These alkaloids were screened from the compound library and the various physiochemical properties of these compounds were also accessed. Further, molecular docking and dynamic simulation studies were also performed to predict whether these inhibitors can target MDM2 and could be a new therapeutic avenue in targeting GBMs.

3.2 MATERIAL AND METHODOLOGY

3.2.1. COLLECTION OF RAW DATA

Datasets that are used in the current study have been extracted from the National Centre of Biotechnology Information (NCBI) gene expression omnibus (GEO) (<https://www.ncbi.nlm.nih.gov/geo/>) [290]. The microarray gene expression profiles were obtained from GSE 4290, GSE 104291, and GSE 50161 datasets. The platform used in GSE 104291, GSE 50161, and GSE4290 is GPL570 [HG-U133_Plus_2] Affymetrix human genome.

3.2.2. IDENTIFICATION OF DIFFERENTIALLY EXPRESSED GENES

The present study utilized GEO2R (<https://www.ncbi.nlm.nih.gov/geo/geo2r>) a web-based interactive tool that works on the R language limma package. GEO2R can be used as a comparative tool for two or more sets of samples and is helpful in the prediction of differential expression in the GEO series[290]. We used GEO2R to filter out the genes which were differentially expressed in these three datasets. To study the biological prospects, biological functions were annotated for differentially expressed genes. P-value <0.05 and the $|\text{Log FC}| > 2$ and $|\text{Log FC}| < 2$ were used as cut-off criteria to filter out the differentially expressed genes (DEGs).

3.2.3. SCREENING OF UBIQUITIN E3 LIGASES AND VENN ANALYSIS

The DEGs from the above three datasets were screened for the presence of any ubiquitin E3 ligases. UbiBrowser2.0 (<http://ubibrowser.bio-it.cn/>), an integrated bioinformatics platform was used as an identification tool for ubiquitin E3 ligases in these DEGs. Final confirmation of these DEGs as ubiquitin E3 ligases was done using UbiNet2.0 (<https://awi.cuhk.edu.cn/~ubinet/index.php>). DEGs that were identified as ubiquitin E3 ligases were then analyzed by VENN analysis to filter out common E3 ligases in these three datasets.

3.2.4. FUNCTIONAL ENRICHMENT ANALYSIS OF IDENTIFIED UBIQUITIN E3 LIGASES

To scrutinize the biological, cellular, and molecular functions and the various pathways involved in these ubiquitin E3 ligases, Gene Ontology (GO) term and pathway prediction was done using SHINYGO 7.16 (<http://bioinformatics.sdstate.edu/go/>). Parameters such as P-value <0.05 and count >3 were set as the threshold for significantly enriched terms. Eventually, the functional enrichment network was constructed.

3.2.5. MUTATIONAL ANALYSIS AND EXPRESSION ANALYSIS OF COMMON UBIQUITIN E3 LIGASE

To predict the mutational signatures of the identified ubiquitin E3 ligases we used the cBioCancer genomic portal (<https://www.cbioportal.org/>). This platform can analyze the molecular data retrieved from cancerous tissues and cytogenetics and is useful in the determination of epigenetics and genetic levels. Expression analysis followed by mutational analysis was done using Gene expression profiling interactive analysis 2 (<http://gepia2.cancer-pku.cn/>) to predict the rate of expression of identified E3 ligases in glioblastoma and to check whether the data is statistically significant or not. Here n represents the number of normal patient count whereas t represents the number of patients affected suffering from glioblastoma. This data was obtained from TCGA and the expression analysis was performed using GEPAL2.

3.2.6. COMPOUND LIBRARY SCREENING

In the present study, 70 alkaloids were taken from the Naturally occurring plant-based anti-cancer compound activity-target (NPACT) database. The 3D chemical structure and canonical smiles of these alkaloids were downloaded using PubChem[291]. Ligand confirmations were downloaded in 2D SDF format and visualization was done using Avogadro (<https://avogadro.cc/>) and then converted to PDB format. These structures were checked for the presence of any H-bond or any other bound group apart from our ligand of interest.

3.2.7. ANALYSIS OF ADMET DESCRIPTORS AND BLOOD-BRAIN BARRIER (BBB)

ADMET profiling (i.e., absorption, distribution, metabolism, excretion, and toxicity) of selected compounds was conducted using SwissADME [292]. Both the physical and pharmaceutical properties were screened using SwissADME. CBligand (<https://www.cbligand.org/CCGS/>) was used as a platform to check the BBB permeability of the compounds used in the study. Based on the results obtained from SwissADME and CBligand analysis, filtered compounds were considered further for molecular docking and simulations with the filtered ubiquitin E3 ligase.

3.2.8. MOLECULAR DOCKING STUDIES

The PDB structure of MDM2 (PDB id: 3JZK) was downloaded from the RCSB PDB database. Molecular docking was performed against MDM2 receptor protein with filtered alkaloids. Docking analysis was performed using WEBINA (<https://durrantlab.pitt.edu/webina/>), a JavaScript that runs Auto Dock Vina entirely in a web browser [293]. Molecular docking of MDM2 was performed with different alkaloids. Heteroatoms that were present within the PDB structure of MDM2 were removed and hydrogen was added by using WEBINA. Structural visualization of MDM2 was done using Avogadro and UCSF chimera (<https://www.cgl.ucsf.edu/chimera/>). Docking was performed by employing a grid size of x-axis= 40, y-axis= 45 and z-axis=40. Prediction of docking results was done based on the best interactions between the receptor and the ligand and on the binding affinity. The 3D and 2D confirmations were generated using Discovery Studio 2020 [294]. The complex which showed the best binding affinity as compared to reference then proceeded for MD simulation studies.

3.2.9. MOLECULAR DYNAMIC SIMULATIONS OF PROTEIN-LIGAND COMPLEXES

MD simulation of the identified compounds with MDM2 was performed individually using GROMACS 2019.3 package (<https://bioexcel.eu/gromacs-2019-6-is-available/>). The top fourteen ligand-protein complexes were first simulated at 20 ns to check the stability of the complexes. Complexes that were found to be stable at 20 ns were then considered for simulation

at a 50 ns timescale to provide an insight into how stable they are and to see how they behave dynamically. Complex preparation was done using CHARMM36 all-atom force field. The charge topology of the compounds was generated using CGenFF and then solvated in a cubical boundary box with the dimensional separation of 1.0nm, using the TIP3 water model. Charge neutralization was done via the addition of precise concentration of chloride [Cl⁻] ions and sodium [Na⁺] ions. Energy minimization was performed at 10 kJ/mol/nm using the long steepest descent algorithm for 10000 steps followed by 10000 steps of a conjugate gradient to avoid any steric clashes. The system was then subjected to equilibration with position-restrained (NVT and NPT) dynamics simulations at a constant temperature and pressure of 300K and 1 bar for a duration of 50 ns. The plot for root-mean-square deviation (RMSD), root mean square fluctuation (RMSF), the radius of gyration (Rg), and the number of hydrogen bonds were then plotted.

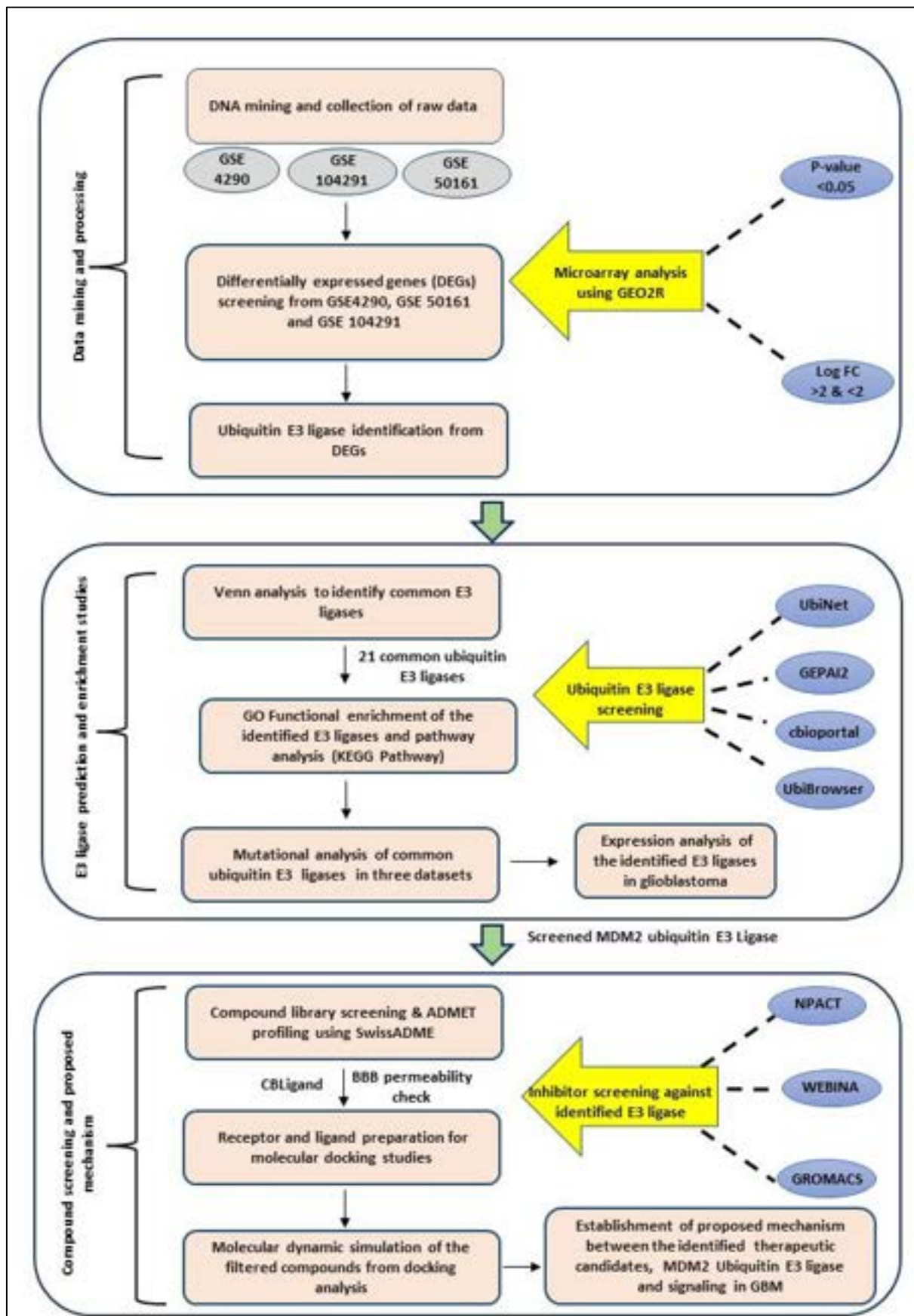


Figure 3.1: Workflow overview: Data extraction was performed from the National Centre of Biotechnology Information (NCBI) gene expression omnibus (GEO). Data analysis and

processing were performed using GEO2R. After data processing, the differentially expressed genes (DEGs) were filtered out from the datasets GSE4290, GSE104291 & GSE50161. These DEGs were then filtered by using parameters such as P-value and the fold change (Log FC) values. prediction of potential ubiquitin E3 ligases present within these three datasets was done using UbiNet and the confirmation of the DEGs acting as ubiquitin E3 ligases was done using UbiBrowser. Post E3 ligase prediction, Venn analysis was done to identify the common ubiquitin E3 ligases present within the three datasets. GO Functional enrichment and pathways analysis was done using SHINYGO 7.16 to identify the functions of each of 21 common ubiquitin E3 ligases and the pathways associated with them. After enrichment and pathway analysis, mutational frequencies of the 21 common E3 ligases were checked using cBiportal to predict the most suitable and targetable ubiquitin E3 ligase for our study focusing on Glioblastomas (GBMs). Using Gene expression profiling interactive analysis 2 (GEPAl2), the expressions were checked for the ligases filtered after mutational analysis. Selection of the most appropriate E3 ligase for our study was preceded by exploring the compound libraries and we selected the Naturally occurring plant-based anti-cancer compound activity-target (NPACT) library and alkaloids class for this study. The blood-brain permeability (BBB) scores were checked to identify the compounds that can cross the BBB using SwissADME. ADMET analysis was then applied to the filtered compound passing BBB to check the parameters such as absorption, distribution, metabolism, excretion, and toxicity of the alkaloids. The protein structure of mouse double minute (MDM2) that was identified as the most suitable target based on mutational frequencies was downloaded using a protein database (PDB). Ligand structures were downloaded using PubChem along with their canonical smiles. After the preparation of the receptor and ligand, docking was carried out to check for the most suitable ligand binding with the receptor (MDM2), showing the highest binding affinity and rate of inhibition. Compounds showing the best interaction and inhibition then proceeded for molecular dynamics simulations (MDS) studies till 50ns to validate the interactions and the stability of the complex (Protein-Ligand). Based on all the analyses performed, a mechanism was proposed for how the identified inhibitors can target the MDM2 that might be able to suppress GBMs.

3.3 RESULTS

3.3.1. RAW DATA COLLECTION AND DEGS SCREENING

The raw data from three gene expression profiles (GSE 4290, GSE 104291, and GSE 50161) were downloaded from NCBI GEO databases. Of these GSE4290 datasets comprised of 81 glioblastoma samples and 23 non-tumor samples, 4 glioblastomata, and 2 non-tumor samples existed in GSE 104291 dataset and, 34 glioblastoma and 13 normal brain samples were present in GSE 50161 dataset. DEGs between the GBM samples and normal control samples were obtained from these three datasets.

3.3.2. UBIQUITIN E3 LIGASE IDENTIFICATION AND VENN ANALYSIS

After the identification of DEGs, screening of ubiquitin E3 ligases was done within these DEGs. These DEGs were individually picked up to check whether they show the activity of an E3 ligase or not. DEGs which functioned as a substrate for a particular ligase were omitted from the study. A total of 181 ligases were predicted out of which 89 were present in GSE4290, 50 in GSE50161, and 42 in GSE104291. Venn analysis was then conducted to deduce the common ligases among all the ligases that were present in these three datasets. Furthermore, 21 overlapping ubiquitin E3 ligases were procured using the Venn diagram and are represented in **Figures 3.2(A)**.

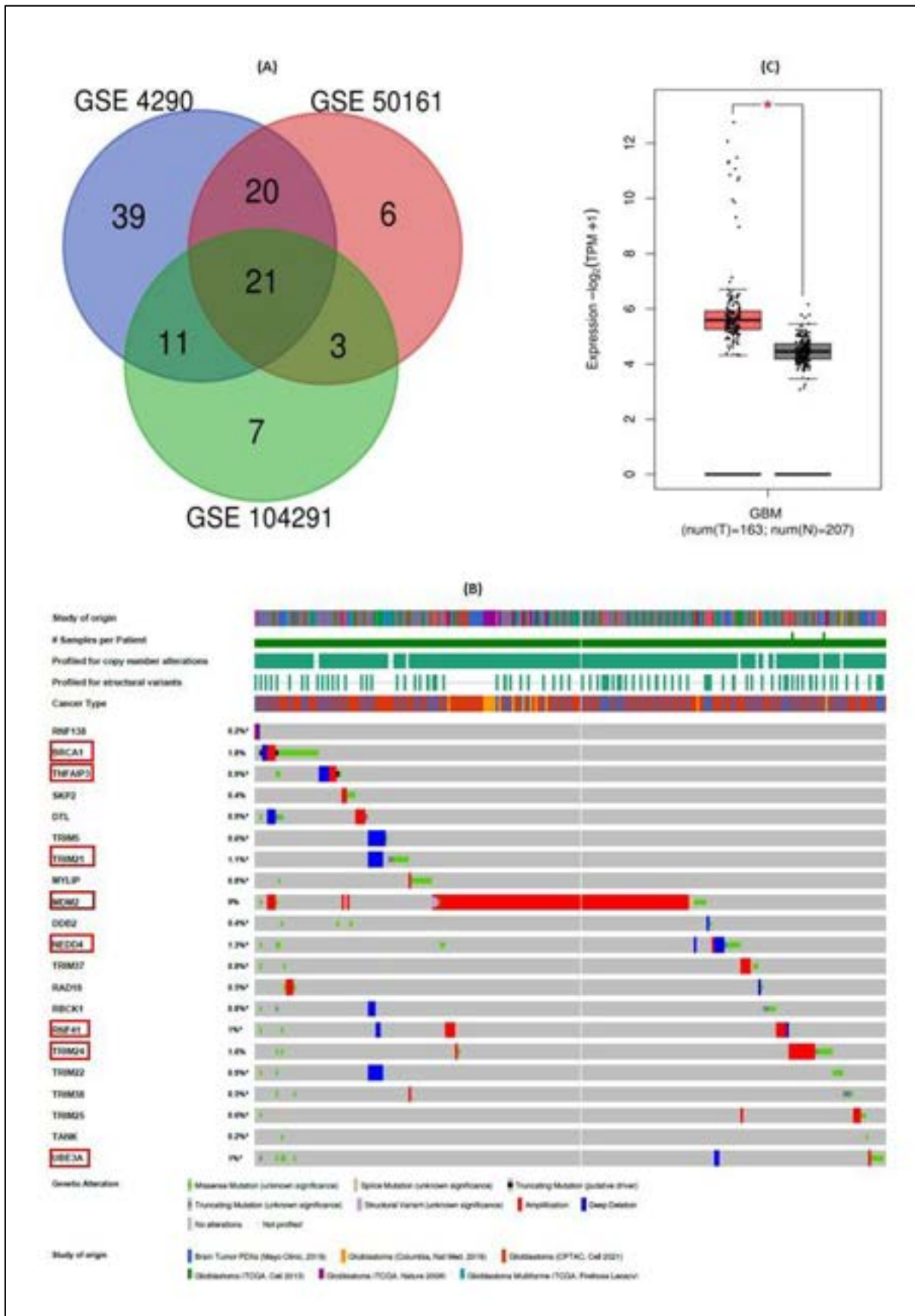


Figure 3.2: (A) Venn diagram and tabular description of the overlap between ubiquitin E3 ligases obtained from the datasets GSE 104291, GSE 4290 and GSE 50161. Significant overlaps show that 21 ubiquitin E3 ligases were commonly shared in these datasets (B) Mutational analysis of

the 21 common ubiquitin E3 ligases revealed that MDM2 showed the highest frequency among all the other ligases in GBM. The percentage of mutations in top 8 ubiquitin E3 ligases was MDM2 (9%), BRCA1 (1.8%), TRIM24 (1.6%), NEDD4 (1.3%), TRIM21 (1.1%), RNF41 (1%) and UBE3A (1%), TNFAIP3 (0.9%). MDM2 was found to be the most favorable ubiquitin E3 ligases that can be targeted in countering GBM (C) Expression levels of MDM2. The expressional rate was defined between the GBM and normal samples from the TGCA database. Plot with an asterisk (*) on the top suggest that the data is statistically significant.

3.3.3. EXPRESSION PROFILING AND MUTATIONAL ANALYSIS

To further substantiate the study, mutational signatures were predicted for 21 E3 ligases. Each gene acting as ubiquitin E3 ligase was checked for to rate of mutational frequencies and the kind of mutations they carry. MDM2 (9%) showed the highest percentage among the 21 ubiquitin E3 ligases. For ligases other than MDM2 the frequency of mutations was BRCA1 (1.8%), TRIM24 (1.6%), NEDD4 (1.3%), TRIM21 (1.1%), RNF41 (1%), and UBE3A (1%) and the mutational signatures that were carried in most of the ligases were of amplification and missense type. An overview of the mutational analysis performed for all the ubiquitin E3 ligases have been shown in **Figure 3.2(B)**. Out of these 21 E3 ligases, the expressional analysis of only those ligases was performed which showed higher mutational frequencies using TGCA GBM data. The expressional analysis was carried out using GEPAI2. Noteworthy, when compared with control samples, the expression levels of MDM2, BRCA1, TRIM24, NEDD4, and TRIM21 were higher in GBM samples and showed statistical significance and the expressional analysis can be derived from **Figure 3.2(C)**. On the other hand, expressional levels in the case of UBE3A and RNF41 were also higher but the data was not significant statistically. On the other hand, expressional levels in the case of UBE3A and RNF41 were also higher but the data was not significant statistically, the expressions can be seen in

3.3.4. FUNCTIONAL ENRICHMENT AND PATHWAY ANALYSIS

Based on the results mentioned above, a functional enrichment analysis of 21 ubiquitin E3 ligases was performed. Three types of enrichment analysis were done, comprising biological process (BP), molecular function (MF), and cellular component (CC). All these enrichments

are shown in **Figure 3.3(A-C)**. The majority of ligases were mainly associated with GO_BP terms such as ubiquitin-protein transferase activity, protein polyubiquitination, ubiquitin-protein ligase activity, and protein autoubiquitination. In the case with GO_CC terms, these genes were involved in the formation of ubiquitin ligase complex, transferase complex, Cul4B-RING E3 ubiquitin ligase complexes, and BRCA1-BARD1 complexes. As for GO_MF, most of the genes were related to ubiquitin binding, ubiquitin-protein transferase activity, ubiquitin-protein ligase activity, ubiquitin-like protein transferase activity, and damaged DNA binding. A detailed overview of the ligases and the process with which they are associated have been summarized in **Table 3.1**.

GO	Category	Description	Log P	Enrichment	Z-score	Hits	Hits list
GO:0016567	GO Biological Processes	Protein ubiquitination	-31.79	42.48	28.79	20	BRCA1 DDB2 MDM2 TRIM37 NEDD4 SKP2 TRIM21 TNFAIP3 UBE3A TRIM25 TRIM24 RN41 TRIM22 TRIM38 RBCK1 MYLIP RN4138 DTL RAD18 TRIM5
GO:0032446	GO Biological Processes	Protein modification by small protein conjugation	-30.96	38.65	27.43	20	BRCA1 DDB2 MDM2 TRIM37 NEDD4 SKP2 TRIM21 TNFAIP3 UBE3A TRIM25 TRIM24 RN41 TRIM22 TRIM38 RBCK1 MYLIP RN4138 DTL RAD18 TRIM5
GO:0000209	GO Biological Processes	Protein polyubiquitination	-24.92	89.47	35.14	14	BRCA1 DDB2 MDM2 NEDD4 SKP2 TRIM21 TNFAIP3 UBE3A RN41 TRIM22 TRIM38 RBCK1 DTL TRIM5
GO:0030163	GO Biological Processes	Protein catabolic process	-14.19	24.27	16.56	12	MDM2 NEDD4 SKP2 TNFAIP3 UBE3A TRIM25 TRIM24 RN41 TRIM38 RBCK1 MYLIP DTL
GO:0051603	GO Biological Processes	Proteolysis is involved in the cellular protein catabolic process	-13.08	25.22	16.17	11	MDM2 NEDD4 SKP2 TNFAIP3 UBE3A TRIM25 RN41 TRIM38 RBCK1 MYLIP DTL
GO:0004842	GO Molecular Functions	ubiquitin-protein transferase activity	-32.88	63.09	34.33	19	BRCA1 DDB2 MDM2 TRIM37 NEDD4 TRIM21 TNFAIP3 UBE3A TRIM25 TRIM24 RN41 TRIM22 TRIM38 RBCK1 MYLIP RN4138 DTL RAD18 TRIM5
GO:0019787	GO Molecular Functions	ubiquitin-like protein transferase activity	-32.41	59.65	33.36	19	BRCA1 DDB2 MDM2 TRIM37 NEDD4 TRIM21 TNFAIP3 UBE3A TRIM25 TRIM24 RN41 TRIM22 TRIM38 RBCK1 MYLIP RN4138 DTL RAD18 TRIM5
GO:0061630	GO Molecular Functions	ubiquitin-protein ligase activity	-22.81	63.70	29.56	14	MDM2 TRIM37 NEDD4 TRIM21 UBE3A TRIM25 TRIM24 RN41 TRIM22 TRIM38 MYLIP RN4138 RAD18 TRIM5
GO:0061659	GO Molecular Functions	ubiquitin-like protein ligase activity	-22.56	61.19	28.95	14	MDM2 TRIM37 NEDD4 TRIM21 UBE3A TRIM25 TRIM24 RN41 TRIM22 TRIM38 MYLIP RN4138 RAD18 TRIM5
GO:0003713	GO Molecular Functions	transcription coactivator activity	-13.12	48.65	20.59	9	BRCA1 TRIM37 TRIM21 UBE3A TRIM25 TRIM24 TRIM22 TRIM38 TRIM5

Table 3.1: Tabular representation of GO Functionally enriched ubiquitin E3 ligases with associated biological processes and molecular functions

Besides, the KEGG pathway analysis showed that these ubiquitin E3 ligases were significantly involved in ubiquitin mediated proteolysis, Epstein-Barr virus infection, p53 signaling, and endocytosis. **Figure 3(D-E)** tried to give an overview of KEGG pathways in which these ligases were involved. Further, all the terms were merged into clusters based on similarities and the top pathways that were enriched with most of the overlapping ligases are represented in **Table 3.2**.

Enrichment FDR	Hits	Fold Enrichment	Pathway	Hit list
1.74E-09	7	53.89125296	Ubiquitin mediated proteolysis	BRCA1, NEDD4, TRIM37, UBE3A, DDB2, MDM2, SKP2
2.55E-05	5	26.86940123	Epstein-Barr virus infection	NEDD4, TNFAIP3, DDB2, MDM2 SKP2
0.013265001	2	29.74037834	Platinum drug resistance	BRCA1, MDM2
0.013265001	2	29.74037834	P53 signaling pathway	DDB2, MDM2
0.013265001	3	12.92290249	Endocytosis	NEDD4, MDM2, RNF41
0.013265001	3	16.04222379	Viral carcinogenesis	UBE3A, MDM2, SKP2
0.013265001	2	28.94730159	Glioma	DDB2, MDM2
0.013265001	2	30.15343915	Melanoma	DDB2, MDM2
0.013265001	2	28.56641604	Chronic myeloid leukemia	DDB2, MDM2
0.017380146	2	23.59834369	Small cell lung cancer	DDB2, SKP2
0.020082398	2	20.87545788	NF-kappa B signaling pathway	TNFAIP3, TRIM25
0.026614554	2	16.57288259	Fox O signaling pathway	MDM2, SKP2

Table 3.2: Tabular representation of KEGG pathway analysis of the predicted ubiquitin E3 ligases along with their fold change and enrichment false discovery rate (FDR).

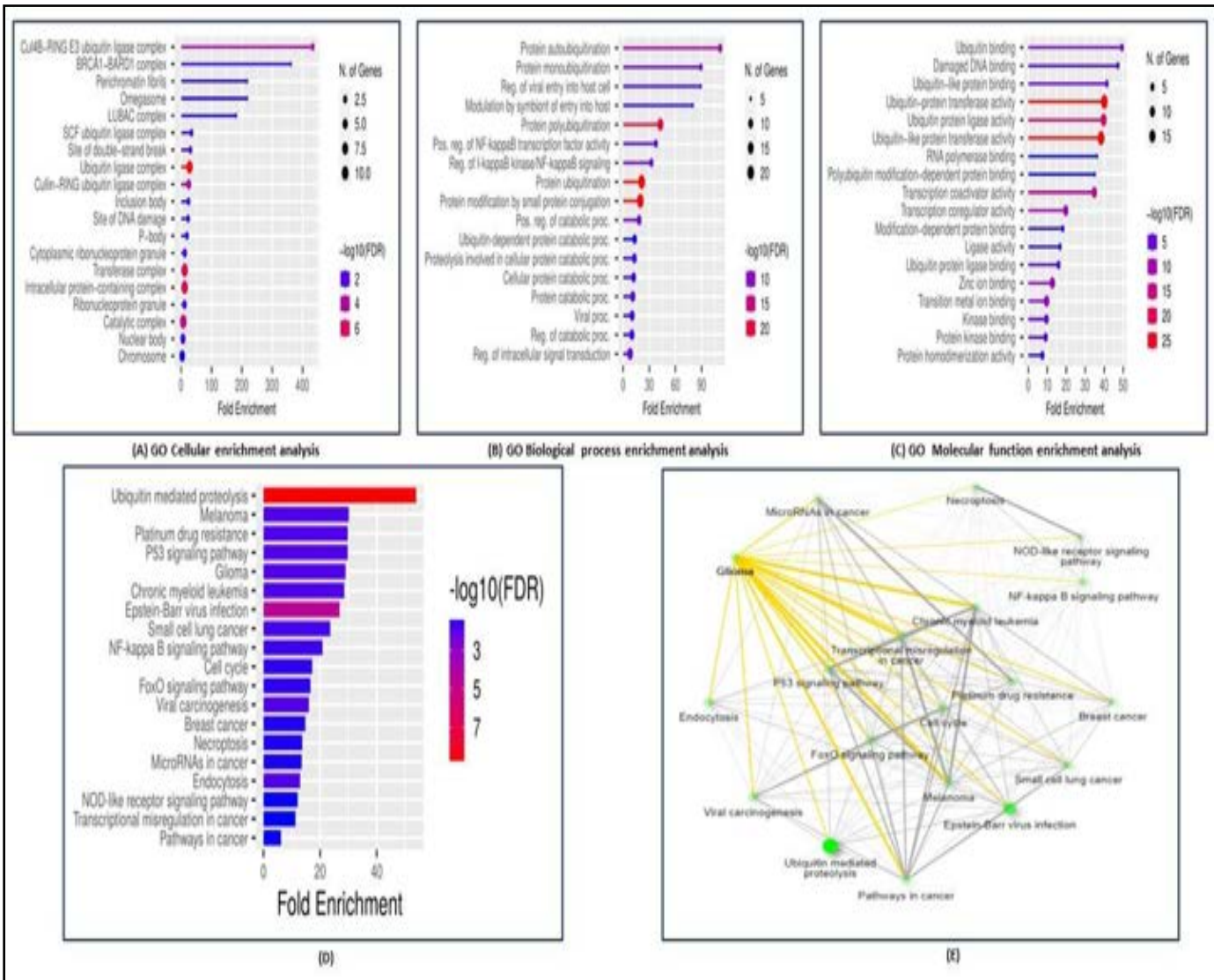


Figure 3.3: (A-C) Gene ontology (GO) functional enrichment analysis of 21 common ubiquitin E3 ligases and (D-E) Schematic representation of the KEGG pathway enrichment. (A) GO cellular Enrichment analysis revealed that the top processes in which most of the ligases are involved were ubiquitin ligase complex, transferases complex, intracellular protein-containing complex, and catalytic complex. The color and the size of the dots represent the false discovery rate (FDR) is significant or not. The bigger the dots, the greater the color is too red, showing the greater significance and number of genes involved in that process. (B) GO Biological process enrichment showed that the majority of ubiquitin E3 ligases were involved in processes like protein ubiquitination, protein modification by small protein conjugation, protein polyubiquitination, and proteolysis involved in the cellular protein catabolic process. (C) GO molecular function enrichment identified that most of the ligases were involved in ubiquitin protein transferase activity, ubiquitin-like protein transferase activity, ubiquitin protein ligase activity, and transcription coactivator activity. The more the red color of the dots the more significant the FDR and the processes in which these ligases are involved. (D) Depicts the bar plot images of the various pathways for 21 ubiquitin E3 ligases and how they are enriched. The red bar here represents the most enriched and significant pathway and the blue represents less significance. Ubiquitin-mediated proteolysis is composed of most of the significant and

overlapped genes followed by Epstein-Barr virus infection, platinum drug resistance, p53 signaling, endocytosis, and glioma. (E) KEGG pathway network based on nodes and edges. The bigger the nodes represent a greater number of genes involved and thicker edges here represent significance. Edges for glioma have been highlighted in yellow.

3.3.5. COMPOUND PREDICTION, BBB, AND ADMET PARAMETERS

Based on the literature mining, we identified NPACT a database comprising different classes of natural compounds, and selected the alkaloid class from the compound library. 70 compounds were selected from the database and the BBB permeability and the BBB score were checked using the SVM algorithm in CBligand. Based on BBB prediction, initially, 54 compounds were filtered. ADMET profiling for these 70 compounds was done to check whether the compounds fall under the prescribed limits of ADMET analysis. Properties such as molecular mass (<500 Da), number of H-bond donors (<5), no. of H-Bond acceptor (< 10), octal water partition coefficient ($\log < 5$), and molar refractivity (40-130) were considered for our study. The no. of violations of the Lipinski rule of five was also taken into consideration for these 70 compounds. Only 54 compounds showed zero violation of the Lipinski rule and also satisfied the ADMET threshold and were further assessed for docking and simulation studies.

3.3.6. MDM2-ALKALOIDS INTERACTION PROFILING

Molecular docking was carried out for the screened ubiquitin E3 ligase (MDM2) with different alkaloid compounds. Any extra residue attached to the ligand was removed along with any heteroatom. Any hydrogen or water attached to either ligand or the receptor was also omitted before proceeding for docking. The reference study conducted before using nutlin-3a as a reference compound with MDM2 shows a binding affinity of -7.9 kcal/mol. However, we used a more stringent threshold of -8.0 kcal/mol in our study to shortlist the compounds, showing specific and non-specific bindings. Docking was performed for 54 compounds and out of these only 14 compounds showed binding energy of above -8.0 kcal/mol. These binding energies demonstrate the high binding affinity of these compounds against MDM2. The higher the

binding in negative terms indicates more inhibition capability of these compounds for MDM2. During MDM2 docking, the maximum no. of compounds along with reference ligand, showed common interactions with the receptor residues at Ile61, His96, Ile99, Leu54, Val93 & Tyr100. Binding potential of above -8.5 kcal/mol was seen in cepharanthine (-9 kcal/mol), sanguinarine (-8.6 kcal/mol), evodiamine (-8.6 kcal/mol), tomatidine (-8.6 kcal/mol), ellipticine (-8.6 kcal/mol) and tylophoridicine F (-8.6 kcal/mol). The binding energies of various alkaloids with the best affinity and the docking coordinates along with other properties can be interpreted in

Table 3.3.

Alkaloid	BBB predictor	BBB Swiss ADMET	Affinity (kcal/mol)	Molecular Mass (<500Da)	Docking coordinates	H-Bond donor (<5)	H-Bond acceptor (<10)	Octal water partition coefficient (log<5)	Molar refractivity (40-130)
Brucine	Yes	Yes	-8.2	394.46 g/mol	40-40-40	0	5	1.84	114.04
Chelerythrine	Yes	Yes	-8.1	348.37 g/mol	40-40-40	0	4	3.02	101.6
Isostrychnine	Yes	Yes	-8.2	334.41 g/mol	40-40-40	1	3	1.85	102.77
Sanguinarine	Yes	Yes	-8.6	334.41 g/mol	40-40-40	0	3	2.09	101.05
Tomatidine	Yes	Yes	-8.6	354.44 g/mol	40-40-40	1	4	2.61	103.74
(R)-cryptopleurine	Yes	Yes	-7.9	393.48 g/mol	40-40-40	0	5	4.04	119.16
Cepharanthine	Yes	Yes	-9	369.45 g/mol	40-40-40	0	5	3.33	108.8
Ellipticine	Yes	Yes	-8.6	303.36 g/mol	40-40-40	1	1	2.7	97.67
Evodiamine	Yes	Yes	-8.6	315.49 g/mol	40-40-40	1	2	3.88	96.52
Isotetrandrine	Yes	No	-8.2	275.26 g/mol	40-40-40	0	4	2.88	76.67
liriodenine	Yes	Yes	-8.3	478.62 g/mol	40-40-40	0	6	4.43	147.34
Tylophoridicine C	Yes	No	-8.1	381.42 g/mol	40-40-40	2	5	0.78	112.73
Tylophoridicine F	Yes	Yes	-8.6	395.45 g/mol	40-40-40	1	5	1.11	117.2
6-O-desmethylantrifine	Yes	Yes	-8.2	349.42 g/mol	40-40-40	1	4	3.67	108.2

Table 3.3: Tabular representation of the various alkaloids docked against MDM2 and their ADMET profiling

*** Alkaloids highlighted in red represent evodiamine and sanguinarine with their binding energies highlighted in yellow**

After the successful completion of docking, these 14 compounds then proceeded for molecular simulation studies. Evodiamine and sanguinarine showed the best possible interactions as compared to the reference used in our study and the binding energies along with interaction can be observed in **Table 3.4**.

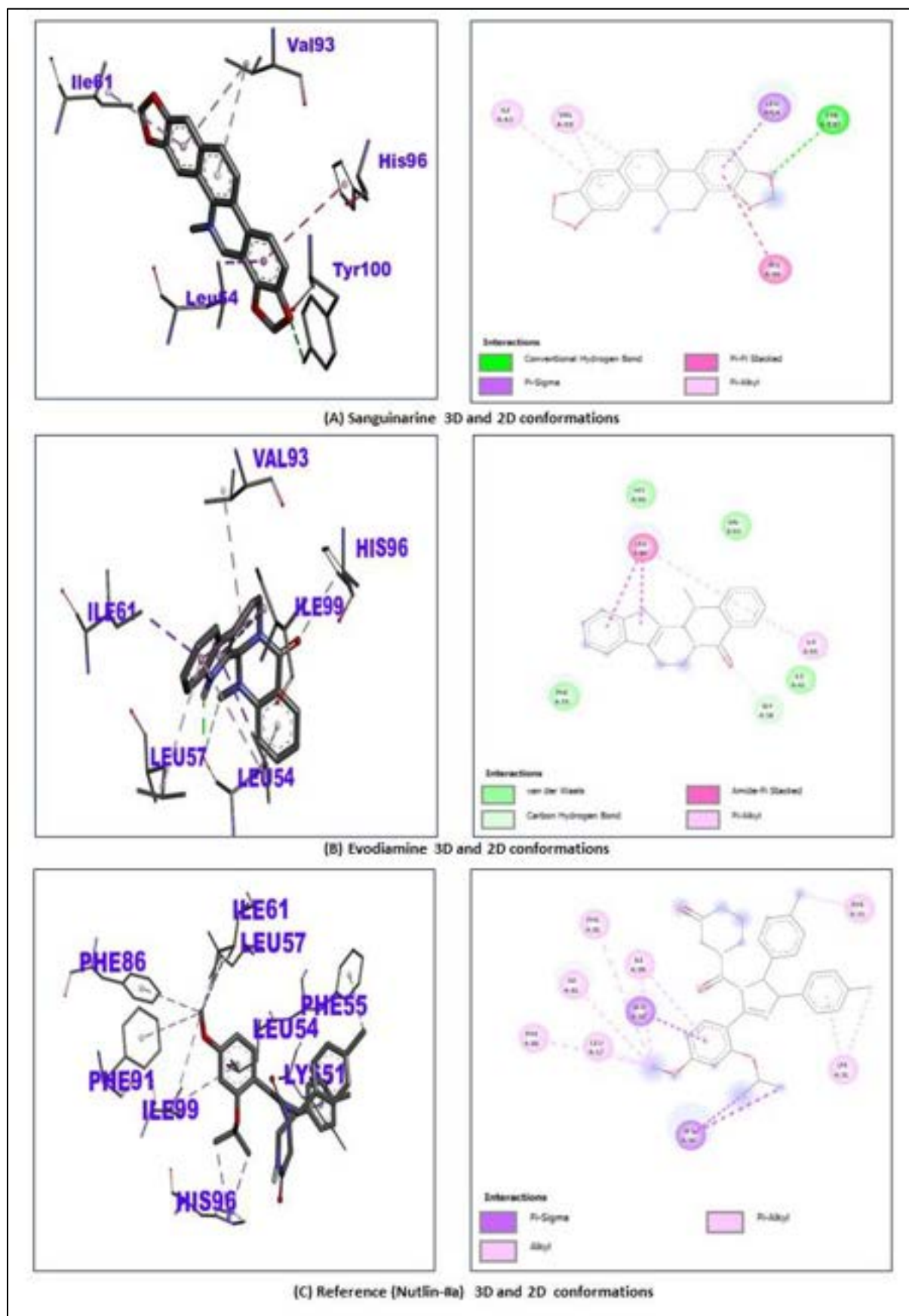


Figure 3.4: (A-C) Molecular docking confirmations: Representation of 2D and 3D confirmation of MDM2 binding with (A) Sanguinarine shows binding at the residue Val93, Ile61, His96, Tyr100,

Leu64 of MDM2 protein (B) Evodiamine represents interaction at the site Val93, Ile61, His96, Ile99, Leu54 and Leu57 of MDM2. (C) Reference ligand (Nutlin-3a) showing interaction with MDM2 at the residues site Val93, Ile61, His96, Ile99, Leu54, Phe55, Phe91, Phe86, Leu57, and Lys51.

The 2D and 3D confirmations of evodiamine, sanguinarine, and reference after binding with MDM2 can be observed in **Figure 3.4 (A-C)**.

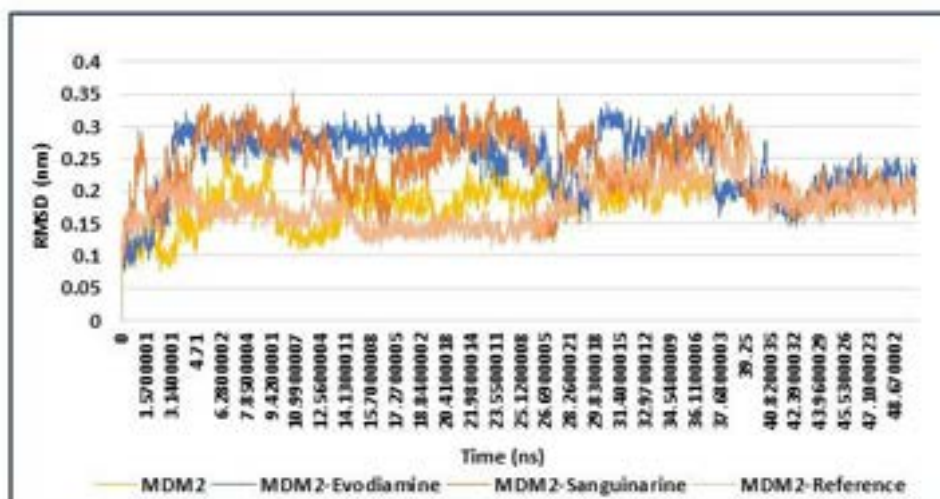
Compounds	Binding energy (KJ/mol)	Interacting residues
Evodiamine	-8.6	Val93, Ile61, His96, Ile99, Leu54 and Leu57
Sanguinarine	-8.6	Val93, Ile61, His96, Tyr100, Leu64
Reference (nutlin)	-7.9	Val93, Ile61, His96, Ile99, Leu54, Phe55, Phe91, Phe86, Leu57 and Lys51.

Table 3.4: Tabular representation of binding energies and the interaction of evodiamine, sanguinarine, and nutlin with MDM2.

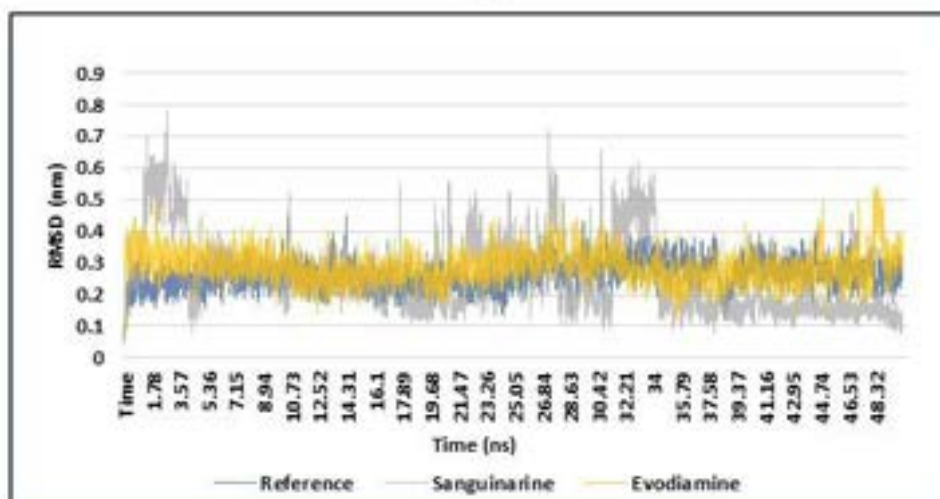
3.3.7. MDM2-ALKALOIDS COMPLEXES DYNAMIC STABILITY

All the 14 compounds having binding energy above -8.0 kcal/mol were subjected to MD simulations for 50 ns which helped us to understand the pattern of interaction and the dynamic behavior. The stability of these compounds with MDM2 was analyzed using RMSD obtained from MD simulations. The RMSD of different protein-ligand complexes along with the RMSD of ligands alone were considered. The backbone of the complexes (MDM2- Sanguinarine & MDM2-Evodiamine) were found to be stable when compared with the MDM2-reference complex or with protein alone. The RMSD showed a fluctuation in the beginning and reached 0.30 nm but gradually decreased and was stable in the range of 0.15 nm to 0.25 nm when compared with the reference complex. Till 20 ns there was a slight deviation in the stability of complexes (MDM2-Sanguinarine and MDM2-Evodiamine) from the MDM2- reference complex. After 25ns of simulation the complexes started stabilizing themselves and after 35ns

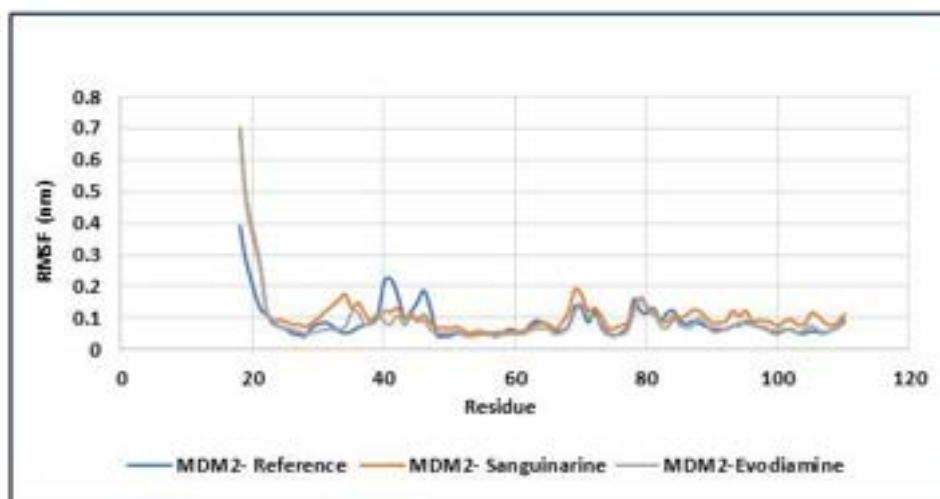
both the complexes achieved better stability and were interactive till 50 ns which can be seen in **Figure 3.5(A)**. Similarly, the RMSD of all the ligands is given in **Figure 3.5(B)** and it is clearly showing that sanguinarine and evodiamine are both stable when compared with the reference compound however, the RMSD of ligand sanguinarine fluctuated in the beginning and reached 0.7 nm but after 32 ns it started to stabilize and was in the range of 0.2 nm to 0.4 nm.



(A)



(B)



(C)

Figure 3.5: (A-C) Plots depicting variations in root mean square deviation (RMSD) and root mean square fluctuations (RMSF) in protein alone, ligand alone, and protein-ligand complexes. (A)

RMSD of MDM2, MDM2-Evodiamine, MDM2-Sanguinarine, and MDM2- Reference complexes were calculated and plotted on the graph. Y-axis represents the RMSD in nanometer (nm) and X-axis represents the time in nanoseconds (ns). The RMSD of each of these was calculated at the timescale of 50 ns. Highlighted in gold represents the RMSD peak of MDM2 protein itself. MDM2-evodiamine RMSD peak can be seen in blue. RMSD peak of MDM2-sanguinarine complex is represented with orange and the peak for MDM2-Reference complex is represented with orange. This graph clearly shows that when overall RMSD was compared, MDM2-Evodiamine and MDM2-sanguinarine complexes were found to be stable against the MDM2-Reference complex till 50 ns. RMSD of these complexes can be seen as stable in the range of 0.15nm to 0.25nm and showed stability after 35ns. (B) Overall RMSD peak of the reference ligand, sanguinarine, and evodiamine are highlighted in blue, gray, and gold. The RMSD of the sanguinarine and evodiamine was found in the range of 0.2nm to 0.4nm and was stable till 50ns. (C) RMSF peaks of MDM2-Reference, MDM2-Sanguinarine, and MDM2-Evodiamine are represented in blue, orange, and gray. The RMSF of MDM2-sanguinarine and MDM2-evodiamine can be seen in range with the MDM2-reference complex.

The RMSF of both the complexes along with MDM2-Reference can be depicted in **Figure 3.5(C)**. Observations can be obtained that the RMSF of the two complexes was in the range with MDM2- Reference complex and are found to be stable in the range of 0.1 nm to 0.2 nm. The Rg is generally identified to check the compactness of the protein structure and if the structure is stably folded it will remain stable over time. It can be seen that the Rg for both MDM2-evodiamine and MDM2-sanguinarine were found to be stable and compact for 50 ns, holding an average Rg of 1.6 nm **Figure. 3.6(A)** when compared with MDM2-Reference. The coulomb's interaction energy of each of the complexes was calculated and from the analysis it was seen that as compared to the reference the interaction energy was more negative in the case of the other two complexes, suggesting a higher binding potential of the MDM2 receptors with ligand sanguinarine and evodiamine. The overall interaction can be seen in **Figure. 3.6(B)**. The plots for H-bonds and pairing within 0.35 nm in **Figure. 3.6(C-D)** shows the interactions of the amino acid residue of MDM2 with evodiamine, sanguinarine, and reference compounds during the 50 ns simulations. The formation of different types of bonds between various complexes, suggests important evidence for the inhibitory potential of evodiamine and sanguinarine.

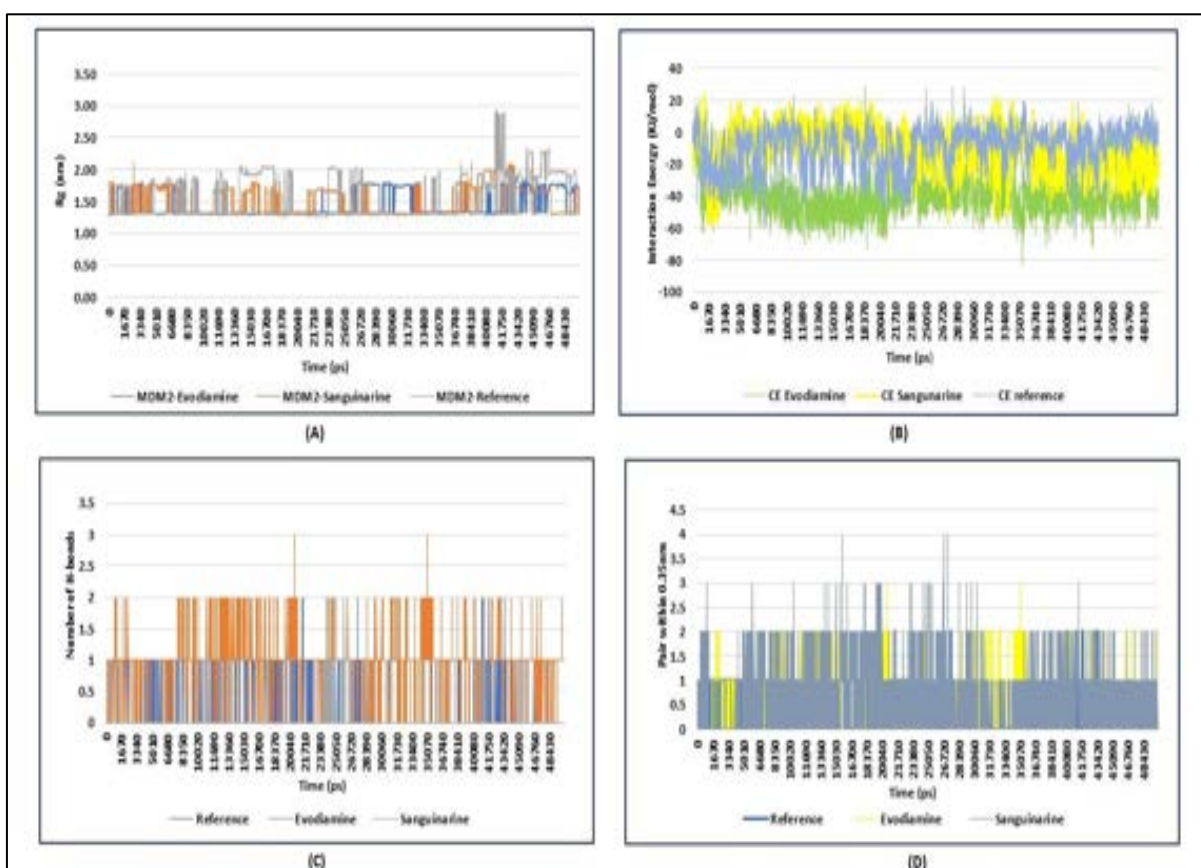


Figure 3.6: (A-D) Plot representing Radius of gyration (Rg), Interaction energy, Number of H-bonds, and H-Bond pairs within 0.35nm. (A) Rg of all the complexes (MDM2- Evodiamine, MDM2-Sanguinarine, and MDM2-Reference) plotted against time with Y-axis representing Rg in nanometer (nm) while the x-axis shows time interval in picoseconds (ps). Peak showing interaction Rg of MDM2- Evodiamine is highlighted in blue, orange in case of MDM2-Sanguinarine, and gray in MDM2-Reference. The Rg of MDM2-Reference showed fluctuations from the other two complexes but in the case of MDM2- Evodiamine and MDM2- Sanguinarine, the peaks were in the range when compared with MDM2-Reference complex, (B) Coulombs interaction energy in KJ/mol plotted against time in ps. The coulomb's interaction energy peaks in the case of MDM2- Evodiamine are shown in light green, MDM2- Sanguinarine in yellow, and for MDM2-Reference in blue. The interaction was more towards the negative and reached -70 KJ/mol in the case of MDM2- Evodiamine and reaching -60KJ/mol in MDM2- Sanguinarine as compared to MDM2-Reference (-40 KJ/mol) suggesting a more stable interaction in case of evodiamine and sanguinarine. (C) Plot for the number of H-bonds on each residue against time in ps. The overall H-bonds in case of reference per residue were comparatively lower and the peak is displayed in blue. The peak for H-bonds in the case of evodiamine is shown in orange and for sanguinarine in gray. The number of H-bonds in the case of evodiamine was higher, followed by sanguinarine and reference. (D) H-bond pairing within a radius of 0.35 nm can be seen in Reference (Blue), Evodiamine (Yellow), and Sanguinarine (Gray). These pairing with MDM2 suggest that the pairs per residues formed in the case of sanguinarine and the pair

formation was almost equal in reference and evodiamine suggesting greater stability of sanguinarine and evodiamine with MDM2 till 50000 ps (50ns).

3.4. DISCUSSION

GBM is highly aggressive and metastatic among other tumors of the central nervous system (CNS) with very complicated biology and carries a poor prognosis. The molecular mechanism and the signaling pathways underlying these tumors are of great significance and therefore in-depth studies are needed to counter these tumors. The overall survival in patients is very less and the therapeutic angles are also fewer. When talking about chemotherapeutics, temozolomide acts as a gold standard against these solid tumors. surgery followed by concurrent radiotherapy remains an option. As ubiquitin E3 ligases target a large number of substrates that are regulators of the majority of cellular functions such as apoptosis, DNA repair, and metabolism hence, they can be the therapeutic drug targets in GBMs [295]. This study has tried to identify the various ubiquitin E3 ligases whose expressions are comparatively higher in GBMs, their involvement in functions operating at molecular and cellular levels, and mutational frequencies of the identified ubiquitin E3 ligase in GBMs. After the identification of targetable E3 ligases, we also tried to predict substantial inhibitors that could inhibit the expression of these identified ubiquitin E3 ligases.

Using high-throughput studies and a bioinformatics approach, DEGs were first extracted from three GBM datasets using the GEO database. These DEGs were analyzed using UbiNet and Ubibrowser (tools to predict whether the DEG is ubiquitin E3 ligase or just the substrate of any ligase). Only 21 ubiquitin E3 ligases were retrieved that were shared equally among the three datasets for GBM. Functional enrichment and KEGG analysis were carried out to see how these ubiquitin E3 ligases are playing an intricate role in glioblastoma at molecular, cellular, and biological levels along with the pathways on which they are acting. It was seen that at biological levels, out of 21 ligases 20 were involved in the process of protein ubiquitination, protein modification by small protein conjugation, and 14 hits were involved in protein

polyubiquitination. At molecular levels, most of the hits were associated with ubiquitin protein transferase activity and ubiquitin protein ligase activity. It was conferred from these functional enrichments that most of the hits that were common in these processes were MDM2, BRCA1, RNF41, TRIM21, NEDD4, and TRIM24. Similarly, the KEGG pathway analysis also revealed that out of these ligases, MDM2 was majorly involved in the pathways like endocytosis, ubiquitin mediated proteolysis, and various pathways in cancer. Researchers have shown that MDM2 plays a prominent role in mediating the activation of p53 during various signaling cascades [296] and therefore they can be better targets as ubiquitin E3 ligases. The mutational frequencies of these ubiquitin ligases were checked using data from TGCA and Mayo clinic and it was found that MDM2 carried a mutational frequency of 9% and the mutations were of amplification type. Expression analysis of MDM2 along with other ubiquitin E3 ligases in GBM revealed that in most of the cases the data showed statistical significance. This tells us that the expression of MDM2 was comparatively higher in patients with GBM as compared to the normal group of people according to TGCA. As very few studies are available on how ubiquitin E3 ligases can be therapeutically important and therefore, by predicting the expression of every ligase, selective targeting using either siRNA or any drug or natural compound can somehow reduce the expression of these ubiquitin E3 ligases.

Molecular docking studies showed that binding energies of evodiamine (-8.6 KJ/Mol) and Sanguinarine (-8.6 KJ/Mol) were comparatively higher than the reference compound (-7.6 KJ/Mol), suggesting a more sustained inhibitory effect of these alkaloid against MDM2. Sanguinarine was able to binding at the residue Val93, Ile61, His96, Tyr100, Leu64 of MDM2 protein while evodiamine represents interaction at the site Val93, Ile61, His96, Ile99, Leu54 and Leu57 of MDM2. Reference showed interaction with MDM2 at the residues site Val93, Ile61, His96, Ile99, Leu54, Phe55, Phe91, Phe86, Leu57, and Lys51. Although evodiamine and sanguinarine predicted less interactions as compared to the reference but based on the affinity score these compounds were checked for stability with MD simulations. From the results

obtained from simulation studies, the fluctuation and stability of the system during simulation and the outcome trajectories for all the complexes were inspected using different simulation parameters. These parameters included the backbone RMSDs for all the atoms and ligands, RMSF of individual amino acid residues, formation of H-bonds and Rg. RMSD plots when compared showed that the hits bounded to MDM2, evodiamine and sanguinarine possessed lower fluctuations in RMSD and greater stability at the active site during simulation at 50ns. The RMSDs were calculated between the initial confirmations and final confirmations throughout 50ns in dynamic simulations. This showed us that evodiamine and sanguinarine showed more stable binding when compared with the reference. RMSF on the other hand represented the important residues that were involved in strong interactions with specific ligands. The pattern of RMSF peaks suggest that the fluctuations in the values of evodiamine and sanguinarine were close to the reference and exhibited almost similar patterns. Coming to the Rg, it was seen that Rg values of the backbone atoms of MDM2 when bound to evodiamine and sanguinarine were nearly same when compared with the reference bound to MDM2 and was maintained thoroughly till 50ns. Results generated from interaction energy peaks, it can be conferred that the interactions between evodiamine, sanguinarine and MDM2 were more stable and stronger as compared to the reference. These findings somewhere reinforced the credibility of docking results, suggesting the potential role of evodiamine and sanguinarine as potent inhibitors of MDM2.

Previous studies have shown that MDM2 acts as ubiquitin E3 ligases and also promotes the ubiquitination of p53 [297]. This process mediated by MDM2 leads to the identification and interaction of proteasome by p53 thereby, causing increased degradation of p53. However, the mechanism by which evodiamine and sanguinarine targets the MDM2 and hence p53 remains unclear. We therefore proposed a mechanism of how both of these compounds could potentially target the MDM2 and can induce a therapeutic response in GBM and the proposed mechanism can be seen in **Figure 3.7**.

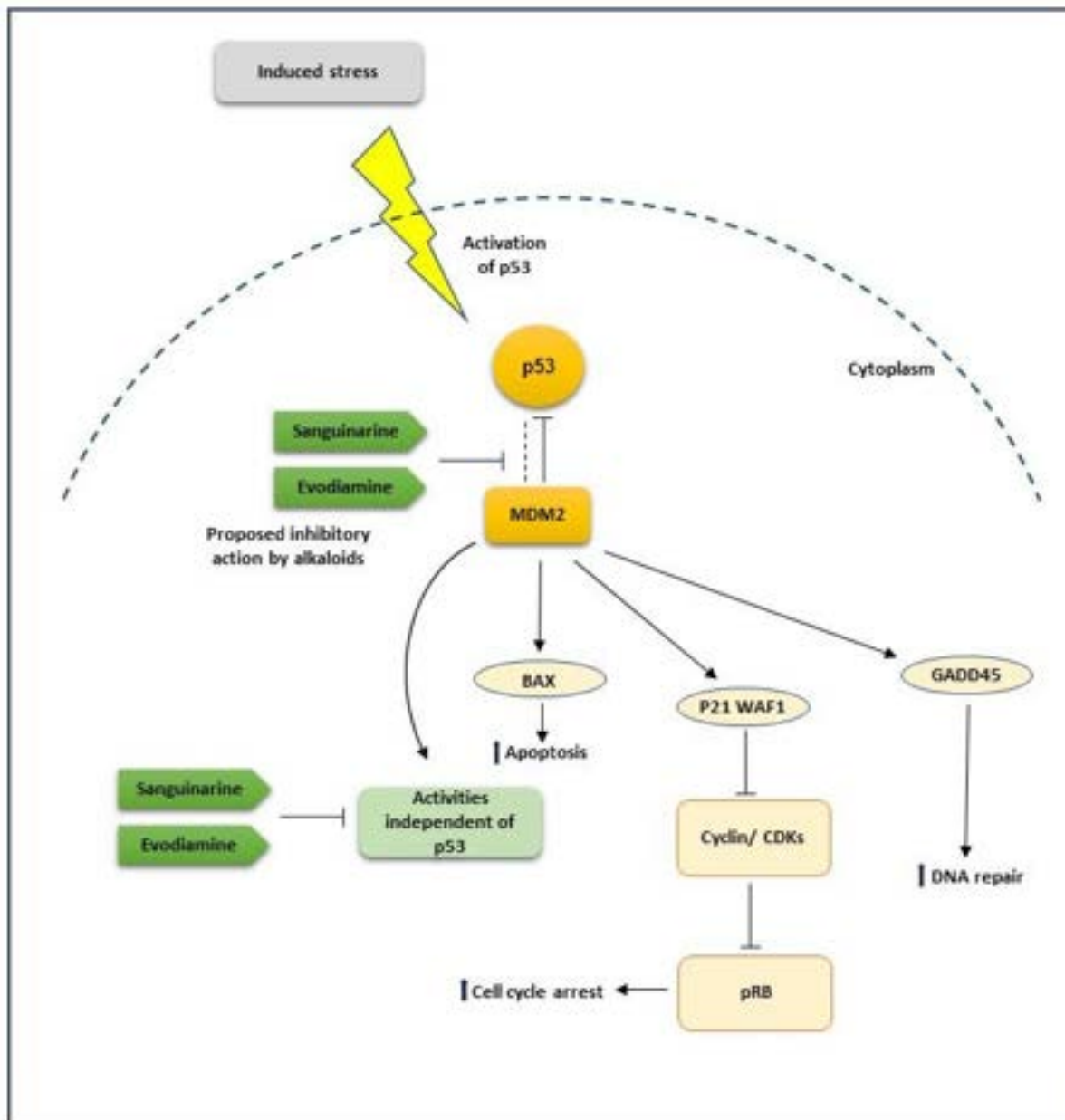


Figure 3.7: Proposed mechanism of action of evodiamine and sanguinarine in MDM2 inhibition. Stress-induced due to genotoxicity, DNA damage, ionizing radiations, and other factors cause the activation of p53(Tumor suppressor gene) bound to MDM2. Overexpressed MDM2 causes the degradation of p53 and is not able to function properly. We hypothesized that breaking the MDM2-p53 interaction by either evodiamine or sanguinarine can prevent the degradation of p53. Upon prevented degradation of p53, activation of downstream targets associated with p53-MDM2 interaction such as Bcl2 associated protein (BAX) causing apoptosis, growth arrest, and DNA-damage inducible gene (GADD45), and the P21 WAF causes an increase in apoptosis, DNA repair, and cell cycle arrest, therefore, restoring the normal cellular mechanism and can suppress glioblastoma.

3.5. KEY FINDINGS OF THE STUDY

- ✓ The role of MDM2 as a potential ubiquitin E3 ligase was identified and how can be the game changer in the therapeutic targeting of GBM.
- ✓ Targeting MDM2 using a natural class of inhibitors instead of synthetic compounds can be more fruitful.
- ✓ We proposed a mechanism of how evodiamine and sanguinarine are disrupting the MDM2-p53 interactions and targeting the p53 signaling in GBM.

CHAPTER IV

DISSECTING THE FUNCTIONAL SIGNIFICANCE OF HEAT SHOCK PROTEINS IN GLIOBLASTOMA AND EPENDYMOMAS USING OMICS ANALYSIS AND DRUG PREDICTION USING VIRTUAL SCREENING

CHAPTER IV: DISSECTING THE FUNCTIONAL SIGNIFICANCE OF HEAT SHOCK PROTEINS IN GLIOBLASTOMA AND EPENDYMOMAS USING OMICS ANALYSIS AND DRUG PREDICTION USING VIRTUAL SCREENING

4.1 INTRODUCTION

Heat shock proteins (HSPs) also known as stress proteins are an important class of proteins that are activated by the cells in response to heat shock or in response to stimuli (external or internal) such as unavailability of nutrition, heat and cold, hypoxia and so on (Bond et al., 1987). These classes of proteins are involved in presentation of antigens, assembly of hormonal receptors, protein folding and cell trafficking [110]. Due to various roles that HSPs play in maintaining the cellular integrity, a disruption in their machinery causes a depletion in cellular proteostasis leading to cell death (Saibil .H, 2013). Due to this malfunction their levels are significantly increased in cancerous cells as compared to the normal tissue [300]. Therefore, their mechanism is taken up by the malignant cells for their proliferation and survival [301]. As HSPs play an intricate role in origin of these cancerous cells, increased cellular growth and in the maintenance of tumor cells, shows their importance in cancer biology and are therefore, can be employed as potential therapeutic targets. HSPs also play important role in cancer cell evasion, tumor cellular division, mechanism of DNA repair, metastasis and invasion into the surrounding normal cells (Hasan et al., 2022). These HSPs are classified based on the molecular weights comprising of different families- HSP90, HSP110, DNAJ and smaller HSPs [150].

Malignant tumors that originate from the brain are hard to treat due to their location of origin as they are deeply embedded within the brain, their ability to metastasize rapidly, aggressive behavior thereby, leading to poor prognosis in patients and decreased overall survival. Glioblastomas (GBMs) and ependymomas are Grade IV tumors that originates from the glial

cells and are most aggressive tumors of the central nervous system (CNS)[303]. Ependymomas are the tumors of the neuroectodermal region and arises from the glial cells and are present in the parenchyma of the brain due to the migration of the ependymal cells of the fetus from the periventricular areas(Centeno et al., 1986). The prevalence of ependymoma is more in males as compared to females and can happen in age groups[306]. Overall survival of the patients suffering from ependymoma remains around 40%[307]. Glioblastoma on the other hand is the most commonly occurring brain tumors and can arise from oligodendrocytes, astrocytes or from the ependymal cells. Their classification is based on the site of the origin and can be defined as either oligodendrogliomas, astrocytoma or glioblastomas[231]. These tumors are more aggressive than ependymomas and are more lethal and account for almost 75 % of the cases as recognized by the World Health organization (WHO). Standard therapy in glioblastoma still remains temozolomide followed by radiotherapy thus, causes short survival and poor prognosis in patients. The median survival in patients suffering from glioblastoma remains only 10-16 months after treatment[234]. In both the tumors described there is a lack in therapeutically targeting these tumors as these tumors have unpredictable etiologies and the complex mechanism of these tumors are still unknown. Availability of the information regarding the role of chemotherapy in case of ependymoma[308] is very less and only surgery remains an option. Although the potency to counter the primary tumors in both the high-grade and low-grade ependymomas is not upon the mark therefore more aggressive therapies are being employed in the clinics to find some better therapeutics in countering ependymomas. Here HSPs comes into counterplay as they mediate a number of cellular processes and could be a potential therapeutic avenue in countering both GBMs and ependymomas.

HSP90 is the most studied class and its inhibitors are found to be effective in the treatment of cancer. One study investigated the role of 17-allylamino-17demethoxygeldanamycin (17-AAG) or Tanespimycin as a therapeutic agent in GBM. This inhibitor was found to be effective in combination with Olaparib and also caused the inhibition of Poly ADP-ribose polymerase

(PARP) in case of glioblastoma. However, no study claims its role in the inhibition of ependymomas. Another study used ZD1839 , which is an inhibitor of epidermal growth factor receptor (EGFR) against the glioma cells[310]. Inhibitors of HSP70 such as VER-155008, MAL3-101 also showed promising results against various brain tumors. Studies have also shown that cannabinoid agonist such as WIN55-212-2 was found to be efficient in human glioblastoma cell line U-251MG and also showed to alter the expressional levels of HSP70, cathepsin and p53(Silva et al., 2019). These studies suggest that targeting HSPs can be more fruitful and hence, more studies are needed to be done against HSPs in understanding the role of HSPs in countering both the tumors. Therefore, our findings may provide a better understanding of the pathways of the HSPs that are mutually dysregulated in both GBMs and ependymomas, and this open new opportunities in the therapeutic options in both the brain malignancies.

4.2. METHODOLOGY

4.2.1. RETRIEVAL OF RAW DATA

Dataset that was employed in the study was extracted from the National Centre of Biotechnology Information (NCBI) gene expression omnibus (GEO) (<https://www.ncbi.nlm.nih.gov/geo/>) [290]. The microarray gene expression profiles were obtained from GSE 50161 dataset. The dataset used for the study was based on the criteria as discussed. First criteria were to use only those datasets that contained the array expressional analysis data of human brain tissue samples from GBM patients, ependymoma and healthy patients. Secondly, the dataset must possess the ependymoma, GBM and the control samples in one dataset itself. Thirdly, all the patient samples present within the dataset whether healthy or tumor are not previously exposed to any kind of prior treatment (chemotherapy or radiotherapy). Fourthly, the number of human patient samples either healthy, GBM and ependymoma affected should not be less than 10 in number within the dataset respectively[313]. The platform that is used in GSE 50161 is GPL570 [HG-U133_Plus_2] Affymetrix human genome.

4.2.2. DATA PROCESSING, ANALYSIS OF DEGS AND PREDICTION OF HSPTS

Raw read counts for input data were obtained from TCGA or GEO dataset. R package DESeq2 was also used for data extraction. The analysis was further nurtured using GEO2R (<https://www.ncbi.nlm.nih.gov/geo/geo2r>) a web-based interactive tool that works on the R language limma package. GEO2R acts as a tool for the comparative establishment for two or more sets of gene samples in the GEO series[290]. To study the underlying biological prospects, biological functions were annotated for the differentially expressed genes. Parameters such as P-value <0.05 and the $|\text{Log FC}| > 2$ and $|\text{Log FC}| < 2$ were used as cut-off criteria to filter the differentially expressed genes. Identification of HSPs from the screened DEGs, commonly regulating in both tumors was done using HSPMdb[314] database and by literature survey.

4.2.3. PROTEIN-PROTEIN FUNCTIONAL INTERACTION AND NETWORK ANALYSIS

Interaction of proteins was committed using Network Analyst[315] which is an online bioinformatic tool(Zhou et al., 2019). All the common heat shock proteins were used as input in network preparation. Network Analyst is used as network construction and visualization tool that incorporates various databases for analysis. Topological parameters such as Degree centrality and distribution of betweenness was done using network analyzer using Cytoscape. Degree centrality refers to the number of connections in the network and also the impact of a node on the network. The betweenness centrality of the nodes represents the shortest distance between the nodes passing through the query node. In addition to this, module explorer panel was also used for the identification of interlinked proteins in the network. Based on the number of proteins involved in the interaction these modules were ranked. First order network analysis was done to reduce the hairball effect. For the analysis of large and complicated biological networks, nodes are considered significant and is hampered by this hairball effect.

4.2.4. FUNCTIONAL ENRICHMENT AND PATHWAY ANALYSIS

To determine the functional aspects of the predicted overlapping HSPs, the functional annotation map module of the database for visualization, annotation and integration we used DAVID bioinformatics database. This database was used for the analysis and to give annotation to the identified overlapping HSPs. We also used another tool for the Gene Ontology (GO) term and the pathway prediction was done using SHINY GO 7.16 (<http://bioinformatics.sdstate.edu/go/>). Parameters such as |P-value <0.05|, |Log Fc >2| and |Log Fc <2| were used as threshold for significantly enriched terms. Eventually, the functional enrichment network was constructed[317]. Enrichment analysis was done to understand the biological process, molecular function and cellular components using GO term analysis. Kyoto encyclopedia of genes and genomes (KEGG) pathway analysis was conducted for the common predicted HSPs in glioblastoma and ependymoma. The analysis was performed using Web-

Gestalt (WEB-based Gene Set Analysis Toolkit). Web-Gestalt which is a web based functional enrichment tool is able to identify the KEGG pathway that are associated with the genes required to be studied. Also helps to identify the genes interacting in each pathway along with their Entrez ID[318][319]. P-value of less than 0.05 was used as cutoff criterion in KEGG analysis. Further, the dot plot for the enriched KEGG pathways was plotted using cluster Profiler package 4.0 [320].

4.2.5. IDENTIFICATION OF COMMON REGULATORY TRANSCRIPTOMES

For the identification of common HSPs transcriptomes, the coinciding genes were targeted in different databases. This analysis was done to identify the common transcription factors (TFs) and miRNAs that were regulatory at both translational and post-translational levels in GBM and ependymoma. The prediction of common regulatory transcriptional factors[321] was done using ENCODE database[322][323], which is a ChIP sequencing data that is based on BETA Minus algorithm(Bisht et al., 2020). The signals with peak intensity <500 and potential regulatory score <1, used as threshold in the BETA algorithm used by this database. Potential prediction of miRNA was done using DIANA-TarBase v8 database(Karagkouni et al., 2018), that encompasses experimentally validated miRNA targets of genes of different species.

4.2.6. TRANSCRIPTIONAL AND POST TRANSCRIPTIONAL REGULATION OF TF-HSP, TF-MIRNA, MIRNA-HSPS AND HSPS-TF

The prediction of TF-HSPs and TF-miRNA interactions was done using Transcription factor (TRANSFAC) database. TRANSFAC[326,327] is a comprehensive database of transcription factor-target genes interactions. We selected only those TF-HSPs pairs that were found to be conserved in humans. To study the post-transcriptional regulation at miRNA and TF levels, we used three reliable databases for miRNA-target prediction. The three databases that were used are miRanda[328], TargetScan[329] and PITA[330]. The data in these databases is obtained from low and high throughput experimental procedures. Only those pairs were selected that were present in atleast two databases. Further, the construction of miRNA-TF-HSPs

coregulatory network was done using Network Analyst.

4.2.7. DRUG SCREENING AND TARGET HSP CONFIRMATION

The common regulatory HSPs and key drivers that were screened from DEGs obtained were then used for CREEDS[331]. The database can be accessed using (<https://maayanlab.cloud/CREEDS/>) After the prediction from CREEDS the results obtained were then subjected to Drug Gene Budger (<https://maayanlab.cloud/DGB/>). Confirmation of the best HSP that could be targeted from the list of identified HSPs was done using Brain-RNA seq (<https://www.brainrnaseq.org/>). Brain-RNA seq is a web-based database containing the RNA sequences information of the cells of the glial and neuronal origin.

4.2.8. RANKING AND SCORING OF PREDICTED DRUGS

Drugs predicted using CREEDs and Drug Gene Budger analysis was then used as an input to computational drug repositioning score (CoDRES) tool. CoDRES[332] is a computational analysis tool that allows a functional score (FS) and structural score (STS) to independent drugs based on the disease of interest. This tool gives the best repositioning score to the identified drugs based on the similarity and functions.

4.2.9. MOLECULAR DOCKING, ADMET AND BLOOD-BRAIN BARRIER (BBB) ANALYSIS

Molecular docking studies were performed for the confirmation of the identification of candidate drugs. The PDB confirmation of HSP90AB1 (PDB ID: 3NMQ) was retrieved from RCSB PDB database. WEBINA (<https://durrantlab.pitt.edu/webina/>) which is a web-based interaction that works on JavaScript and runs AUTODOCK Vina on web. Heteroatoms within the HSP90AB1 structure were omitted and addition of hydrogen was done using UCSF chimera and Avogadro. The grid size was set with the following coordinates (X-axis=30, Y-axis=30 and Z-axis=30). The 2D and the 3D interactions of the complexes were visualized using Discovery Studio (<https://biovia-discovery-studio-2022-client.software.informer.com/>). The ADMET (absorption, distribution, metabolism, excretion and toxicity) of the predicted candidate drugs

was done using SWISSADME. The BBB permeability[333] of the predicted candidate drugs was checked using CBligand (<https://www.cbligand.org/BBB/mainpage.php>).

4.2.10. MOLECULAR DYNAMIC (MD) SIMULATION STUDIES

Dynamic simulation studies were performed using GROMACS 2019.3 package (<https://bioexcel.eu/software/gromacs/>) following docking analysis for final validation. Preparation of the complexes was done using Charmm37 all atom forcefield. The generation of the charge topology was conducted using CGenFF along with solvation in cubical boundary box with a dimensional gap of 1.0nm (applying TIP3 water model). The addition of Na⁺ and Cl⁻ ion was done to perform charge neutralization. Minimization of energy carried out at 20KJ/mol/nm by implementing a descent long algorithm of 10000 steps proceeded by 10000 steps of conjugate gradient to remove any steric hinderance. Calculation for the root mean square fluctuation (RMSF), root mean square deviations (RMSD), Interaction energy and radius of gyration was done and then plots were constructed.

The detailed pipeline of the study is represented in **Figure 4.1**.

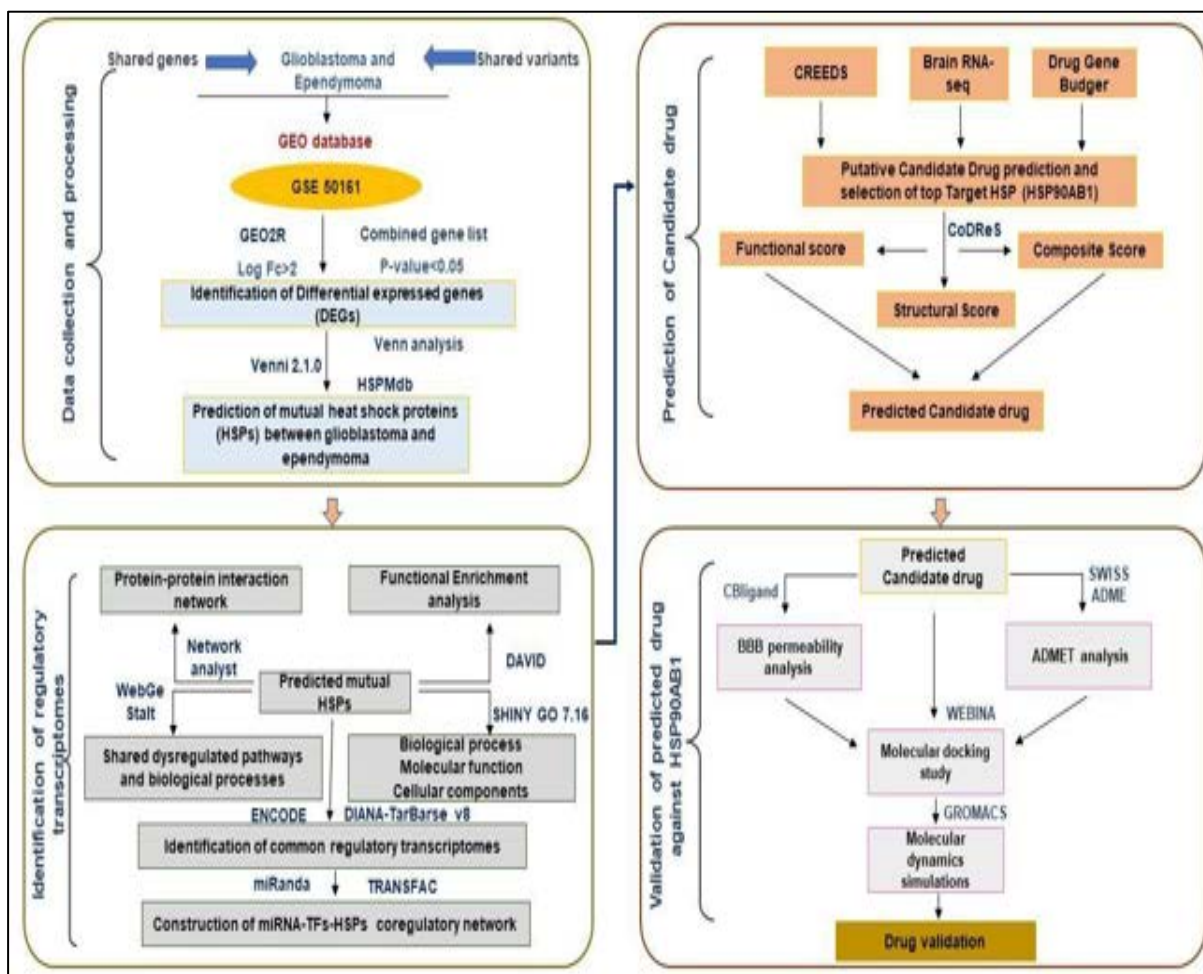


Figure 4.1. Workflow pipeline: Data was retrieved from Gene expression omnibus (GEO) database for transcriptomics studies. Data processing was done using Gene expression profiling interactive analysis 2 (GEPAl2) After data processing the identification of putative Heat shock proteins (HSPs) was carried out using literature survey and HSPMdb database. Following the prediction, the intersection of common HPSs in Glioblastoma (GBMs)and ependymoma was done using Venn diagrams. Protein-protein interaction (PPI) analysis extracted common hub genes to search for disease-disease similarity. These hub genes were further subjected to enrichment analysis and pathway analysis to obtain significant pathways and common GO terms. The common regulation of the two indications was further confirmed by identifying common transcription factors (TFs) and microRNAs (miRNA). CREEDs analysis and LINC1000 Drug Gene Budger was used to identify potential candidate drugs targeting HSPs mutually in GBMs and ependymoma. Finally, the ranking of the candidate drugs was done using CoDRoS giving the functional, structural and composite scores of the candidate drugs.

4.3. RESULTS

4.3.1. COLLECTION OF RAW DATA

Microarray data from the gene expression profile GSE 50161 was downloaded from NCBI GEO databases. A total of 130 human surgical samples of the brain were present in the dataset.

Out of these the count of the diseased ependymoma samples present in this dataset was 46, count for diseased glioblastoma samples was 33 and the number of normal brain samples that were present in this dataset was 13. Rest of the samples were not employed for analysis as those were astrocytoma and medulloblastoma samples and our study was focused to GBM and ependymoma only.

4.3.2. DIFFERENTIAL EXPRESSION OF HSPTS IN EPENDYMOMA AND GBM SAMPLES

Identification of the DEGs of which the expression levels were highly correlated may highlight the pathological and the biological events occurring between GBMs, ependymoma and the potential signature genes. The DEGs were picked by comparing the genes between the normal and the diseased samples. In case of glioblastoma based on the P-value out of 20713 genes, 9261 genes were filtered out. A total of 6107 genes were identified to be differentially expressed and downregulated after applying a fold change of less than or equals 2 and 1736 genes found to be upregulated when the fold change was above or equal to 2. When talking about ependymoma, out of 21051 gene, 9222 genes were filtered out based on the P-value. From these 7214 gene were identified to be downregulated based on $\text{Log Fc} < 2$ and 1919 genes found to be upregulated when we applied a $\text{Log Fc} > 2$. After the prediction of DEGs in both the diseased states, evaluation of the heat shock proteins in both GBM and ependymoma was done. Based on the data available from HSPMdb and literature mining, HSPs were selected from these DEGs. A total of 52 HSPs were identified from the DEGs obtained from GBM samples and 41 HSPs was obtained from DEGs of ependymoma samples. Following Venn analysis, a total of 22 HSPs was predicted, commonly regulating in both the tumors. The summarization of the overlapping HSPs can be seen in **Figure 4.2**. These 22 HSPs were preceded for further analysis.

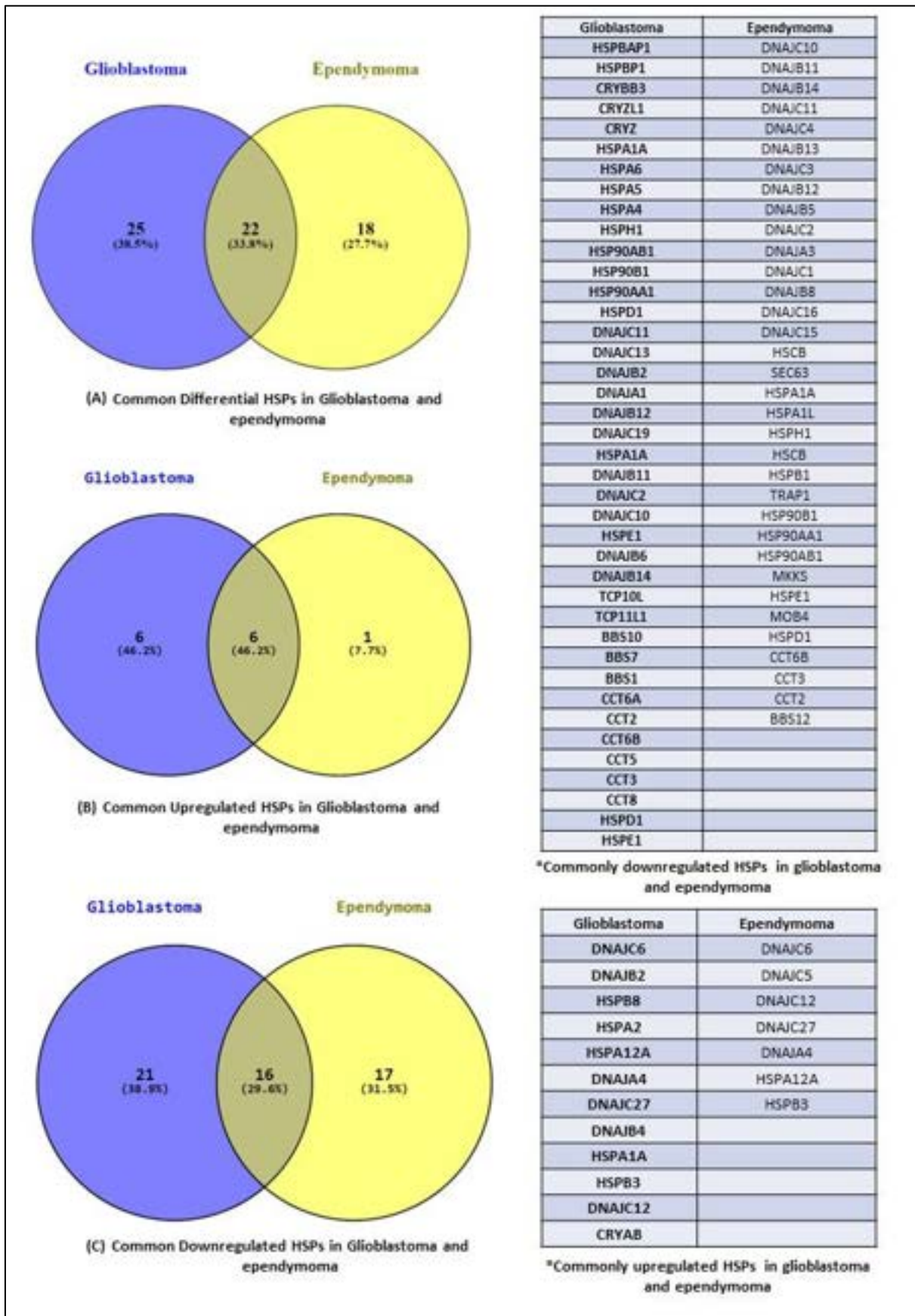


Figure 4.2: Representation of the various heat shock proteins (HSPs) identified to be common in both Glioblastoma and ependymoma. (A) 22 out of 65 HSPs predicted using literature survey

were found to be overlapping in Glioblastomas and ependymomas. (B) 6 out of 7 predicted HSPs identified to be upregulated in both glioblastoma and ependymomas. (C) 16 out of 38 HSPs predicted to be mutually occurring in both glioblastoma and ependymomas.

4.3.3. CONSTRUCTION OF HSPS PPIN IDENTIFIES DYSREGULATED GENES LINKING GBM AND EPENDYMOMA

HSPs are known to possess many important biological functions and a vast biological significance. 22 regulatory HSPs obtained after Venn analysis were used to construct a panorama of the protein-protein interaction network. This interaction network was plotted to predict the biological interactions that were significant commonly in glioblastoma and ependymoma. These 22 differentially expressed HSPs were used for mapping to the parental network as the hub nodes which later formed subnetwork comprising of all the interactions. Resultant PPI network showed 8 different subnetworks with several nodes and intercalating edges. To further reduce the 'hairball effect' PPI network mapping of first order was done that only contained the seed nodes and other interconnecting nodes. From these 8 different subnetworks only the largest subnetwork comprising of 669 nodes and 1247 edges, which are known to be differential HSPs interaction and were used for further analysis. The assessment of the subnetwork was based on different topological parameters consisting of betweenness and degree centrality. We found that degree ranging from 1 to 371 and betweenness ranging from 0 to 137466.1 in the largest subnetwork. Nodes with the higher values were predicted to be the hub nodes while with higher betweenness values were known to be bottleneck nodes. Through our observations we predicted that HSP90AA1 (Degree:371; Betweenness: 137466.1), HSPD1 (Degree:103; Betweenness: 41658.09), CCT2 (Degree:103; Betweenness: 31247.69), HSP90AB1 (Degree:172; Betweenness: 29831.8), HSPA1A (Degree:106; Betweenness: 26204.73) as the top five hub nodes with the highest values of degrees. These hub nodes can be seen as the possible therapeutic targets in both glioblastoma and ependymoma as they show the largest involvement with the interacting signaling cascades. To further give a better illustration

of the network we performed module analysis to identify modules possessing identical biological functions. Out of different modules, we only selected top 3 modules based on the P-value ≥ 0.05 and the size of the module ranging from 5 to 70 genes. Module 0 (p -value $6.34E-11$) consisted of HSP90AB1, DNAJC2, DNAJC4, HSPA1A, HSPA12A and HSPH1 as hub nodes, module 1 (p -value $7.66E-19$) had CCT2, CCT6B and CCT3 hub nodes while module 2 (p -value $3.04E-03$) had HSPD1 and HSPE1 hub nodes.

4.3.4. FUNCTIONAL ENRICHMENT AND PATHWAY ANALYSIS OF THE PREDICTED HSPS

Gene ontology (GO) enrichment analysis of 22 HSPs was performed using DAVID database and with SHINY GO enrichment tool. Based on the above-mentioned results, three types of functional enrichment analysis were performed. This analysis was done to look at the biological process (BP), cellular component (CC) and molecular functions (MF). These enrichments can be seen in **Figure 4.3**.

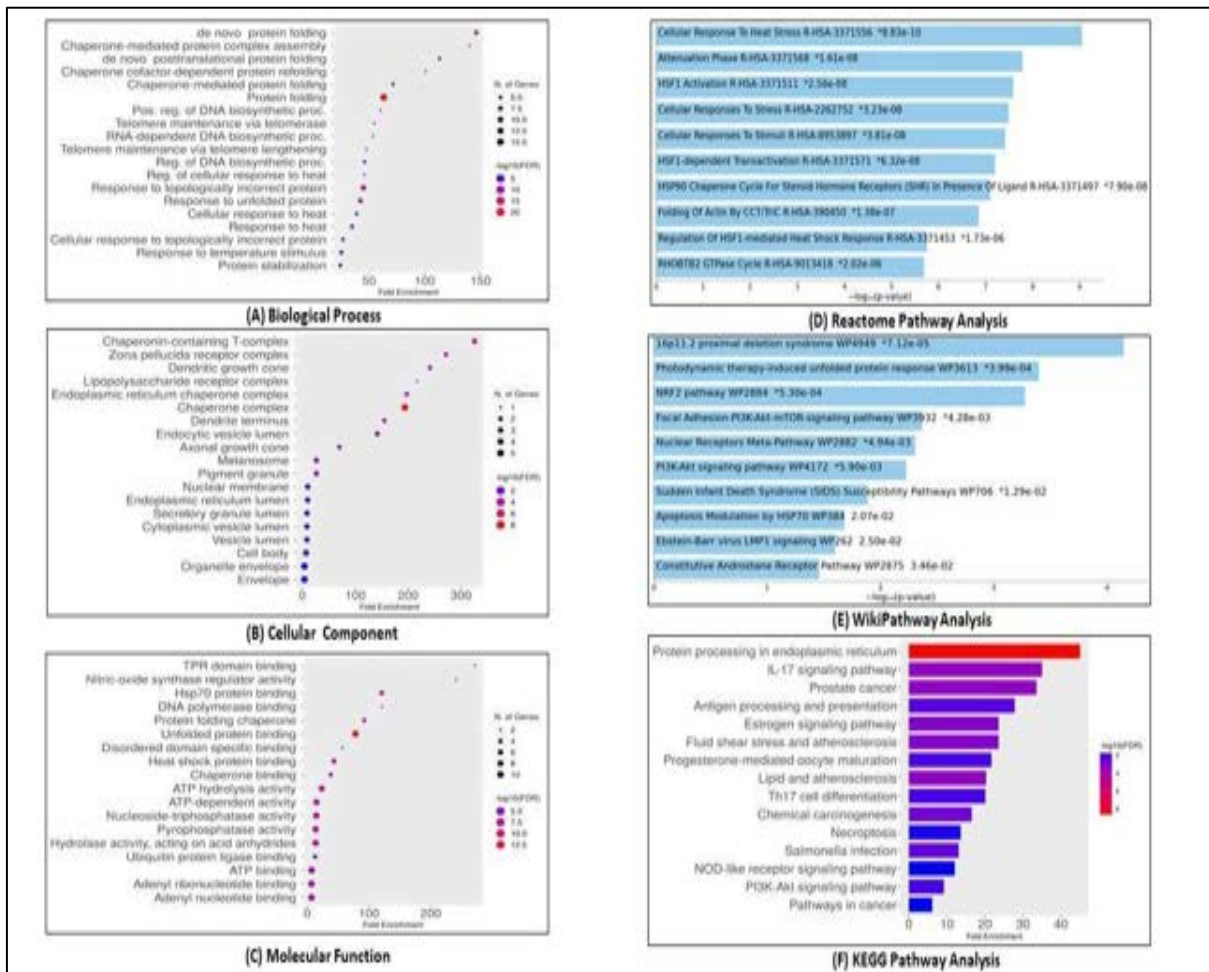


Figure 4.3: (A-C) Gene ontology (GO) functional enrichment analysis of 22 common ubiquitin E3 ligases. (A) GO Biological Enrichment analysis involved in protein folding, chaperone-mediated protein complex assembly and chaperone-mediated protein folding requiring cofactors. The bigger the dots, the greater the color is too red, showing the greater significance and number of genes involved in that process. (B) GO Cellular process enrichment showed that the majority of HSPs were associated with extracellular exosomes, endoplasmic reticulum, membrane formation, endoplasmic reticulum chaperone complexes and endocytic vesicle lumens. (C) GO Molecular function enrichment identified that majority of the HSPs can be seen in processes such as unfolded protein binding, ATP binding, ATPase activity, RNA binding and ubiquitin protein ligase binding. (D-F) Depicts the images of the various pathways for 22 Heat Shock proteins (HSPs) and how they are enriched in Reactome, WikiPathway and KEGG analysis. Most of overlapping HSPs can be visualized in pathways such as ‘protein processing in endoplasmic reticulum (Enrichment FDR: 2.43E-09)’, ‘IL-signaling pathway reticulum (Enrichment FDR: 0.000493)’, ‘Pathway involved in Glioma reticulum (Enrichment FDR: 0.000498)’, ‘Antigen processing and presentation reticulum (Enrichment FDR: 0.000543)’, ‘Estrogen signaling pathways reticulum (Enrichment FDR: 0.000933)’, ‘Lipid and atherosclerosis pathway reticulum (Enrichment FDR: 0.000419)’, and ‘Pathways in cancer (Enrichment FDR: 0.017039)’. HSP90AB1, HSP90B1 and HSP90B1 found to be involved in most of the intersecting pathways in both glioblastoma and ependymoma. Other HSPs that were identified in other pathways were

DNAJC10, DNAJB11, HSPH1 and DNAJB12. The bigger the nodes represent a greater number of genes involved and thicker edges here represent significance.

Most of the HSPs in GO_BP were involved in protein folding, chaperone-mediated protein complex assembly and chaperone-mediated protein folding requiring cofactors. When taking about the GO_CC, these HSPs were associated with extracellular exosomes, endoplasmic reticulum, membrane formation, endoplasmic reticulum chaperone complexes and endocytic vesicle lumens. Coming to the GO_MF, majority of the HSPs can be seen in processes such as unfolded protein binding, ATP binding, ATPase activity, RNA binding and ubiquitin protein ligase binding. A comprehensive overview of these heat shock proteins commanding various processes in GBMs and ependymoma can be visualized in **Table 4.1**. To enumerate the various common regulatory pathways that are deregulated mutually in GBMs and ependymoma, we conducted pathway enrichment of the hub HSPs using reactome, wiki and KEGG analysis. The 22 differentially expressed HSPs were used as an input for enrichment. A distinct count of 15 pathways had been enriched for this study. These are represented in **Figure 4.3 (D-F)**.

Category	Term	Hit Count	GO	P-Value	Genes Hit list	List Total	Fold Enrichment	Benjamini	FDR
GO Biological Processes	Protein folding	15	GO:0006457	2.04E-16	DNAJC10, HSP90AA1, DNAJB11, HSP90AB1, DNAJC2, HSPE1, HSPH1, CCT6B, DNAJA4, HSPD1, DNAJB12, CCT3, DNAJB14, CCT2, HSP90B1	22	61.82063953	3.67667E-14	3.28858E-14
GO Biological Processes	Chaperone-mediated protein complex assembly	5	GO:0051131	4.82E-09	CCT2, HSP90AA1, HSP90AB1, HSPD1, HSPA1A	22	219.6931818	2.89097E-07	2.58581E-07
GO Biological Processes	Chaperone mediated protein folding requiring cofactor	5	GO:0051085	3.03E-08	HSPH1, DNAJB12, DNAJB14, HSPE1, HSPA1A	22	142.1544118	1.36441E-06	1.22039E-06
GO Biological Processes	Protein refolding	4	GO:0042026	1.83E-06	HSP90AA1, DNAJA4, HSPD1, HSPA1A	22	154.664	5.58535E-05	4.99579E-05
GO Biological Processes	Protein stabilization	6	GO:0050821	1.86E-06	CCT3, CCT2, HSP90AA1, HSP90AB1, HSPD1, HSPA1A	22	26.36318182	5.58535E-05	4.99579E-05
GO Biological Processes	Cellular response to heat	4	GO:0034605	1.93E-05	HSP90AA1, HSP90AB1, HSPD1, HSPA1A	22	71.6037037	0.000497264	0.000444775
GO Biological Processes	Ubiquitin-independent ERAD pathway	4	GO:0030433	6.54E-05	DNAJC10, DNAJB12, DNAJB14, HSP90B1	22	47.73580247	0.001471778	0.001316424
GO Biological	Regulation of	3	GO:00	0.000139	HSP90AA1, HSP90AB1,	22	161.1083333	0.002773943	0.0024811

I Processes	protein ubiquitination		31396		HSPA1A				38
GO Biological Processes	Positive regulation of telomerase activity	3	GO:0051973	0.000504	CCT2, HSP90AA1, HSP90AB1	22	85.29264706	0.009068588	0.008111348
GO Biological Processes	Regulation of cellular protein localization	2	GO:01903827	0.014646	HSP90AA1, HSP90AB1	20	128.8866667	0.125536434	0.112285366
GO Molecular Functions	Unfolded protein binding	11	GO:0051082	3.11E-17	CCT3, CCT2, HSP90AA1, HSP90AB1, DNAJA4, DNAJB11, HSPE1, HSP90B1, HSPD1, CCT6B, HSPA1A	21	75.60450745	2.30298E-15	1.8984E-15
GO Molecular Functions	ATPase activity	8	GO:0016887	4.78E-08	CCT3, CCT2, HSP90AA1, HSP90AB1, HSP90B1, HSPD1, CCT6B, HSPA1A	21	20.34759214	1.76753E-06	1.45702E-06
GO Molecular Functions	ATP binding	12	GO:0005524	8.57E-08	CCT3, CCT2, HSP90AA1, HSPH1, HSP90AB1, DNAJA4, HSPA12A, HSPE1, HSP90B1, HSPD1, CCT6B, HSPA1A	21	7.011402614	2.11353E-06	1.74224E-06
GO Molecular Functions	Hsp70 protein binding	5	GO:0030544	1.58E-07	DNAJC2, DNAJA4, DNAJC10, DNAJB12, DNAJB14	21	95.7852077	2.76797E-06	2.28171E-06
GO Molecular Functions	Protein binding involved in protein folding	5	GO:0044183	1.87E-07	CCT3, CCT2, HSP90AB1, CCT6B, HSPA1A	21	91.87560739	2.76797E-06	2.28171E-06

GO Molecular Functions	Chaperone binding	4	GO :0051087	0.000203	DNAJA4, DNAJC10, HSPE1, HSPD1	21	32.74112554	0.002506195	0.002065917
GO Molecular Functions	Ubiquitin protein ligase binding	5	GO :0031625	0.000269	CCT2, HSP90AA1, HSP90AB1, HSPD1, HSPA1A	21	14.66418489	0.00284237	0.002343035
GO Molecular Functions	RNA binding	8	GO :0003723	0.000533	CCT3, DNAJC2, HSP90AA1, HSP90AB1, HSPE1, HSP90B1, HSPD1, HSPA1A	21	4.896701305	0.004386134	0.003615597
GO Molecular Functions	Disordered domain specific binding	3	GO :0097718	0.000692	HSP90AA1, HSP90AB1, HSPA1A	21	73.003861	0.00512362	0.004223524
GO Molecular Functions	TPR domain binding	2	GO :0030911	0.008432	HSP90AA1, HSP90AB1	21	225.0952381	0.052958379	0.04365488
GO Cellular component	Endoplasmic reticulum chaperone complex	3	GO :0034663	5.42E-05	DNAJB11, DNAJC10, HSP90B1	22	255.1239669	0.002088319	0.001627261
GO Cellular component	Chaperonin-containing T-complex	3	GO :0005832	5.42E-05	CCT3, CCT2, CCT6B	22	255.1239669	0.002088319	0.001627261
GO Cellular component	Endocytic vesicle lumen	3	GO :0071682	0.00015	HSP90AA1, HSPH1, HSP90B1	22	155.9090909	0.003267354	0.00254599
GO Cellular component	Extracellular exosome	10	GO :0070062	0.00017	CCT3, CCT2, HSP90AA1, HSPH1, HSP90AB1, HSPA12A, HSPE1, HSP90B1, HSPD1, HSPA1A	22	4.215658159	0.003267354	0.00254599

GO Cellular component	Melanosome	3	GO:0042470	0.004989	HSP90AA1, HSP90AB1, HSP90B1	22	26.98426573	0.055795764	0.043477219
GO Cellular component	Endoplasmic reticulum	6	GO:0005783	0.005072	DNAJB11, DNAJC10, DNAJB12, DNAJB14, HSP90B1, HSPA1A	22	4.906230134	0.055795764	0.043477219
GO Cellular component	Ficolin-1-rich granule lumen	3	GO:01904813	0.007017	HSP90AA1, HSP90AB1, HSPA1A	22	22.63196481	0.058322387	0.045446016
GO Cellular component	Sperm plasma membrane	2	GO:00097524	0.007122	HSP90B1, HSPD1	22	267.2727273	0.058322387	0.045446016
GO Cellular component	Zona pellucida receptor complex	2	GO:0002199	0.008136	CCT3, CCT2	22	233.8636364	0.058322387	0.045446016
GO Cellular component	Membrane	10	GO:0016020	0.008332	HSP90AA1, HSP90AB1, DNAJA4, DNAJB11, DNAJC10, DNAJB12, DNAJB14, HSPE1, HSP90B1, HSPD1	22	2.468869215	0.058322387	0.045446016

Table 4.1: Tabular representation of GO functionally enriched heat shock proteins (HSPs) with associated biological processes, molecular functions and cellular components in glioblastoma and ependymoma.

Pathways having high enrichment FDR values were selected for the study. Most of overlapping HSPs can be visualized in pathways such as ‘protein processing in endoplasmic reticulum (Enrichment FDR: 2.43E-09)’, ‘IL-signaling pathway reticulum (Enrichment FDR: 0.000493)’, ‘Pathway involved in Glioma reticulum (Enrichment FDR: 0.000498)’, ‘Antigen processing and presentation reticulum (Enrichment FDR: 0.000543)’, ‘Estrogen signaling pathways reticulum (Enrichment FDR: 0.000933)’, ‘Lipid and atherosclerosis pathway reticulum (Enrichment FDR: 0.000419)’, and ‘Pathways in cancer (Enrichment FDR: 0.017039)’.

HSP90AB1, HSP90B1 and HSP90B1 found to be involved in most of the intersecting pathways

in both glioblastoma and ependymoma. Other HSPs that were identified in other pathways were DNAJC10, DNAJB11, HSPH1 and DNAJB12. These results suggests that HSP90AB1, HSP90b1 and HSP90B1 have multiple metabolic functions and are involved in various processes in human body. The detailed information is summarized in **Table 4.2**

Enrichment FDR	Hits	Pathway Genes	Fold Enrichment	Pathway	Genes Hit list
2.43E-09	7	169	44.96252	Protein processing in endoplasmic reticulum	DNAJC10 HSP90AA1 DNAJB11 HSP90AB1 HSPH1 DNAJB12 HSP90B1
0.000493	3	93	35.0169	IL-17 signaling pathway	HSP90AA1 HSP90AB1 HSP90B1
0.000498	3	97	33.5729	Glioma	HSP90AA1 HSP90AB1 HSP90B1
0.00543	2	78	27.83394	Antigen processing and presentation	HSP90AA1 HSP90AB1
0.000933	3	138	23.59834	Estrogen signaling pathway	HSP90AA1 HSP90AB1 HSP90B1
0.000933	3	138	23.59834	Fluid shear stress and atherosclerosis	HSP90AA1 HSP90AB1 HSP90B1
0.00766	2	100	21.71048	Progesterone-mediated oocyte maturation	HSP90AA1 HSP90AB1
0.000419	4	214	20.29016	Lipid and atherosclerosis	HSP90AA1 HSP90AB1 HSPD1 HSP90B1
0.007706	2	108	20.10229	Th17 cell differentiation	HSP90AA1 HSP90AB1
0.002261	3	197	16.53082	Chemical carcinogenesis	HSP90AA1 HSP90AB1 HSP90B1
0.015034	2	159	13.65439	Necroptosis	HSP90AA1 HSP90AB1
0.003886	3	249	13.0786	Salmonella infection	HSP90AA1 HSP90AB1 HSP90B1
0.017039	2	180	12.06138	NOD-like receptor signaling pathway	HSP90AA1 HSP90AB1
0.00766	3	354	9.199354	PI3K-Akt signaling pathway	HSP90AA1 HSP90AB1 HSP90B1
0.017039	3	530	6.144474	Pathways in cancer	HSP90AA1 HSP90AB1 HSP90B1

Table 4.2: Tabular representation of KEGG pathway analysis of the predicted HSPs along with their fold change and enrichment false discovery rate (FDR) in glioblastoma and ependymoma.

4.3.5. IDENTIFICATION OF MUTUAL REGULATORY TRANSCRIPTOMES LINKING HSPS IN GBMS AND EPENDYMOMA

To study the mutualistic role of each of the predicted HSPs and to establish a link in glioblastoma and ependymoma at transcriptional and post-transcriptional levels, we tried to decipher a connection of the hub genes with the miRNAs and TFs. GATA2, FOXC1, USF2, NFIC, FOXL1, RELA, YY1, CREB1, NFKB1 and E2F1 were disclosed to be the top 10 interacting transcription factors with the hub HSPs and are summarized in **Table 4.3**. The link can be visualized in **Figure 4.4**

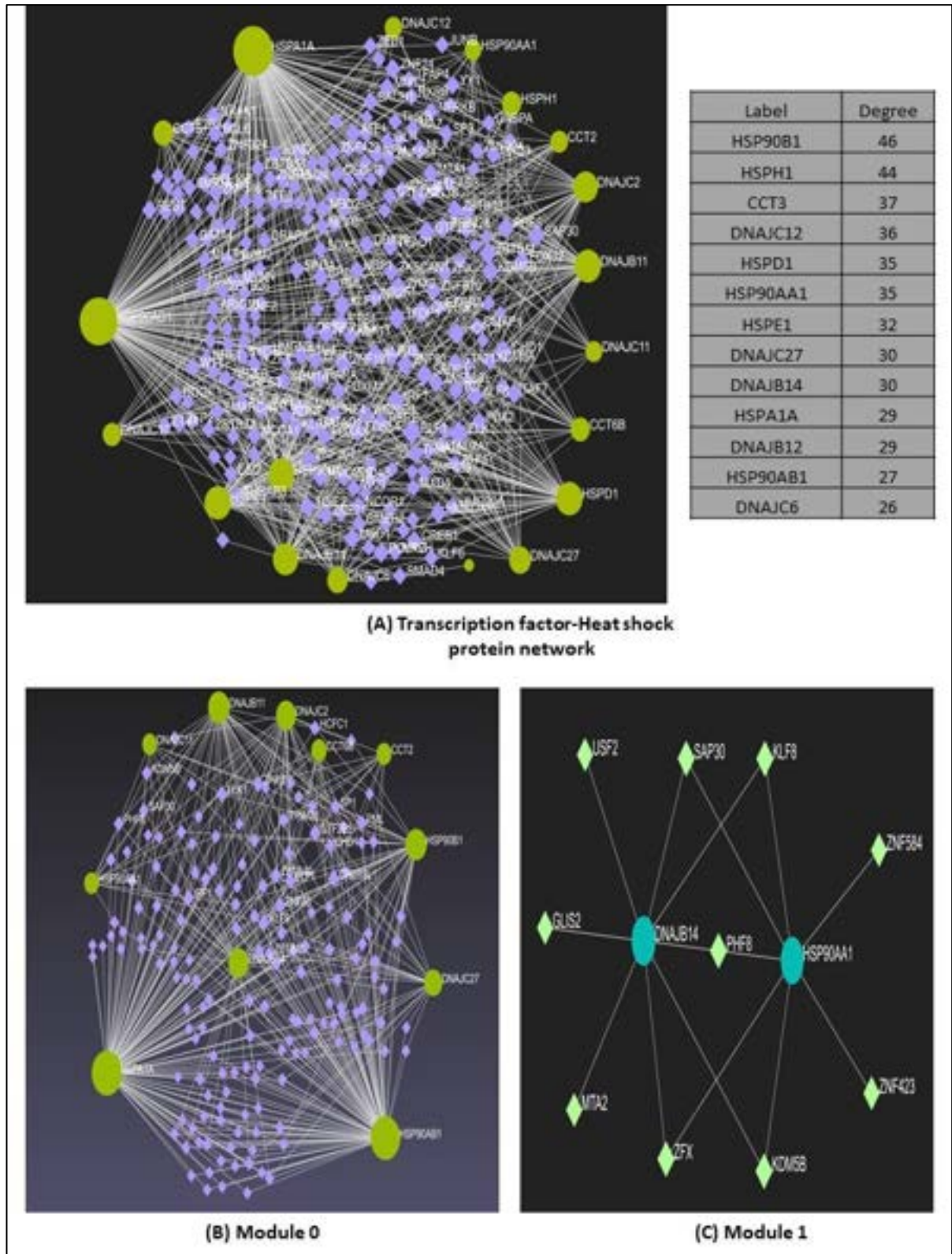


Figure 4.4 (A) Transcription Factor-Heat shock protein networks showing the interaction between the hub HSPs and associated transcription factors (TFs). The red circles represent the hub genes and the blue diamond represent the associated TFs. (B) Module 0 represent 11 query nodes, HSP90AB1, HSPA1A, HSP90B1, CCT2, DNAJC2, DNAJB11 and CCT6B. (C) Module 1 represent 2

query nodes DNAJb14 and HSP90AA1. Yellow diamond in the module represents interacting TFs

Id	Transcription factor (TFs)	Associated HSPs	Degree	Betweenness
2624	GATA2	CCT2, DNAJC12, HSP90AB1, HSP90AA1, HSPH1, CCT3, DNAJC11, DNAJC2, HSP90B1, DNAJA4, HSPA12A, DNAJB14, HSPD1	14	188.62
2296	FOXC1	CCT2, DNAJC12, DNAJC6, HSPB3, HSP90AA1, HSPH1, DNAJC2, DNAJC10, DNAJC27, DNAJA4, DNAJB14, HSPD1, HSPE1	13	171.09
7392	USF2	HSPA1A, HSPH1, CCT3, HSP90B1, DNAJC27, HSPE1, DNAJB11, DNAJB12	8	66.85
4782	NFIC	HSPA1A, DNAJC12, HSP90AB1, DNAJC10, HSP90B1, HSPD1, CCT6B, DNAJB11	8	54.68
2300	FOXL1	CCT2, HSPB3, HSP90AA1, HSPH1, DNAJB14, HSPD1, HSPE1, CCT6B	8	51.5
5970	RELA	HSP90AB1, HSP90AA1, DNAJC11, HSP90B1, DNAJA4, HSPA12A, DNAJB11	7	48.25
7528	YY1	CCT2, HSPH1, CCT3, DNAJA4, DNAJB14, DNAJB11	7	31.86
1385	CREB1	DNAJC6, HSP90AB1, HSP90B1, DNAJC27, DNAJA4, HSPA12A	6	23.18
4790	NFKB1	HSP90AB1, DNAJC2, HSP90B1, HSPA12A, DNAJB11	5	14.14
1869	E2F1	DNAJC12, HSP90B1, DNAJA4, DNAJB14, HSPE1	5	12.81

common in Glioblastoma (GBMs) and Ependymoma.

Table 4.3: Tabular summarization of top transcription factors and their associated heat shock proteins (HSPs) common both in glioblastoma and ependymoma.

Likewise, hsa-miR-16-5p, hsa-miR-26b-5p, hsa-miR-92a-3p, hsa-miR-335-5p and hsa-miR-92a-

3p, hsa-miR-15a-5p, hsa-miR-193b-3p, hsa-miR-218-5p, hsa-miR-501-5p, hsa-miR-1-3p/ hsa-miR-206/hsa-miR-613 were selected as the top interacting miRNAs with hub HSPs and can be visualized in **Figure 4.5A**.

All of these interacting miRNAs are summarized in **Table 4.4**.

microRNA	p-value	FDR	Odd ratio	Number of interactions	Target Genes
hsa-miR-16-5p	1.63361E-05	0.008462105	0.217053903	10	HSPA1A, HSP90B1, DNAJC2, DNAJA4, CCT6B, CCT3, HSPD1, HSPH1, HSP90AA1, DNAJC10
hsa-miR-26b-5p	0.038242532	0.354424512	0.435408922	6	DNAJC2, DNAJC12, HSPA12A, DNAJC11, DNAJC6, HSPD1
hsa-miR-92a-3p	0.040501731	0.354424512	0.392286245	5	HSP90B1, HSP90AB1, HSPH1, DNAJB12, DNAJC27
hsa-miR-335-5p	0.298229545	0.392050052	0.732434944	5	HSPB3, DNAJB14, HSP90B1, HSPA1A, HSP90AB1
hsa-miR-92a-3p	0.040501731	0.354424512	0.392286245	5	HSP90B1, HSP90AB1, HSPH1, DNAJB12, DNAJC27
hsa-miR-15a-5p	0.015947705	0.354424512	0.249883829	4	HSPA1A, HSP90B1, CCT6B, DNAJC10
hsa-miR-193b-3p	0.02825663	0.354424512	0.297281599	4	HSP90AB1, DNAJC11, CCT2, HSPH1
hsa-miR-218-5p	0.02446857	0.354424512	0.284386617	4	HSP90B1, DNAJC2, DNAJC11, DNAJA4
hsa-miR-501-5p	0.001310597	0.339444689	0.073420074	3	HSP90AB1, HSP90AA1, DNAJB14
hsa-miR-1-3p/ hsa-miR-206/ hsa-miR-613	0.133738208	0.354424512	0.427973978	3	HSPD1, HSP90B1, DNAJC10

Table 4.4: Tabular representation of common regulatory miRNAs targeting various heat shock proteins (HSPs) in glioblastoma and ependymoma.

4.3.6. ESTABLISHMENT OF MIRNA-TFS- TARGET HSPS COREGULATORY NETWORK

In order to understand the regulatory relationship between miRNAs and TFs, the miRNA-TFs-HSPs regulation network was constructed as shown in **Figure 4.5B**. hsa-miR-181d and has-miR-23a had the rate of connectivity with the target HSPs and TFs. Whereas, several miRNAs were

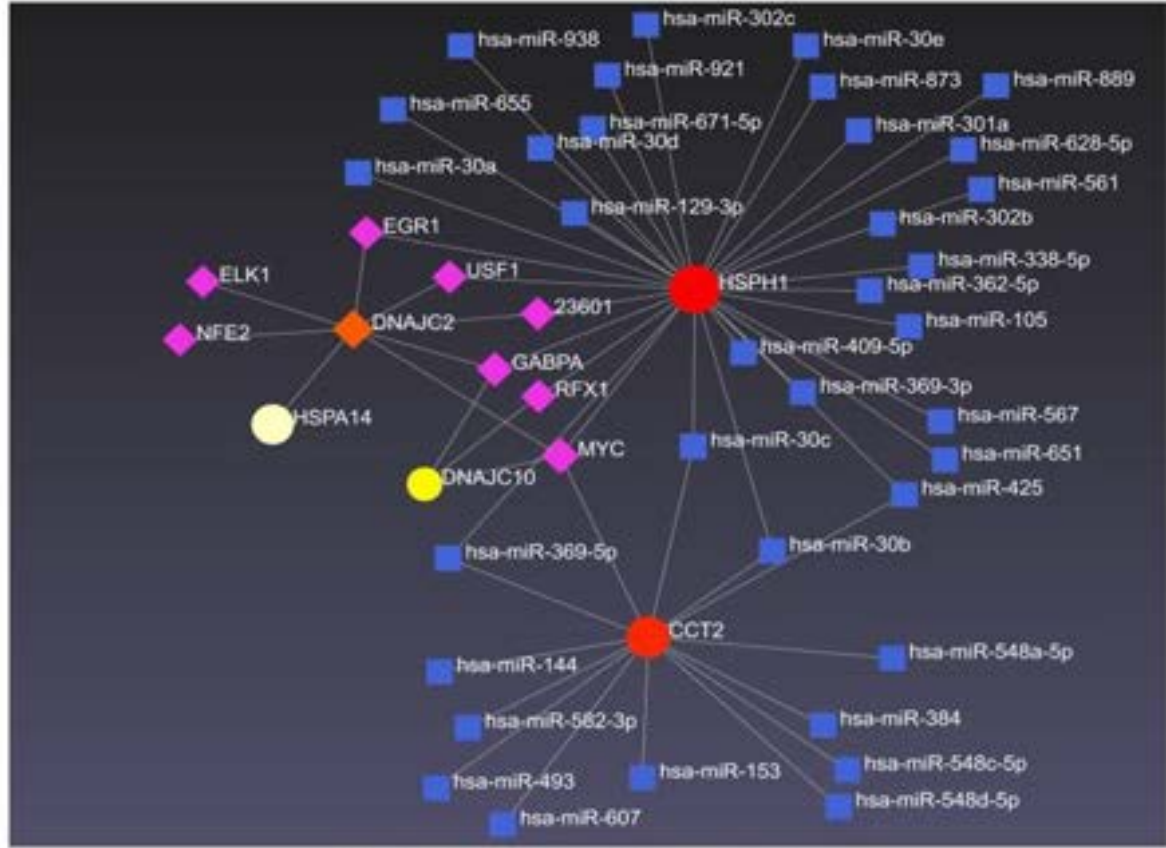
identified to have mutual targets such as has-miR-30C and has-miR-30b showed interactions with HSPH1 and CCT2. Also, various TFs were also found to be interconnected with different HSPs like GABA, MYC, RFX1 and EGFR1. These regulatory TFs interacted with DNAJC2, DNAJC10, HSPH1 and CCT2. We also visualized different modules to develop a better relationship amongst the transcriptomes and the target HSPs.

Module 0 shows the interaction of CCT3 with E2F1 that was interacting with DNAJC10. hsa-miR-141 was found to be interacting with HSPD1 and with E2F1. Other miRNA has-miR-206 showed interlink with HSPD1 and HSF2. Similarly, hsa-miR-217 interacted with CCT2 and with transcription factor E2F7. From module 1 we predicted that HSP90B1 was interacting with has-miR-522 which in turn was regulated by ZEB1. HSP90B1 was also interacting with NFYA, SREBF1 and BPTF along with has-miR-99a, hsa-miR-148 and has-miR-624. Module 2 revealed interaction of DNAJC6 with FOXO3B, FOXO1, NFIL3 which in turn also showed interactions with has-miR-323-3p, hsa-miR-876-3p and hsa-miR-501-5p.



Label	Betweenness
hsa-miR-23a	561.68
hsa-miR-23b	561.68
hsa-miR-181d	748.6
hsa-miR-548a-5p	607.18
hsa-miR-27a	463.79
hsa-miR-144	364.51
hsa-miR-544	316.79
hsa-miR-203	266.37
hsa-miR-548a-3p	256.44
hsa-miR-425	240.79

(A) miRNA-HSPs interaction network



(B) TF-miRNA-HSPs coregulatory network

Figure 4.5. (A): Representation of the miRNAs showing interacting with Heat shock proteins (HSPs) common in GBMs and ependymoma. The green circles represent the HSPs and the blue squares represent the associated. (B) The regulatory relationship between miRNAs and TFs, the

miRNA-TFs-HSPs regulation network was constructed highlighting HSP90B1 interacting with various miRNAs that are mutually associated in both the tumors. Similarly, hsa-miR-217 interacted with CCT2 and with transcription factor E2F7. HSP90B1 was interacting with has-miR-522 which in turn was regulated by ZEB1. HSP90B1 was also interacting with NFYA, SREBF1 and BPTF along with has-miR-99a, hsa-miR-148 and has-miR-624.

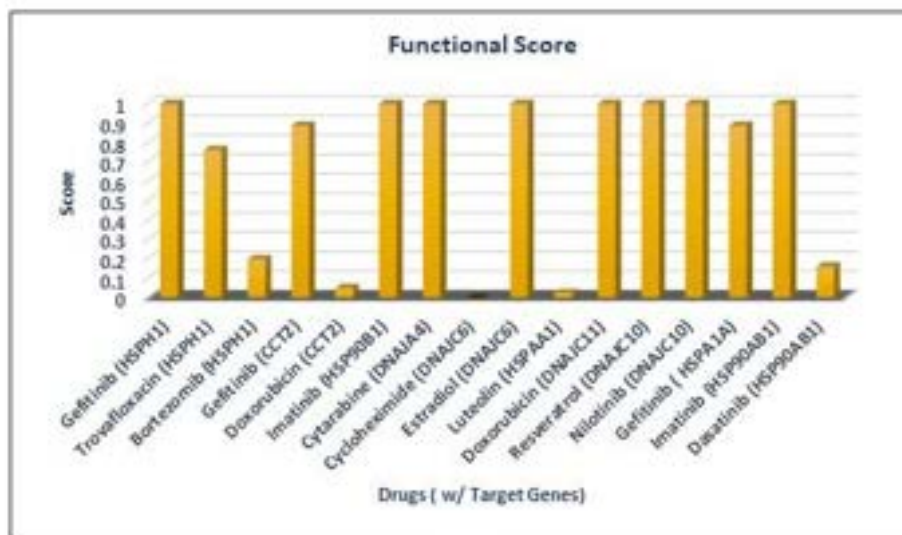
4.3.7. PREDICTION OF POTENTIAL DRUG CANDIDATES AND PUTATIVE TARGETABLE HSP VALIDATION

To identify therapeutic candidates that could potentially target HSPs in GBMs and ependymoma, we performed the CREEDS analysis followed by Drug Gene Budger from LINC1000. As CREEDS dataset comprises of thousands of single-drugs induced gene expression signatures obtained from GEO, these drugs could be possibly be used as therapeutics in the reversal of GBMs and ependymoma. To nurture our study, we used those gene set-drug pairs that carried significant p-values. In the initial screening we identified 26 drugs when we feed the upregulated hub HSPs into CREEDS with P-value $<10^{-10}$ as threshold. Similarly, 148 drugs were obtained when downregulated hub HSPs were screened against the CREEDS database with same filters. From further analysis we predicted 5 drugs that could reverse the expression of the upregulated hub HSPs and 30 drugs which could reverse the expressional signature of the downregulated hub HSPs by checking the drug profiles. To crosscheck our results, we used Drug Gene Budger to explore our predicted drugs in L1000 database. Only the drugs that caused the differential gene expression of important HSPs, followed by Log Fc higher than 2 for upregulated HSPs and Log Fc lower than 2 for downregulated HSPs were considered for analysis using Drug Gene Budger. We found that only 2 drugs could reverse the expression pattern of upregulated HSPs in glioblastoma and ependymoma and 11 drugs for the expression reversal in downregulated HSPs. Resveratrol and cycloheximide was found to be changing the expression patterns of the upregulated HSPs. Similarly, Gefitinib, trovafloxacin, bortezomib, doxorubicin, imatinib, cytarabine, estradiol, luteolin, nilotinib and dasatinib were able to reverse the activity in downregulation hub HSPs. Out of 22 HSPs only 9 were found targetable based on the analysis

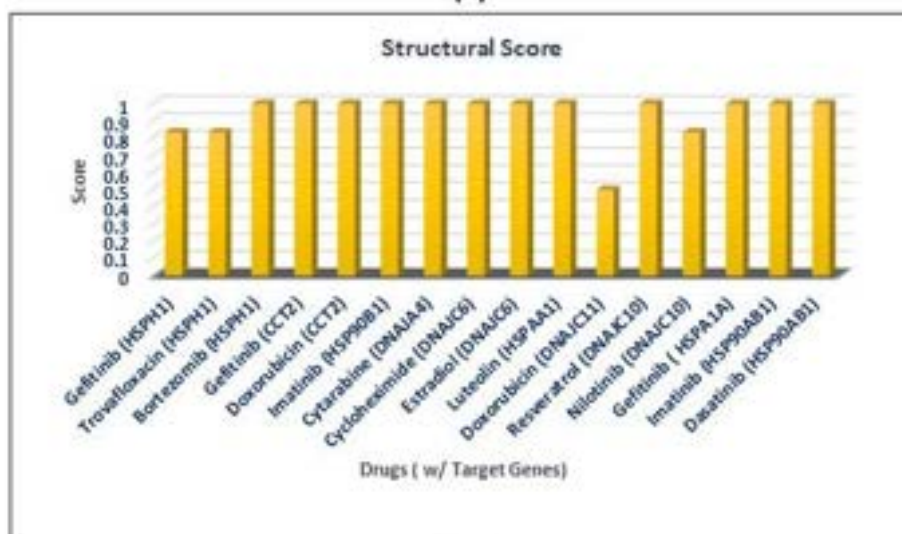
made from CREEDS and Drug Gene Budger. These HSPs were HSP90AB1, HSPH1, CCT2, HSP90B1, DNAJA4, DNAJC6, HSPAA1, DNAJC10 and HSPA1A. We further proceeded to identify the most suitable HSP among all as a target against all the predicted drugs. Based on the RNA sequencing data and expression pattern of these HSPs, HSP90AB1 was found to be the most prominent HSPs against the identified ones. The expression rate in the microglial cells was 227.30 in case of HSP90AB1, 92.03 in case of HSPH1, 18.67 in DNAJC10, 15.93 in CCT2, 0.33 in DNAJC6 and 120.37 in case of HSP90B1. Therefore, HSP90AB1 was used to target for further analysis.

4.3.8. DRUG PRIORITIZATION BASED ON RANKING SCORES USING CODRES

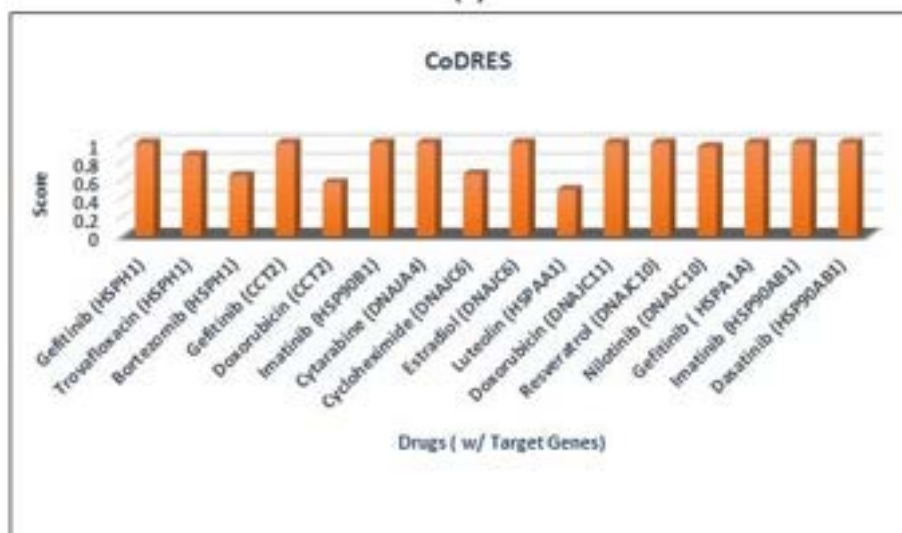
The results obtained from CREEDS and LINC 1000 Drug Gene Budger analysis were then checked for the functional and structural properties. The comprehensive comparative scores representing the structural, functional and composite scores are shown in **Figure 4.6**.



(A)



(B)



(C)

Figure 4.6. Representation of the scores of the candidate drugs obtained using CoDRES (A) Function scores of the candidate drugs. We predicted that four drugs- imatinib, cytarabine, estradiol and resveratrol have functional score value of 1 (B) Structural score value of 1 while

three drugs- Nilotinib, gefitinib, doxorubicin have a functional score of 1 but structural score was less than one (C) Composite CoDReS scores of various candidate drugs. With these observations we considered that resveratrol, cycloheximide and gefitinib as the most promising candidates.

From the analysis, we predicted that four drugs- imatinib, cytarabine, estradiol and resveratrol have functional and structural score value of 1 while three drugs- Nilotinib, gefitinib, doxorubicin have a functional score of 1 but structural score was less than one. On the other hand, bortezomib, cycloheximide, luteolin and dasatinib had a structural score of 1 but the functional score was less than 1. These drugs were repositioned based on their composite CoDReS scores and imatinib, cytarabine, estradiol, resveratrol, and cycloheximide were identified as the top drugs. With these observations we considered that resveratrol, cycloheximide, gefitinib and imatinib as the most promising candidates for this study. The details of the individual scores are summarized in **Table 4.5**.

Drug name	Targetable Heat shock proteins (HSPs)	Expression Pattern	Drug Bank ID	Functiona I Score	Structural Score	CoDReS
Gefitinib	HSPH1	Downregulat e	DB00137	1	0.833333	1
Trovafloracin	HSPH1	Downregulat e	DB00685	0.762656	0.833333	0.87054
Bortezomib	HSPH1	Downregulat e	DB00188	0.199532	1	0.65429
Gefitinib	CCT2	Downregulat e	DB00317	0.887728	1	1
Doxorubicin	CCT2	Downregulat e	DB00997	0.050992	1	0.573268
Imatinib	HSP90B1	Downregulat e	DB00619	1	1	1
Cytarabine	DNAJA4	Downregulat e	DB00987	1	1	1
Cycloheximide	HSP90AB1	Upregulate	N/A	0	1	0.666667
Estradiol	DNAJC6	Downregulat e	DB00783	1	1	1
Luteolin	HSPAA1	Downregulat e	DB15584	0.024504	1	0.5

Doxorubicin	DNAJC11	Downregulate	DB00997	1	0.5	1
Resveratrol	HSP90AB1	Upregulate	DB02709	1	1	1
Nilotinib	DNAJC10	Downregulate	DB04868	1	0.833333	0.959982
Gefitinib	HSPA1A	Downregulate	DB00317	0.887728	1	1
Imatinib	HSP90AB1	Upregulate	DB00619	1	1	1
Dasatinib	HSP90AB1	Upregulate	DB01254	0.161974	1	1

Table 4.5: Tabular representation of the comparative scores of different drug targeting heat shock proteins (HSPs)

4.3.9. DOCKING, ADMET AND BBB STUDIES AGAINST HSP90AB1

Drugs that were prioritized based on the drug ranking and various scores were then proceeded for docking analysis. Docking analysis of HSP90AB1 was done against a reference drug (cepharanthine) to compare the binding scores and with imatinib, gefitinib, cycloheximide and resveratrol. All these four drugs along with the reference were checked for the presence of any extra residue or any heteroatom. Any extra water atoms were removed before docking analysis. Reference drug (Cepharanthine) to compare the binding affinity of HSP90AB1 shows a score of -9.1 Kcal/mol. Binding energy here shows the overall affinity of the drugs for HSP90AB1. The greater the binding scores in negative terms displays more inhibition capacity of all these four prioritized drugs against HSP90AB1. The common residues identified during the docking analysis of all these targets along with reference were Met98, Gly135 and Val186. The binding

energies calculated post docking analysis were -9.1 Kcal/mol for the reference drug, -9.3 Kcal/mol for resveratrol, -9.2 Kcal/mol in case of cycloheximide, -9.7 Kcal/mol for gefitinib and -10.9 in case of imatinib. The results obtained after docking analysis can be visualized in **Figure 4.7**.

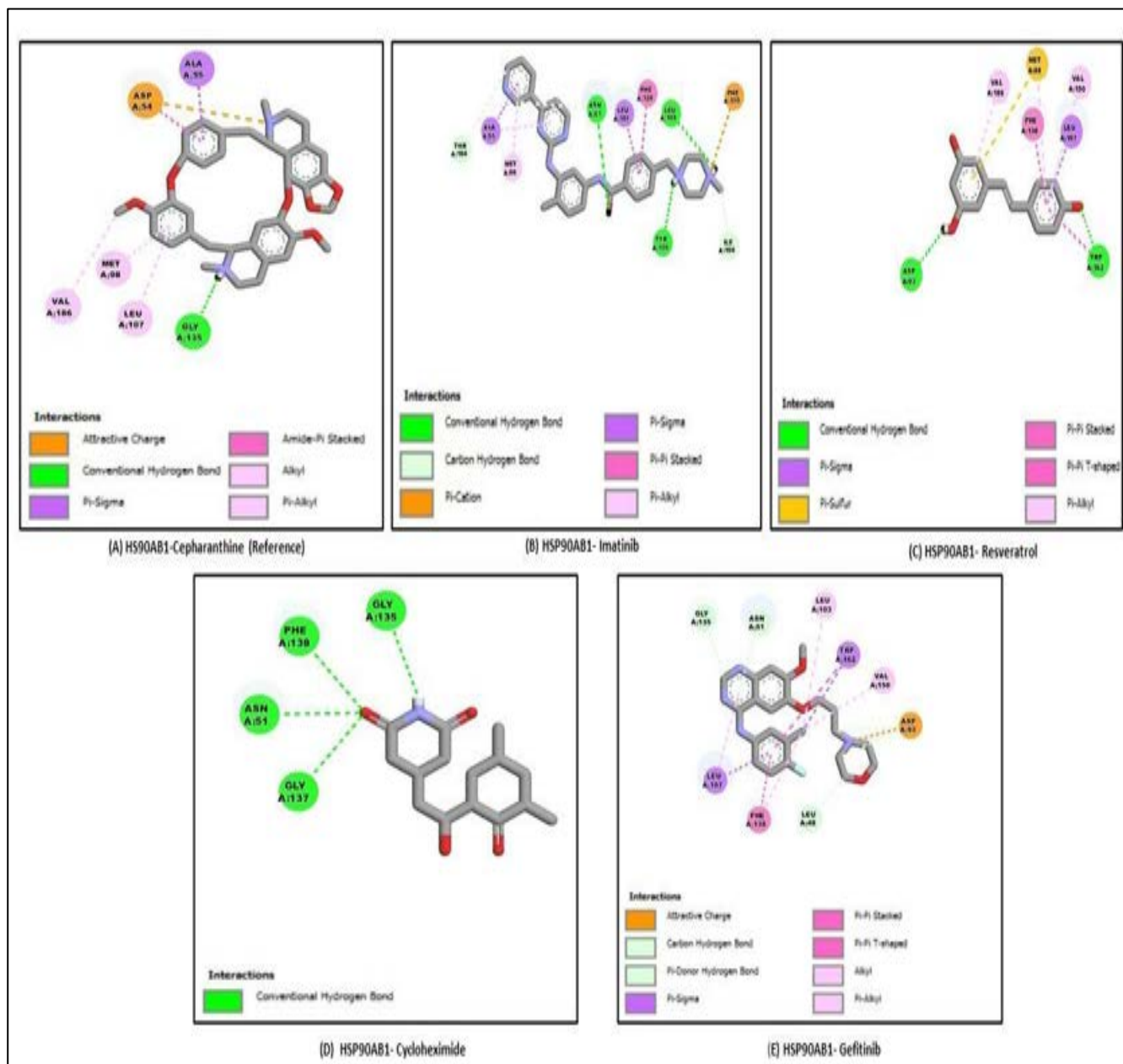


Figure 4.7: (A-F) Molecular docking confirmations: Representation of 2D interactions of the various ligands with HSP90AB1 along with the number of interacting residues. (A) Interaction of the cepharanthine with the HSP90AB1 showing an affinity score of -9.1 and interacting residues are Asp54, Ala55, Met98, Leu107, Gly135, Val186. (B) Interaction of imatinib with the HSP90AB1 showing an affinity score of -10.9 and interacting residues are Ala55, Met98, Leu103, Phe170, Phe138, Leu107, Asn51, Ile104 (C) Interaction of resveratrol with the HSP90AB1 showing an affinity

score of -9.3 and interacting residues are Met98; Val150; Leu107; Phe138; Val186; Trp162; Asp93. (D) Interaction of cycloheximide with the HSP90AB1 showing an affinity score of -9.2 and interacting residues are Phe138, Gly135, Asn51, Gly137. (E) Interaction of gefitinib with the HSP90AB1 showing an affinity score of -9.7 and interacting residues are Leu107, Phe138, Leu48, Asp93, Val150, Trp162, Leu103, Asn51, Gly135.

Compound	Affinity (kcal/mol)	Grid Size	Interacting residues	Canonical smiles	BBB CBligand	CBligand Score	Molecular Mass (g/mol)	H-bond donor (<5)	H-bond donor (<10)	Octal partition coefficient (Log <5)	Molar Refractivity
Reference (Cepharanthine)	-9.1	30-30-30	Asp54; Ala55; Met98; Leu107; Gly135; Val186	CN1CC C2=CC3 =C(C4= C2C1CC 5=CC=C (C=C5) OC6=C(C=CC(= C6) CC7C8= CC=C(C=C8C CN7C) OC) O4) OC) OCO3	Yes	0.076	493.6	2	6	3.49	154.5
Resveratrol	-9.3	30-30-30	Met98; Val150; Leu107; Phe138; Val186; Trp162; Asp93	C1=CC(=CC=C1 C=CC2= CC(=CC (=C2) O) O) O	Yes	0.041	228.24	3	3	2.48	67.88
Cycloheximide	-9.2	30-30-30	Phe138; Gly135; Asn51; Gly137	CC1CC(C(=O) C(C1) C(CC2C C(=O) NC(=O) C2) O) C	Yes	0.05	281.35	2	4	1.3	78.47
Gefitinib	-9.7	30-30-30	Leu107; Phe138; Leu48; Asp93; Val150; Trp162; Leu103; Asn51; Gly135	COC1= C(C=C2 C(=C1) N=CN= C2NC3= CC(=C(C=C3) F) Cl) OCCCN 4CCOC C4	Yes	0.027	446.9	7	1	3.92	121.66
Imatinib	-10.9	30-30-30	Ala55; Met98; Leu103; Phe170; Phe138; Leu107; Asn51; Ile104	CC1=C(C=C(C= C1) NC(=O) C2=CC= C(C=C2) CN3CC N(CC3) C) NC4=N C=CC(= N4)	Yes	0.03	606.71	0	8	3.96	179.18

				C5=CN= CC=C5							
--	--	--	--	-----------------	--	--	--	--	--	--	--

Table 4.6: Tabular representation of scores for binding affinity, ADMET and BBB permeability

After docking analysis, these drugs were targeted for the ADMET to check for any violation of the Lipinski rule of five for better results and whether they are able to cross the BBB parameter. Our results demonstrated that all the drugs fitted to the ADMET scores and all of them were able to cross the BBB permeability filter that was done using CBligand. All the docking scores along with the ADMET and BBB scores can be visualized in **Table 4.6**.

4.3.10. MD SIMULATIONS

After the docking analysis for the final confirmational studies, drugs were subjected to MD simulations till 50 nanoseconds to check whether the complexes were stable or not. These simulations will help to identify the expression patterns and the dynamic nature. The pattern of stability was checked by calculating the RMSD plot of the all the complexes with HSP90AB1. The RMSD of all the ligands complexed with protein and the ligands alone was calculated. The comparison of all the complexes with the reference (HSP90AB1-Cephatanthine) revealed that the backbone of complexes (HSP90AB1-resveratrol, HSP90AB1-gefitinib, HSP90AB1-imatinib, HSP90AB1-Cycloheximide) were stable and integrated. There was a slight fluctuation in the starting and the peak intensity reached between 0.30nm and 0.33nm for all the complexes but its decreased eventually thereby showing a stability ranging from 0.15nm to 0.25nm as compared to the reference. A deviation was observed in the beginning up to 20ns but as the simulation time increased the complex started to stabilize themselves and all the complexes achieved defined stability till 50 ns and can be visualized in **Figure 4.8(A)**. The compactness in the protein-ligand complex and the folding capacity of protein over time was calculated using the Rg of 1.7nm. However, a increase in the Rg in case of HSP90AB1-Gefitinb was observed and the peak intensity of 2.70nm was observed at around 43 nanoseconds but the compactness was maintained in all the

structure at an average Rg of 1.8nm and can be seen in **Figure 4.8(B)**. Interaction energy of every complex was measured and it can be preferred from the observations that binding potential of all the four complexes was more as compared to the reference complex **Figure 4.8(C)**. The greater the values in negative terms suggests a stronger binding and more stability. Coming to the RMSF which measure the rate of displacement of atoms around the reference, the stability in the peaks of all the complexes (HSP90AB1-cycloheximide, HSP90AB1-resveratrol, HSP90AB1-Imatinib, HSP90AB1-gefitinib) was more as compared to the reference complex and can be observed from **Figure 4.8(D)**.

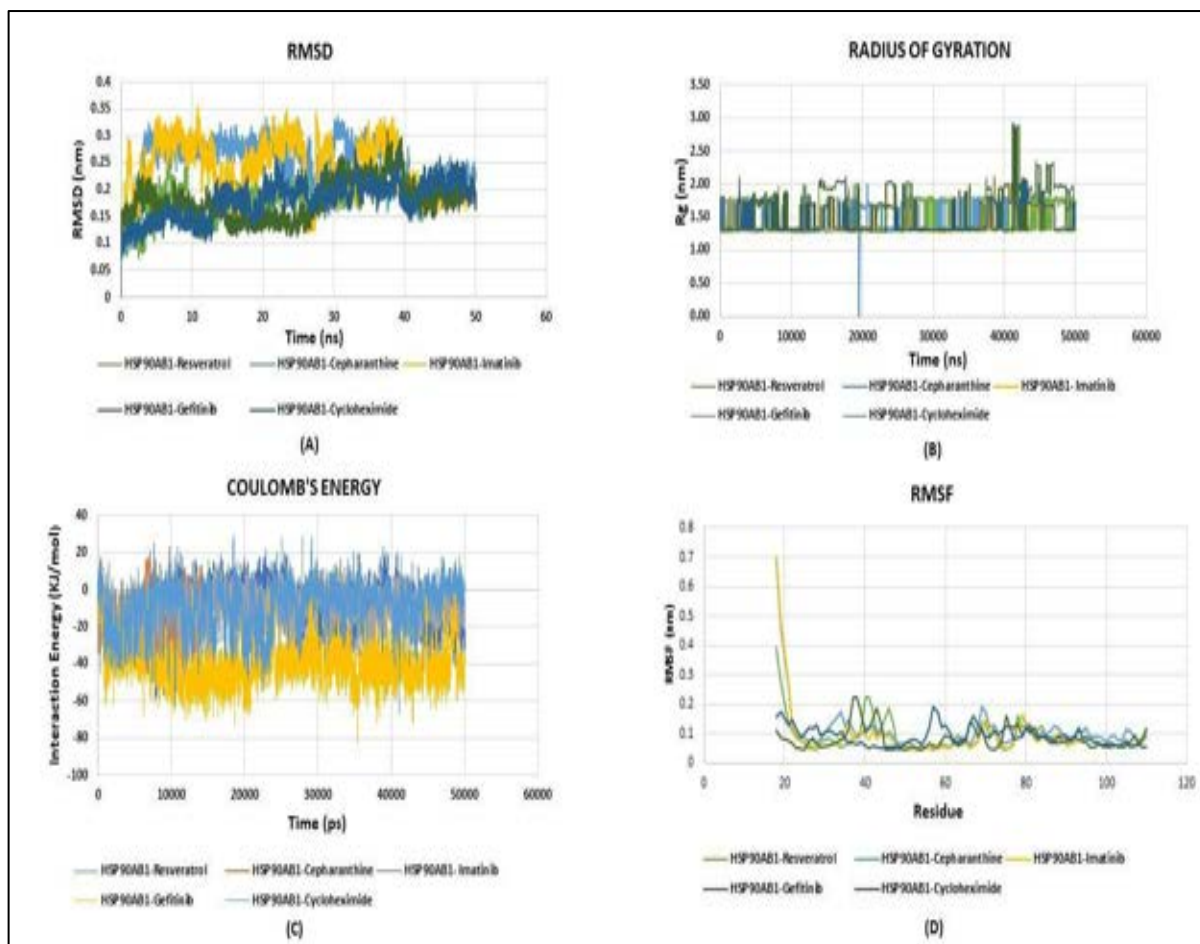


Figure 4.8: (A-D) Plot representing the root mean square deviation (RMSD), Radius of gyration (Rg) of all the complexes, interaction energies and the root mean square fluctuations (RMSF) till 50 ns. (A) Represent the various RMSD of different complexes. RMSD values of the complexes when compared with the reference complex (HSP90AB1-Cepharanthine) showed that the backbone of complexes (HSP90AB1-resveratrol, HSP90AB1-gefitinib, HSP90AB1-imatinib, HSP90AB1-Cycloheximide) were more stable and integrated. (B) Radius of gyration of all the complexes showing the folding capacity of the protein over a period of time and the peak intensity showed a slight deviation of peak value 2.70nm. Rest all the complexes were under the limit and better peaks were observed. (C) Coulombs energy represent the interaction energy of the complexes. Binding affinities of all the four complexes was better than the reference complex. (D) RMSF represents the rate of displacement of atoms around the target atom. Stability can be seen to be more in all the four complexes when compared with the reference complex.

4.4. DISSCUSSION

HSPs comprises a family of proteins that are conserved in both the eukaryotes and prokaryotes and plays significant role in the regulation of apoptosis and autophagy, proteostasis and regulation of polypeptides. They also act to prevent the cells from various stresses like ionizing radiations, heat shock and hypoxia. Coming from the class of molecular chaperones they are involved in

protein folding under normal metabolic conditions and thus, are the enhancers in protein repair during molecular stress. When talking about tumors cells the expression of HSPs is highly elevated as compared to the normal cells. We retrieved the data for both GBM and ependymoma from GEO and also studied the transcriptomic data and further analyzed the integrated pathways, biological processes and therapeutic targets. Starting with the analysis we first identified the overlapping differentially expressed genes in both the tumors. From the list of filtered DEGs, identification of potential HSPs was done using literature mining and from HSPMdb database. Based on Venn analysis, 22 overlapping HSPs were obtained that were called as differentially expressed HSPs.

We constructed a protein-protein interaction network with all the predicted 22 differentially expressed HSPs based on different topological parameters. The hub HSPs obtained after network analysis are known to be the mediators in a variety of biological processes in both glioblastoma and ependymoma. HSP90AA1 one of the hub proteins is found to be overexpressed in IDH-wild type GBMs[334] although the role of HSP90AA1 in ependymoma is still unclear. HSP90AA1 plays significant role in maintaining the integrity of various signaling pathways and resistance to stress-induced apoptosis in normal cells. Another hub protein HSPD1 is known to play an important role in folding of proteins imported from mitochondria or their refolding under mitochondrial stress. Studies have also shown that HSPD1 are involved in many diseases such as neurodegenerative diseases and cardiovascular diseases(Teng et al., 2019). They are also reported to play an important role in cancer development. Very few studies are available on their role in brain tumors, however their expression was seen elevated in meningiomas. Ependymomas do not show any positive immunohistochemical reaction and show lower expression levels of HSPD1. CCT2 (Chaperonin containing tailless complex, TCP) are the members of HSP60 family and their expression is found to be elevated in cancerous brain tissues as compared to normal brain tissues. Studies have shown that the expression of these proteins are elevated in Grade IV glioblastomas and can be used as a diagnostic markers[338]. Role of CCT2 in ependymoma remains still

unexplored. HSP90AB1 comes under the class of HSP90 superfamily and are known to be overexpressed in tumors of glial origin[136]. HSP90AB1 levels are seen to be elevated in recurrent GBMs(Zhang et al., 2005). Expression levels of HSP90AB1 was found to be highly elevated in carcinomas of head and neck and showed poor prognosis along with high mortality rate. Researchers have shown that HSP90AB1 can be a better prognostic factor and therapeutic option in both the malignancies[340]. Gefitinib is also known to induce cell death and decreased cell proliferation in non-small cell lung carcinomas[341]. Imatinib on the other hand is known to be an effective treatment in case of stromal tumors of gastrointestinal origin and in a variety of malignancies(Venkataraman et al., 2023). HSPA1A another class coming from HSP70 family are found to be interacting with endoplasmic reticulum-alpha and causes its increased expression and leads to an increase in cellular proliferation in MCF-7 breast cancer[343]. Higher expression level of HSPA1A are observed in ependymoma[344] suggestive of a better therapeutic targets in combating these lethal tumors.

To better understand the functional aspects of the identified HSPs and what are the mutual role they play in GBMs and ependymoma, different enrichments have been done to predict a relationship of the interconnected dysregulated pathways between these two tumors. Functional enrichment and KEGG pathway analysis revealed the role of these 22 HSPs and how they play an intricate role at biological, molecular and cellular levels along with the pathways on which they act. From the enrichment done at biological levels, out of 22 HSPs, 15 differentially expressed HSPs were involved in protein folding, 6 HSPs were involved in protein stabilization and 5 were involved in chaperone mediated protein complex assembly and chaperone mediated protein folding requiring cofactors. Out of these HSP90AA1, HSP90AB1, HSPD1, HSPA1A and CCT2 were commonly present in every biological process. Studies suggest that HSP90AA1 is exploited by the tumor cells to enhance and support their activation of oncoproteins, comprising of several kinases and TFs[345]. Researchers have seen that the product of HSP90AA1 protein is known to act as a key player in tumor invasion and proliferation[346]. At molecular levels, 11

of the counts were associated with unfolded protein binding, 12 were involved in ATP binding and 8 were involved in ATPase activity. Here also the prevalence of HSP90AB1, HSPA1A, CCT2, HSPD1 and HSP90AA1 was the most even at molecular levels. Coming to the cellular counterpart, out of 22 hub HSPs, 10 were present in extracellular exosomes, 6 were in endoplasmic reticulum and 10 HSPs were present in the membrane. HSP90AA1 was present in almost all the cellular counterpart suggesting its major role in GBMs and ependymoma. The expression of HSP90AA1 is found to be elevated in various cancers and studies have predicted that the therapeutic inhibition of HSP90AA1 results in good prognosis and increased overall survival of lung cancer patients[347]. When we performed the KEGG pathway analysis, we observed that most of the HSPs were involved in protein processing in the endoplasmic reticulum, pathways in cancer and in glioma signaling. [339]. Studies have shown that the activator also acting HSPs in various pathways like the PI3K/AKT/mTORc1[348] and the sonic hedgehog signaling are found to be related with various high-grade tumors of glial origin[349]. These were the common dysregulated pathways identified in GBMs and ependymoma. Studies have defined the role of endoplasmic reticulum (ER) stress in the unfolded protein responses (UFP). These ER stress are the modulators of cancer progression and are known to play an important role in chemotherapeutic resistance in glioblastoma[350]. Some common regulatory signaling pathways such as the Wnt signaling(Manfreda et al., 2023; Misawa-Omori et al., 2023), the sonic hedgehog signaling[353], the IGF-IR signaling and the ERbB signaling are shared in both of these malignancies giving us a better insight of how these both can be targeted from the therapeutic aspects. IGF-IR is known to be involved in epithelial to mesenchymal transitions in both the brain tumors and can be seen as important target[354]. Researchers have also shown that the aberrant levels of the EGFR, Platelet derived growth factor receptors β (PDGFR- β) and the vascular endothelial growth factor receptors-2 (VEGFR-2) are identified as important regulators and important prognostic markers in both the malignancies[303,355,356]. Dysregulated expression levels of the receptor tyrosine kinases (RTKs) and various other growth factors such as the PDGF,

HGF in both these tumors, leads to increased tumor proliferation and can be used as an important prognostic markers(Weiner et al., 1996). Therefore, it can be conferred that the therapeutic side of these 5 HSPs can be explored to counter these malignant brain tumors as they major involvement in their pathology and occurrence.

To further nurture our study and to establish a more concrete connection of the identified HSPs with GBMs and ependymomas, we explored the regulatory signatures of the transcriptomes (TFs and miRNAs). Among the top identified TFs, GATA2 (GATA-binding factor 2) was found to be the most interactive in both the pathologies. GATA2 is known to be the regulator of constitutive PD-L1 and PD-L2 expression in most of the brain tumors[358]. Another interacting TF Forkhead box C1 (FOXC1) is a known conserved TF and play an important role in the tumorigenesis and is also involved in epithelial-to-mesenchymal transitions (EMT) in gliomas[359].Upstream transcription factor 2 (USF2) is known to be a modulators of the cellular proliferation and its silencing can reduce the tumor load in glioblastomas[360]. Among the top interacting miRNAs, hsa-miR-16-5p is known to be involved in the pathogenesis of glioblastoma and astrocytoma however, no study claims the involvement of hsa-miR-26b-5p in ependymomas and glioblastoma, hsa-miR-16-5p are reported to be the regulators of signaling cascades along with WEE1, CHEK1 and MCL1. Here the increased expression of this miRNA, reduced cellular proliferation, increased cell viability, increased the cell cycle arrest and increased response to irradiation and chemotherapy[361]. Another miRNA hsa-miR-26b-5p is known to inhibit the cellular proliferation and EMT in triple negative breast cancer[362]. Also, miR-26b-5p is found to be an important regulator in Burkitt lymphoma cellular growth[363]. We also established a miRNA-TFs-HSPs coregulatory network to understand how these TFs and miRNAs are commanding the HSPs in both of these morbidities. Using an integrative miRNA-TF- HSPs target network we identified several dysregulated miRNAs that were connective to the various HSPs and the associate TFs. GABA, MYC, RFX1 and EGFR were the major TFs that were interconnected with the HSPs along with the miRNAs. MYC is an important TFs family and is composed of TFs c-

myc, Mycn and Mycl. These regulatory TFs are required for the development of the brain and its overexpression induces cellular proliferation in gliomas[364] and medulloblastomas[365,366]. Regulatory factor X1 (RFX1) is known to play an intricate role in causing chemoresistance and recurrence in glioblastoma[367]. However, their role is unknown in ependymomas. From the modules prepared from network, it was found that CCT3 was interacting with E2F1 and DNAJC10. Another module showed interaction of HSP90B1 with BPTF, SREBF1 and NFYA. Through these interactions we can conclude that these HSPs are interacting commonly with regulatory miRNAs and TFs.

In order to understand the potential role of different drugs and to identify putative candidates that can reverse the effect of both GBMs and ependymomas, we analyzed the CREEDS database and the LINC1000 Drug Gene Budger. From the drug screening it was found that 2 drugs were able to reverse the effects of the HSPs whose expressions were upregulated while 11 drugs were able to reverse the effect of the downregulated HSPs. Resveratrol a polyphenol is present in plants such as grapes and peanuts is known to possess properties of antioxidants[368]. Studies have shown that resveratrol have been found to shown suppression activity in various neurological disorders like Alzheimer's disease[369] and Parkinson's disease[370]. Cycloheximide is known to induce paraptosis that is induced by the inhibition of cyclophilins in GBMs[371]. However, the role of cycloheximide in ependymoma remains unclear. Various inhibitors like the ganetespib and cycloheximide is known to induce apoptotic arrest and reduced tumorigenicity targeting HSP90 class in various cancers(Youssef et al., 2023). Cycloheximide is also known to cause differential effect in neuronal and glioma cells that are treated with chemotherapy and radiotherapy[373]. To further validate our results and the drugs obtained we performed the drug ranking and predicted the structural, functional and composite scores of the drugs obtained after the analysis from CREEDS and Drug gene Budger. Imatinib, cytarabine, gefitinib, estradiol, resveratrol, and cycloheximide were predicted as the top 5 drugs. With these observations we considered that resveratrol, cycloheximide, gefitinib and imatinib as the most promising

candidates for this study and the hub HSPs that were found targetable with these drugs were HSP90AB1, CCT2, HSPH1, DNAJC10. We further proceeded the study by identifying the most suitable HSPs candidate amongst all the top HSPs. Using Brain-RNA sequencing data, the expression patterns of the individual HSPs was checked whether the expression levels are higher in glial cells or not as both of these tumors originates from microglial cells within the brain. From our results discussed above, HSP90AB1 was found to be the most promising HSPs and the expression levels were elevated in both the GBM and ependymoma. Studies have shown that inhibition of HSP90AB1 significantly reduced the activity of adenylate cyclase post chronic morphine treatment[374]. Another study identified the role of gallic acid has an inhibitory effect on skin squamous cell carcinomas and reduced expression of HSP90AB1[375]. Expression levels of HSP90AB1 in recurrent glioblastomas. Inhibitor NW457 is known to suppress glioblastoma when given in combination with radiotherapy[376]. This shows that the effective targeting of HSP90AB1 could ideally suppress the activity of both of these tumors.

To validate the drugs identified from CREEDS and DrugGene Budger we performed molecular docking and MD simulations of all the four predicted drugs (gefitinib, imatinib, cycloheximide and resveratrol) against HSP90AB1. Cepharanthine was used as a reference drug to compare to docking scores of our predicted drugs against HSP90AB1[377]. From docking analysis, it was identified that the binding affinities for resveratrol (-9.3 Kcal/mol), cycloheximide (-9.2 Kcal/mol), gefitinib (-9.7 Kcal/mol), imatinib (-10.9 Kcal/mol) were comparatively higher when checked with the reference drug (-9.1 Kcal/mol), suggesting an inhibitory effect of these drugs against HSP90AB1. As the docking results were favorable, we further validated our study using MD simulations at till 50ns. The stability index and the fluctuations in the system and probable result trajectories of all the complexes were seen by applying different parameters during simulations. The parameters used while conducting the analysis were RMSD for all the complexes, RMSF of all the amino acid residues, Rg and the interaction energies of each of the individual complexes. The RMSD of all the complexes was measured between the initial and the

final confirmations of the protein-ligand complexes till 50ns. A stable binding was observed in all the complexes when compared with the reference complex. The peak pattern of RMSF showed us that all the four complexes were in close proximity during fluctuations in amino acids residue when compared with reference complex suggesting a much stronger bonding. When talking about the Rg and the coulombs interaction energy, all the findings showed a much better interactions pattern of HP90AB1 with resveratrol, gefitinib, imatinib and cycloheximide. Overall, these findings were able to nurture the credibility of the results obtained using CREEDS, DrugGene Budger and docking analysis, suggesting the potential therapeutic efficiency of these drugs in therapeutics suppression of GBMs and ependymomas. We also proposed an inhibitory mechanism of how these drugs are acting in the signaling cascades in both the diseases and how targeting HSP90AB1 can mutually suppress both the tumors. A proposed mechanism of these inhibitors can target the HSP machinery has been shown in **Figure 4.9**.

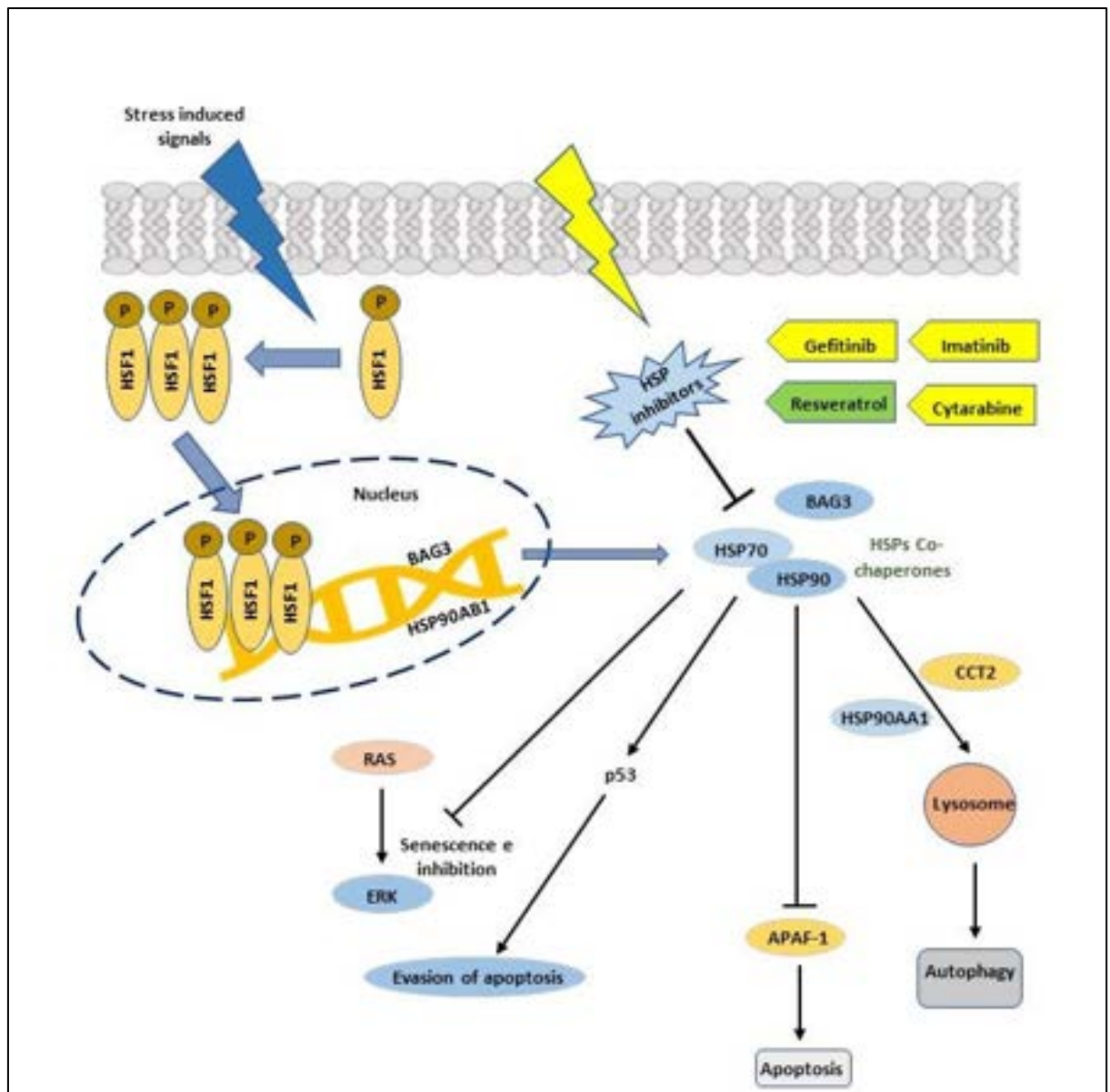


Figure 4.9: Diagrammatic representation of proposed mechanism of inhibitory action of HSPs inhibitors in Heat Shock Protein (HSPs) mediated pathway. Binding of the HSPs inhibitors to HSP70 and HSP90 cochaperone machinery can cause an increased in the level of the apoptotic protease activating factor-1 (APAF-1) which is suppressed under normal conditions. This activation can cause an increase in the levels of the apoptotic machinery. We also hypothesized that gefitinib, imatinib, cytarabine and cycloheximide directly could prevent the binding of cochaperones that are induced in response to stress and hence, promotes autophagy. Gefitinib, imatinib, cytarabine and resveratrol binding to the target HSP causes inhibition of the downstream targets and prevents the binding of HSPs co-chaperones with HSP70 and HSP90 assembly causing cell cycle arrest, increased apoptosis and other cellular processes finally, causing death of tumor cells. Also, these inhibitors could possibly induce senescence and inhibition in the progression of ependymomas and glioblastomas.

4.5. CONCLUSION

This study has tried to identify the molecular mechanism and the common regulatory pathway of HSPs and how they are sharing various transcriptomes and regulatory signatures mutually in GBMs and ependymomas. With our findings we have explored a mechanistic approach to understand the interlink of HSPs in between GBMs and ependymoma. We identified HSP90AB1, HSPA1A, CCT2, HSPD1 and HSP90AA1 as the key candidate HSPs that can be used as therapeutic targets in countering GBMs and ependymomas. With this study we identified HSP90AB1 as a promising candidate in the therapeutic targeting of GBM and ependymomas. We proposed that gefitinib, imatinib, resveratrol and cytarabine could potentially target HSP90AB1 and can promote cell death in both glioblastoma and ependymomas. This study will provide a more mechanistic link of how these two malignancies can be targeted mutually and the interlinked molecular mechanisms. However, more concrete studies are needed how these drugs are actually working against HSP90AB1 in both of the morbidities.

***IN-SILICO* MOLECULAR DOCKING AND
SIMULATION ANALYSIS TO IDENTIFY
NATURAL COMPOUNDS TARGETING HEAT
SHOCK PROTEINS IN BRAIN TUMORS**

CHAPTER V: IN SILICO MOLECULAR DOCKING AND SIMULATION ANALYSIS TO IDENTIFY NATURAL COMPOUNDS TARGETING HEAT SHOCK PROTEINS IN BRAIN TUMORS

5.1 INTRODUCTION

Heat shock proteins are known to be an important category of proteins and are involved in a variety of biological processes and are activated in response to heat shock or any other stimuli[124]. Their machinery is taken up by the malignant cells for their survival and growth. Glioblastomas (GBMs) are Grade IV tumors seen by the World health organization. Chemotherapy and radiotherapy only remain an option and the overall survival of the patient is around 10-14 months. Therefore, more stringent strategies are needed against this morbidity. HSP90 is the most studied class of HSPs are various studies have shown that can be targeted in various cancers[376]. HSP90AB1 expressions are found to be elevated in case of recurrent GBMs along with poor prognosis[339]. Another class HSP70 is also known to target various cancers. Studies have shown that WIN55-212-2 which is a cannabinoid agonist is effective in human glioblastoma cell line U-251 MG[378]. Alkaloids are the valuable category of natural compounds known to possess the property of antioxidants and have been shown to promote cell death in GBM[379]. Papaverin an alkaloid was found to suppress GBM and is a non-narcotic opium alkaloid[380]. Another alkaloid melatonin was found to inhibit the activity of phosphorylation in the MDM2 gene[270,317]. This shows that alkaloids can be an important parameter in the suppression of GBMs and with the current study, we have tried to show the prospects of various alkaloids importantly chelerythrine and cepharanthine as therapeutics in countering GBMs.

5. 2. COMPUTATIONAL METHODS AND METHODOLOGY

5.2.1. DATA SOURCE

Data used in the study were retrieve using NCBI from the gene expression omnibus (GEO) (<https://www.ncbi.nlm.nih.gov/gds>). The gene expression profile was taken from GSE 50161 datasets.

5.2.2. SCREENING OF DIFFERENTIALLY EXPRESSED GENES AND HEAT SHOCK PROTEIN

We used GEO2R which is a web-based interaction tool. GEO2R (<https://www.ncbi.nlm.nih.gov/geo/geo2r>) a web-based interactive tool using the R language limma package. In order to understand the biological aspects, functions were put for the DEGs. Further, P-value <0.05 and the Log Fc were used to filter the DEGs. Prediction of the HSPs was committed through the literature survey.

5.2.3. ENRICHMENT AND PATHWAY ANALYSIS

To understand the cellular, molecular, and biological functions and the various pathways involved with the predicted. The tool used for these enrichment and pathway analyses performed by using SHINYGO (<http://bioinformatics.sdstate.edu/go/>).

5.2.4. MUTATIONAL ANALYSIS OF PREDICTED HSPS

Prediction of the mutational signatures of the identified HSP, cBIOCancer genomic portal was used for the analysis (<https://www.cbioportal.org/>). This tool is helpful in the analysis of the molecular data obtained from the tumorous tissues and for analysis at genetic and epigenetic levels.

5.2.5. COMPOUND SCREENING, ADMET ANALYSIS, AND BBB PERMEABILITY CHECK

For this study, 95 alkaloids were taken from the naturally occurring plant-based anti-cancer compound activity target database (NPACT). Canonical smiles and 3D structures of these

compounds were obtained using PubChem. ADMET was checked using SwissADME. To access the blood-brain permeability (BBB) CBligand (<https://www.cbligand.org/CCGS/>) used in the study.

5.2.6. MOLECULAR DOCKING ANALYSIS

The receptor structure of HSP90AB1 (PDB id: 1UYM) was taken from the RCSB PDB database. Molecular Docking analysis done using the WEBINA software (<https://durrantlab.pitt.edu/webina/>), which is a script running Autodock vina in web browser mode. 65 alkaloids were docked against the identified HSP. The grid box of dimensions, x-axis=30, y-axis=30, and z-axis=30 was taken. Visualization of the structures was done using UCSF chimera (<https://www.cgl.ucsf.edu/chimera/>). Generation of the 3D conformers was done using Discovery Studio 2021.

5.2.7. MOLECULAR DYNAMIC SIMULATION STUDIES

Following docking analysis, all the three compounds were then proceeded for MD simulations studies. MD simulations was performed using GROMACS till 100 ns. The plots were generated for RMSD, RMSF and the radius of gyration.

5.3. RESULTS

5.3.1. DATA COLLECTION AND IDENTIFICATION OF DEGS

The gene expression profile GSE 50161 comprised 13 normal brain samples and 34 GBM samples. From these 9262 genes were filtered based on the P-value and Log Fc. Following the prediction of DEGs, the identification of HSPs was done using the literature survey.

5.3.2. FUNCTIONAL ENRICHMENT AND PATHWAY ANALYSIS OF IDENTIFIED HSPS

Enrichment analysis of the predicted HSPs to determine the molecular, cellular, and biological process was done to identify their role in GBMs. 44 HSPs were targeted for this analysis. Most of the HSPs were involved in processing in the ER and antigen processing in biological enrichment. At molecular levels, most of the HSPs were functioning in chaperone-containing T-complex and the formation of chaperone complexes. At cellular levels, these HSPs were found to be involved in protein folding chaperone assembly and ATPase activator activity. From KEGG analysis, de novo protein folding and chaperone-mediated protein folding were the major pathways in which most of the HSPs were involved. All these enrichments can be seen in **Figure 5.1.**

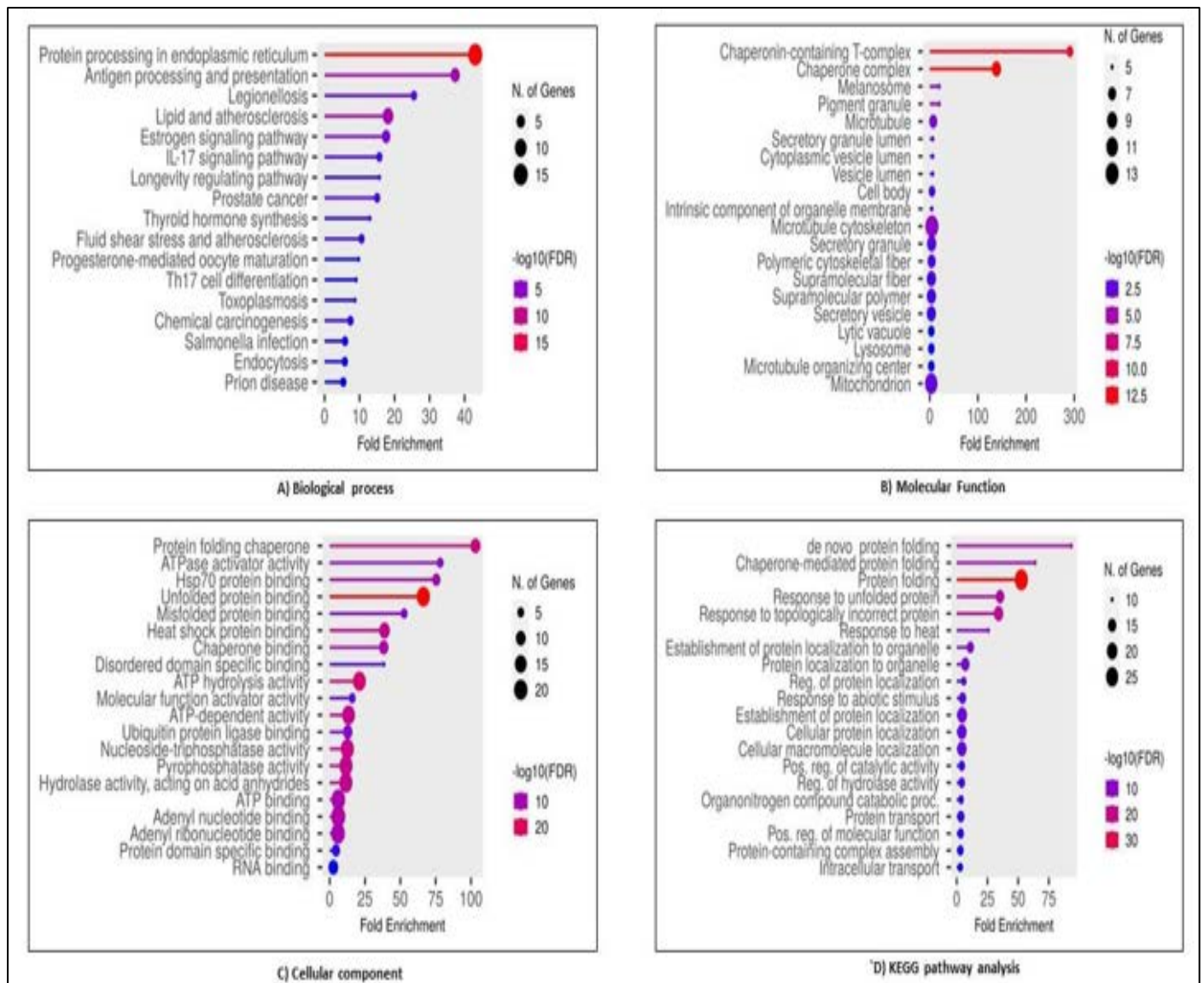


Figure 5.1: Representation of the enrichments of the Heat shock proteins (HSPs) and KEGG analysis.

5.3.3. MUTATIONAL ANALYSIS

All 44 predicted HSPs were subjected to mutational analysis using the cbioportal genomic portal. The rate of mutation was maximum in the case of HSPH1 (3%), HSP90AB1 (1%), and HSPB1 (1%). The mutation identified was of missense type and out of these HSP90AB1 was used for further analysis. The analysis could be visualized in **Figure 5.2**.

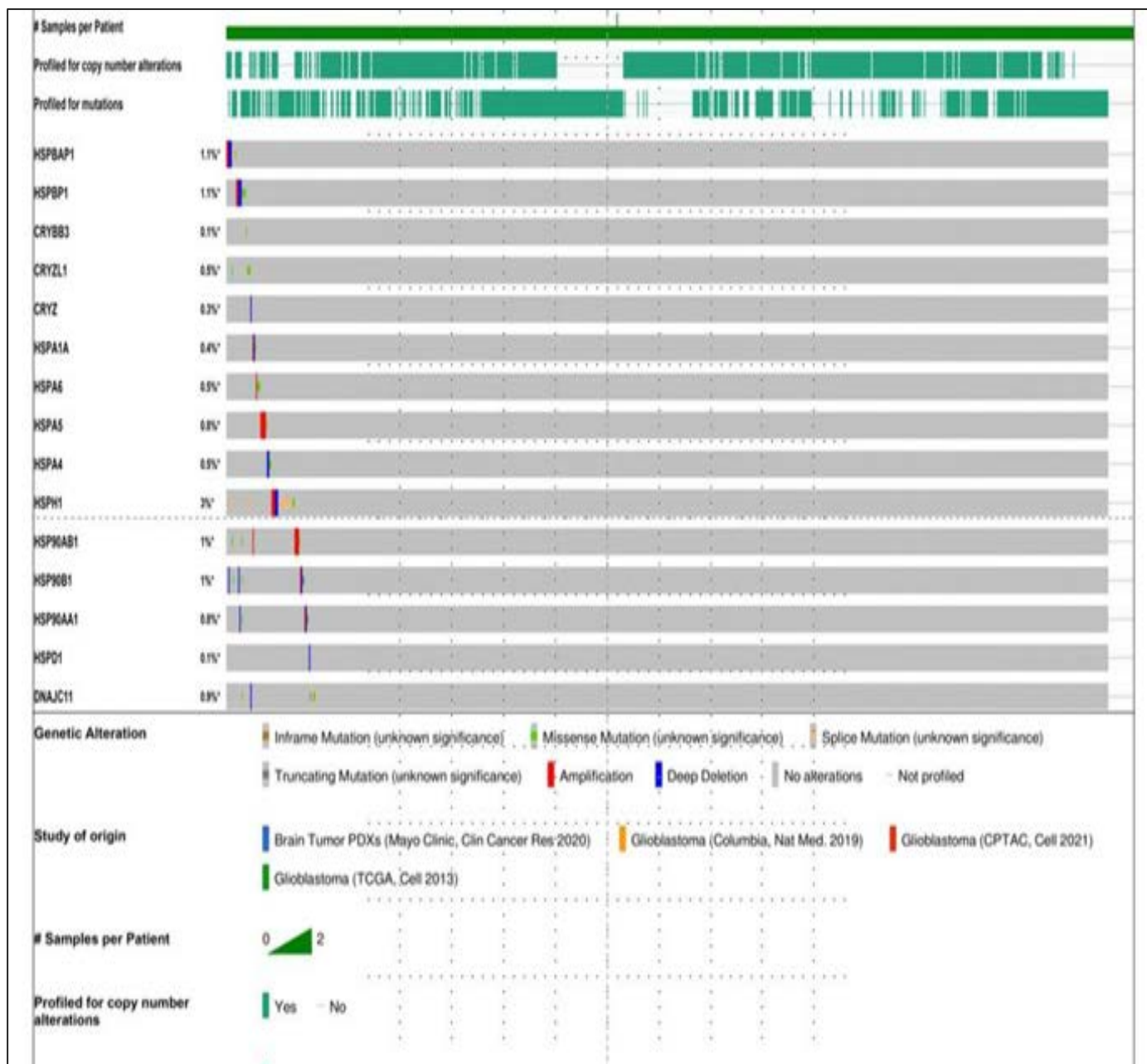


Figure 5.2: Mutational analysis of the identified HSP.

5.3.4. COMPOUND SELECTION, BBB CHECK, AND ADMET ANALYSIS

Using the NPACT library, 95 alkaloids were screened in the preliminary stage. By further applying the BBB and ADMET filters only 65 compounds were found suitable for further analysis using SwissADME and BBB using CBligand. These compounds were selected based on the drug-likeness and bio-availability scores.

5.3.5. MOLECULAR DOCKING ANALYSIS AND INTERPRETATION

Molecular docking analysis of HSP90AB1 with the identified 65 alkaloids was carried out. Removal of any kind of extra residue in conjugation with any kind of heteroatom was done. Docking was conducted for 65 alkaloid was performed. 10 alkaloids represented better binding affinity of above -8.5 Kcal/mol. Binding energy here shows the highest rate of binding of these compounds with HSP90AB1. From docking analysis, it was seen that chelerythrine and

Compounds	Blood brain barrier permeability	SWISS ADM E	Binding Affinity (kcal/mol)	Molecular Mass (<500Da)	Grid size	Hydrogen bond donor	Hydrogen bond acceptor	Partition coefficient (log<5)	Molar refraction (30-150)
Brucine	yes	yes	-8.7	397.45 g/mol	30-30-30	0	4	1.83	115.02
Chelerythrine	yes	yes	-10.3	344.38 g/mol	30-30-30	0	5	3.01	103.6
Isostrychnine	yes	yes	-9.4	340.40 g/mol	30-30-30	2	2	1.90	104.77
Sanguinarine	yes	yes	-9.6	384.42 g/mol	30-30-30	1	2	2.19	103.05
Tomatidine	yes	yes	-9.3	360.43 g/mol	30-30-30	2	6	2.62	102.74
Cryptopleurine	yes	yes	-9.0	390.46 g/mol	30-30-30	0	4	4.14	118.16
Cepharanthine	yes	yes	-10.0	370.43 g/mol	30-30-30	0	5	3.33	108.8
Ellipticine	yes	yes	-8.8	305.37 g/mol	30-30-30	0	2	2.6	96.47
Evodiamine	yes	yes	-9.7	314.43 g/mol	30-30-30	0	1	3.78	95.22
Isotetrandrine	yes	no	-8.8	272.22 g/mol	30-30-30	0	3	2.78	73.57

cepharanthine showed the maximum binding affinities of -10.3 Kcal/mol and -10.0 Kcal/mol. These two were identified to be the most ideal inhibitors against HSP90AB1. Overall scores can be seen in **Table 5.1**.

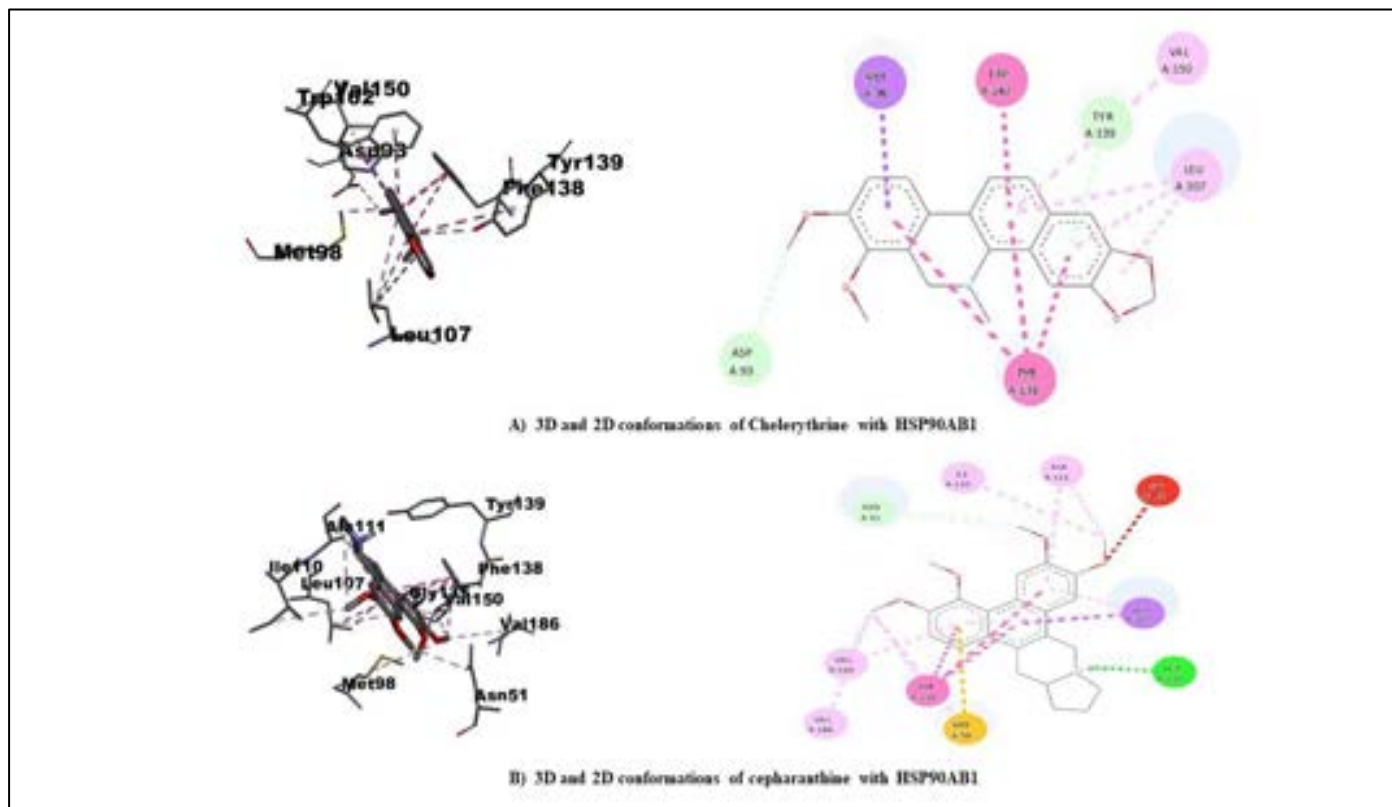
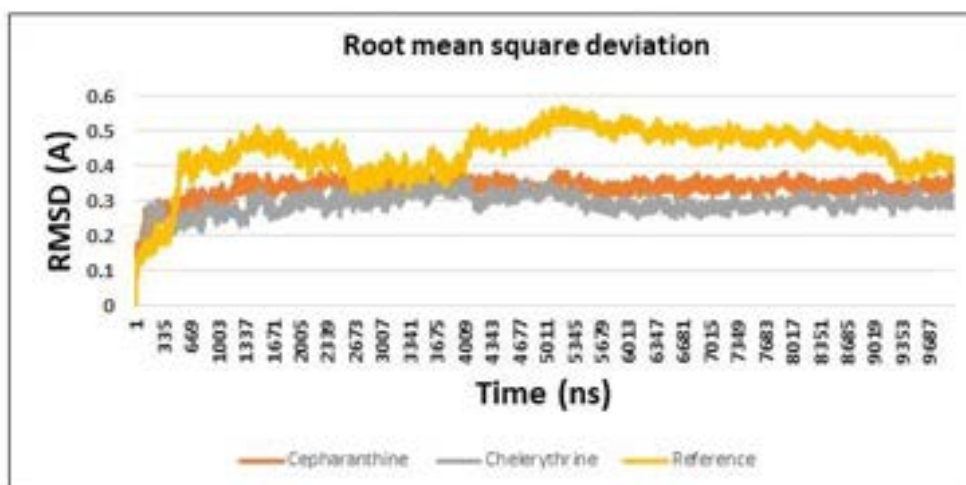


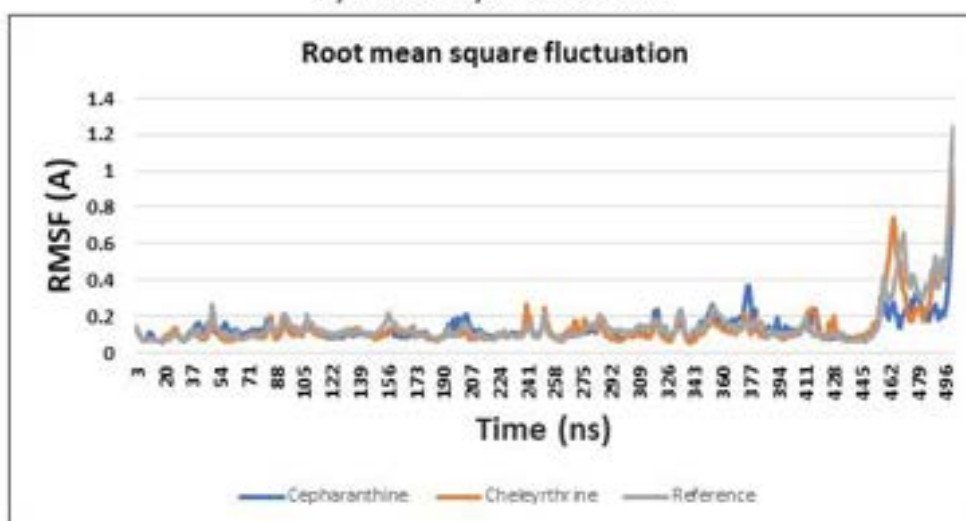
Figure 5.3: Representation of the 3D and 2D conformation of alkaloids

5.3.6. MOLECULAR DYNAMIC SIMULATION ANALYSIS AND INTERPRETATION

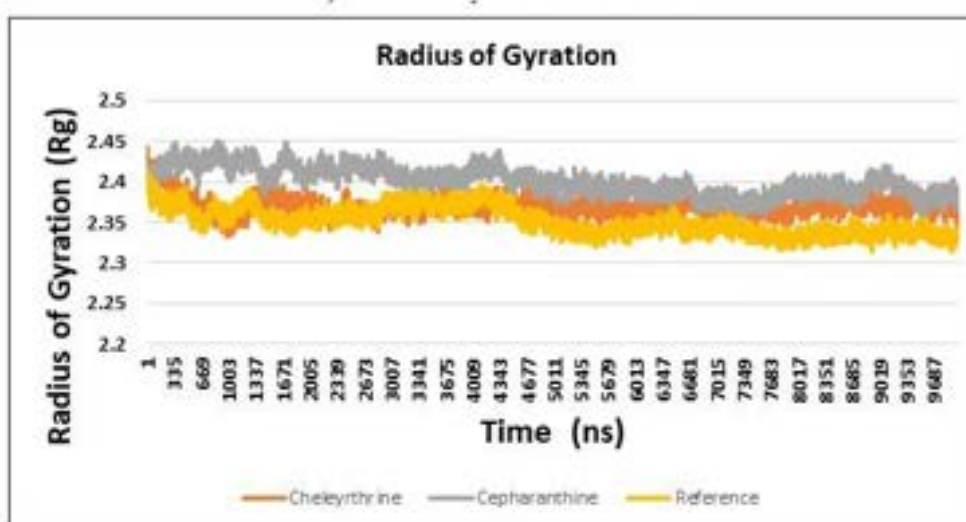
The RMSD, RMSF and Rg of chelerythrine and cepharanthine were calculated against the target protein HSP90AB1 and were compared against the reference compound tomatidine. The simulation was conducted till 100 ns and the peaks were observed against the reference compound tomatidine. The peaks were comparatively stable for chelerythrine-HSP90AB1 and cepharanthine-HSP90AB1 in the beginning and no fluctuations in the peaks were observed.



A) RMSD analysis for HSP90AB1



B) RMSF analysis for HSP90AB1



C) Rg analysis for HSP90AB1

Figure 5.3: Representation of the 3D and 2 D conformation of alkaloids

5.4. DISCUSSION

Despite several advancements chemotherapy and radiotherapy only remains a standard for the treatment of GBMs. Here HSPs can be an important target for therapeutic purposes as they are involved in various signaling cascades. Using the dataset GSE50161, DEGs were screened based on the P-value and Log Fc. From these DEGs, we predicted the potential HSPs using literature mining. Following the identification, functional enrichment comprising the biological processes, cellular components, and molecular functions was done for these HSPs. 44 HSPs were predicted. Mutational analysis was then carried out to determine the rate of mutation frequency of these HSPs in GBMs and the rates were higher for HSPH1, HSP90AB1, HSP90B1, and HSP90AA1[381]. Based on the literature survey and the availability of the HSP90AB1 was found to be the most suitable for this study. Alkaloids were used for targeting HSP90AB1 as they show the property of antioxidants and also possess anti-cancer properties. From ADMET and BBB analysis, only 65 compounds were used for further screening. From docking analysis, it was revealed that chelerythrine[382] and cepharanthine showed the maximum binding affinities of -10.3 Kcal/mol and -10.0 Kcal/mol which can be visualized in

5.5. CONCLUSION AND FUTURE PROSPECTS

Overall, the efficiency and efficacy of HSPS could be further explored to predict their role in the therapeutic targeting of GBMs. Using the expressional signatures of HSP90AB1 and their interaction in GBMs these can be seen from the therapeutic prospects. With this study chelerythrine and cepharanthine were found to be the most promising candidates against HSP90AB1 in GBMs. However, more studies are required to determine how these inhibitors can be fruitful against GBMs.

CHAPTER VI

DISCUSSION, LIMITATIONS OF THE STUDY AND FUTURE PROSPECTS

CHAPTER VI: DISCUSSION, LIMITATIONS OF THE STUDY AND FUTURE PROSPECTS

6.1. DISCUSSION

Brain tumors represents a heterogenous group of tumors arising from abnormal mass of cells in the brain. These tumors are categorized based on the site from which they originate within the brain along with the cells of the origin. Despite various advancements chemotherapy and radiotherapy only remains an option in the therapeutic aspects. Very few inhibitors are available that could possibly counter these tumors with bortezomib and carfilzomib remaining the only options besides radiotherapy. Even after these treatments the overall survival of the patients suffering from glioblastoma and ependymomas remains 10-12 months. Ubiquitination and heat shock proteins shows an electrifying option for the development of new treatments in these brain tumors. Current therapeutics does not guarantee a better survival outcome and the levels of toxicity is higher in case of the drugs that are currently available. Also, the various signaling pathways associated with ubiquitin E3 ligases and HSPs are somewhere interconnected with the ability of the cells to proliferate, metastasize to other regions of the body, autophagy and vascularization. As these two mechanisms, ubiquitination and HSP assembly are the two key processes that are involved in the post-translational modifications, and are required for the correct dumping of the proteins that have been mutated or becomes unnecessary for the proteasome machinery, therefore, targeting these two mechanisms could possibly be an emerging therapeutic approach, and how these HSPs and ubiquitin E3 ligases could be used as biomarkers still needs a spotlight. Even the exact mechanism of how these two machineries is eroded by these abnormal cells and the various pathways associated along with the mechanistic side of them still remains unanswered, and requires further investigations.

The current study was based on the identification of potential ubiquitin E3 ligases that were highly upregulated in glioblastomas and to predict various other E3 ligases that can be possible therapeutic targets in combating GBMs. After the identification of ubiquitin E3 ligase, screening of inhibitors was done based on molecular docking and simulation studies. The second part of the study was based on the prediction of HSPs that were mutually occurring in GBMs and ependymomas, and also to identify the various regulatory signatures that were associated with them. This part was further preceded with the identification of various inhibitors that could possibly target the predicted HSP in both GBMs and ependymomas. The third part of the study brings into spotlight the identification of various natural compounds can actually target the predicted HSPs from part second.

In the initial steps, we utilized the microarray expression data from different datasets, and the extraction of this data was done using the gene expression omnibus. We then identified the various differentially expressed genes based on the parameters like P-value and Log Fc. After the confirmation of the DEGs, screening of the ubiquitin E3 ligases was done using the computational tools Ubinet and Ubibrowser. Venn analysis was also done to screen the most common occurring ubiquitin E3 ligases in all the three datasets. Based on the preliminary screening, 21 ubiquitin E3 ligases were taken. The mutational analysis and expression analysis of all these ubiquitin E3 ligases was done to identify the ligase that was showing the highest levels of expression in GBM. We then performed the functional enrichment and pathway analysis to check the various regulatory pathways in GBMs. MDM2 was identified as the most promising candidate E3 ligase from our study. BRCA1, TRIM22, TRIM24, UBE3A and RNF41 were some of the other E3 ligases that were identified but the best results were shown by MDM2. We targeted MDM2 with various alkaloids and studied their inhibitory effects based on the molecular docking studies and molecular dynamic simulation studies. Evodiamine and sanguinarine were

identified as the most promising candidates based on docking and simulation studies that were showing the highest level of interactions with MDM2. We therefore proposed that evodiamine and sanguinarine could potentially target the p53-MDM2 signaling axis in GBMS. The binding of either these of them would possibly prevent the activation of MDM2 by p53, the machinery which is taken up by cancer cells and therefore can lead to increased apoptosis, autophagy and finally cell death.

The second part of the study was based on the prediction of a common regulatory HSP in both GBMs and ependymoma. As HSPs are a diverse class of proteins that are activated in response to any kind of cellular stress, however, the exact mechanism still remains a question to answer. We performed the literature survey and used the HSPMDB database to screen all the HSPs that were present in the DEGs. We identified that the HSP90AB1 was the most ideal HSPs for the therapeutic targeting in both GBMs and ependymomas. We also identified the various regulatory pathways and the proteins interconnected in both the malignancies at transcriptomic levels. hsa-miR-16-5p, hsa-miR-26b-5p and hsa-miR-92a-3p were identified as the most potential regulatory miRNAs in both GBMs and ependymoma that could be used as potent biomarkers. Another finding revealed that GABA, MYC, RFX1 and EGFR were the major interconnected transcription factors in both of these tumors. We also conducted the PPI network analysis to identify the hub proteins, and we screened 6 hub proteins from this analysis. Based on the drug ranking and CoDReS analysis, we screened inhibitors that could possibly target HSP90AB1. For the final confirmations of the screened inhibitors, molecular docking and simulation studies were performed till 50 nanoseconds, and based on these finding Gefitinib, imatinib, resveratrol, and cytarabine were identified as the most promising candidate drugs that could possibly be seen as therapeutic options in countering mutually both GBM and ependymomas. We proposed a mechanism of how these drugs could possibly break the HSP70-HSP90 chaperone interactions,

and could regulate the various downstream targets. This break in the interaction further leads to an increased level of autophagy, mitophagy, decreased cell proliferation, invasion and finally leading to the death of cancerous cells.

Another important finding of the study was the identification of putative alkaloids chelerythrine and cepharanthine that could possibly be used as natural inhibitors in targeting HSP90AB1. From the mutational analysis and functional enrichment analysis it was identified that HSP90AB1 was involved in various major regulating pathways. We used the NPACT library to screen various alkaloids and further used these alkaloids after passing them through the BBB permeability analysis and ADMET analysis. Validation of how these compounds were actually targeting the predicted HSP90AB1 and the various possible number of interactions was done using molecular docking and dynamic simulation studies. After plotting the graphs for the final RMSD, RMSF and Rg till 100 ns, we came to conclusion that cepharanthine and chelerythrine could be the promising candidates in the natural therapeutic in glioblastoma suppression.

Overall summarization of the study showed various significant outcomes that were achieved from this work. The most interesting finding was the role of various ubiquitin E3 ligases specifically the MDM2 E3 ligases and its interaction in GBM p53-MDM2 signaling. Another important finding revealed the role of HSP90AB1 in the suppression of GBMs and ependymomas and how various inhibitors could possibly target these HSPs. All the mechanism and summarization of this study is shown in **Figure 6.1**. Despite all the findings, experimental studies are still necessary to understand the complete role and how these proposed drugs are actually targeting the ubiquitin E3 ligases and HSPs.

6.2. LIMITATIONS OF THE STUDY

The present study has some of the limitations. This study is entirely based on the computational analysis based on the utilization of different tools and filters for result interpretations and analysis. However, the result may slightly vary based on different tools and software applied during various stages of screening of different drugs. Also, these proposed drugs and candidates' genes needs wet lab validations for their final confirmation either *in-vitro* or *in-vivo*. This validation will be able to show the efficacy of these predicted candidate drugs and how they showing the mechanism of action, BBB permeability factors and other downstream and upstream targets.

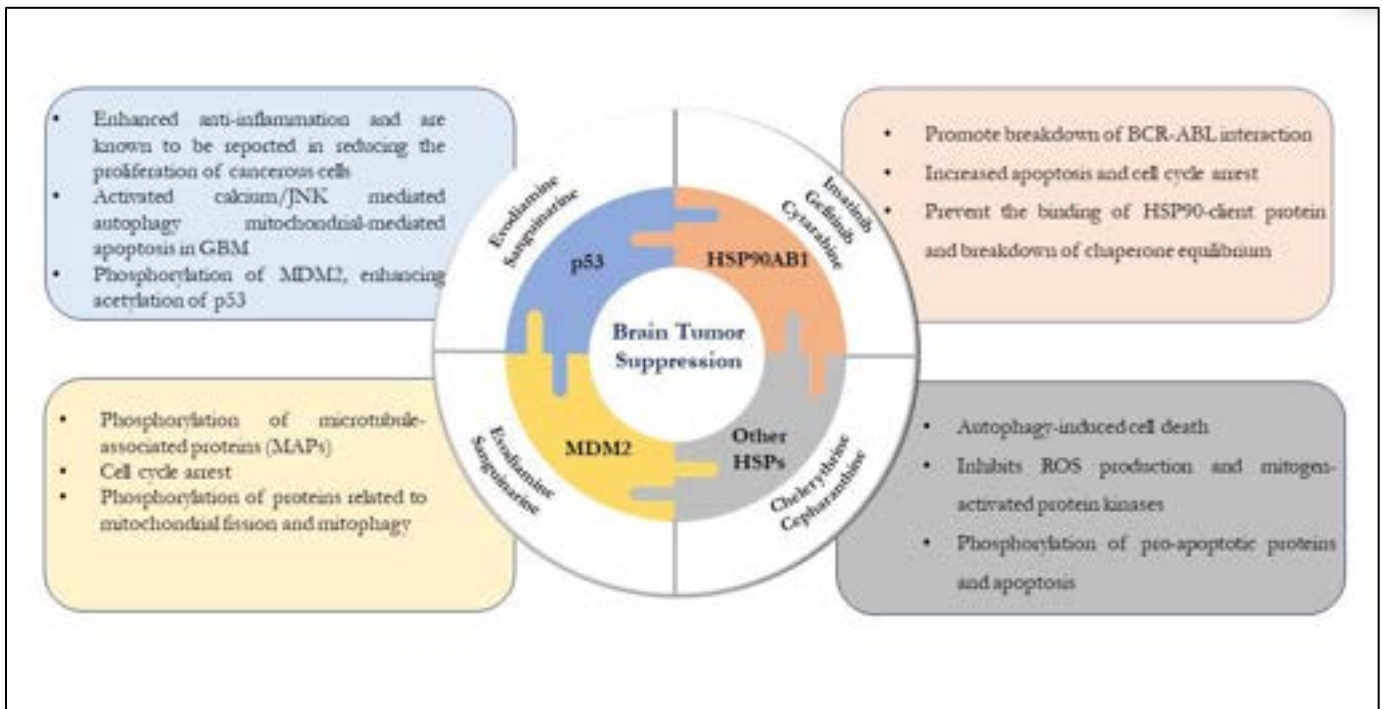


Figure 6.1: The function of various signaling targets associated with glioblastoma and endependymomas and the drugs targeting them.

6.3. FUTURE PROSPECTS

- Through the integrated studies and using various computational analysis tools, identification of the putative ubiquitin E3 ligases and heat shock proteins would possibly bring in spotlight the therapeutic targeting of them with reduced burden on the use of cytotoxic drugs that actually even kills healthy cells.
- The findings from the study would actually bring a breakthrough in the development of new therapeutic strategies by targeting the ubiquitin E3 ligases and HSPs and the exploration of interconnected pathways will open more therapeutic opportunities in the therapeutic suppression of these morbidities.
- This study has identified the role of various potential biomarkers that can be further explored for the development of novel therapeutic avenues in GBMs and ependymomas.
- The study pipeline and the methodology adopted would be extremely useful for identifying the therapeutic capacity of new drugs and the use of natural inhibitors and small molecules in combating brain tumors.

ANNEXURES

Annexure 1: Representation of various ubiquitin E3 ligases present in datasets GSE4290, GSE50161, and GSE 104291

	GSE4290 (89)	GSE 50161 (50)	GSE 104291 (42)
Ubiquitin E3 Ligases	<p>UHRF1, DTL, MDM2, TRIM5, FBXO4, CDCA3, NEDD4</p> <p>, UBE3C, TRIM22, SOCS3, TRIM38, BRCA1, MAP3K1, ITCH, TRAF4, SMURF2, CBL, DYRK2, RBCK1, SIAH1, BARD1, ARID1B, CCNB1P1, TANK, RNF216, HUWE1, RBBP6, RNF115, CNOT4, CHFR, RNF40, MKRN1, RLIM, VHL, RAD18, TRIM13, DDB2, KLHL20, MIB2, SKP2, CBLB, TRIM25, WWP2, TNFAIP3, SH3RF1, TRAF2, TRIM21, RAG1, MIB1, RNF138, TRAF6, XIAP, F2R1, TRIM65, DCAF1, RNF4, SMURF1, KCTD10, FBXO45, FBXO21, RBX1, WWP1, RNF2, RCHY1, TRIM32, PJA2, RNF43</p> <p>FBXO3, MYLIP, RNF14, TRIM62, TRAF3, STUB1, RNF8, CDC34, RFFL, FBXW11, UBE4B, TRIM17, CRBN, RNF220, TRIM37, TRIM9, TRIM24, KLHL2, RNF41, LNX1, FBXO2, FBXW7, UBE3A, NEDD4L</p>	<p>RNF220, TRIM25, TANK, RBCK1, MDM2, SKP2, STUB1, TRIM21</p> <p>RNF41, ITCH, FBXD4</p> <p>RFWD3, RAD18</p> <p>BRCA1, BARD1, TRIM24, TRIM5, TRIM37, DTL, CDCA3, CDC20, NEDD4, TNFAIP3</p> <p>RNF8, CRBN</p> <p>RNF13, UBE3A</p> <p>TRAF3, PELI1</p> <p>TRIM17, SMURF1</p> <p>MYLIP, UBE4B, CHFR, RHOTB1</p> <p>RNF43, BIRC2</p> <p>TRIM38, CBLB</p> <p>TRIM22, WWP1</p> <p>RLIM, DDB2, PJA2</p> <p>FBXO28, CBL, HUWE1, BIRC3, NEDD4L</p>	<p>TRIM21, TANK, TRIM37, BRCA1, TRIM38, DTL, RAD18, FBXO4, TRIM5, UBE3C, RBCK1, MIB1, RNF138, TNFAIP3, CDC20, BIRC2, MDM2, TRIM22, RNF41, MYLIP, MAP3K1, TRIM25, DDB2, FBXO28, SIAH1, TRAF6, ARID1B, CNOT4, TRIM62, TRIM9, NEDD4, TRIM2, BRAP, CISH, SMURF2, FBXO31, CCNB1IP1</p> <p>, ASB2, SKP2, FBXO32, TRIM24, UBE3A</p>

Annexure 2: Tabular representation of common interacting ubiquitin E3 ligases filtered using Venn analysis

Names	Total	Elements
GSE 104291; GSE 4290; GSE 50161	21	RNF138, BRCA1, TNFAIP3, SKP2, DTL, TRIM5, TRIM21, MYLIP, MDM2, DDB2, NEDD4, TRIM37, RAD18, RBCK1, RNF41, TRIM24, TRIM22, TRIM38, TRIM25, TANK, UBE3A, CDCA3, STUB1, UBE4B, BARD1, CBLB, WWP1, RNF43, CHFR, PJA2, RNF220, NEDD4L, TRAF3, CBL, RNF8, CRBN, TRIM17, SMURF1, HUWE1, RLIM, ITCH
GSE 4290; GSE 50161	20	STUB1, UBE4B, BARD1, CBLB, WWP1, RNF43, CHFR, PJA2, RNF220, NEDD4L, TRAF3, CBL, RNF8, CRBN, TRIM17, SMURF1, HUWE1, RLIM, ITCH
GSE 104291; GSE 4290	11	UBE3C, MIB1, FBXO4, TRIM9, TRIM62, CNOT4, SMURF2, TRAF6, SIAH1, ARID1B, MAP3K1
GSE 104291; GSE 50161	3	CDC20, FBXO28, BIRC2

Annexure 3: Tabular representation of various alkaloids with their BBB scores and ADMET profiling

Final List of alkaloids crosses BBB												
PubChem Id	Alkaloid	Canonical SMILES	SV_M_A_C_C_S_F_P_B_B_S_c_o_r_e	B_B_B_p_r_e_d_i_c_t_o_r	B_B_B_S_c_o_r_e	BBB_SW_ISS_ADM_E	MOLECULAR MASS (<500Da)	H-BOND DONOR (<5)	H-BOND ACCEPTOR (<10)	OCTAL WATER PARTITION COEFFICIENT (log<5)	MOLA R REFRACTIVITY (40-130)	LIPINSKI RULE
10723258	3,5'-dihydroxythalifabramine	CN1CCC2=C3C1CC4=C(C(=C(C=C4C3=C(C(=C2O)OC)OC)OC)OC5=CC=C(C=C5)C6C7=CC(=C(C(=C7CCN6C)O)OC)OC	0.044	yes	1.22	no	684.77 g/mol	3	11	4.72	197.55	No; 2 violations

10170	Berbamine	<chem>CN1CCC2=CC(=C3C=C2C1CC4=CC=C(C=C4)OC5=C(C=CC(=C5)CC6C7=C(O3)C=C(C=C7CCN6C)OC)OC)OC</chem>	0.036	YES	294	no	608.72 g/mol	1	8	5.15	181.6	Yes; 1 violation
442021	Brucine	<chem>COC1=C(C=C2C(=C1)C34CCN5C3CC6C7C4N2C(=O)CC7OCC=C6C5)OC</chem>	0.064	YES	474	yes	394.46 g/mol	0	5	1.84	114.04	Yes; 0 violation
161215	Brucine N-oxide	<chem>COC1=C(C=C2C(=C1)C34CCN+15(C3CC6C7C4N2C(=O)CC7OCC=C6C5)[O])OC</chem>	0.082	YES	406	no	410.46 g/mol	0	5	0.49	117.41	Yes; 0 violation
2703	Chelerythrine	<chem>C[N+1]=C2C(=C3C=CC(=C1C3=CC4=CC5=C(C=C42)OCO5</chem>	0.058	YES	412	yes	348.37 g/mol	0	4	3.02	101.6	Yes; 0 violation
82143	Cryptolepine	<chem>CN1C2=CC=C=C2C=C3C1=C4C=CC=CC4=N3</chem>	0.115	YES	398	yes	232.28 g/mol	0	1	3.29	76.01	Yes; 0 violation

73481	Fangchinoline	<chem>CN1CCC2=CC(=C3C=C2C1CC4=CC=C(C=C4)OC5=C(C=CC(=C5)CC6C7=C(O3)C=C(C=C7CCN6C)OC)OC)OC</chem>	0.036	YES	296	no	608.72 g/mol	1	8	5.16	181.6	Yes; 1 violation
3565	Harmalol	<chem>CC1=NCCC2=C1NC3=C2C=C(C=C3)O</chem>	0.046	YES	516	yes	200.24 g/mol	2	2	1.99	64.76	Yes; 0 violation
5281404	Harmane	<chem>CC1=NC=CC2=C1NC3=CC=C(C=C23</chem>	0.105	YES	514	yes	182.22 g/mol	1	1	2.7	58.57	Yes; 0 violation
5280953	Harmine	<chem>CC1=NC=CC2=C1NC3=C2C=C(C=C3)OC</chem>	0.058	YES	521	yes	212.25 g/mol	1	1	2.78	65.06	Yes; 0 violation
68094	Harmol	<chem>CC1=C2C(=C3C=CC(=O)C=C3N2)C=CN1</chem>	0.037	YES	457	yes	198.22 g/mol	2	0	1.86	61.39	Yes; 0 violation
197835	Hydrastine	<chem>CN1CCC2=CC3=C(C=C2C1C4C5=C(C(=C1C(=C5)OC)OC)C(=O)O4)OCO3</chem>	0.061	YES	411	yes	383.39 g/mol	0	7	2.55	103.38	Yes; 0 violation

11024113	Isostrychnine	<chem>C1CN2CC(=CCO)C3CC2C14C5C3=CCC(=O)N5C6=CC=CC=C46</chem>	<u>0.18</u> 3	Y E S	<u>5</u> + <u>1</u> <u>1</u>	yes	<u>334.41</u> g/mol	1	3	<u>1.85</u>	<u>102.77</u>	Yes: <u>0</u> violation
4072580	Mahanimbine	<chem>CC1=CC2=C(C=C1)NC3=C2C=CC4=C3C=CC(O4)(C)CCC=C(C)C</chem>	<u>0.09</u> 4	Y E S	<u>4</u> + <u>5</u> <u>5</u>	no	<u>331.45</u> g/mol	1	1	<u>5.63</u>	<u>108.45</u>	Yes: <u>1</u> violation
167963	Mahanimbine	<chem>CC1=CC2=C(C3=C1OC(C=C3)(C)CCC=C(C)C)NC4=CC=CC=C42</chem>	<u>0.09</u> 4	Y E S	<u>4</u> + <u>5</u> <u>6</u>	no	<u>331.45</u> g/mol	1	1	<u>5.62</u>	<u>108.45</u>	Yes: <u>1</u> violation
36689305	Mahanine	<chem>CC1=CC2=C(C3=C1OC(C=C3)(C)CCC=C(C)C)NC4=C2C=CC(=C4)O</chem>	<u>0.02</u> 2	Y E S	<u>4</u> + <u>6</u> <u>1</u>	no	<u>347.45</u> g/mol	2	2	<u>5.2</u>	<u>110.48</u>	Yes: <u>0</u> violation
10105653	Marcanine A	<chem>CC1=CC(=O)NC2=C1C(=O)C3=CC=CC=C3C2=O</chem>	<u>0.10</u> 6	Y E S	<u>3</u> + <u>0</u> <u>9</u>	yes	<u>239.23</u> g/mol	1	3	<u>1.72</u>	<u>65.34</u>	Yes: <u>0</u> violation

91466	Matrine	<chem>C1CC2C3CCC4C3C(CCC4)CN2C(=O)C1</chem>	<u>0.12</u> 1	Y E S	<u>5</u> + <u>0</u> <u>2</u>	yes	<u>248.36</u> g/mol	0	2	<u>1.79</u>	<u>79.59</u>	Yes: <u>0</u> violation
124256	N-(4-hydroxyundecanoyl)anabasine	<chem>CCCCCCCC(CCC(=O)N1CCC(CC1)C2=CN=C(C=C2)O</chem>	<u>0.09</u> 8	Y E S	<u>4</u> + <u>5</u> <u>3</u>	yes	<u>346.51</u> g/mol	1	3	<u>3.78</u>	<u>107.37</u>	Yes: <u>0</u> violation
390526	Neocryptolepine	<chem>CN1C2=CC=C(C=C2)C3=C2C=C3C1=NC4=CC=CC=C43</chem>	<u>0.15</u> 8	Y E S	<u>3</u> + <u>8</u> <u>2</u>	yes	<u>232.28</u> g/mol	0	1	<u>3.47</u>	<u>76.01</u>	Yes: <u>0</u> violation
162334	N-n-octanoylnornicotine	<chem>CCCCCCCC(=O)N1CCCC1C2=CN=CC=C2</chem>	<u>0.12</u> 2	Y E S	<u>4</u> + <u>9</u> <u>4</u>	yes	<u>274.40</u> g/mol	0	2	<u>3.35</u>	<u>86.98</u>	Yes: <u>0</u> violation
275196	Noscapine	<chem>CN1CCC2=CC3=C(C(=C2)C1C4C5=C(C(=C(C=C5)OC)OC)C(=O)O4)OC)OC3O</chem>	<u>0.04</u> 2	Y E S	<u>3</u> + <u>7</u>	no	<u>413.42</u> g/mol	0	8	<u>2.55</u>	<u>109.88</u>	Yes: <u>0</u> violation
4680	Papaverine	<chem>COC1=C(C(=C(C=C1)CC2=NC=CC3=CC(=C(C=C32)OC)OC)OC</chem>	<u>0.09</u> 2	Y E S	<u>4</u> + <u>7</u> <u>6</u>	yes	<u>339.39</u> g/mol	0	5	<u>3.32</u>	<u>97.16</u>	Yes: <u>0</u> violation
5983	Physostigmine	<chem>CC12CCN(C1N(C3=C2C=C(C=C3)OC(=O)NC)C)C</chem>	<u>0.14</u>	Y E S	<u>5</u> + <u>0</u> <u>3</u>	yes	<u>275.35</u> g/mol	1	3	<u>1.68</u>	<u>84.93</u>	Yes: <u>0</u> violation

5281408	Rhynco phylline	<chem>C=CC1C(=C OC)C(=O)OC)C 4=CC=CC=C4N C3=O</chem>	0.06	Y E S	3 . 9	yes	384.47 g/mol	1	5	2.46	113.39	Yes: 0 violation
13422573	Rohituki ne	<chem>CC1=CC(=O)C 2=C(O1)C(=C/ C=C2O)O)C3C CN(CC3O)C</chem>	0.06 8	Y E S	3 . 2 7	no	332.33 g/mol	0	4	2.88	94.68	Yes: 0 violation
5154	Sanguin arine	<chem>C[N+]=C2C(= C3C=CC4=C(C 3=C1)OCO4)C =CC5=CC6=C(C=C52)OCO6</chem>	0.11 5	Y E S	4 . 1 3	yes	334.41 g/mol	0	3	2.09	101.05	Yes: 0 violation
441071	Strychni ne	<chem>C1CN2CC3=C COC4CC(=O)N 5C6C4C3CC2C 61C7=CC=CC= C75</chem>	0.12 8	Y E S	5 . 2 5	yes	622.75 g/mol	0	8	5.41	186.07	Yes: 1 violation

73078	Tetrandr ine	<chem>CN1CCC2=CC(=C3C=C2C1CC 4=CC=C(C=C4) OC5=C(C=CC(=C5)CC6C7=C(O3)C(=C(C=C7 CCN6C)OC)OC)OC)OC</chem>	0.05 6	Y E S	3 . 1 5	no	413.64 g/mol	2	3	4.67	127.23	Yes: 1 violation
12442871	Tomatid enol	<chem>CC1CCC2(C(C 3C(O2)CC4C3(CCC5C4CC=C 6C5(CCC(C6)O)C)C)NC1</chem>	0.13	Y E S	4 . 5	yes	415.65 g/mol	2	3	4.9	127.7	Yes: 1 violation
65576	Tomatidi ne	<chem>CC1CCC2(C(C 3C(O2)CC4C3(CCC5C4CC6 C5(CCC(C6)O)C)C)NC1</chem>	0.10 5	Y E S	4 . 5 1	yes	354.44 g/mol	1	4	2.61	103.74	Yes: 0 violation
15376	Vincami ne	<chem>CCC12CCCN3 C1C4=C(CC3) C5=CC=CC=C5 N4C(C2)(C(=O) OC)O</chem>	0.04 7	Y E S	4 . 8 8	yes	265.31 g/mol	1	3	2.88	80.13	Yes: 0 violation
160597	(-)- anonain e	<chem>C1CNC2CC3= CC=CC=C3C4= C2C1=CC5=C4 OCO5</chem>	0.11	Y E S	5 . 4 3	yes	365.42 g/mol	2	5	2.96	109.37	Yes: 0 violation
161749	(+)- tylophori nidine	<chem>COC1=CC2=C(C=C1)C3=C(C N4CCCC4C3O) C5=CC(=C(C=C C52)O)OC</chem>	0.04 9	Y E S	4 . 2 3	yes	363.45 g/mol	0	4	4.07	112.67	Yes: 0 violation
639288	(R)- antofine	<chem>COC1=CC2=C(C=C1)C3=C(C C4CCCN4C3)C 5=CC(=C(C=C5 2)OC)OC</chem>	0.09 8	Y E S	5 . 1 8	yes	377.48 g/mol	0	4	4.35	117.48	Yes: 0 violation

92765	(R)- cryptoplu reine	<chem>COC1=CC2=C(C=C1)C3=C(C4CCCCN4C3)C5=CC(=C(C=C5)OC)OC</chem>	0.07 6	Y E S	5 + 1 4	yes	393.48 g/mol	0	5	4.04	119.16	Yes; 0 violation
92114	(R)- tylophori ne	<chem>COC1=C(C=C2C(=C1)C3=C(C4CCCC4C3)C5=CC(=C(C=C5)2)OC)OC)OC</chem>	0.08	Y E S	4 + 9 4	yes	409.47 g/mol	1	5	3.47	120.75	Yes; 0 violation
373661	(S)- tyloindici ne I	<chem>COC1=C(C=C(C=C1)C2=CN3CCCC3C=C2C4=CC(=C(C=C4)OC)OC)O)OC</chem>	0.02 4	Y E S	4 + 2 3	yes	250.25 g/mol	0	3	2.38	74.15	Yes; 0 violation
9881423	9- methoxy canthin- 6-one	<chem>COC1=CC2=C(C=C1)C3=C4N2C(=O)C=CC4=NC=C3</chem>	0.11 6	Y E S	4 + 6 7	yes	266.25 g/mol	0	3	1.72	77.52	Yes; 0 violation

44593495	9- methoxy canthin- 6-one 3N- oxide	<chem>COC1=CC2=C(C=C1)C3=C4N2C(=O)C=CC4=[N+](C=C3)O-</chem>	0.12 1	Y E S	4 + 3 5	yes	240.26 g/mol	2	3	2.15	69.95	Yes; 0 violation
5375436	beta- carbolin e-1- propioni c acid	<chem>C1=CC=C2C(=C1)C3=C(N2)C(=NC=C3)CCC(=O)O</chem>	0.04 9	Y E S	4 + 1 8	yes	220.23 g/mol	0	2	2.39	67.66	Yes; 0 violation
97176	canthin- 6-one	<chem>C1=CC=C2C(=C1)C3=C4N2C(=O)C=CC4=NC=C3</chem>	0.13 7	Y E S	4 + 8 2	yes	305.41 g/mol	2	3	3.43	90.52	Yes; 0 violation
1548943	Capsaici n	<chem>CC(C)C=CCCCC(=O)NCC1=CC(=C(C=C1)O)OC</chem>	0.06 4	Y E S	4 + 1 6	yes	331.36 g/mol	1	5	0.53	91.35	Yes; 0 violation
637173	Cephalo taxine alpha-N- oxide	<chem>COC1=CC23C CC(N+)[2](CCC4=CC5=C(C=C4)C3C1O)OCO5]O-</chem>	0.06 8	Y E S		no	331.36 g/mol	1	5	0.53	91.35	Yes; 0 violation
10404434	Cephalo taxine beta-N- oxide	<chem>COC1=CC23C CC(N+)[2](CCC4=CC5=C(C=C4)C3C1O)OCO5]O-</chem>	0.06 8	Y E S		no	606.71 g/mol	0	8	5.36	179.15	Yes; 1 violation
10206	Cephara nthine	<chem>CN1CCC2=CC3=C(C4=C2C1CC5=CC=C(C=C5)OC6=C(C=CC(=C6)CC7C8=CC(=C(C=C8)CCN7C)OC)O4)OC)OCO3</chem>	0.07 6	Y E S		no	369.45g/m ol	0	5	3.33	108.8	Yes; 0 violation

101301	Corydali ne	<chem>CC1C2C3=CC(=C(C=C3CCN2)CC4=C1C=CC(=C4OC)OC)OC</chem>	0.021	Y E S		yes	622.75 g/mol	0	8	5.47	186.07	Yes: 1 violation
121313	Cycleani ne	<chem>CN1CCC2=CC(=C(C3=C2C1C)C4=CC=C(C=C4)OC5=C6C(C7=CC=C(O3)C=C7)N(CCC6=CC(=C5OC)OC)OC)OC</chem>	0.056	Y E S		no	246.31 g/mol	1	1	3.92	81.04	Yes: 0 violation
3213	Ellipticin e	<chem>CC1=C2C=CN=CC2=C(C3=C1NC4=CC=CC=C43)C</chem>	0.118	Y E S		yes	303.36 g/mol	1	1	2.7	97.67	Yes: 0 violation

151289	Evodiam ine	<chem>CN1C2C3=C(C)CN2C(=O)C4=CC=CC=C41)C5=CC=CC=C5N3</chem>	0.139	Y E S		yes	315.49 g/mol	1	2	3.88	96.52	Yes: 0 violation
12310548	Holamin e	<chem>CC(=O)C1CCC2C1(CCC3C2C)C=C4C3(CCC(C4)N)C)C</chem>	0.069	Y E S	4 : 6 6	yes	315.36 g/mol	1	5	1.98	88.77	Yes: 0 violation
10245167	Isoceph alotaxi ne	<chem>COC1=C2C3=CC4=C(C=C3C)CN5C2(CCC5)CC1O)OCO4</chem>	0.025	Y E S		yes	622.75 g/mol	0	8	5.41	186.07	Yes: 1 violation
5351212	Isotetran drine	<chem>CN1CCC2=CC(=C3C=C2C1CC4=CC=C(C=C4)OC5=C(C=CC(=C5)CC6C7=C(O3)C=C(C=C7)CCN6C)OC)OC)OC</chem>	0.056	Y E S		no	275.26 g/mol	0	4	2.88	76.67	Yes: 0 violation
10144	liriodeni ne	<chem>C1OC2=C(O1)C3=C4C(=C2)C=CN=C4C(=O)C5=CC=CC=C53</chem>	0.157	Y E S		yes	478.62 g/mol	0	6	4.43	147.34	Yes: 0 violation
15560508	Psychotr ine	<chem>CCC1CN2CCC3=CC(=C(C=C3)C2CC1CC4=NCCC5=CC(=C(C=C54)OC)OC)OC)OC</chem>	0.021	Y E S	4 : 8 1	yes	393.48 g/mol	0	5	4.08	119.16	Yes: 0 violation

637044	Secoantofine	<chem>COC1=CC=C(C=C1)C2=C(CC3CCCN3C2)C4=CC(=C(C=C4)O)C)OC</chem>	0.09 1	Y E S	5 4 5	yes	381.46 g/mol	1	5	3.32	113.12	Yes; 0 violation
246845	tylocrebrine	<chem>COC1=C(C2=C(C=C1)C3=C(C4CCCC4C3)C5=CC(=C(C=C5)2)OC)OC)OC</chem>	0.08	Y E S	4 9 5	yes	393.48 g/mol	0	5	4.08	119.16	Yes; 0 violation
373658	tyloindicine F	<chem>COC1=CC=C(C=C1)C2=CC3(CCCN3CC2)C4=CC(=C(C=C4)O)C)OC)O</chem>	0.07 4	Y E S	4 9 6	yes	381.46 g/mol	1	5	3.32	113.12	Yes; 0 violation
373659	tyloindicine G	<chem>COC1=C(C=C2C(=C1)C3CN4CCCC4(C=C3)C5=CC(=C(C=C2)5)OC)OC)O)OC</chem>	0.08 2	Y E S	4 5 7	yes	409.47 g/mol	1	6	3.24	118.61	Yes; 0 violation
44443382	tylophoridine C	<chem>COC1=CC2=C(C=C1)C3=C(C1N+14(CCCC4C3O))O-)C5=CC(=C(C=C5)2)O)OC</chem>	0.08 5	Y E S		no	381.42 g/mol	2	5	0.78	112.73	Yes; 0 violation
44443383	tylophoridine F	<chem>COC1=CC2=C(C=C1)C3=C(C1N+14(CCCC4C3O))O-)C5=CC(=C(C=C5)2)OC)OC</chem>	0.10 2	Y E S		yes	395.45 g/mol	1	5	1.11	117.2	Yes; 0 violation
249332	Vincristine sulfate	<chem>CCCC1(CC2CC(C3=C(CCN(C2)C1)C4=CC=CC=C4N3)(C5=C(C=C6C(=C5)C78CCN9C7C(C=C8)C(C(C8N6C=O)(C(=O)C)O)OC(=O)C)CC)OC)C(=O)OC)O.OS(=O)(=O)O</chem>	0.04 7	Y E S		no	923.04 g/mol	5	16	2.26	247.33	No; 2 violations
92114	(S)-tylophorine	<chem>COC1=C(C=C2C(=C1)C3=C(C4CCCC4C3)C5=CC(=C(C=C5)2)OC)OC)OC</chem>	0.08	Y E S		yes	393.48 g/mol	0	5	4.04	119.16	Yes; 0 violation
9975115	6-O-desmethylvantofine	<chem>COC1=C(C=C2C(=C1)C3=C(C4CCCC4C3)C5=C2C=C(C=C5)O)OC</chem>	0.09 6	Y E S		yes	349.42 g/mol	1	4	3.67	108.2	Yes; 0 violation

11741391	13(R)-14(R)-hydroxyantofine-N-oxide	<chem>COC1=CC2=C(C=C1)C3=C(C(C4CCCIN+14(C3)O)C5=CC(=C(C=C5)OC)OC</chem>	0.096	YES		yes	395.45 g/mol	1	5	1.74	117.2	Yes: 0 violation
51041425	Sapros mine B	<chem>CCOC1(C2=CC=CC=C2C(=O)C3=C1C(=CC(=O)N3)C)OC</chem>	0.026	YES		yes	299.32 g/mol	1	4	2.24	81.39	Yes: 0 violation
10263500	9-hydroxycanthin-6-one	<chem>C1=CC2=C3C=CNC4=C3N(C2=CC1=O)C(=O)C=C4</chem>	0.051	YES		yes	236.23 g/mol	1	2	1.55	70.49	Yes: 0 violation
10408269	Isotylcrobribe	<chem>COC1=C(C2=C(C=C1)C3=C(C4CCCC4C3)C5=CC(=C(C=C5)2)OC)OC</chem>	0.080	YES	494	yes	393.48 g/mol	0	5	4.04	119.16	Yes: 0 violation

Annexure 4: Representation of Various Heat shock proteins in different tumors from GSE50161

Glioblastoma	Medulloblastoma	Ependymoma	Astrocytoma
DNAJC6	DNAJC5	DNAJC6	DNAJC6
DNAJB2	DNAJC6	DNAJC5	DNAJC27
HSPB8	HSPA12A	DNAJC12	HSPA4L
HSPA2	DNAJA4	DNAJC27	DNAJA4
HSPA12A	HSPA4L	DNAJA4	HSPH1
DNAJA4	DNAJC27	HSPA12A	HSPA4L
DNAJC27	DNAJC12	HSPB3	HSPB3
DNAJB4	HSPB3		CRY2
HSPA1A	HSPA2		CRYM
HSPB3	CRY2		
DNAJC12	CRYM		
CRYAB			

Annexure 5: Representation of TFs interacting with HSPs with their Degree and Betweenness

Id	Label	Degree	Betweenness	Expression
3303	HSPA1A	174	17613.78	0
3326	HSP90AB1	151	12793.97	0
3329	HSPD1	48	1221.89	0
3336	HSPE1	48	1221.89	0
51726	DNAJB11	47	1629.38	0
7184	HSP90B1	46	1654.28	0
79982	DNAJB14	41	1759.37	0
27000	DNAJC2	38	1211.68	0
51277	DNAJC27	26	917.65	0
9829	DNAJC6	22	1625.29	0
7203	CCT3	21	412.22	0
10693	CCT6B	18	703.06	0
10808	HSPH1	18	681.23	0
54431	DNAJC10	16	423.05	0
10576	CCT2	14	83.25	0
56521	DNAJC12	13	149.87	0
55735	DNAJC11	12	65.33	0
3320	HSP90AA1	12	57.83	0
2002	ELK1	10	440.9	0
1997	ELF1	9	468.73	0
90993	CREB3L1	9	355.87	0
687	KLF9	9	289.8	0
1105	CHD1	8	309.17	0
22882	ZHX2	8	180.99	0
7027	TFDP1	7	207.59	0
2961	GTF2E2	7	198.36	0
8462	KLF11	7	188.83	0
3659	IRF1	7	170.88	0
3054	HCFC1	7	123.47	0
27107	ZBTB11	6	211.1	0
55769	ZNF83	6	183.57	0
6749	SSRP1	6	148.86	0
8061	FOSL1	6	144.24	0
10168	ZNF197	6	144.24	0
473	RERE	6	144.24	0
4090	SMAD5	6	143.81	0
10155	TRIM28	6	135.37	0
2113	ETS1	6	124.28	0
8625	RFXANK	6	122.91	0
23133	PHF8	6	119.83	0

10765	KDM5B	6	119.83	0
8819	SAP30	6	119.83	0
11279	KLF8	6	109.2	0
80108	ZFP2	5	212.58	0
3399	ID3	5	180.3	0
5437	POLR2H	5	136.3	0
79618	HMBOX1	5	134.68	0
466	ATF1	5	122.17	0
9923	ZBTB40	5	103.83	0
57798	GATAD1	5	101.22	0
7572	ZNF24	5	100.92	0
55810	FOXJ2	5	95.78	0
5371	PML	5	89	0
6667	SP1	5	89	0
60436	TGIF2	5	87.57	0
4152	MBD1	5	70.47	0
6879	TAF7	5	65.19	0
56897	WRNIP1	5	60.33	0
7490	WT1	4	155.02	0
7003	TEAD1	4	100.86	0
51385	ZNF589	4	97.41	0
26959	HBP1	4	93.02	0
2305	FOXM1	4	89.11	0
3662	IRF4	4	89.11	0
1958	EGR1	4	89.11	0
5978	REST	4	83.37	0
5430	POLR2A	4	83.01	0
571	BACH1	4	78.56	0
83881	MIXL1	4	78.56	0
51621	KLF13	4	77.51	0
7025	NR2F1	4	75.67	0
11218	DDX20	4	75.67	0
162963	ZNF610	4	69.92	0
7528	YY1	4	69.27	0
7030	TFE3	4	67.64	0
604	BCL6	4	67.64	0
25942	SIN3A	4	67.61	0
7586	ZKSCAN1	4	66.32	0
64919	BCL11B	4	66.21	0
6945	MLX	4	64.6	0
23309	SIN3B	4	64.6	0

9112	MTA1	4	64.6	0
10346	TRIM22	4	61.52	0
5927	KDM5A	4	60.25	0

3164	NR4A1	4	59.32	0
9611	NCOR1	4	54.74	0
83855	KLF16	4	53.8	0
84146	ZNF644	4	53.8	0
5914	RARA	4	53.8	0
2118	ETV4	4	53.8	0
10362	HMG20B	4	53.8	0
8648	NCOA1	4	53.8	0
3171	FOXA3	4	53.8	0
23028	KDM1A	4	53.8	0
7543	ZFX	4	51.05	0
4798	NFRKB	4	49.96	0
5089	PBX2	4	49.22	0
6772	STAT1	4	41.57	0
6932	TCF7	4	40.69	0
1385	CREB1	4	35.48	0
58491	ZNF71	4	34.86	0
51548	SIRT6	3	119.25	0
6597	SMARCA4	3	119.25	0
10320	IKZF1	3	119.25	0
10488	CREB3	3	119.25	0
51193	ZNF639	3	88.93	0
5977	DPF2	3	75.2	0
6257	RXRB	3	72.72	0
84905	ZNF341	3	54.43	0
3726	JUNB	3	51.09	0
10589	DRAP1	3	50.51	0
6670	SP3	3	49.64	0
3727	JUND	3	49.49	0
10009	ZBTB33	3	49.49	0
6935	ZEB1	3	49.12	0
4899	NRF1	3	48.88	0
3068	HDGF	3	48.88	0
2063	NR2F6	3	48.88	0
2115	ETV1	3	48.88	0
51341	ZBTB7A	3	48.88	0
9324	HMG3	3	48.88	0

2551	GABPA	3	47.04	0
23394	ADNP	3	46.14	0
84124	ZNF394	3	46.12	0
55892	MYNN	3	40.87	0
4298	MLLT1	3	40.87	0
7549	ZNF2	3	40.87	0
57684	ZBTB26	3	40.87	0

7799	PRDM2	3	40.87	0
2626	GATA4	3	40.87	0
1054	CEBPG	3	40.47	0
7756	ZNF207	3	40.35	0
1875	E2F5	3	39.78	0
25799	ZNF324	3	39.78	0
8467	SMARCA5	3	39.78	0
8805	TRIM24	3	38.75	0
7023	TFAP4	3	38.31	0
4774	NFIA	3	38.31	0
2101	ESRRA	3	37.81	0
23090	ZNF423	3	37.36	0
2738	GLI4	3	37.05	0
7068	THRB	3	37.05	0
6660	SOX5	3	37.05	0
4150	MAZ	3	37.05	0
55929	DMAP1	3	36.09	0
2958	GTF2A2	3	35.94	0
167465	ZNF366	3	35.55	0
9967	THRAP3	3	34.21	0
8726	EED	3	34.21	0
1316	KLF6	3	31.53	0
4802	NFYC	3	31.04	0
57492	ARID1B	3	29.05	0
4149	MAX	3	29.05	0
7629	ZNF76	3	28.36	0
201514	ZNF584	3	28.01	0
83463	MXD3	3	27.14	0
8932	MBD2	3	26.51	0
10608	MXD4	3	21.79	0
54815	GATAD2A	3	21.79	0
7005	TEAD3	3	19.56	0
4601	MXI1	3	16.48	0
26205	GMEB2	3	16.48	0

51742	ARID4B	3	16.48	0
4089	SMAD4	3	14.11	0
10363	HMG20A	3	8.62	0
4609	MYC	3	8.47	0
468	ATF4	3	7.68	0
2623	GATA1	2	267	0
54880	BCOR	2	47.96	0
84450	ZNF512	2	47.96	0
30009	TBX21	2	30.78	0
2114	ETS2	2	23.18	0

7799	PRDM2	3	40.87	0
2626	GATA4	3	40.87	0
1054	CEBPG	3	40.47	0
7756	ZNF207	3	40.35	0
1875	E2F5	3	39.78	0
25799	ZNF324	3	39.78	0
8467	SMARCA5	3	39.78	0
8805	TRIM24	3	38.75	0
7023	TFAP4	3	38.31	0
4774	NFIA	3	38.31	0
2101	ESRRA	3	37.81	0
23090	ZNF423	3	37.36	0
2738	GLI4	3	37.05	0
7068	THRB	3	37.05	0
6660	SOX5	3	37.05	0
4150	MAZ	3	37.05	0
55929	DMAP1	3	36.09	0
2958	GTF2A2	3	35.94	0
167465	ZNF366	3	35.55	0
9967	THRAP3	3	34.21	0
8726	EED	3	34.21	0
1316	KLF6	3	31.53	0
4802	NFYC	3	31.04	0
57492	ARID1B	3	29.05	0
4149	MAX	3	29.05	0
7629	ZNF76	3	28.36	0
201514	ZNF584	3	28.01	0
83463	MXD3	3	27.14	0
8932	MBD2	3	26.51	0
10608	MXD4	3	21.79	0

54815	GATAD2A	3	21.79	0
7005	TEAD3	3	19.56	0
4601	MXI1	3	16.48	0
26205	GMEB2	3	16.48	0
51742	ARID4B	3	16.48	0
4089	SMAD4	3	14.11	0
10363	HMG20A	3	8.62	0
4609	MYC	3	8.47	0
468	ATF4	3	7.68	0
2623	GATA1	2	267	0
54880	BCOR	2	47.96	0
84450	ZNF512	2	47.96	0
30009	TBX21	2	30.78	0
2114	ETS2	2	23.18	0

84733	CBX2	1	0	0
10919	EHMT2	1	0	0
3065	HDAC1	1	0	0
148979	GLIS1	1	0	0
5316	PKNOX1	1	0	0
6668	SP2	1	0	0
4335	MNT	1	0	0
9831	ZNF623	1	0	0
5452	POU2F2	1	0	0
639	PRDM1	1	0	0
7182	NR2C2	1	0	0
7004	TEAD4	1	0	0
1052	CEBPD	1	0	0
3170	FOXA2	1	0	0
7702	ZNF143	1	0	0
1879	EBF1	1	0	0
9126	SMC3	1	0	0
118738	ZNF488	1	0	0
3087	HHEX	1	0	0
8328	GFI1B	1	0	0
7566	ZNF18	1	0	0
1106	CHD2	1	0	0
6045	RNF2	1	0	0
1999	ELF3	1	0	0
1959	EGR2	1	0	0
6829	SUPT5H	1	0	0

10127	ZNF263	1	0	0
83746	L3MBTL2	1	0	0
7709	ZBTB17	1	0	0
90780	PYGO2	1	0	0
7728	ZNF175	1	0	0
6908	TBP	1	0	0
2120	ETV6	1	0	0
4209	MEF2D	1	0	0
23186	RCOR1	1	0	0
7675	ZNF121	1	0	0
2033	EP300	1	0	0
11244	ZHX1	1	0	0
9232	PTTG1	1	0	0
3660	IRF2	1	0	0
3090	HIC1	1	0	0
5970	RELA	1	0	0
6721	SREBF2	1	0	0
4286	MITF	1	0	0
1523	CUX1	1	0	0
10661	KLF1	1	0	0
6934	TCF7L2	1	0	0
1390	CREM	1	0	0
2959	GTF2B	1	0	0
861	RUNX1	1	0	0
4602	MYB	1	0	0
9314	KLF4	1	0	0
7539	ZFP37	1	0	0

REFERENCES

- [1] Louis DN, Perry A, Reifenberger G, von Deimling A, Figarella-Branger D, Cavenee WK, et al. The 2016 World Health Organization Classification of Tumors of the Central Nervous System: a summary. *Acta Neuropathol* 2016. <https://doi.org/10.1007/s00401-016-1545-1>.
- [2] Ho IAW, Shim WSN. Contribution of the microenvironmental niche to glioblastoma heterogeneity. *Biomed Res Int* 2017. <https://doi.org/10.1155/2017/9634172>.
- [3] Weller M, van den Bent M, Hopkins K, Tonn JC, Stupp R, Falini A, et al. EANO guideline for the diagnosis and treatment of anaplastic gliomas and glioblastoma. *Lancet Oncol* 2014. [https://doi.org/10.1016/S1470-2045\(14\)70011-7](https://doi.org/10.1016/S1470-2045(14)70011-7).
- [4] Biau J, Chautard E, De Schlichting E, Dupic G, Pereira B, Fogli A, et al. Radiotherapy plus temozolomide in elderly patients with glioblastoma: a “real-life” report. *Radiat Oncol* 2017. <https://doi.org/10.1186/s13014-017-0929-2>.
- [5] Adams J. The proteasome: Structure, function, and role in the cell. *Cancer Treat Rev* 2003. [https://doi.org/10.1016/S0305-7372\(03\)00081-1](https://doi.org/10.1016/S0305-7372(03)00081-1).
- [6] Ciechanover A, Orian A, Schwartz AL. Ubiquitin-mediated proteolysis: Biological regulation via destruction. *BioEssays* 2000. [https://doi.org/10.1002/\(SICI\)1521-1878\(200005\)22:5<442::AID-BIES6>3.0.CO;2-Q](https://doi.org/10.1002/(SICI)1521-1878(200005)22:5<442::AID-BIES6>3.0.CO;2-Q).
- [7] Komander D, Rape M. The Ubiquitin Code. *Annu Rev Biochem* 2012. <https://doi.org/10.1146/annurev-biochem-060310-170328>.
- [8] Kane RC, Farrell AT, Sridhara R, Pazdur R. United States Food and Drug Administration approval summary: Bortezomib for the treatment of progressive multiple myeloma after one

prior therapy. *Clin Cancer Res* 2006. <https://doi.org/10.1158/1078-0432.CCR-06-0170>.

[9] Orłowski RZ, Kuhn DJ. Proteasome inhibitors in cancer therapy: Lessons from the first decade. *Clin Cancer Res* 2008. <https://doi.org/10.1158/1078-0432.CCR-07-2218>.

[10] Chen D, Frezza M, Schmitt S, Kanwar J, P. Dou Q. Bortezomib as the First Proteasome Inhibitor Anticancer Drug: Current Status and Future Perspectives. *Curr Cancer Drug Targets* 2011. <https://doi.org/10.2174/156800911794519752>.

[11] Li W, Bengtson MH, Ulbrich A, Matsuda A, Reddy VA, Orth A, et al. Genome-wide and functional annotation of human E3 ubiquitin ligases identifies MULAN, a mitochondrial E3 that regulates the organelle's dynamics and signaling. *PLoS One* 2008. <https://doi.org/10.1371/journal.pone.0001487>.

[12] Scheffner M, Kumar S. Mammalian HECT ubiquitin-protein ligases: Biological and pathophysiological aspects. *Biochim Biophys Acta - Mol Cell Res* 2014. <https://doi.org/10.1016/j.bbamcr.2013.03.024>.

[13] Kitching R, Wong MJ, Koehler D, Burger AM, Landberg G, Gish G, et al. The RING-H2 protein RNF11 is differentially expressed in breast tumours and interacts with HECT-type E3 ligases. *Biochim Biophys Acta - Mol Basis Dis* 2003. <https://doi.org/10.1016/j.bbadis.2003.07.001>.

[14] Scheffner M, Werness BA, Huibregtse JM, Levine AJ, Howley PM. The E6 oncoprotein encoded by human papillomavirus types 16 and 18 promotes the degradation of p53. *Cell* 1990. [https://doi.org/10.1016/0092-8674\(90\)90409-8](https://doi.org/10.1016/0092-8674(90)90409-8).

[15] Alejo M, Alemany L, Clavero O, Quiros B, Vighi S, Seoud M, et al. Contribution of Human papillomavirus in neuroendocrine tumors from a series of 10,575 invasive cervical cancer cases. *Papillomavirus Res* 2018. <https://doi.org/10.1016/j.pvr.2018.03.005>.

- [16] Thomas M, Banks L. Inhibition of Bak-induced apoptosis by HPV-18 E6. *Oncogene* 1998. <https://doi.org/10.1038/sj.onc.1202223>.
- [17] Raghu D, Paul PJ, Gulati T, Deb S, Khoo C, Russo A, et al. E6AP promotes prostate cancer by reducing p27 expression. *Oncotarget* 2017. <https://doi.org/10.18632/oncotarget.17224>.
- [18] Wang Y, Liu X, Zhou L, Duong D, Bhuripanyo K, Zhao B, et al. Identifying the ubiquitination targets of E6AP by orthogonal ubiquitin transfer. *Nat Commun* 2017. <https://doi.org/10.1038/s41467-017-01974-7>.
- [19] Wade M, Li YC, Wahl GM. MDM2, MDMX and p53 in oncogenesis and cancer therapy. *Nat Rev Cancer* 2013. <https://doi.org/10.1038/nrc3430>.
- [20] Cahilly-Snyder L, Yang-Feng T, Francke U, George DL. Molecular analysis and chromosomal mapping of amplified genes isolated from a transformed mouse 3T3 cell line. *Somat Cell Mol Genet* 1987. <https://doi.org/10.1007/BF01535205>.
- [21] Itahana K, Mao H, Jin A, Itahana Y, Clegg H V., Lindström MS, et al. Targeted Inactivation of Mdm2 RING Finger E3 Ubiquitin Ligase Activity in the Mouse Reveals Mechanistic Insights into p53 Regulation. *Cancer Cell* 2007. <https://doi.org/10.1016/j.ccr.2007.09.007>.
- [22] Wang X, Jiang X. Mdm2 and MdmX partner to regulate p53. *FEBS Lett* 2012. <https://doi.org/10.1016/j.febslet.2012.02.049>.
- [23] Momand J, Jung D, Wilczynski S, Niland J. The MDM2 gene amplification database. *Nucleic Acids Res* 1998. <https://doi.org/10.1093/nar/26.15.3453>.
- [24] Zhang R, Wang H. MDM2 Oncogene as a Novel Target for Human Cancer Therapy. *Curr Pharm Des* 2005. <https://doi.org/10.2174/1381612003400911>.

- [25] Freedman DA, Wu L, Levine AJ. Functions of the MDM2 oncoprotein. *Cell Mol Life Sci* 1999. <https://doi.org/10.1007/s000180050273>.
- [26] Kussie PH, Gorina S, Marechal V, Elenbaas B, Moreau J, Levine AJ, et al. Structure of the MDM2 oncoprotein bound to the p53 tumor suppressor transactivation domain. *Science* (80-) 1996. <https://doi.org/10.1126/science.274.5289.948>.
- [27] Poyurovsky M V., Katz C, Laptenko O, Beckerman R, Lokshin M, Ahn J, et al. The C terminus of p53 binds the N-terminal domain of MDM2. *Nat Struct Mol Biol* 2010. <https://doi.org/10.1038/nsmb.1872>.
- [28] Grossman SR, Deato ME, Brignone C, Chan HM, Kung AL, Tagami H, et al. Polyubiquitination of p53 by a ubiquitin ligase activity of p300. *Science* (80-) 2003. <https://doi.org/10.1126/science.1080386>.
- [29] Ferreone JC, Lee CW, Arai M, Martinez-Yamout MA, Dyson HJ, Wright PE. Cooperative regulation of p53 by modulation of ternary complex formation with CBP/p300 and HDM2. *Proc Natl Acad Sci U S A* 2009. <https://doi.org/10.1073/pnas.0811023106>.
- [30] Greenblatt MS, Bennett WP, Hollstein M, Harris CC. Mutations in the p53 tumor suppressor gene: clues to cancer etiology and molecular pathogenesis. *Cancer Res* 1994.
- [31] Deshaies RJ. SCF and Cullin/RING H2-Based Ubiquitin Ligases. *Annu Rev Cell Dev Biol* 1999. <https://doi.org/10.1146/annurev.cellbio.15.1.435>.
- [32] Sun Y, Tan M, Duan H, Swaroop M. SAG/ROC/Rbx/Hrt, a zinc RING finger gene family: Molecular cloning, biochemical properties, and biological functions. *Antioxidants Redox Signal* 2001. <https://doi.org/10.1089/15230860152542989>.
- [33] Soucy TA, Smith PG, Milhollen MA, Berger AJ, Gavin JM, Adhikari S, et al. An inhibitor of NEDD8-activating enzyme as a new approach to treat cancer. *Nature* 2009.

<https://doi.org/10.1038/nature07884>.

[34] Jia L, Sun Y. RBX1/ROC1-SCF E3 ubiquitin ligase is required for mouse embryogenesis and cancer cell survival. *Cell Div* 2009. <https://doi.org/10.1186/1747-1028-4-16>.

[35] Nakayama KI, Nakayama K. Ubiquitin ligases: Cell-cycle control and cancer. *Nat Rev Cancer* 2006. <https://doi.org/10.1038/nrc1881>.

[36] Wang Z, Liu P, Inuzuka H, Wei W. Roles of F-box proteins in cancer. *Nat Rev Cancer* 2014. <https://doi.org/10.1038/nrc3700>.

[37] Plechanovov A, Jaffray EG, Tatham MH, Naismith JH, Hay RT. Structure of a RING E3 ligase and ubiquitin-loaded E2 primed for catalysis. *Nature* 2012.

<https://doi.org/10.1038/nature11376>.

[38] Zheng N, Schulman BA, Song L, Miller JJ, Jeffrey PD, Wang P, et al. Structure of the Cul1-Rbx1-Skp1-F boxSkp2 SCF ubiquitin ligase complex. *Nature* 2002.

<https://doi.org/10.1038/416703a>.

[39] Wu K, Fuchs SY, Chen A, Tan P, Gomez C, Ronai Z, et al. The SCFHOS/ β -TRCP-ROC1 E3 Ubiquitin Ligase Utilizes Two Distinct Domains within CUL1 for Substrate Targeting and Ubiquitin Ligation. *Mol Cell Biol* 2000.

<https://doi.org/10.1128/mcb.20.4.1382-1393.2000>.

[40] Duan H, Wang Y, Aviram M, Swaroop M, Loo JA, Bian J, et al. SAG, a Novel Zinc RING Finger Protein That Protects Cells from Apoptosis Induced by Redox Agents. *Mol Cell Biol* 1999. <https://doi.org/10.1128/mcb.19.4.3145>.

[41] Kim SY, Kim MY, Mo JS, Park JW, Park HS. SAG protects human neuroblastoma SH-SY5Y cells against 1-methyl-4-phenylpyridinium ion (MPP⁺)-induced cytotoxicity via the

downregulation of ROS generation and JNK signaling. *Neurosci Lett* 2007.

<https://doi.org/10.1016/j.neulet.2006.11.074>.

[42] Ohta T, Michel JJ, Schottelius AJ, Xiong Y. ROC1, a homolog of APC11, represents a family of cullin partners with an associated ubiquitin ligase activity. *Mol Cell* 1999.

[https://doi.org/10.1016/S1097-2765\(00\)80482-7](https://doi.org/10.1016/S1097-2765(00)80482-7).

[43] Jin J, Cardozo T, Lovering RC, Elledge SJ, Pagano M, Harper JW. Systematic analysis and nomenclature of mammalian F-box proteins. *Genes Dev* 2004.

<https://doi.org/10.1101/gad.1255304>.

[44] Welcker M, Clurman BE. FBW7 ubiquitin ligase: A tumour suppressor at the crossroads of cell division, growth and differentiation. *Nat Rev Cancer* 2008.

<https://doi.org/10.1038/nrc2290>.

[45] Mao JH, Kim IJ, Wu D, Climent J, Hio CK, DelRosario R, et al. FBXW7 targets mTOR for degradation and cooperates with PTEN in tumor suppression. *Science* (80-) 2008.

<https://doi.org/10.1126/science.1162981>.

[46] Petroski MD, Deshaies RJ. Function and regulation of cullin-RING ubiquitin ligases. *Nat Rev Mol Cell Biol* 2005. <https://doi.org/10.1038/nrm1547>.

[47] Deshaies RJ, Joazeiro CAP. RING Domain E3 Ubiquitin Ligases. *Annu Rev Biochem* 2009. <https://doi.org/10.1146/annurev.biochem.78.101807.093809>.

[48] Swaroop M, Wang Y, Miller P, Duan H, Jatkoa T, Madore SJ, et al. Yeast homolog of human SAG/ROC2/Rbx2/Hrt2 is essential for cell growth, but not for germination: Chip profiling implicates its role in cell cycle regulation. *Oncogene* 2000.

<https://doi.org/10.1038/sj.onc.1203635>.

[49] Furukawa M, Ohta T, Xiong Y. Activation of UBC5 ubiquitin-conjugating enzyme by

the RING finger of ROC1 and assembly of active ubiquitin ligases by all cullins. *J Biol Chem* 2002. <https://doi.org/10.1074/jbc.M108565200>.

[50] Kamura T, Maenaka K, Kotoshiba S, Matsumoto M, Kohda D, Conaway RC, et al. VHL-box and SOCS-box domains determine binding specificity for Cul2-Rbx1 and Cul5-Rbx2 modules of ubiquitin ligases. *Genes Dev* 2004. <https://doi.org/10.1101/gad.1252404>.

[51] Jia L, Soengas MS, Sun Y. ROC1/RBX1 E3 ubiquitin ligase silencing suppresses tumor cell growth via sequential induction of G2-M arrest, apoptosis, and senescence. *Cancer Res* 2009. <https://doi.org/10.1158/0008-5472.CAN-08-4671>.

[52] Li X, Zhao Q, Liao R, Sun P, Wu X. The SCFSkp2 ubiquitin ligase complex interacts with the human replication licensing factor Cdt1 and regulates Cdt1 degradation. *J Biol Chem* 2003. <https://doi.org/10.1074/jbc.C300251200>.

[53] Arias EE, Walter JC. PCNA functions as a molecular platform to trigger Cdt1 destruction and prevent re-replication. *Nat Cell Biol* 2006. <https://doi.org/10.1038/ncb1346>.

[54] Nishitani H, Sugimoto N, Roukos V, Nakanishi Y, Saijo M, Obuse C, et al. Two E3 ubiquitin ligases, SCF-Skp2 and DDB1-Cul4, target human Cdt1 for proteolysis. *EMBO J* 2006. <https://doi.org/10.1038/sj.emboj.7601002>.

[55] Lechner E, Achard P, Vansiri A, Potuschak T, Genschik P. F-box proteins everywhere. *Curr Opin Plant Biol* 2006. <https://doi.org/10.1016/j.pbi.2006.09.003>.

[56] Swaroop M, Bian J, Aviram M, Duan H, Bisgaier CL, Loo JA, et al. Expression, purification, and biochemical characterization of SAG, a ring finger redox-sensitive protein. *Free Radic Biol Med* 1999. [https://doi.org/10.1016/S0891-5849\(99\)00078-7](https://doi.org/10.1016/S0891-5849(99)00078-7).

[57] Sun Y. Alterations of SAG mRNA in human cancer cell lines: Requirement for the RING finger domain for apoptosis protection. *Carcinogenesis* 1999.

<https://doi.org/10.1093/carcin/20.10.1899>.

[58] Chanalaris A, Sun Y, Latchman DS, Stephanou A. SAG attenuates apoptotic cell death caused by simulated ischaemia/reoxygenation in rat cardiomyocytes. *J Mol Cell Cardiol* 2003.

[https://doi.org/10.1016/S0022-2828\(03\)00003-8](https://doi.org/10.1016/S0022-2828(03)00003-8).

[59] Lee SJ, Yang ES, Kim SY, Kim SY, Shin SW, Park JW. Regulation of heat shock-induced apoptosis by sensitive to apoptosis gene protein. *Free Radic Biol Med* 2008.

<https://doi.org/10.1016/j.freeradbiomed.2008.03.026>.

[60] Jia L, Sun Y. SCF E3 Ubiquitin Ligases as Anticancer Targets. *Curr Cancer Drug Targets* 2011. <https://doi.org/10.2174/156800911794519734>.

[61] Sasaki H, Yukiue H, Kobayashi Y, Moriyama S, Nakashima Y, Kaji M, et al.

Expression of the sensitive to apoptosis gene, SAG, as a prognostic marker in nonsmall cell lung cancer. *Int J Cancer* 2001. [https://doi.org/10.1002/1097-0215\(20011120\)95:6<375::AID-IJC1066>3.0.CO;2-L](https://doi.org/10.1002/1097-0215(20011120)95:6<375::AID-IJC1066>3.0.CO;2-L).

[62] Duan H, Tsvetkov LM, Liu Y, Song Y, Swaroop M, Wen R, et al. Promotion of S-phase entry and cell growth under serum starvation by SAG/ROC2/Rbx2/Hrt2, an E3 ubiquitin ligase component: Association with inhibition of p27 accumulation: Association of SAG-Induced Growth with Inhibition of p27 Accumulation. *Mol Carcinog* 2001.

[https://doi.org/10.1002/1098-2744\(200101\)30:1<37::AID-MC1011>3.0.CO;2-7](https://doi.org/10.1002/1098-2744(200101)30:1<37::AID-MC1011>3.0.CO;2-7).

[63] Tan M, Gallegos JR, Gu Q, Huang Y, Li J, Jin Y, et al. SAG/ROC-SCF β -TrCP E3 ubiquitin ligase promotes pro-caspase-3 degradation as a mechanism of apoptosis protection. *Neoplasia* 2006. <https://doi.org/10.1593/neo.06568>.

[64] Tan M, Gu Q, He H, Pamarthy D, Semenza GL, Sun Y. SAG/ROC2/RBX2 is a HIF-1 target gene that promotes HIF-1 α ubiquitination and degradation. *Oncogene* 2008.

<https://doi.org/10.1038/sj.onc.1210780>.

[65] Jia L, Yang J, Hao X, Zheng M, He H, Xiong X, et al. Validation of SAG/RBX2/ROC2 E3 ubiquitin ligase as an anticancer and radiosensitizing target. *Clin Cancer Res* 2010.

<https://doi.org/10.1158/1078-0432.CCR-09-1592>.

[66] Kipreos ET, Pagano M. The F-box protein family. *Genome Biol* 2000.

<https://doi.org/10.1186/gb-2000-1-5-reviews3002>.

[67] Frescas D, Pagano M. Deregulated proteolysis by the F-box proteins SKP2 and β -TrCP: Tipping the scales of cancer. *Nat Rev Cancer* 2008. <https://doi.org/10.1038/nrc2396>.

[68] Lee SH, McCormick F. Downregulation of Skp2 and p27/Kip1 synergistically induces apoptosis in T98G glioblastoma cells. *J Mol Med* 2005. <https://doi.org/10.1007/s00109-004-0611-7>.

[69] Jiang F, Caraway NP, Li RY, Katz RL. RNA silencing of S-phase kinase-interacting protein 2 inhibits proliferation and centrosome amplification in lung cancer cells. *Oncogene* 2005. <https://doi.org/10.1038/sj.onc.1208459>.

[70] Winston JT, Strack P, Beer-Romero P, Chu CY, Elledge SJ, Harper JW. The SCF(β -TRCP)-ubiquitin ligase complex associates specifically with phosphorylated destruction motifs in I κ B α and β -catenin and stimulates I κ B α ubiquitination in vitro. *Genes Dev* 1999. <https://doi.org/10.1101/gad.13.3.270>.

[71] Karin M, Ben-Neriah Y. Phosphorylation Meets Ubiquitination: The Control of NF- κ B Activity. *Annu Rev Immunol* 2000. <https://doi.org/10.1146/annurev.immunol.18.1.621>.

[72] Uddin S, Bhat AA, Krishnankutty R, Mir F, Kulinski M, Mohammad RM. Involvement of F-BOX proteins in progression and development of human malignancies. *Semin Cancer Biol* 2016. <https://doi.org/10.1016/j.semcancer.2015.09.008>.

- [73] Skaar JR, Pagan JK, Pagano M. Mechanisms and function of substrate recruitment by F-box proteins. *Nat Rev Mol Cell Biol* 2013. <https://doi.org/10.1038/nrm3582>.
- [74] Skaar JR, Pagan JK, Pagano M. SCF ubiquitin ligase-targeted therapies. *Nat Rev Drug Discov* 2014. <https://doi.org/10.1038/nrd4432>.
- [75] Peters JM. The anaphase promoting complex/cyclosome: A machine designed to destroy. *Nat Rev Mol Cell Biol* 2006. <https://doi.org/10.1038/nrm1988>.
- [76] Chang L, Zhang Z, Yang J, McLaughlin SH, Barford D. Atomic structure of the APC/C and its mechanism of protein ubiquitination. *Nature* 2015. <https://doi.org/10.1038/nature14471>.
- [77] De Boer HR, Guerrero Llobet S, Van Vugt MATM. Controlling the response to DNA damage by the APC/C-Cdh1. *Cell Mol Life Sci* 2016. <https://doi.org/10.1007/s00018-015-2096-7>.
- [78] Chang L, Zhang Z, Yang J, McLaughlin SH, Barford D. Molecular architecture and mechanism of the anaphase-promoting complex. *Nature* 2014. <https://doi.org/10.1038/nature13543>.
- [79] Primorac I, Musacchio A. Panta rhei: The APC/C at steady state. *J Cell Biol* 2013. <https://doi.org/10.1083/jcb.201301130>.
- [80] Wang Q, Moyret-Lalle C, Couzon F, Surbiguet-Clippe C, Saurin JC, Lorca T, et al. Alterations of anaphase-promoting complex genes in human colon cancer cells. *Oncogene* 2003. <https://doi.org/10.1038/sj.onc.1206224>.
- [81] Venere M, Horbinski C, Crish JF, Jin X, VasANJI A, Major J, et al. The mitotic kinesin KIF11 is a driver of invasion, proliferation, and self-renewal in glioblastoma. *Sci Transl Med* 2015. <https://doi.org/10.1126/scitranslmed.aac6762>.

[82] Mao DD, Gujar AD, Mahlokozera T, Chen I, Pan Y, Luo J, et al. A CDC20-APC/SOX2 Signaling Axis Regulates Human Glioblastoma Stem-like Cells. *Cell Rep* 2015.

<https://doi.org/10.1016/j.celrep.2015.05.027>.

[83] Xie Q, Wu Q, Mack SC, Yang K, Kim L, Hubert CG, et al. CDC20 maintains tumor initiating cells. *Oncotarget* 2015. <https://doi.org/10.18632/oncotarget.3676>.

[84] Fulda S, Debatin KM. 5-Aza-2'-deoxycytidine and IFN- γ cooperate to sensitize for TRAIL-induced apoptosis by upregulating caspase-8. *Oncogene* 2006.

<https://doi.org/10.1038/sj.onc.1209518>.

[85] Gu L, Zhu N, Zhang H, Durden DL, Feng Y, Zhou M. Regulation of XIAP Translation and Induction by MDM2 following Irradiation. *Cancer Cell* 2009.

<https://doi.org/10.1016/j.ccr.2009.03.002>.

[86] Vucic D, Fairbrother WJ. The inhibitor of apoptosis proteins as therapeutic targets in cancer. *Clin Cancer Res* 2007. <https://doi.org/10.1158/1078-0432.CCR-07-0729>.

[87] Fulda S, Vucic D. Targeting IAP proteins for therapeutic intervention in cancer. *Nat Rev Drug Discov* 2012. <https://doi.org/10.1038/nrd3627>.

[88] Hu S, Yang X. Cellular inhibitor of apoptosis 1 and 2 are ubiquitin ligases for the apoptosis inducer Smac/DIABLO. *J Biol Chem* 2003.

<https://doi.org/10.1074/jbc.M207197200>.

[89] MacFarlane M, Merrison W, Bratton SB, Cohen GM. Proteasome-mediated degradation of Smac during apoptosis: XIAP promotes Smac ubiquitination in vitro. *J Biol Chem* 2002. <https://doi.org/10.1074/jbc.M200317200>.

[90] Deveraux QL, Reed JC. IAP family proteins - Suppressors of apoptosis. *Genes Dev* 1999. <https://doi.org/10.1101/gad.13.3.239>.

- [91] Eckhardt I, Roesler S, Fulda S. Identification of DR5 as a critical, NF- κ B-regulated mediator of Smac-induced apoptosis. *Cell Death Dis* 2013. <https://doi.org/10.1038/cddis.2013.457>.
- [92] Giagkousiklidis S, Vogler M, Westhoff MA, Kasperczyk H, Debatin KM, Fulda S. Sensitization for γ -irradiation-induced apoptosis by second mitochondria-derived activator of caspase. *Cancer Res* 2005. <https://doi.org/10.1158/0008-5472.CAN-05-0866>.
- [93] Riley BE, Loughheed JC, Callaway K, Velasquez M, Brecht E, Nguyen L, et al. Structure and function of Parkin E3 ubiquitin ligase reveals aspects of RING and HECT ligases. *Nat Commun* 2013. <https://doi.org/10.1038/ncomms2982>.
- [94] Cesari R, Martin ES, Calin GA, Pentimalli F, Bichi R, McAdams H, et al. Parkin, a gene implicated in autosomal recessive juvenile parkinsonism, is a candidate tumor suppressor gene on chromosome 6q25-q27. *Proc Natl Acad Sci U S A* 2003. <https://doi.org/10.1073/pnas.0931262100>.
- [95] Chourasia AH, Boland ML, Macleod KF. Mitophagy and cancer. *Cancer Metab* 2015. <https://doi.org/10.1186/s40170-015-0130-8>.
- [96] Suen DF, Narendra DP, Tanaka A, Manfredi G, Youle RJ. Parkin overexpression selects against a deleterious mtDNA mutation in heteroplasmic cybrid cells. *Proc Natl Acad Sci U S A* 2010. <https://doi.org/10.1073/pnas.0914569107>.
- [97] Gupta A, Anjomani-Virmouni S, Koundouros N, Dimitriadi M, Choo-Wing R, Valle A, et al. PARK2 Depletion Connects Energy and Oxidative Stress to PI3K/Akt Activation via PTEN S-Nitrosylation. *Mol Cell* 2017. <https://doi.org/10.1016/j.molcel.2017.02.019>.
- [98] Yeo CWS, Ng FSL, Chai C, Tan JMM, Koh GRH, Chong YK, et al. Parkin pathway activation mitigates glioma cell proliferation and predicts patient survival. *Cancer Res* 2012.

<https://doi.org/10.1158/0008-5472.CAN-11-3060>.

[99] Staropoli JF, McDermott C, Martinat C, Schulman B, Demireva E, Abeliovich A. Parkin Is a Component of an SCF-like Ubiquitin Ligase Complex and Protects Postmitotic Neurons from Kainate Excitotoxicity. *Neuron* 2003. [https://doi.org/10.1016/S0896-6273\(03\)00084-9](https://doi.org/10.1016/S0896-6273(03)00084-9).

[100] Gong Y, Zack TI, Morris LGT, Lin K, Hukkelhoven E, Raheja R, et al. Pan-cancer genetic analysis identifies PARK2 as a master regulator of G1/S cyclins. *Nat Genet* 2014. <https://doi.org/10.1038/ng.2981>.

[101] Wang H, Jiang Z, Na M, Ge H, Tang C, Shen H, et al. PARK2 negatively regulates the metastasis and epithelial-mesenchymal transition of glioblastoma cells via ZEB1. *Oncol Lett* 2017. <https://doi.org/10.3892/ol.2017.6488>.

[102] Liu J, Zhang C, Zhao Y, Yue X, Wu H, Huang S, et al. Parkin targets HIF-1 α for ubiquitination and degradation to inhibit breast tumor progression. *Nat Commun* 2017. <https://doi.org/10.1038/s41467-017-01947-w>.

[103] Wu J, Liu T, Rios Z, Mei Q, Lin X, Cao S. Heat Shock Proteins and Cancer. *Trends Pharmacol Sci* 2017. <https://doi.org/10.1016/j.tips.2016.11.009>.

[104] Jegou G, Hazoumé A, Seigneuric R, Garrido C. Targeting heat shock proteins in cancer. *Cancer Lett* 2013. <https://doi.org/10.1016/j.canlet.2010.10.014>.

[105] Liu T, Daniels CK, Cao S. Comprehensive review on the HSC70 functions, interactions with related molecules and involvement in clinical diseases and therapeutic potential. *Pharmacol Ther* 2012. <https://doi.org/10.1016/j.pharmthera.2012.08.014>.

[106] Macario AJL, De Macario EC. Molecular chaperones: Multiple functions, pathologies, and potential applications. *Front Biosci* 2007. <https://doi.org/10.2741/2257>.

- [107] Wang X, Chen M, Zhou J, Zhang X. HSP27, 70 and 90, anti-apoptotic proteins, in clinical cancer therapy (review). *Int J Oncol* 2014. <https://doi.org/10.3892/ijo.2014.2399>.
- [108] Ciocca DR, Calderwood SK. Heat shock proteins in cancer: Diagnostic, prognostic, predictive, and treatment implications. *Cell Stress Chaperones* 2005. <https://doi.org/10.1379/CSC-99r.1>.
- [109] Bepperling A, Alte F, Kriehuber T, Braun N, Weinkauff S, Groll M, et al. Alternative bacterial two-component small heat shock protein systems. *Proc Natl Acad Sci U S A* 2012. <https://doi.org/10.1073/pnas.1209565109>.
- [110] Lianos GD, Alexiou GA, Mangano A, Mangano A, Rausei S, Boni L, et al. The role of heat shock proteins in cancer. *Cancer Lett* 2015. <https://doi.org/10.1016/j.canlet.2015.02.026>.
- [111] Xia Y, Rocchi P, Iovanna JL, Peng L. Targeting heat shock response pathways to treat pancreatic cancer. *Drug Discov Today* 2012. <https://doi.org/10.1016/j.drudis.2011.09.016>.
- [112] Shamovsky I, Nudler E. New insights into the mechanism of heat shock response activation. *Cell Mol Life Sci* 2008. <https://doi.org/10.1007/s00018-008-7458-y>.
- [113] Garrido C, Brunet M, Didelot C, Zermati Y, Schmitt E, Kroemer G. Heat shock proteins 27 and 70: Anti-apoptotic proteins with tumorigenic properties. *Cell Cycle* 2006. <https://doi.org/10.4161/cc.5.22.3448>.
- [114] Åkerfelt M, Morimoto RI, Sistonen L. Heat shock factors: Integrators of cell stress, development and lifespan. *Nat Rev Mol Cell Biol* 2010. <https://doi.org/10.1038/nrm2938>.
- [115] De Maio A. Heat shock proteins: Facts, thoughts, and dreams. *Shock* 1999. <https://doi.org/10.1097/00024382-199901000-00001>.
- [116] Fan GC. Role of heat shock proteins in stem cell behavior. *Prog. Mol. Biol. Transl. Sci.*, 2012. <https://doi.org/10.1016/B978-0-12-398459-3.00014-9>.

- [117] Meshalkina DA, Shevtsov MA, Dobrodumov A V., Komarova EY, Voronkina I V., Lazarev VF, et al. Knock-down of Hdj2/DNAJA1 co-chaperone results in an unexpected burst of tumorigenicity of C6 glioblastoma cells. *Oncotarget* 2016.
<https://doi.org/10.18632/oncotarget.7872>.
- [118] Jolly C, Morimoto RI. Role of the heat shock response and molecular chaperones in oncogenesis and cell death. *J Natl Cancer Inst* 2000. <https://doi.org/10.1093/jnci/92.19.1564>.
- [119] Ghosh JC, Siegelin MD, Dohi T, Altieri DC. Heat shock protein 60 regulation of the mitochondrial permeability transition pore in tumor cells. *Cancer Res* 2010;70:8988–93.
<https://doi.org/10.1158/0008-5472.CAN-10-2225>.
- [120] Tang H, Li J, Liu X, Wang G, Luo M, Deng H. Down-regulation of HSP60 Suppresses the Proliferation of Glioblastoma Cells via the ROS/AMPK/mTOR Pathway. *Sci Rep* 2016;6:1–11. <https://doi.org/10.1038/srep28388>.
- [121] Alexiou GA, Karamoutsios A, Lallas G, Ragos V, Goussia A, Kyritsis AP, et al. Expression of heat shock proteins in brain tumors. *Turk Neurosurg* 2014;24:745–9.
<https://doi.org/10.5137/1019-5149.JTN.9852-13.0>.
- [122] Ishida CT, Shu C, Halatsch ME, Westhoff MA, Altieri DC, Karpel-Massler G, et al. Mitochondrial matrix chaperone and c-myc inhibition causes enhanced lethality in glioblastoma. *Oncotarget* 2017. <https://doi.org/10.18632/oncotarget.16202>.
- [123] Kopecek P, Altmannová K, Weigl E. Stress proteins: nomenclature, division and functions. *Biomed Pap Med Fac Univ Palacky Olomouc Czech Repub* 2001.
<https://doi.org/10.5507/bp.2001.010>.
- [124] Murphy ME. The HSP70 family and cancer. *Carcinogenesis* 2013;34:1181–8.
<https://doi.org/10.1093/carcin/bgt111>.

[125] Gaspar N, Sharp SY, Pacey S, Jones C, Walton M, Vassal G, et al. Acquired resistance to 17-Allylamino-17-Demethoxygeldanamycin (17-A AG, Tanespimycin) in glioblastoma cells. *Cancer Res* 2009. <https://doi.org/10.1158/0008-5472.CAN-08-3131>.

[126] Patel HJ, Modi S, Chiosis G, Taldone T. Advances in the discovery and development of heat-shock protein 90 inhibitors for cancer treatment. *Expert Opin Drug Discov* 2011. <https://doi.org/10.1517/17460441.2011.563296>.

[127] Supko JG, Hickman RL, Grever MR, Malspeis L. Preclinical pharmacologic evaluation of geldanamycin as an antitumor agent. *Cancer Chemother Pharmacol* 1995. <https://doi.org/10.1007/BF00689048>.

[128] Austin CD, De Mazière AM, Pisacane PI, Van Dijk SM, Eigenbrot C, Sliwkowski MX, et al. Endocytosis and sorting of ErbB2 and the site of action of cancer therapeutics trastuzumab and geldanamycin. *Mol Biol Cell* 2004. <https://doi.org/10.1091/mbc.E04-07-0591>.

[129] Castagnola P, Bellese G, Birocchi F, Gagliani MC, Tacchetti C, Cortese K. Identification of an HSP90 modulated multi-step process for ERBB2 degradation in breast cancer cells. *Oncotarget* 2016. <https://doi.org/10.18632/oncotarget.13392>.

[130] Kummar S, Gutierrez ME, Gardner ER, Chen X, Figg WD, Zajac-Kaye M, et al. Phase I trial of 17-dimethylaminoethylamino-17-demethoxygeldanamycin (17-DMAG), a heat shock protein inhibitor, administered twice weekly in patients with advanced malignancies. *Eur J Cancer* 2010. <https://doi.org/10.1016/j.ejca.2009.10.026>.

[131] Lancet JE, Gojo I, Burton M, Quinn M, Tighe SM, Kersey K, et al. Phase i study of the heat shock protein 90 inhibitor alvespimycin (KOS-1022, 17-DMAG) administered intravenously twice weekly to patients with acute myeloid leukemia. *Leukemia* 2010.

<https://doi.org/10.1038/leu.2009.292>.

[132] Hanson BE, Vesole DH. Retaspimycin hydrochloride (IPI-504): A novel heat shock protein inhibitor as an anticancer agent. *Expert Opin Investig Drugs* 2009.

<https://doi.org/10.1517/13543780903158934>.

[133] Brough PA, Aherne W, Barril X, Borgognoni J, Boxall K, Cansfield JE, et al. 4,5-Diarylisoxazole Hsp90 chaperone inhibitors: Potential therapeutic agents for the treatment of cancer. *J Med Chem* 2008. <https://doi.org/10.1021/jm701018h>.

[134] Seul-Ki C, Kam H, Kye-Young K, In Park S, Yun-Sil L. Targeting heat shock protein 27 in cancer: A druggable target for cancer treatment? *Cancers (Basel)* 2019.

<https://doi.org/10.3390/cancers11081195>.

[135] Kato K, Goto S, Hasegawa K, Shinohara H, Inaguma Y. Responses to heat shock of α B crystallin and HSP28 in U373 MG human glioma cells. *BBA - Mol Cell Res* 1993.

[https://doi.org/10.1016/0167-4889\(93\)90214-A](https://doi.org/10.1016/0167-4889(93)90214-A).

[136] Hermisson M, Strik H, Rieger J, Dichgans J, Meyermann R, Weller M. Expression and functional activity of heat shock proteins in human glioblastoma multiforme. *Neurology* 2000.

<https://doi.org/10.1212/wnl.54.6.1357>.

[137] Jakubowicz-Gil J, Langner E, Badziul D, Wertel I, Rzeski W. Silencing of Hsp27 and Hsp72 in glioma cells as a tool for programmed cell death induction upon temozolomide and quercetin treatment. *Toxicol Appl Pharmacol* 2013.

<https://doi.org/10.1016/j.taap.2013.10.003>.

[138] Volloch VZ, Sherman MY. Oncogenic potential of Hsp72. *Oncogene* 1999.

<https://doi.org/10.1038/sj.onc.1202525>.

[139] Park SH, Won J, Kim SI, Lee Y, Park CK, Kim SK, et al. Molecular testing of brain

- tumor. *J Pathol Transl Med* 2017;51:205–23. <https://doi.org/10.4132/jptm.2017.03.08>.
- [140] Khalil AA, Kabapy NF, Deraz SF, Smith C. Heat shock proteins in oncology: Diagnostic biomarkers or therapeutic targets? *Biochim Biophys Acta - Rev Cancer* 2011. <https://doi.org/10.1016/j.bbcan.2011.05.001>.
- [141] Cayado-Gutiérrez N, Moncalero VL, Rosales EM, Berón W, Salvatierra EE, Alvarez-Olmedo D, et al. Downregulation of Hsp27 (HSPB1) in MCF-7 human breast cancer cells induces upregulation of PTEN. *Cell Stress Chaperones* 2013. <https://doi.org/10.1007/s12192-012-0367-x>.
- [142] Gozé C, Rigau V, Gibert L, Maudelonde T, Duffau H. Lack of complete 1p19q deletion in a consecutive series of 12 WHO grade II gliomas involving the insula: A marker of worse prognosis? *J Neurooncol* 2009. <https://doi.org/10.1007/s11060-008-9680-8>.
- [143] Zanini C, Pulerà F, Carta F, Giribaldi G, Mandili G, Maule MM, et al. Proteomic identification of heat shock protein 27 as a differentiation and prognostic marker in neuroblastoma but not in Ewing's sarcoma. *Virchows Arch* 2008. <https://doi.org/10.1007/s00428-007-0549-6>.
- [144] Acunzo J, Katsogiannou M, Rocchi P. Small heat shock proteins HSP27 (HspB1), α -crystallin (HspB5) and HSP22 (HspB8) as regulators of cell death. *Int J Biochem Cell Biol* 2012. <https://doi.org/10.1016/j.biocel.2012.04.002>.
- [145] Voss OH, Batra S, Kolattukudy SJ, Gonzalez-Mejia ME, Smith JB, Doseff AI. Binding of caspase-3 prodomain to heat shock protein 27 regulates monocyte apoptosis by inhibiting caspase-3 proteolytic activation. *J Biol Chem* 2007. <https://doi.org/10.1074/jbc.M701740200>.
- [146] Zhao M, Shen F, Yin YX, Yang YY, Xiang DJ, Chen Q. Increased expression of heat shock protein 27 correlates with peritoneal metastasis in epithelial ovarian cancer. *Reprod Sci*

2012. <https://doi.org/10.1177/1933719111432875>.

[147] O'Callaghan-Sunol C, Gabai VL, Sherman MY. Hsp27 modulates p53 signaling and suppresses cellular senescence. *Cancer Res* 2007. <https://doi.org/10.1158/0008-5472.CAN-07-2441>.

[148] Bruey JM, Ducasse C, Bonniaud P, Ravagnan L, Susin SA, Diaz-Latoud C, et al. Hsp27 negatively regulates cell death by interacting with cytochrome c. *Nat Cell Biol* 2000. <https://doi.org/10.1038/35023595>.

[149] Lin SP, Lee YT, Wang JY, Miller SA, Chiou SH, Hung MC, et al. Survival of Cancer Stem Cells under Hypoxia and Serum Depletion via Decrease in PP2A Activity and Activation of p38-MAPKAPK2-Hsp27. *PLoS One* 2012. <https://doi.org/10.1371/journal.pone.0049605>.

[150] Kampinga HH, Hageman J, Vos MJ, Kubota H, Tanguay RM, Bruford EA, et al. Guidelines for the nomenclature of the human heat shock proteins. *Cell Stress Chaperones* 2009. <https://doi.org/10.1007/s12192-008-0068-7>.

[151] Hata M, Ohtsuka K. Characterization of HSE sequences in human Hsp40 gene: Structural and promoter analysis. *Biochim Biophys Acta - Gene Struct Expr* 1998. [https://doi.org/10.1016/S0167-4781\(97\)00208-X](https://doi.org/10.1016/S0167-4781(97)00208-X).

[152] Sterrenberg JN, Blatch GL, Edkins AL. Human DNAJ in cancer and stem cells. *Cancer Lett* 2011. <https://doi.org/10.1016/j.canlet.2011.08.019>.

[153] Mosser DD, Morimoto RI. Molecular chaperones and the stress of oncogenesis. *Oncogene* 2004. <https://doi.org/10.1038/sj.onc.1207529>.

[154] Trinh DLN, Elwi AN, Kim SW. Direct interaction between p53 and Tid1 proteins affects p53 mitochondrial localization and apoptosis. *Oncotarget* 2010.

<https://doi.org/10.18632/oncotarget.174>.

[155] Edwards KM, Münger K. Depletion of physiological levels of the human TID1 protein renders cancer cell lines resistant to apoptosis mediated by multiple exogenous stimuli.

Oncogene 2004. <https://doi.org/10.1038/sj.onc.1207732>.

[156] Syken J, De-Medina T, Münger K. TID1, a human homolog of the Drosophila tumor suppressor l(2)tid, encodes two mitochondrial modulators of apoptosis with opposing functions. Proc Natl Acad Sci U S A 1999. <https://doi.org/10.1073/pnas.96.15.8499>.

[157] Kim SW, Hayashi M, Lo JF, Fearn C, Xiang R, Lazennec G, et al. Tid1 negatively regulates the migratory potential of cancer cells by inhibiting the production of interleukin-8. Cancer Res 2005. <https://doi.org/10.1158/0008-5472.CAN-04-4422>.

[158] Kurzik-Dumke U, Hörner M, Czaja J, Nicotra MR, Simiantonaki N, Koslowski M, et al. Progression of colorectal cancers correlates with overexpression and loss of polarization of expression of the htid-1 tumor suppressor. Int J Mol Med 2008.

<https://doi.org/10.3892/ijmm.21.1.19>.

[159] Chen HW, Lee JY, Huang JY, Wang CC, Chen WJ, Su SF, et al. Curcumin inhibits lung cancer cell invasion and metastasis through the tumor suppressor HLJ1. Cancer Res 2008. <https://doi.org/10.1158/0008-5472.CAN-07-6734>.

[160] Tsai MF, Wang CC, Chang GC, Chen CY, Chen HY, Cheng CL, et al. A new tumor suppressor DnaJ-like heat shock protein, HLJ1, and survival of patients with non-small-cell lung carcinoma. J Natl Cancer Inst 2006. <https://doi.org/10.1093/jnci/djj229>.

[161] Wen KW, Damania B. Hsp90 and Hsp40/Erdj3 are required for the expression and anti-apoptotic function of KSHV K1. Oncogene 2010. <https://doi.org/10.1038/onc.2010.124>.

[162] Nishizawa S, Hirohashi Y, Torigoe T, Takahashi A, Tamura Y, Mori T, et al. HSP

DNAJB8 controls tumor-initiating ability in renal cancer stem-like cells. *Cancer Res* 2012.

<https://doi.org/10.1158/0008-5472.CAN-11-3062>.

[163] Yang T, Li XN, Li XG, Li M, Gao PZ. DNAJC6 promotes hepatocellular carcinoma progression through induction of epithelial-mesenchymal transition. *Biochem Biophys Res Commun* 2014. <https://doi.org/10.1016/j.bbrc.2014.11.011>.

[164] Desmetz C, Bibeau F, Boissière F, Bellet V, Rouanet P, Maudelonde T, et al. Proteomics-based identification of HSP60 as a tumor-associated antigen in early stage breast cancer and ductal carcinoma in situ. *J Proteome Res* 2008. <https://doi.org/10.1021/pr800130d>.

[165] Hjerpe E, Egyhazi S, Carlson J, Stolt MF, Schedvins K, Johansson H, et al. HSP60 predicts survival in advanced serous ovarian cancer. *Int J Gynecol Cancer* 2013. <https://doi.org/10.1097/IGC.0b013e318284308b>.

[166] Pang Q, Christianson TA, Keeble W, Koretsky T, Bagby GC. The anti-apoptotic function of Hsp70 in the interferon-inducible double-stranded RNA-dependent protein kinase-mediated death signaling pathway requires the Fanconi anemia protein, FANCC. *J Biol Chem* 2002. <https://doi.org/10.1074/jbc.M209386200>.

[167] Calderwood SK, Khaleque MA, Sawyer DB, Ciocca DR. Heat shock proteins in cancer: Chaperones of tumorigenesis. *Trends Biochem Sci* 2006. <https://doi.org/10.1016/j.tibs.2006.01.006>.

[168] Basu S, Binder RJ, Ramalingam T, Srivastava PK. CD91 is a common receptor for heat shock proteins gp96, hsp90, hsp70, and calreticulin. *Immunity* 2001. [https://doi.org/10.1016/S1074-7613\(01\)00111-X](https://doi.org/10.1016/S1074-7613(01)00111-X).

[169] Binder RJ, Srivastava PK. Essential role of CD91 in re-presentation of gp96-chaperoned peptides. *Proc Natl Acad Sci U S A* 2004.

<https://doi.org/10.1073/pnas.0308180101>.

[170] Srivastava P. Roles of heat-shock proteins in innate and adaptive immunity. *Nat Rev Immunol* 2002. <https://doi.org/10.1038/nri749>.

[171] Khan F, Ricks-Santi L, Hudson T, Beyene D, Naab T. HSP90 Expression Associated with HER2 Overexpressing Breast Ductal Carcinomas in African American Women. *Am J Clin Pathol* 2016. <https://doi.org/10.1093/ajcp/aqw159.068>.

[172] Ghosh JC, Siegelin MD, Dohi T, Altieri DC. Heat shock protein 60 regulation of the mitochondrial permeability transition pore in tumor cells. *Cancer Res* 2010. <https://doi.org/10.1158/0008-5472.CAN-10-2225>.

[173] Bloch O, Crane CA, Fuks Y, Kaur R, Aghi MK, Berger MS, et al. Heat-shock protein peptide complex-96 vaccination for recurrent glioblastoma: A phase II, single-arm trial. *Neuro Oncol* 2014. <https://doi.org/10.1093/neuonc/not203>.

[174] Crane CA, Han SJ, Ahn B, Oehlke J, Kivett V, Fedoroff A, et al. Individual patient-specific immunity against high-grade glioma after vaccination with autologous tumor derived peptides bound to the 96 KD chaperone protein. *Clin Cancer Res* 2013. <https://doi.org/10.1158/1078-0432.CCR-11-3358>.

[175] Rappa F, Farina F, Zummo G, David S, Campanella C, Carini F, et al. HSP-Molecular chaperones in cancer biogenesis and tumor therapy: An overview. *Anticancer Res* 2012.

[176] Kumar SJ, Stokes J, Singh UP, Scissum Gunn K, Acharya A, Manne U, et al. Targeting Hsp70: A possible therapy for cancer. *Cancer Lett* 2016. <https://doi.org/10.1016/j.canlet.2016.01.056>.

[177] Boudesco C, Cause S, Jegou G, Garrido C. Hsp70: A cancer target inside and outside the cell. *Methods Mol. Biol.*, 2018. https://doi.org/10.1007/978-1-4939-7477-1_27.

- [178] Sherman MY, Gabai VL. Hsp70 in cancer: Back to the future. *Oncogene* 2015. <https://doi.org/10.1038/onc.2014.349>.
- [179] Liu C, Li D, Zhang S, Liu Z. A Structural View of α B-crystallin Assembly and Amyloid Aggregation. *Protein Pept Lett* 2017. <https://doi.org/10.2174/0929866524666170206122616>.
- [180] Gotoh T, Terada K, Oyadomari S, Mori M. hsp70-DnaJ chaperone pair prevents nitric oxide- and CHOP-induced apoptosis by inhibiting translocation of Bax to mitochondria. *Cell Death Differ* 2004. <https://doi.org/10.1038/sj.cdd.4401369>.
- [181] Saleh A, Srinivasula SM, Balkir L, Robbins PD, Alnemri ES. Negative regulation of the Apaf-1 apoptosome by Hsp70. *Nat Cell Biol* 2000. <https://doi.org/10.1038/35019510>.
- [182] Gabai VL, Meriin AB, Mosser DD, Caron AW, Rits S, Shifrin VI, et al. Hsp70 prevents activation of stress kinases: A novel pathway of cellular thermotolerance. *J Biol Chem* 1997. <https://doi.org/10.1074/jbc.272.29.18033>.
- [183] Ravagnan L, Gurbuxani S, Susin SA, Maise C, Daugas E, Zamzami N, et al. Heat-shock protein 70 antagonizes apoptosis-inducing factor. *Nat Cell Biol* 2001. <https://doi.org/10.1038/ncb0901-839>.
- [184] Dugaard M, Kirkegaard-Sørensen T, Ostefeld MS, Aaboe M, Høyer-Hansen M, Ørntoft TF, et al. Lens epithelium-derived growth factor is an Hsp70-2 regulated guardian of lysosomal stability in human cancer. *Cancer Res* 2007. <https://doi.org/10.1158/0008-5472.CAN-06-4121>.
- [185] Nylandsted J, Gyrd-Hansen M, Danielewicz A, Fehrenbacher N, Lademann U, Høyer-Hansen M, et al. Heat shock protein 70 promotes cell survival by inhibiting lysosomal membrane permeabilization. *J Exp Med* 2004. <https://doi.org/10.1084/jem.20040531>.

[186] Chatterjee S, Bhattacharya S, Socinski MA, Burns TF. HSP90 inhibitors in lung cancer: Promise still unfulfilled. *Clin Adv Hematol Oncol* 2016.

[187] Yi X, Luk JM, Lee NP, Peng J, Leng X, Guan XY, et al. Association of mortalin (HSPA9) with liver cancer metastasis and prediction for early tumor recurrence. *Mol Cell Proteomics* 2008. <https://doi.org/10.1074/mcp.M700116-MCP200>.

[188] Schopf FH, Biebl MM, Buchner J. The HSP90 chaperone machinery. *Nat Rev Mol Cell Biol* 2017. <https://doi.org/10.1038/nrm.2017.20>.

[189] Gopal U, Bohonowych JE, Lema-Tome C, Liu A, Garrett-Mayer E, Wang B, et al. A novel extracellular Hsp90 mediated co-receptor function for LRP1 regulates EphA2 dependent glioblastoma cell invasion. *PLoS One* 2011. <https://doi.org/10.1371/journal.pone.0017649>.

[190] Thuringer D, Hammann A, Benikhlef N, Fourmaux E, Bouchot A, Wettstein G, et al. Transactivation of the epidermal growth factor receptor by heat shock protein 90 via toll-like receptor 4 contributes to the migration of glioblastoma cells. *J Biol Chem* 2011. <https://doi.org/10.1074/jbc.M110.154823>.

[191] O'Leary B, Finn RS, Turner NC. Treating cancer with selective CDK4/6 inhibitors. *Nat Rev Clin Oncol* 2016. <https://doi.org/10.1038/nrclinonc.2016.26>.

[192] Hanahan D, Weinberg RA. Hallmarks of cancer: The next generation. *Cell* 2011. <https://doi.org/10.1016/j.cell.2011.02.013>.

[193] Peyressatre M, Prével C, Pellerano M, Morris MC. Targeting cyclin-dependent kinases in human cancers: From small molecules to peptide inhibitors. *Cancers (Basel)* 2015. <https://doi.org/10.3390/cancers7010179>.

[194] Malumbres M, Barbacid M. Mammalian cyclin-dependent kinases. *Trends Biochem Sci*

2005. <https://doi.org/10.1016/j.tibs.2005.09.005>.

[195] Wohlschlegel JA, Dwyer BT, Takeda DY, Dutta A. Mutational Analysis of the Cyclin Motif from p21 Reveals Sequence Degeneracy and Specificity for Different Cyclin-Dependent Kinases. *Mol Cell Biol* 2001. <https://doi.org/10.1128/mcb.21.15.4868-4874.2001>.

[196] Errico A, Deshmukh K, Tanaka Y, Pozniakovsky A, Hunt T. Identification of substrates for cyclin dependent kinases. *Adv Enzyme Regul* 2010. <https://doi.org/10.1016/j.advenzreg.2009.12.001>.

[197] Modrek AS. Brain stem cells as the cell of origin in glioma. *World J Stem Cells* 2014. <https://doi.org/10.4252/wjsc.v6.i1.43>.

[198] Asghar U, Witkiewicz AK, Turner NC, Knudsen ES. The history and future of targeting cyclin-dependent kinases in cancer therapy. *Nat Rev Drug Discov* 2015. <https://doi.org/10.1038/nrd4504>.

[199] Rastogi N, Mishra DP. Therapeutic targeting of cancer cell cycle using proteasome inhibitors. *Cell Div* 2012. <https://doi.org/10.1186/1747-1028-7-26>.

[200] Cobanoglu G, Turacli I, Ozkan A, Ekmekci A. Flavopiridol's antiproliferative effects in glioblastoma multiforme. *J Cancer Res Ther* 2016. <https://doi.org/10.4103/0973-1482.172132>.

[201] Raub TJ, Wishart GN, Kulanthaivel P, Staton BA, Ajamie RT, Sawada GA, et al. Brain exposure of two selective dual CDK4 and CDK6 inhibitors and the antitumor activity of CDK4 and CDK6 inhibition in combination with temozolomide in an intracranial glioblastoma xenograft. *Drug Metab Dispos* 2015. <https://doi.org/10.1124/dmd.114.062745>.

[202] Zhou B, Bu G, Zhou Y, Zhao Y, Li W, Li M. Knockdown of CDC2 expression inhibits proliferation, enhances apoptosis, and increases chemosensitivity to temozolomide in

glioblastoma cells. *Med Oncol* 2015. <https://doi.org/10.1007/s12032-014-0378-9>.

[203] Aggarwal P, Vaites LP, Kim JK, Mellert H, Gurung B, Nakagawa H, et al. Nuclear cyclin D1/CDK4 kinase regulates CUL4 expression and triggers neoplastic growth via activation of the PRMT5 methyltransferase. *Cancer Cell* 2010. <https://doi.org/10.1016/j.ccr.2010.08.012>.

[204] Lam PYP, Ditomaso E, Ng HK, Pang JCS, Roussel MF, Hjelm NM. Expression of p19(INK4d), CDK4, CDK6 in glioblastoma multiforme. *Br J Neurosurg* 2000. <https://doi.org/10.1080/02688690042870>.

[205] Michaud K, Solomon DA, Oermann E, Kim JS, Zhong WZ, Prados MD, et al. Pharmacologic inhibition of cyclin-dependent kinases 4 and 6 arrests the growth of glioblastoma multiforme intracranial xenografts. *Cancer Res* 2010. <https://doi.org/10.1158/0008-5472.CAN-09-4559>.

[206] Parrish KE, Pokorny J, Mittapalli RK, Bakken K, Sarkaria JN, Elmquist WF. Efflux transporters at the blood-brain barrier limit delivery and efficacy of cyclin-dependent kinase 4/6 inhibitor palbociclib (PD-0332991) in an orthotopic brain tumor model. *J Pharmacol Exp Ther* 2015. <https://doi.org/10.1124/jpet.115.228213>.

[207] Chen YJ, Dominguez-Brauer C, Wang Z, Asara JM, Costa RH, Tyner AL, et al. A conserved phosphorylation site within the forkhead domain of FoxM1B is required for its activation by cyclin-CDK1. *J Biol Chem* 2009. <https://doi.org/10.1074/jbc.M109.007997>.

[208] Marais A, Ji Z, Child ES, Krause E, Mann DJ, Sharrocks AD. Cell cycle-dependent regulation of the forkhead transcription factor FOXK2 by CDK-cyclin complexes. *J Biol Chem* 2010. <https://doi.org/10.1074/jbc.M110.154005>.

[209] Kolodziej M, Goetz C, Di Fazio P, Montalbano R, Ocker M, Strik H, et al. Roscovitine

has anti-proliferative and pro-apoptotic effects on glioblastoma cell lines: A pilot study. *Oncol Rep* 2015. <https://doi.org/10.3892/or.2015.4105>.

[210] Patnaik A, Rosen LS, Tolaney SM, Tolcher AW, Goldman JW, Gandhi L, et al. Efficacy and safety of Abemaciclib, an inhibitor of CDK4 and CDK6, for patients with breast cancer, non-small cell lung cancer, and other solid tumors. *Cancer Discov* 2016.

<https://doi.org/10.1158/2159-8290.CD-16-0095>.

[211] Hou H, Nemani VK, Du G, Montano R, Song R, Gimi B, et al. Monitoring oxygen levels in orthotopic human glioma xenograft following carbogen inhalation and chemotherapy by implantable resonator-based oximetry. *Int J Cancer* 2015.

<https://doi.org/10.1002/ijc.29132>.

[212] Hayashi T, Adachi K, Ohba S, Hirose Y. The Cdk inhibitor flavopiridol enhances temozolomide-induced cytotoxicity in human glioma cells. *J Neurooncol* 2013.

<https://doi.org/10.1007/s11060-013-1220-5>.

[213] Alonso M, Tamasdan C, Miller DC, Newcomb EW. Flavopiridol induces apoptosis in glioma cell lines independent of retinoblastoma and p53 tumor suppressor pathway alterations by a caspase-independent pathway. *Mol Cancer Ther* 2003.

[214] Cimini A, d'Angelo M, Benedetti E, D'Angelo B, Laurenti G, Antonosante A, et al. Flavopiridol: An Old Drug With New Perspectives? Implication for Development of New Drugs. *J Cell Physiol* 2017. <https://doi.org/10.1002/jcp.25421>.

[215] Patel YT, Davis A, Baker SJ, Campagne O, Stewart CF. CNS penetration of the CDK4/6 inhibitor ribociclib in non-tumor bearing mice and mice bearing pediatric brain tumors. *Cancer Chemother Pharmacol* 2019. <https://doi.org/10.1007/s00280-019-03864-9>.

[216] Martínez-Chávez A, Van Hoppe S, Rosing H, Lebre MC, Tibben M, Beijnen JH, et al.

P-glycoprotein Limits Ribociclib Brain Exposure and CYP3A4 Restricts Its Oral

Bioavailability. *Mol Pharm* 2019. <https://doi.org/10.1021/acs.molpharmaceut.9b00475>.

[217] Tien AC, Li J, Bao X, Derogatis A, Kim S, Mehta S, et al. A phase 0 trial of ribociclib in recurrent glioblastoma patients incorporating a tumor pharmacodynamic- And pharmacokinetic-guided expansion cohort. *Clin Cancer Res* 2019.

<https://doi.org/10.1158/1078-0432.CCR-19-0133>.

[218] Zhang X, Lv H, Zhou Q, Elkholi R, Chipuk JE, Reddy MVR, et al. Preclinical pharmacological evaluation of a novel multiple kinase inhibitor, ON123300, in brain tumor models. *Mol Cancer Ther* 2014. <https://doi.org/10.1158/1535-7163.MCT-13-0847>.

[219] Jane EP, Premkumar DR, Cavaleri JM, Sutera PA, Rajasekar T, Pollack IF. Dinaciclib, a cyclin-dependent kinase inhibitor promotes proteasomal degradation of Mcl-1 and enhances ABT-737-mediated cell death in malignant human glioma cell lines. *J Pharmacol Exp Ther* 2016. <https://doi.org/10.1124/jpet.115.230052>.

[220] Parry D, Guzi T, Shanahan F, Davis N, Prabhavalkar D, Wiswell D, et al. Dinaciclib (SCH 727965), a novel and potent cyclin-dependent kinase inhibitor. *Mol Cancer Ther* 2010. <https://doi.org/10.1158/1535-7163.MCT-10-0324>.

[221] Paruch K, Dwyer MP, Alvarez C, Brown C, Chan TY, Doll RJ, et al. Discovery of dinaciclib (SCH 727965): A potent and selective inhibitor of cyclin-dependent kinases. *ACS Med Chem Lett* 2010. <https://doi.org/10.1021/ml100051d>.

[222] Chalmers AJ, Ruff EM, Martindale C, Lovegrove N, Short SC. Cytotoxic Effects of Temozolomide and Radiation are Additive- and Schedule-Dependent. *Int J Radiat Oncol Biol Phys* 2009. <https://doi.org/10.1016/j.ijrobp.2009.07.1703>.

[223] Nadkarni A, Shrivastav M, Mladek AC, Schwingler PM, Grogan PT, Chen J, et al.

- ATM inhibitor KU-55933 increases the TMZ responsiveness of only inherently TMZ sensitive GBM cells. *J Neurooncol* 2012. <https://doi.org/10.1007/s11060-012-0979-0>.
- [224] Vecchio D, Daga A, Carra E, Marubbi D, Baio G, Neumaier CE, et al. Predictability, efficacy and safety of radiosensitization of glioblastoma-initiating cells by the ATM inhibitor KU-60019. *Int J Cancer* 2014. <https://doi.org/10.1002/ijc.28680>.
- [225] Lescarbeau RS, Lei L, Bakken KK, Sims PA, Sarkaria JN, Canoll P, et al. Quantitative phosphoproteomics reveals wee1 kinase as a therapeutic target in a model of proneural glioblastoma. *Mol Cancer Ther* 2016. <https://doi.org/10.1158/1535-7163.MCT-15-0692-T>.
- [226] Sarcar B, Kahali S, Prabhu AH, Shumway SD, Xu Y, Demuth T, et al. Targeting radiation-induced G2 checkpoint activation with the wee-1 inhibitor MK-1775 in glioblastoma cell lines. *Mol Cancer Ther* 2011. <https://doi.org/10.1158/1535-7163.MCT-11-0469>.
- [227] Zitouni S, Nabais C, Jana SC, Guerrero A, Bettencourt-Dias M. Polo-like kinases: Structural variations lead to multiple functions. *Nat Rev Mol Cell Biol* 2014. <https://doi.org/10.1038/nrm3819>.
- [228] Triscott J, Lee C, Foster C, Manoranjan B, Pambid MR, Berns R, et al. Personalizing the treatment of pediatric medulloblastoma: Polo-like kinase 1 as a molecular target in high-risk children. *Cancer Res* 2013. <https://doi.org/10.1158/0008-5472.CAN-12-4331>.
- [229] Harris PS, Venkataraman S, Alimova I, Birks DK, Donson AM, Knipstein J, et al. Polo-like kinase 1 (PLK1) inhibition suppresses cell growth and enhances radiation sensitivity in medulloblastoma cells. *BMC Cancer* 2012. <https://doi.org/10.1186/1471-2407-12-80>.
- [230] Investigation TK-L, 2022 undefined. Grading of adult diffuse gliomas according to the 2021 WHO Classification of Tumors of the Central Nervous System. NatureCom n.d.

- [231] Masui K, Mischel PS, Reifenberger G. Molecular classification of gliomas. *Handb Clin Neurol* 2016;134:97–120. <https://doi.org/10.1016/B978-0-12-802997-8.00006-2>.
- [232] Gupta A, Dwivedi T. A simplified overview of World Health Organization classification update of central nervous system tumors 2016. *J Neurosci Rural Pract* 2017;8:629–41. https://doi.org/10.4103/JNRP.JNRP_168_17.
- [233] Di Carlo DT, Cagnazzo F, Benedetto N, Morganti R, Perrini P. Multiple high-grade gliomas: epidemiology, management, and outcome. A systematic review and meta-analysis. *Neurosurg Rev* 2019;42:263–75. <https://doi.org/10.1007/S10143-017-0928-7>.
- [234] Krex D, Klink B, Hartmann C, Von Deimling A, Pietsch T, Simon M, et al. Long-term survival with glioblastoma multiforme. *Brain* 2007;130:2596–606. <https://doi.org/10.1093/BRAIN/AWM204>.
- [235] Donehower LA, Soussi T, Korkut A, Liu Y, Schultz A, Cardenas M, et al. Integrated Analysis of TP53 Gene and Pathway Alterations in The Cancer Genome Atlas. *Cell Rep* 2019;28:1370-1384.e5. <https://doi.org/10.1016/J.CELREP.2019.07.001>.
- [236] Frosina G. Limited advances in therapy of glioblastoma trigger re-consideration of research policy. *Crit Rev Oncol Hematol* 2015;96:257–61. <https://doi.org/10.1016/J.CRITREVONC.2015.05.013>.
- [237] Brooks CL, Gu W. Dynamics in the p53-Mdm2 Ubiquitination Pathway. <https://doi.org/10.4161/CC.3.7.997>.
- [238] Zheng N, Shabek N. Ubiquitin Ligases: Structure, Function, and Regulation. <https://doi.org/10.1146/ANNUREV-BIOCHEM-060815-014922>.
- [239] Huang X, Dixit VM. Drugging the undruggables: exploring the ubiquitin system for

- drug development. *Cell Res* 2016 264 2016;26:484–98. <https://doi.org/10.1038/cr.2016.31>.
- [240] Clegg H V., Itahana K, Zhang Y. Unlocking the Mdm2-p53 loop: Ubiquitin is the key. <Http://DxDoiOrg/104161/Cc735358> 2008;7:287–92. <https://doi.org/10.4161/CC.7.3.5358>.
- [241] Umphlett M, Shea S, Tome-Garcia J, Zhang Y, Hormigo A, Fowkes M, et al. Widely metastatic glioblastoma with BRCA1 and ARID1A mutations: A case report. *BMC Cancer* 2020;20. <https://doi.org/10.1186/S12885-020-6540-1>.
- [242] Huang X, Chen J, Cao W, Yang L, Chen Q, ... JH-C death &, et al. The many substrates and functions of NEDD4-1. *NatureCom* n.d.
- [243] Alomari M. TRIM21 – A potential novel therapeutic target in cancer. *Pharmacol Res* 2021;165:105443. <https://doi.org/10.1016/J.PHRS.2021.105443>.
- [244] Humphreys L, Smith P, Chen Z, ... SF-CD&, 2021 undefined. The role of E3 ubiquitin ligases in the development and progression of glioblastoma. *NatureCom* n.d.
- [245] Simchi L, Panov J, Morsy O, ... YF-J of clinical, 2020 undefined. Novel insights into the role of UBE3A in regulating apoptosis and proliferation. *MdpiCom* n.d. <https://doi.org/10.3390/jcm9051573>.
- [246] Zhang S, Peng X, Li X, Liu H, Zhao B, ... ME-C death &, et al. BKM120 sensitizes glioblastoma to the PARP inhibitor rucaparib by suppressing homologous recombination repair. *NatureCom* n.d.
- [247] Lian Y, Huang Y, Zhang Y, Chen D, Theranostics JW-, 2019 undefined. CACYBP enhances cytoplasmic retention of P27Kip1 to promote hepatocellular carcinoma progression in the absence of RNF41 mediated degradation. *NcbiNlmNihGov* n.d.
- [248] Zhao Z, Wang Y, Yun D, Huang Q, ... DM-A journal of, 2020 undefined. TRIM21 overexpression promotes tumor progression by regulating cell proliferation, cell migration

and cell senescence in human glioma. NcbiNlmNihGov n.d.

[249] Haupt Y, Maya R, Kazaz A, Oren M. Mdm2 promotes the rapid degradation of p53.

Nat 1997 3876630 1997;387:296–9. <https://doi.org/10.1038/387296a0>.

[250] England B, Huang T, Karsy M. Current understanding of the role and targeting of tumor suppressor p53 in glioblastoma multiforme. Tumor Biol 2013 344 2013;34:2063–74.

<https://doi.org/10.1007/S13277-013-0871-3>.

[251] Yujun Zhao M, Aguilar A, Bernard D, Wang S. Small-molecule inhibitors of the MDM2–p53 protein–protein interaction (MDM2 Inhibitors) in clinical trials for cancer treatment: miniperspective. ACS Publ 2014;58:1038–52. <https://doi.org/10.1021/jm501092z>.

[252] Mello SS, Attardi LD. Deciphering p53 signaling in tumor suppression. Curr Opin Cell Biol 2018;51:65–72. <https://doi.org/10.1016/J.CEB.2017.11.005>.

[253] Kurki S, Latonen L, Laiho M. Cellular stress and DNA damage invoke temporally distinct Mdm2, p53 and PML complexes and damage-specific nuclear relocalization. J Cell Sci 2003;116:3917–25. <https://doi.org/10.1242/JCS.00714>.

[254] Jin Y, Xiao W, Song T, Feng G, Dai Z. Expression and Prognostic Significance of p53 in Glioma Patients: A Meta-analysis. Neurochem Res 2016;41:1723–31.

<https://doi.org/10.1007/S11064-016-1888-Y>.

[255] Schiebe M, Ohneseit P, Hoffmann W, Meyermann R, Rodemann HP, Bamberg M.

Analysis of mdm2 and p53 Gene Alterations in Glioblastomas and its Correlation with Clinical Factors. J Neuro-Oncology 2000 493 2000;49:197–203.

<https://doi.org/10.1023/A:1006410702284>.

[256] Nag S, Zhang X, Srivenugopal KS, Wang M-H, Wang W, Zhang R. Targeting MDM2–p53 Interaction for Cancer Therapy: Are We There Yet? n.d.

- [257] Her NG, Oh JW, Oh YJ, Han S, Cho HJ, Lee Y, et al. Potent effect of the MDM2 inhibitor AMG232 on suppression of glioblastoma stem cells. *Cell Death Dis* 2018 98 2018;9:1–12. <https://doi.org/10.1038/s41419-018-0825-1>.
- [258] Wang B, Fang L, Zhao H, Xiang T, Wang D. MDM2 inhibitor Nutlin-3a suppresses proliferation and promotes apoptosis in osteosarcoma cells. *Acta Biochim Biophys Sin (Shanghai)* 2012;44:685–91. <https://doi.org/10.1093/ABBS/GMS053>.
- [259] Ding Q, Zhang Z, Liu JJ, Jiang N, Zhang J, Ross TM, et al. Discovery of RG7388, a potent and selective p53-MDM2 inhibitor in clinical development. *J Med Chem* 2013. <https://doi.org/10.1021/jm400487c>.
- [260] Wang Y, Hoi P, Chan J, Lee S. New Perspective on the Dual Functions of Indirubins in Cancer Therapy and Neuroprotection. *Anticancer Agents Med Chem* 2014;14:1213–9. <https://doi.org/10.2174/1871520614666140825112924>.
- [261] Holzer P, Masuya K, Furet P, Kallen J, Valat-Stachyra T, Ferretti SS, et al. Discovery of a dihydroisoquinolinone derivative (NVP-CGM097): a highly potent and selective MDM2 inhibitor undergoing phase 1 clinical trials in p53wt tumors. *J Med Chem* 2015;58:22. <https://doi.org/10.1021/acs.jmedchem.5b00810>.
- [262] Sun D, Li Z, Rew Y, Gribble M, Bartberger MD, Beck HP, et al. Discovery of AMG 232, a potent, selective, and orally bioavailable MDM2-p53 inhibitor in clinical development. *J Med Chem* 2014;57:1454–72. https://doi.org/10.1021/JM401753E/SUPPL_FILE/JM401753E_SI_001.PDF.
- [263] Canon J, Osgood T, Olson SH, Saiki AY, Robertson R, Yu D, et al. The MDM2 Inhibitor AMG 232 Demonstrates Robust Antitumor Efficacy and Potentiates the Activity of p53-Inducing Cytotoxic Agents AMG 232 Regresses Tumors and. *AACR* 2015.

<https://doi.org/10.1158/1535-7163.MCT-14-0710>.

[264] Al-Ghabkari A, Narendran A. In Vitro Characterization of a Potent p53-MDM2 Inhibitor, RG7112 in Neuroblastoma Cancer Cell Lines. <https://HomeLieberpubCom/Cbr> 2019;34:252–7. <https://doi.org/10.1089/CBR.2018.2732>.

[265] Sirous H, Chemi G, Campiani G, Brogi S. An integrated in silico screening strategy for identifying promising disruptors of p53-MDM2 interaction. *Comput Biol Chem* 2019;83:107105. <https://doi.org/10.1016/J.COMPBIOLCHEM.2019.107105>.

[266] Lemos A, Gomes A, Loureiro J, Molecules PB-, 2019 undefined. Synthesis, biological evaluation, and in silico studies of novel aminated xanthenes as potential p53-activating agents. *MdpiCom* n.d.

[267] Zhai K, Siddiqui M, Abdellatif B, Liskova A, Kubatka P, Büsselberg D. Natural Compounds in Glioblastoma Therapy: Preclinical Insights, Mechanistic Pathways, and Outlook. *Cancers (Basel)* 2021;13. <https://doi.org/10.3390/CANCERS13102317>.

[268] Rehman S, Khan H. *Advances in Antioxidant Potential of Natural Alkaloids* n.d.

[269] Cos S, Sánchez-Barceló EJ. Melatonin inhibition of MCF-7 human breast-cancer cells growth: influence of cell proliferation rate. *Cancer Lett* 1995;93:207–12. [https://doi.org/10.1016/0304-3835\(95\)03811-A](https://doi.org/10.1016/0304-3835(95)03811-A).

[270] Proietti S, Cucina A, Dobrowolny G, D'Anselmi F, Dinicola S, Masiello MG, et al. Melatonin down-regulates MDM2 gene expression and enhances p53 acetylation in MCF-7 cells. *J Pineal Res* 2014;57:120–9. <https://doi.org/10.1111/JPI.12150>.

[271] Inada M, Shindo M, Kobayashi K, Sato A, Yamamoto Y, Akasaki Y, et al. Anticancer effects of a non-narcotic opium alkaloid medicine, papaverine, in human glioblastoma cells. *PLoS One* 2019; 14:e0216358. <https://doi.org/10.1371/JOURNAL.PONE.0216358>.

- [272] Gavaraskar K, Dhulap S, Hirwani RR. Therapeutic and cosmetic applications of Evodiamine and its derivatives—A patent review. *Fitoterapia* 2015;106:22–35.
<https://doi.org/10.1016/J.FITOTE.2015.07.019>.
- [273] Jiang J, Hu C. Evodiamine: A Novel Anti-Cancer Alkaloid from *Evodia rutaecarpa*. *Mol* 2009, Vol 14, Pages 1852-1859 2009;14:1852–9.
<https://doi.org/10.3390/MOLECULES14051852>.
- [274] Liu AJ, Wang SH, Chen KC, Kuei HP, Shih YL, Hou SY, et al. Evodiamine, a plant alkaloid, induces calcium/JNK-mediated autophagy and calcium/mitochondria-mediated apoptosis in human glioblastoma cells. *Chem Biol Interact* 2013;205:20–8.
<https://doi.org/10.1016/J.CBI.2013.06.004>.
- [275] Liang Z, Wang Y, Zhang H, Deng J, Lei F, Li J, et al. Design, synthesis and bioactivity evaluation of favorable evodiamine derivative scaffold for developing cancer therapy. *Eur J Med Chem* 2022;239:114530. <https://doi.org/10.1016/J.EJMECH.2022.114530>.
- [276] Choi WY, Kim GY, Lee WH, Choi YH. Sanguinarine, a Benzophenanthridine Alkaloid, Induces Apoptosis in MDA-MB-231 Human Breast Carcinoma Cells through a Reactive Oxygen Species-Mediated Mitochondrial Pathway. *Chemotherapy* 2008;54:279–87.
<https://doi.org/10.1159/000149719>.
- [277] Du H, Peng Q, Gu J, Qiu P, Liu L, Du B, et al. Effect of Evodiamine on Cancer Metabolism of Liver Tumor Through Met/EGFR and HIF Pathways. *SSRN Electron J* 2022.
<https://doi.org/10.2139/SSRN.4095315>.
- [278] Mohan V, Agarwal R, Singh RP. A novel alkaloid, evodiamine causes nuclear localization of cytochrome-c and induces apoptosis independent of p53 in human lung cancer cells. *Biochem Biophys Res Commun* 2016;477:1065–71.

<https://doi.org/10.1016/J.BBRC.2016.07.037>.

[279] Han S, Woo JK, Jung Y, Jeong D, Kang M, Yoo YJ, et al. Evodiamine selectively targets cancer stem-like cells through the p53-p21-Rb pathway. *Biochem Biophys Res Commun* 2016;469:1153–8. <https://doi.org/10.1016/J.BBRC.2015.12.066>.

[280] Basu P, diseases GK-A nutraceuticals and chronic, 2016 undefined. *Sanguinarine and its role in chronic diseases*. Springer n.d.

[281] Zhang B, Wang X, Deng J, Zheng H, Liu W, Chen S, et al. p53-dependent upregulation of miR-16-2 by sanguinarine induces cell cycle arrest and apoptosis in hepatocellular carcinoma. *Cancer Lett* 2019;459:50–8. <https://doi.org/10.1016/J.CANLET.2019.05.042>.

[282] Han MH, Kim SO, Kim GY, Kwon TK, Choi BT, Lee WH, et al. Induction of apoptosis by sanguinarine in C6 rat glioblastoma cells is associated with the modulation of the Bcl-2 family and activation of caspases through downregulation of extracellular signal-regulated kinase and Akt. *Anticancer Drugs* 2007;18:913–21. <https://doi.org/10.1097/CAD.0B013E328117F463>.

[283] Ghauri MA, Su Q, Ullah A, Wang J, Sarwar A, Wu Q, et al. Sanguinarine impedes metastasis and causes inversion of epithelial to mesenchymal transition in breast cancer. *Phytomedicine* 2021;84:153500. <https://doi.org/10.1016/J.PHYMED.2021.153500>.

[284] Pallichankandy S, Rahman A, ... FT-FRB, 2015 undefined. ROS-dependent activation of autophagy is a critical mechanism for the induction of anti-glioma effect of sanguinarine. Elsevier n.d.

[285] Kulikov R, Letienne J, Kaur M, Grossman SR, Arts J, Blattner C. Mdm2 facilitates the association of p53 with the proteasome. *Proc Natl Acad Sci U S A* 2010;107:10038–43. <https://doi.org/10.1073/PNAS.0911716107>.

- [286] Zhang X, Gu L, Li J, Shah N, He J, Yang L, et al. Degradation of MDM2 by the Interaction between Berberine and DAXX Leads to Potent Apoptosis in MDM2-Overexpressing Cancer Cells Berberine Inhibits MDM2 in. AACR n.d.
- [287] Zhou N, Li J, Li T, ... GC-M medicine, 2017 undefined. Matrine-induced apoptosis in Hep3B cells via the inhibition of MDM2. Spandidos-PublicationsCom n.d.
- [288] Brew CT, Aronchik I, Hsu JC, Sheen J-H, Dickson RB, Bjeldanes LF, et al. Indole-3-carbinol activates the ATM signaling pathway independent of DNA damage to stabilize p53 and induce G1 arrest of human mammary epithelial [1] C. T. Brew et al., "Indole-3-carbinol activates the ATM signaling pathway independent of DNA damage to st. Wiley Online Libr 2006;118:857–68. <https://doi.org/10.1002/ijc.21445>.
- [289] Patil SP, Pacitti MF, Gilroy KS, Ruggiero JC, Griffin JD, Butera JJ, et al. Identification of antipsychotic drug fluspirilene as a potential p53-MDM2 inhibitor: A combined computational and experimental study. J Comput Aided Mol Des 2015;29:155–63. <https://doi.org/10.1007/S10822-014-9811-6/FIGURES/4>.
- [290] Clough E, Barrett T. The Gene Expression Omnibus database. Methods Mol Biol 2016;1418:93–110. https://doi.org/10.1007/978-1-4939-3578-9_5.
- [291] Kim S, Thiessen PA, Bolton EE, Chen J, Fu G, Gindulyte A, et al. PubChem Substance and Compound databases. Nucleic Acids Res 2016;44:D1202–13. <https://doi.org/10.1093/NAR/GKV951>.
- [292] Daina A, Michielin O, Zoete V. SwissADME: a free web tool to evaluate pharmacokinetics, drug-likeness and medicinal chemistry friendliness of small molecules. Sci Reports 2017 7:1 2017;7:1–13. <https://doi.org/10.1038/srep42717>.
- [293] Kochnev Y, Hellemann E, Cassidy KC, Durrant JD. Webina: an open-source library

and web app that runs AutoDock Vina entirely in the web browser. *Bioinformatics* 2020;36:4513–5. <https://doi.org/10.1093/BIOINFORMATICS/BTAA579>.

[294] Pawar SS, Rohane SH. Review on Discovery Studio: An important Tool for Molecular Docking. *Asian J Res Chem* 2021;14:1–3. <https://doi.org/10.5958/0974-4150.2021.00014.6>.

[295] Humphreys L, Smith P, Chen Z, ... SF-CD&, 2021 undefined. The role of E3 ubiquitin ligases in the development and progression of glioblastoma. *NatureCom* n.d.

[296] Daniele S, Costa B, Zappelli E, Pozzo E Da, reports SS-S, 2015 undefined. Combined inhibition of AKT/mTOR and MDM2 enhances Glioblastoma Multiforme cell apoptosis and differentiation of cancer stem cells. *NatureCom* n.d.

[297] Kubbutat MHG, Jones SN, Vousden KH. Regulation of p53 stability by Mdm2. *Nature* 1997;387:299–303. <https://doi.org/10.1038/387299A0>.

[298] Bond U, genetics MS-A in, 1987 undefined. Heat-shock proteins and development. *Elsevier* n.d.

[299] biology HS-N reviews M cell, 2013 undefined. Chaperone machines for protein folding, unfolding and disaggregation. *NatureCom* n.d.

[300] Hu C, Yang J, Qi Z, Wu H, Wang B, Zou F, et al. Heat shock proteins: Biological functions, pathological roles, and therapeutic opportunities. *Wiley Online Libr* 2022;3. <https://doi.org/10.1002/mco2.161>.

[301] Sherman M, of GM-A of the NYA, 2007 undefined. Heat shock proteins in cancer. *Wiley Online Libr* 2007;1113:192–201. <https://doi.org/10.1196/annals.1391.030>.

[302] Hasan A, Rizvi S, Parveen S, Sciences SM-L, 2022 undefined. Molecular chaperones in DNA repair mechanisms: Role in genomic instability and proteostasis in cancer. *Elsevier* n.d.

- [303] Han L, Tang L, Jiang Z, Jiang Y. Enhanced radiosensitization of human glioblastoma multiforme cells with phosphorylated peptides derived from Gli2. *Neuropeptides* 2018;70:87–92. <https://doi.org/10.1016/J.NPEP.2018.05.009>.
- [304] Oppenheim J, Strauss R, ... JM-, 1994 undefined. Ependymomas of the third ventricle. *JournalsLwwCom* n.d.
- [305] Centeno R, Lee A, Winter J, neurosurgery DB-J of, 1986 undefined. Supratentorial ependymomas: neuroimaging and clinicopathological correlation. *ThejnsOrg* n.d.
- [306] De Angelis R, Sant M, Coleman MP, Francisci S, Baili P, Pierannunzio D, et al. Cancer survival in Europe 1999–2007 by country and age: results of EURO CARE-5—a population-based study. *TheLancetCom* 2013. [https://doi.org/10.1016/S1470-2045\(13\)70546-1](https://doi.org/10.1016/S1470-2045(13)70546-1).
- [307] Gatta G, Capocaccia R, Coleman MP, Gloeckler Ries LA, Berrino F. Childhood cancer survival in Europe and the United States. *Wiley Online Libr* 2002;95:1767–72. <https://doi.org/10.1002/cncr.10833>.
- [308] Bouffet E, Foreman N. Chemotherapy for intracranial ependymomas. *Child’s Nerv Syst* 1999;15:563–70. <https://doi.org/10.1007/S003810050544>.
- [309] Sauvageot C, Weatherbee J, ... SK-N, 2009 undefined. Efficacy of the HSP90 inhibitor 17-AAG in human glioma cell lines and tumorigenic glioma stem cells. *AcademicOupCom* n.d.
- [310] Premkumar DR, Arnold B, Pollack IF. Cooperative inhibitory effect of ZD1839 (Iressa) in combination with 17-AAG on glioma cell growth. *Mol Carcinog* 2006;45:288–301. <https://doi.org/10.1002/MC.20141>.
- [311] Braunstein M, Scott S, Scott C, ... SB-J of, 2011 undefined. Antimyeloma effects of the heat shock protein 70 molecular chaperone inhibitor MAL3-101. *HindawiCom* n.d.

- [312] Silva A, Lopes C, Júnior C, Vitro RT-T in, 2019 undefined. WIN55, 212-2 induces caspase-independent apoptosis on human glioblastoma cells by regulating HSP70, p53 and Cathepsin D. Elsevier n.d.
- [313] Yao F, Zhang K, Zhang Y, Guo Y, Li A, Xiao S, et al. Identification of Blood Biomarkers for Alzheimer's Disease Through Computational Prediction and Experimental Validation. *Front Neurol* 2019;9. <https://doi.org/10.3389/FNEUR.2018.01158>.
- [314] Singh P, Unik B, Puri A, Nagpal G, Singh B, Gautam A, et al. HSPMdb: a computational repository of heat shock protein modulators. *Database* 2020;2020:3. <https://doi.org/10.1093/DATABASE/BAAA003>.
- [315] Advani D, Kumar P. Deciphering the molecular mechanism and crosstalk between Parkinson's disease and breast cancer through multi-omics and drug repurposing approach. *Neuropeptides* 2022;96:102283. <https://doi.org/10.1016/J.NPEP.2022.102283>.
- [316] Zhou G, Soufan O, Ewald J, ... RH-N acids, 2019 undefined. NetworkAnalyst 3.0: a visual analytics platform for comprehensive gene expression profiling and meta-analysis. AcademicOupCom n.d.
- [317] Sharma S, Kumar P. Decoding the Role of MDM2 as a Potential Ubiquitin E3 Ligase and Identifying the Therapeutic Efficiency of Alkaloids against MDM2 in Combating Glioblastoma. *ACS Omega* 2023;8:5072–87. https://doi.org/10.1021/ACSOMEGA.2C07904/ASSET/IMAGES/MEDIUM/AO2C07904_0003.GIF.
- [318] Liao Y, Wang J, Jaehnig EJ, Shi Z, Zhang B. WebGestalt 2019: gene set analysis toolkit with revamped UIs and APIs. *Nucleic Acids Res* 2019;47:W199–205. <https://doi.org/10.1093/NAR/GKZ401>.

[319] Zhang B, Kirov S, Snoddy J. WebGestalt: An integrated system for exploring gene sets in various biological contexts. *Nucleic Acids Res* 2005;33.

<https://doi.org/10.1093/NAR/GKI475>.

[320] Wu T, Hu E, Xu S, Chen M, Guo P, Dai Z, et al. clusterProfiler 4.0: A universal enrichment tool for interpreting omics data. *Innov* 2021;2:100141.

<https://doi.org/10.1016/J.XINN.2021.100141>.

[321] Falktoft B, Georg B, Fahrenkrug J. Calmodulin interacts with PAC1 and VPAC2 receptors and regulates PACAP-induced FOS expression in human neuroblastoma cells. *Neuropeptides* 2009;43:53–61.

<https://doi.org/10.1016/J.NPEP.2009.02.001>.

[322] Auerbach RK, Chen B, Butte AJ. Relating genes to function: identifying enriched transcription factors using the ENCODE ChIP-Seq significance tool. *Bioinformatics* 2013;29:1922–4.

<https://doi.org/10.1093/BIOINFORMATICS/BTT316>.

[323] Goi CL, Little P, Xie C. Cell-type and transcription factor specific enrichment of transcriptional cofactor motifs in ENCODE ChIP-seq data. *BMC Genomics* 2013;14:1–11.

<https://doi.org/10.1186/1471-2164-14-S5-S2/FIGURES/4>.

[324] Bisht I, Ambasta R, *Neuropeptides PK-*, 2020 undefined. An integrated approach to unravel a putative crosstalk network in Alzheimer’s disease and Parkinson’s disease. Elsevier n.d.

[325] Karagkouni D, ... *MP-N acids*, 2018 undefined. DIANA-TarBase v8: a decade-long collection of experimentally supported miRNA–gene interactions. AcademicOupCom n.d.

[326] Wingender E, Kel A, Krull M. Transcription Factor Databases. *Encycl Bioinforma Comput Biol ABC Bioinforma* 2019;1–3:134–41. <https://doi.org/10.1016/B978-0-12-809633-8.20216-1>.

- [327] Matys V, Kel-Margoulis O V., Fricke E, Liebich I, Land S, Barre-Dirrie A, et al. TRANSFAC and its module TRANSCompel: transcriptional gene regulation in eukaryotes. *Nucleic Acids Res* 2006;34. <https://doi.org/10.1093/NAR/GKJ143>.
- [328] Betel D, Wilson M, Gabow A, Marks DS, Sander C. The microRNA.org resource: targets and expression. *Nucleic Acids Res* 2008;36:D149. <https://doi.org/10.1093/NAR/GKM995>.
- [329] Agarwal V, Bell GW, Nam JW, Bartel DP. Predicting effective microRNA target sites in mammalian mRNAs. *Elife* 2015;4. <https://doi.org/10.7554/ELIFE.05005>.
- [330] Kertesz M, Iovino N, Unnerstall U, Gaul U, Segal E. The role of site accessibility in microRNA target recognition. *Nat Genet* 2007 3910 2007;39:1278–84. <https://doi.org/10.1038/ng2135>.
- [331] Wang Z, Monteiro CD, Jagodnik KM, Fernandez NF, Gundersen GW, Rouillard AD, et al. Extraction and analysis of signatures from the Gene Expression Omnibus by the crowd. *Nat Commun* 2016 71 2016;7:1–11. <https://doi.org/10.1038/ncomms12846>.
- [332] Karatzas E, Minadakis G, Kolios G, Delis A, Spyrou GM. A Web Tool for Ranking Candidate Drugs Against a Selected Disease Based on a Combination of Functional and Structural Criteria. *Comput Struct Biotechnol J* 2019;17:939–45. <https://doi.org/10.1016/J.CSBJ.2019.05.010>.
- [333] Masoumi J, Abbasloui M, Parvan R, Mohammadnejad D, Pavon-Djavid G, Barzegari A, et al. *ne. Neuropeptides* 2018;70:76–86. <https://doi.org/10.1016/J.NPEP.2018.05.008>.
- [334] Zuehlke AD, Beebe K, Neckers L, Prince T. Regulation and function of the human HSP90AA1 gene. *Gene* 2015;570:8–16. <https://doi.org/10.1016/J.GENE.2015.06.018>.
- [335] Gomez-Llorente Y, Jebara F, Patra M, ... RM-N, 2020 undefined. Structural basis for

active single and double ring complexes in human mitochondrial Hsp60-Hsp10 chaperonin. NatureCom n.d.

[336] Teng R, Liu Z, Tang H, Zhang W, Chen Y, Xu R, et al. HSP60 silencing promotes Warburg-like phenotypes and switches the mitochondrial function from ATP production to biosynthesis in ccRCC cells. Elsevier n.d.

[337] Rappa F, Unti E, Baiamonte P, ... FC-EJ of, 2013 undefined. Different immunohistochemical levels of Hsp60 and Hsp70 in a subset of brain tumors and putative role of Hsp60 in neuroepithelial tumorigenesis. NcbiNlmNihGov n.d.

[338] Hallal S, Russell BP, Wei H, Yuk Lee MT, Toon CW, Sy J, et al. Extracellular vesicles from neurosurgical aspirates identifies chaperonin containing TCP1 subunit 6A as a potential glioblastoma biomarker with prognostic. Wiley Online Libr 2019;19.

<https://doi.org/10.1002/pmic.201800157>.

[339] Zhang M, Pan Y, Qi X, Liu Y, ... RD-A, 2018 undefined. Identification of new biomarkers associated with IDH mutation and prognosis in astrocytic tumors using NanoString nCounter analysis system. IngentaconnectCom n.d.

[340] Zhang H, Yin X, Zhang X, Zhou M, Xu W, Wei Z, et al. HSP90AB1 Promotes the Proliferation, Migration, and Glycolysis of Head and Neck Squamous Cell Carcinoma. Technol Cancer Res Treat 2022;21. <https://doi.org/10.1177/15330338221118202>.

[341] Zhou G, Pu Y, Zhao K, Chen Y, Zhang G. Heat Shock Proteins in Non-Small-Cell Lung Cancer-Functional Mechanism. Front Biosci - Landmark 2023;28. <https://doi.org/10.31083/J.FBL2803056/HTM>.

[342] Venkataraman V, George S, Oncologist GC-T, 2023 undefined. Molecular Advances in the Treatment of Advanced Gastrointestinal Stromal Tumor. AcademicOupCom n.d.

- [343] Yano M, Naito Z, Tanaka S, Asano G. Expression and roles of heat shock proteins in human breast cancer. *Japanese J Cancer Res* 1996;87:908–15. <https://doi.org/10.1111/J.1349-7006.1996.TB02119.X>.
- [344] Liu SJ, Magill ST, Vasudevan HN, Hilz S, Villanueva-Meyer JE, Lastella S, et al. Multiplatform Molecular Profiling Reveals Epigenomic Intratumor Heterogeneity in Ependymoma. *Cell Rep* 2020;30:1300. <https://doi.org/10.1016/J.CELREP.2020.01.018>.
- [345] Xu W, Mollapour M, Prodromou C, Wang S, Scroggins BT, Palchick Z, et al. Dynamic Tyrosine Phosphorylation Modulates Cycling of the HSP90-P50 CDC37-AHA1 Chaperone Machine. *Mol Cell* 2012;47:434–43. <https://doi.org/10.1016/j.molcel.2012.05.015>.
- [346] Sims JD, McCready J, Jay DG. Extracellular heat shock protein (Hsp)70 and Hsp90 α assist in matrix metalloproteinase-2 activation and breast cancer cell migration and invasion. *PLoS One* 2011;6. <https://doi.org/10.1371/JOURNAL.PONE.0018848>.
- [347] Niu M, Zhang B, Li L, Su Z, Pu W, Zhao C, et al. Targeting HSP90 Inhibits Proliferation and Induces Apoptosis Through AKT1/ERK Pathway in Lung Cancer. *Front Pharmacol* 2022;12. <https://doi.org/10.3389/FPHAR.2021.724192/FULL>.
- [348] Amini-Khoei H, Saghaei E, Mobini G-R, Sabzevary-Ghahfarokhi M, Ahmadi R, Bagheri N, et al. Possible involvement of PI3K/AKT/mTOR signaling pathway in the protective effect of selegiline (deprenyl) against memory impairment following ischemia reperfusion. *Elsevier* 1942:101942. <https://doi.org/10.1016/j.npep.2019.101942>.
- [349] Henao-Restrepo J, Caro-Urrego YA, Barrera-Arenas LM, Arango-Viana JC, Bermudez-Munoz M. Expression of activator proteins of SHH/GLI and PI3K/Akt/mTORC1 signaling pathways in human gliomas is associated with high grade tumors. *Exp Mol Pathol* 2021; 122:104673. <https://doi.org/10.1016/J.YEXMP.2021.104673>.

[350] Obacz J, Avril T, Le Reste PJ, Urra H, Quillien V, Hetz C, et al. Endoplasmic reticulum proteostasis in glioblastoma—From molecular mechanisms to therapeutic perspectives. *Sci Signal* 2017;10. <https://doi.org/10.1126/SCISIGNAL.AAL2323>.

[351] Manfreda L, Rampazzo E, *Biology LP-*, 2023 undefined. Wnt Signaling in Brain Tumors: A Challenging Therapeutic Target. *MdpiCom* 2023. <https://doi.org/10.3390/biology>.

[352] Misawa-Omori E, Okihara H, Ogawa T, Abe Y, *Neuropeptides CK-*, 2023 undefined. Reduced mastication during growth inhibits cognitive function by affecting trigeminal ganglia and modulating Wnt signaling pathway and ARHGAP33 molecular. *Elsevier* n.d.

[353] Carballo GB, Honorato JR, De Lopes GPF, Spohr TCLDSE. A highlight on Sonic hedgehog pathway. *Cell Commun Signal* 2018;16. <https://doi.org/10.1186/S12964-018-0220-7>.

[354] Li H, Batth IS, Qu X, Xu L, Song N, Wang R, et al. IGF-IR signaling in epithelial to mesenchymal transition and targeting IGF-IR therapy: overview and new insights. *Mol Cancer* 2017 161 2017;16:1–15. <https://doi.org/10.1186/S12943-016-0576-5>.

[355] Abounader R, *Neuro-oncology JL-*, 2005 undefined. Scatter factor/hepatocyte growth factor in brain tumor growth and angiogenesis. *Acad Abounader, J LaterraNeuro-Oncology*, 2005•academicOupCom 2005. <https://doi.org/10.1215/S1152851705000050>.

[356] Sie M, Den Dunnen WFA, Lourens HJ, Meeuwssen-De Boer TGJ, Scherpen FJG, Zommerman WW, et al. Growth-factor-driven rescue to Receptor Tyrosine Kinase (RTK) inhibitors through Akt and Erk phosphorylation in pediatric low grade astrocytoma and ependymoma. *PLoS One* 2015;10. <https://doi.org/10.1371/JOURNAL.PONE.0122555>.

[357] Weiner H, Rothman M, Miller D, *neurosurgery EZ-P*, 1996 undefined. Pediatric brain tumors express multiple receptor tyrosine kinases including novel cell adhesion kinases.

KargerComHL Weiner, M Rothman, DC Miller, EB ZiffPediatric Neurosurgery,

1996•kargerCom n.d.

[358] Fu Y, Liu CJ, Kobayashi DK, Johanns TM, Bowman-Kirigin JA, Schaettler MO, et al. GATA2 Regulates Constitutive PD-L1 and PD-L2 Expression in Brain Tumors. *Sci Rep* 2020;10. <https://doi.org/10.1038/S41598-020-65915-Z>.

[359] Cao Q, Wang X, Shi Y, Zhang M, Yang J, Dong M, et al. FOXC1 silencing inhibits the epithelial-to-mesenchymal transition of glioma cells: Involvement of [beta]-catenin signaling. *Mol Med Rep* 2019;19:251–62.

[360] Cox JL, Wilder PJ, Gilmore JM, Wuebben EL, Washburn MP, Rizzino A. The SOX2-Interactome in Brain Cancer Cells Identifies the Requirement of MSI2 and USP9X for the Growth of Brain Tumor Cells. *PLoS One* 2013;8:62857. <https://doi.org/10.1371/JOURNAL.PONE.0062857>.

[361] Krell A, Wolter M, Stojcheva N, Hertler C, Liesenberg F, Zapatka M, et al. MiR-16-5p is frequently down-regulated in astrocytic gliomas and modulates glioma cell proliferation, apoptosis and response to cytotoxic therapy. *Neuropathol Appl Neurobiol* 2019;45:441–58. <https://doi.org/10.1111/NAN.12532>.

[362] Ma S, Wei H, Wang C, Han J, Chen X, Li Y. MiR-26b-5p inhibits cell proliferation and EMT by targeting MYCBP in triple-negative breast cancer. *Cell Mol Biol Lett* 2021;26. <https://doi.org/10.1186/S11658-021-00288-3>.

[363] Niu F, Kazimierska M, Nolte IM, Terpstra MM, de Jong D, Koerts J, et al. The miR-26b-5p/KPNA2 Axis Is an Important Regulator of Burkitt Lymphoma Cell Growth. *Cancers* 2020, Vol 12, Page 1464 2020;12:1464. <https://doi.org/10.3390/CANCERS12061464>.

[364] Perry A, Miller CR, Gujrati M, Scheithauer BW, Zambrano SC, Jost SC, et al.

Malignant gliomas with primitive neuroectodermal tumor-like components: A

clinicopathologic and genetic study of 53 cases. *Brain Pathol* 2009;19:81–90.

<https://doi.org/10.1111/J.1750-3639.2008.00167.X>.

[365] Haberler C, Slavc I, Czech T, Gelpi E, Heinzl H, Budka H, et al. Histopathological prognostic factors in medulloblastoma: High expression of survivin is related to unfavourable outcome. *Eur J Cancer* 2006;42:2996–3003. <https://doi.org/10.1016/j.ejca.2006.05.038>.

[366] Shrestha S, Morcavallo A, Gorrini C, Chesler L. Biological Role of MYCN in Medulloblastoma: Novel Therapeutic Opportunities and Challenges Ahead. *Front Oncol* 2021;11. <https://doi.org/10.3389/FONC.2021.694320/FULL>.

[367] Issac J, Raveendran PS, Das A V. RFX1: a promising therapeutic arsenal against cancer. *Cancer Cell Int* 2021;21:1–19. <https://doi.org/10.1186/S12935-021-01952-6/FIGURES/5>.

[368] Shankar S, Singh G, Srivastava RK. Chemoprevention by resveratrol: Molecular mechanisms and therapeutic potential. *Front Biosci* 2007;12:4839–54. <https://doi.org/10.2741/2432>.

[369] Ma XR, Sun ZK, Han X, Li S, Jiang X, Chen S, et al. Neuroprotective Effect of Resveratrol via Activation of Sirt1 Signaling in a Rat Model of Combined Diabetes and Alzheimer's Disease. *Front Neurosci* 2020;13. <https://doi.org/10.3389/FNINS.2019.01400/FULL>.

[370] Öztürk Y, Günaydın C, Yalçın F, Nazıroğlu M, Braidy N. Resveratrol Enhances Apoptotic and Oxidant Effects of Paclitaxel through TRPM2 Channel Activation in DBTRG Glioblastoma Cells. *Oxid Med Cell Longev* 2019;2019. <https://doi.org/10.1155/2019/4619865>.

[371] Wang L, Gundelach JH, Bram RJ. Cycloheximide promotes paraptosis induced by inhibition of cyclophilins in glioblastoma multiforme. *Cell Death Dis* 2017 8:5 2017;8:e2807–e2807. <https://doi.org/10.1038/cddis.2017.217>.

[372] Youssef M, Cavalu S, Hasan A, ... GY-IJ of, 2023 undefined. Role of Ganetespib, an HSP90 Inhibitor, in Cancer Therapy: From Molecular Mechanisms to Clinical Practice. MdpiCom n.d.

[373] Chao KSC, Hsu JSJ, Xu J, Ezekiel UR, Eves E, Rosner M, et al. Differential effect of cycloheximide on neuronal and glioma cells treated with chemotherapy and radiation. *J Neurooncol* 1999;45:19–26. <https://doi.org/10.1023/A:1006342006836/METRICS>.

[374] Koshimizu T aki, Tsuchiya H, Tsuda H, Fujiwara Y, Shibata K, Hirasawa A, et al. Inhibition of heat shock protein 90 attenuates adenylate cyclase sensitization after chronic morphine treatment. *Biochem Biophys Res Commun* 2010;392:603–7. <https://doi.org/10.1016/J.BBRC.2010.01.089>.

[375] de Jesus SF, de Souza MG, Queiroz L dos RP, de Paula DPS, Tabosa ATL, Alves WSM, et al. Gallic acid has an inhibitory effect on skin squamous cell carcinoma and acts on the heat shock protein HSP90AB1. *Gene* 2023;851:147041. <https://doi.org/10.1016/J.GENE.2022.147041>.

[376] Orth M, Albrecht V, Seidl K, Kinzel L, Unger K, Hess J, et al. Inhibition of HSP90 as a Strategy to Radiosensitize Glioblastoma: Targeting the DNA Damage Response and Beyond. *Front Oncol* 2021;11. <https://doi.org/10.3389/FONC.2021.612354/FULL>.

[377] Liu J, Sun T, Liu S, Liu J, Fang S, Tan S, et al. Dissecting the molecular mechanism of cepharanthine against COVID-19, based on a network pharmacology strategy combined with RNA-sequencing analysis, molecular docking, and molecular dynamics simulation. *Comput*

Biol Med 2022;151. <https://doi.org/10.1016/J.COMPBIOMED.2022.106298>.

[378] Blázquez C, González-Feria L, Lvarez LA', Haro A, Llanos Casanova M, Guzmán M. Cannabinoids inhibit the vascular endothelial growth factor pathway in gliomas. AACR 2004;64:5617–23.

[379] Mondal A, Gandhi A, Fimognari C, ... AA-E journal of, 2019 undefined. Alkaloids for cancer prevention and therapy: Current progress and future perspectives. Elsevier n.d.

[380] Karim I, Hojat I, Journal AS-C and T, 2017 undefined. Silencing of final gene involved in biosynthesis of papaverin and sanguinarin alkaloids (DBOX) using VIGS technique in *Papaver somniferum* L. JctArakuAcIr n.d.

[381] Sidera K, drug EP-R patents on anti-cancer, 2014 undefined. HSP90 inhibitors: current development and potential in cancer therapy. IngentaconnectCom 2014.

[382] Zhu M, Niu J, Jiang J, Dong T, Chen Y, Yang X, et al. Chelerythrine inhibits the progression of glioblastoma by suppressing the TGFB1-ERK1/2/Smad2/3-Snail/ZEB1 signaling pathway. Elsevier n.d.

LIST OF PUBLICATIONS

Cumulative impact factor of all publications	= 35.669
h-index and i-10 index	= 5 and 3
Number of citations	= 107

PUBLICATIONS FROM THESIS

1. **Sharma S**, Kumar P. Decoding the role of MDM2 as a potential ubiquitin E3 ligase and identifying the therapeutic efficiency of alkaloids against MDM2 in combating glioblastoma. ACS omega. 2023 Jan 26;8(5): 5072-87.DOI: <https://doi.org/10.1021/acsomega.2c07904>. IF: 4.13 (ACS)
2. **Sharma, S.** and Kumar, P., Dissecting the Functional Significance of Hsp90ab1 and Other Heat Shock Proteins in Countering Glioblastomas and Ependymomas Using Omics Analysis and Drug Prediction Using Virtual Screening 2023 September, 10. DOI: <https://doi.org/10.1016/j.npep.2023.102383>. IF: 3.152 (Neuropeptide)

OTHER PUBLICATIONS

1. **Sharma S**, Advani D, Das A, Malhotra N, Khosla A, Arora V, Jha A, Yadav M, Ambasta RK, Kumar P. Pharmacological intervention in oxidative stress as a therapeutic target in neurological disorders. Journal of Pharmacy and Pharmacology. 2022 Apr;74(4):461-84. DOI: <https://doi.org/10.1093/jpp/rgab064> .IF: 4.81 (Wiley)
2. Dia Advani, **Sudhanshu Sharma**, Smita Kumari, Rashmi K Ambasta and Pravir Kumar Precision Oncology, Signaling, and Anticancer Agents in Cancer Therapeutics.” *Anti-cancer agents in medicinal chemistry* vol. 22,3 (2022):433-468.
doi:10.2174/1871520621666210308101029IF: 2.47 (Bentham)

3. Smita Kumari, Dia Advani, **Sudhanshu Sharma**, Rashmi K Ambasta, and Pravir Kumar “Combinatorial therapy in tumor microenvironment: Where do we stand?” *Biochimica et biophysica acta. Reviews on cancer* vol. 1876,2 (2021): 188585. doi: 10.1016/j.bbcan.2021.188585. Combinatorial therapy in tumor microenvironment: where do we stand? *Biochimica et Biophysica Acta (BBA)-Reviews on Cancer*. 2021 Dec 1;1876(2):188585. DOI: [10.1016/j.bbcan.2021.188585](https://doi.org/10.1016/j.bbcan.2021.188585). IF: 11.41 (Elsevier)
4. Smita Kamari, **Sudhanshu Sharma**, Dia Advani, Aakansha Khosla, Pravir Kumar, and Rashmi K Ambasta. “Unboxing the molecular modalities of mutagens in cancer.” *Environmental science and pollution research international* vol. 29,41 (2022): 62111-62159. doi:10.1007/s11356-021-16726-wIF: 5.4 (Springer)
5. **Dia Advani**, Rohan Gupta, Rahul Tripathi, Sudhanshu Sharma, Rashmi K Ambasta, and Pravir Kumar. “Protective role of anticancer drugs in neurodegenerative disorders: A drug repurposing approach.” *Neurochemistry international* vol. 140 (2020):104841. doi: 10.1016/j.neuint.2020.104841IF: 4.297 (Elsevier)

BOOK CHAPTERS

1. Dia Advani, **Sudhanshu Sharma**, Rahul Tripathi, Rohan Gupta, Asmita Jaiswal, Rashmi K Ambasta, and Pravir Kumar, “Mitochondrial dysfunction in metabolic disorders”, “Mitochondrial Dysfunction and Nanotherapeutics (Elsevier), Aging, Diseases, and Nanotechnology-Related Strategies in Mitochondrial Medicine”

CONFERENCE PROCEEDINGS

1. **Sudhanshu Sharma** and Pravir Kumar, “Dissecting the molecular mechanism of HSP90AB1 as a potential heat shock protein and understanding the role of alkaloids in the therapeutic suppression of Glioblastoma (GBMs)” 3rd International Conference on Innovative

Sustainable Computational Technologies, 2023 [**Oral presentation, IEEE conference, 2023**]

2. **Sudhanshu Sharma** and Pravir Kumar, “Deciphering the role of ubiquitin E3 ligases as potential targets and to identify their therapeutic efficiency in combating glioblastoma”, National Conference on “Neurodegeneration and Cognition-Recent Advances in Neurological diseases”, 02nd to 04th December,2021, SNCI, Jamia Hamdard, Delhi, India. [**Oral presentation**]

WORKSHOPS ATTENDED

1. National workshop on “Advance Research Technique for Cellular and Molecular System in Neuroscience”, 08th to 14th December, 2021, SNCI, Jamia Hamdard University, Delhi, India.
2. Advance course on Care, Management of Laboratory Animals, and Experimental Techniques (LAE) Organized by CSIR-Central Drug Research Institute, Lucknow, India Conducted from 06th to 24th September,2021
3. Post-conference workshop on " Neurodegeneration and Cognition-Recent Advances in Neurological diseases ", 02nd to 04th December,2021, SNCI, Jamia Hamdard, Delhi, India.

INVITED SPEAKER

1. Guest speaker for Symposium on “Future without Cancer” organized by the Department of Life Sciences, School of Basic and Applied Sciences, Galgotias University, on February 04, 2021.

BIOSKETCH

SUDHANSHU SHARMA

Corresponding address:

A-792 Awas Vikas Colony Meerut Road, Hapur-245101, UP (India)

sudhanshu.sharma812@gmail.com; +(91) 8377860524

NAME

SHARMA, SUDHANSHU

POSITION TITLE

PhD thesis (in the submission stage)

Title:

COLLABORATIVE ACTION OF MOLECULAR CHAPERONES, UBIQUITIN E3 LIGASES, AND OTHER SIGNALING MOLECULES IN THE REVERSAL OF GLIOBLASTOMA AND OTHER BRAIN TUMORS

EDUCATION/TRAINING

INSTITUTION AND LOCATION	POSITION	YEAR(s)	FIELD OF STUDY
Delhi Technological University (Formerly Delhi College of Engineering), Delhi	P. HD (DST-INSPIRE SRF)	July 2021-present	Neuro-oncology, Cancer Biology and Neuroscience
Delhi Technological University (Formerly Delhi College of Engineering), Delhi	P. HD (DST-INSPIRE JRF)	July 2019- 2021	Neuro-oncology, Cancer Biology and Neuroscience
Galgotias University, Greater Noida (India)	M.Sc. Biochemistry (Gold Medalist)- 91.56 %	2017-2019	Biochemistry
Ramjas College, University of Delhi (India)	B.Sc. Life Sciences (First Division)- 77.74 %	2012-2015	Life Sciences

Dewan public School, Hapur, U.P, (India)	Higher Secondary School Examination, C.B.S.E. (Distinction) -82.56%	2012	Physics, Chemistry, Biology, English, Informatics Practice
S.D.A. Mission Senior Secondary School, Hapur, U.P (India)	Senior Secondary School I.C.S.E. (First Division) - 70.85 %	2010	Science, Mathematics, Social Sciences, EVS, English, Computer Sciences, Hindi

SALIENT FEATURES OF YOUR RESEARCH WORK

- Animal handling, cell culture, microscopy and computation work- Full proficiency
- Cancer biology, Neuro-oncology, Neurodegenerative diseases, Radiation biology, Immunotherapy, Targeted therapies, Chemotherapy, Bioinformatics, Machine Learning
- Ubiquitination and molecular chaperones, Cell cycle and signaling pathways
- Senior Research Fellow-DST INSPIRE fellow (Department of Science and Technology, Ministry of Science, Government of India)
- Junior Research Fellow-DST INSPIRE fellow (Department of Science and Technology, Ministry of Science, Government of India)

PEER-REVIEWED PUBLICATIONS

Cumulative impact factor of all publications	=	35.669
h-index and i-10 index	=	5 and 3
Total number of citations	=	107

1. **Sharma S**, Kumar P. Decoding the role of MDM2 as a potential ubiquitin E3 ligase and identifying the therapeutic efficiency of alkaloids against MDM2 in combating glioblastoma. ACS omega. 2023 Jan 26;8(5):5072-87. [IF: 4.132]
2. **Sharma S**, Kumar P. Dissecting the functional significance of HSP90AB1 and other heat shock proteins in countering Glioblastomas and ependymomas using omics analysis and drug prediction using virtual screening (**Submitted under review;** https://papers.ssrn.com/sol3/papers.cfm?abstract_id=4511958)

3. **Sharma S**, Advani D, Das A, Malhotra N, Khosla A, Arora V, Jha A, Yadav M, Ambasta RK, Kumar P. Pharmacological intervention in oxidative stress as a therapeutic target in neurological disorders. *Journal of Pharmacy and Pharmacology*. 2022 Apr 1;74(4):461-84. [IF: 4.81]
4. Kumari S, **Sharma S**, Advani D, Khosla A, Kumar P, Ambasta RK. Unboxing the molecular modalities of mutagens in cancer. *Environ Sci Pollut Res Int*. 2021 Oct 5:1–49. doi: 10.1007/s11356-021-16726-w. PMID: 34611806; PMCID: PMC8492102. [IF: 5.19]
5. Advani D, **Sharma S**, Kumari S, Ambasta RK, Kumar P. Precision Oncology, Signaling and Anticancer Agents in Cancer Therapeutics. *Anticancer Agents Med Chem*. 2021 Mar 7. doi: 10.2174/1871520621666210308101029. PMID: 33687887. [IF: 2.527]
6. Kumari S, Advani D, **Sharma S**, Ambasta RK, Kumar P. Combinatorial therapy in tumor microenvironment: Where do we stand? *Biochim Biophys Acta Rev Cancer*. 2021 Jul 2;1876(2):188585. doi: 10.1016/j.bbcan.2021.188585. PMID: 34224836. [IF: 11.414]
7. Advani D, Gupta R, Tripathi R, **Sharma S**, Ambasta RK, Kumar P. Protective role of anticancer drugs in neurodegenerative disorders: a drug repurposing approach. *Neurochemistry international*. 2020 Aug 24:104841. [IF: 4.297]

BOOK CHAPTERS

- Advani D, **Sharma S**, Tripathi R, Gupta R, Jaiswal A, Ambasta RK, Kumar P. Mitochondrial dysfunction in metabolic disorders. In *Mitochondrial Dysfunction and Nanotherapeutics* 2021 Jan 1 (pp. 91-137). Academic Press.

INVITED SPEAKER

- Guest speaker for Symposium on “Future without Cancer” organized by the Department of Life Sciences, School of Basic and Applied Sciences, Galgotias University, on February 04, 2021.

CONFERENCE, PROCEEDINGS AND SYMPOSIUM

- National Conference on “Neurodegeneration and Cognition-Recent Advances in Neurological diseases”, 02nd to 04th December, 2021, SNCI, Jamia Hamdard, Delhi, India. [Oral presentation]

- National workshop on “Advance Research Technique for Cellular and Molecular System in Neuroscience”, 08th to 14th December, 2021, SNCI, Jamia Hamdard University, Delhi, India.
- Advance course on Care, Management of Laboratory Animals, and Experimental Techniques (LAE) Organized by CSIR-Central Drug Research Institute, Lucknow, India Conducted from 06th to 24th September, 2021
- Participated in Mini Symposium on “Tackling Antimicrobial Drug Resistance in Tuberculosis: Novel Approaches” as organizer at V.P.C.I. University of Delhi on 17 April, 2019.
- Attended One Day Workshop on “Frontiers of Nanotechnology “and gave an Oral presentation on “Use of nanoparticles in cancer therapeutics and diagnosis”, at Galgotias University, 19th Sept 2018.
- Attended International Conference on Advances in Biosciences and Biotechnology at Jaypee Institute of information technology (JIIT), 1-3 Feb, 2018.
- Participated and “Presented poster entitled ‘Mitochondrial Outer Membrane Permeabilization: A New Insight for The Regulation of Cancer Cells’ at National conference on Recent advancements in Biotechnology and Bioengineering at Sharda University 2-3 Nov, 2017.

PROFESSIONAL MEMBERSHIPS

Society for Neuroscience, India

PROFICIENCY IN TECHNIQUES

- ***In-vitro* characterization:**

Cell culture expertise of handling adherent brain tumor cell lines such as LN-229, U-87MG, SH-SY5Y and LN-18, MTT cytotoxicity assays, Cryopreservation of heterogeneous cancer cell population, clonogenic assays or cell death assay, Protein isolation, SDS-PAGE, Soft agar assay and Drug stability studies.

- **Gene expression studies:**

Gradient PCR, RT-PCR, DNA and RNA isolations from Blood, Cell line and tissue samples.

- **Microbiological studies:**

Culturing and co-culturing of various strains of Mycobacterium tuberculosis (Both MDR and

XDR strains), Minimum inhibitory concentration (MIC) analysis, AFB staining and colony PCR, Drug resistance studies.

- **Animal handling:**

Basic knowledge of handling of various strains of rodents (Wistar rat, DB/DB mice, Gerbil rat) and lagomorphs (Hamster, Rabbits), Oral gavaging technique, IV infusion from intraperitoneal, intramuscular and intradermal.

- **In-silico studies:**

Microarray dataset collection and analysis, Drug Repurposing using Molecular Docking, Molecular Dynamic Simulations (MDS) studies using CHARMM Forcefield in GROMACS, Basic knowledge of Python, CytoScape and Network analysis.

HONOURS AND AWARDS

- Prestigious DST-INSPIRE FELLOWSHIP (2019-Present).
- University Gold medalist (Masters in Biochemistry)
- Delhi University Volleyball intercollege Gold Medalist.
- CBSE cluster district level athlete.

REFERENCES

1. Professor Pravir Kumar (Ph.D. Guide and Supervisor)

Professor and Head, Department of Biotechnology

Molecular Neuroscience and Functional Genomics Laboratory

Former Dean, Delhi Technological University (Formerly Delhi College of Engineering)

Former Faculty, Tufts University School of Medicine, Boston, MA, USA

Room# FW4TF3, Mechanical Engineering Building

Shahbad Daulatpur, Bawana Road, Delhi 110042; Phone: +91- 9818898622

Email: pravirkumar@dtu.ac.in; kpravir@gmail.com

<https://www.ncbi.nlm.nih.gov/myncbi/1DW465XG9bp5p/bibliography/public/>

<https://scholar.google.co.in/citations?user=WVLI4i4AAAAJ&hl=en>

ORCID ID: 0000-0001-7444-2344; **Scopus ID:** 14831447800; **ISI Research ID:** B-2164-2015

2. Professor Chiranjib Chakraborty

Department of Biotechnology

Adamas University, Barasat

Kolkata, West Bengal, India

Email: drchiranjib@yahoo.com

Phone: +91- 9871608125

PAPER NAME

THESIS FINAL 26.09.2023_SUDHANSHU SHARMA.docx

AUTHOR

Sudhanshu Sharma

WORD COUNT

45765 Words

CHARACTER COUNT

274852 Characters

PAGE COUNT

226 Pages

FILE SIZE

5.8MB

SUBMISSION DATE

Oct 3, 2023 3:30 PM GMT+5:30

REPORT DATE

Oct 3, 2023 3:33 PM GMT+5:30**● 5% Overall Similarity**

The combined total of all matches, including overlapping sources, for each database.

- 2% Internet database
- 2% Publications database
- Crossref database
- Crossref Posted Content database
- 3% Submitted Works database

● Excluded from Similarity Report

- Bibliographic material
- Quoted material
- Cited material
- Small Matches (Less than 10 words)
- Manually excluded sources

● **5% Overall Similarity**

Top sources found in the following databases:

- 2% Internet database
- Crossref database
- 3% Submitted Works database
- 2% Publications database
- Crossref Posted Content database

TOP SOURCES

The sources with the highest number of matches within the submission. Overlapping sources will not be displayed.

1	Brunel University on 2023-09-30 Submitted works	<1%
2	dspace.dtu.ac.in:8080 Internet	<1%
3	d3amtssd1tejdt.cloudfront.net Internet	<1%
4	Dia Advani, Pravir Kumar. "Deciphering the molecular mechanism and ... Crossref	<1%
5	storage.googleapis.com Internet	<1%
6	namiki-s.co.jp Internet	<1%
7	assets.researchsquare.com Internet	<1%
8	"Molecular Diagnostics in Cancer Patients", Springer Nature, 2019 Crossref	<1%

9	Hajar Sirous, Giulia Chemi, Giuseppe Campiani, Simone Brogi. "An inte... Crossref	<1%
10	Mamun Mia, Arafat Rahman Oany, Mousumi Bhowmik, Tahmina Pervin... Crossref posted content	<1%
11	lifekb.org Internet	<1%
12	pure.mpg.de Internet	<1%
13	Shalja Verma, Anand Kumar Pandey. "Epicatechin an incredible tool to ... Crossref	<1%
14	Wei-cheng Lu, Hui Xie, Ce Yuan, Jin-jiang Li, Zhao-yang Li, An-hua Wu. ... Crossref posted content	<1%
15	Yi Sun. "Targeting E3 Ubiquitin Ligases for Cancer Therapy", Cancer Bi... Crossref	<1%
16	Monjur Ahmed Laskar, Moriom Begam, Manabendra Dutta Choudhury. ... Crossref posted content	<1%
17	Karunya University on 2019-09-23 Submitted works	<1%
18	University of Nottingham on 2023-08-17 Submitted works	<1%
19	link.springer.com Internet	<1%
20	github.com Internet	<1%

21	"Heat Shock Proteins in Inflammatory Diseases", Springer Science and ...	<1%
	Crossref	
22	University of Hong Kong on 2022-11-04	<1%
	Submitted works	
23	University of KwaZulu-Natal on 2015-07-20	<1%
	Submitted works	
24	files.docking.org	<1%
	Internet	
25	static-site-aging-prod2.impactaging.com	<1%
	Internet	
26	University of Hong Kong on 2011-03-09	<1%
	Submitted works	
27	Rahul Tripathi, Pravir Kumar. "Preliminary study to identify CXCR4 inhi...	<1%
	Crossref	
28	"Heat Shock Proteins and Stress", Springer Science and Business Medi...	<1%
	Crossref	
29	Carnegie Mellon University on 2022-11-22	<1%
	Submitted works	
30	Heat Shock Proteins, 2015.	<1%
	Crossref	
31	University of Hull on 2014-06-06	<1%
	Submitted works	
32	mdpi.com	<1%
	Internet	

33	"Apoptosis and Cancer Therapy", Wiley, 2006	<1%
	Crossref	
34	"Targeting the DNA Damage Response for Anti-Cancer Therapy", Sprin...	<1%
	Crossref	
35	Dia Advani, Rohan Gupta, Rahul Tripathi, Sudhanshu Sharma, Rashmi K...	<1%
	Crossref	
36	Trent E. Balius, Mayukh Chakrabarti, Y. Stanley Tan. "DOCK 6: Incorpor...	<1%
	Crossref posted content	
37	Xingguang Zhang, Binghan Jia, Yanqi Zhang, Haijie Wu, Sen Zhang. "LI...	<1%
	Crossref posted content	
38	"Bioactive Natural products in Drug Discovery", Springer Science and B...	<1%
	Crossref	
39	"Computational Methods for Drug Repurposing", Springer Science and ...	<1%
	Crossref	
40	Chunping Wu, Mei Wang, Qiang Huang, Yang Guo, Hongli Gong, Chuny...	<1%
	Crossref posted content	
41	Isabelle Ferry, Claudia M. Kuzan-Fischer, Emilie Ernoult, James T. Rutk...	<1%
	Crossref	
42	Jawaharlal Nehru Technological University on 2010-01-27	<1%
	Submitted works	
43	Natural Products, 2013.	<1%
	Crossref	
44	Translation and Its Regulation in Cancer Biology and Medicine, 2014.	<1%
	Crossref	

45	University of Central Lancashire on 2013-09-19	<1%
	Submitted works	
46	University of Sydney on 2022-02-08	<1%
	Submitted works	
47	Yuxin Zhang, Yuehui Wang, Ruoxuan Zhang, Quanwang Li. "Genes asso..."	<1%
	Crossref posted content	
48	d-nb.info	<1%
	Internet	
49	ebin.pub	<1%
	Internet	

● Excluded from Similarity Report

- Bibliographic material
- Cited material
- Manually excluded sources
- Quoted material
- Small Matches (Less than 10 words)

EXCLUDED SOURCES

Sudhanshu Sharma, Pravir Kumar. "Dissecting the functional significance of H... 19%

Crossref

Sudhanshu Sharma, Pravir Kumar. "Decoding the Role of MDM2 as a Potential... 14%

Crossref

ncbi.nlm.nih.gov 13%

Internet

Decoding the Role of MDM2 as a Potential Ubiquitin E3 Ligase and Identifying the Therapeutic Efficiency of Alkaloids against MDM2 in Combating Glioblastoma

Sudhanshu Sharma and Pravir Kumar*

Cite This: *ACS Omega* 2023, 8, 5072–5087

Read Online

ACCESS |



Metrics & More



Article Recommendations



Supporting Information

ABSTRACT: Glioblastomas (GBMs) represent the most aggressive form of brain tumor arising from the malignant transformation of astrocytes. Despite various advancements, treatment options remain limited to chemotherapy and radiotherapy followed by surgery giving an overall survival of 14–15 months. These therapies are somewhere restricted in giving a better survival and cure. There is a need for new therapeutics that could potentially target GBM based on molecular pathways and pathology. Here, ubiquitin E3 ligases can be used as targets as they bind a wide array of substrates and therefore can be attractive targets for new inhibitors. Through this study, we have tried to sort various ubiquitin E3 ligases based on their expression, pathways to which these ligases are associated, and mutational frequencies, and then we tried to screen potent inhibitors against the most favorable E3 ligase as very few studies are available concerning inhibition of E3 ligase in GBM. Our study found MDM2 to be the most ideal E3 ligase and further we tried to target MDM2 against various compounds under the alkaloid class. Molecular Docking and MD simulations combined with ADMET properties and BBB scores revealed that only evodiamine and sanguinarine were effective in inhibiting MDM2. We also tried to give a proposed mechanism of how these inhibitors mediate the p53 signaling in GBM. Therefore, the new scaffolds predicted by the computational approach could help in designing promising therapeutic agents targeting MDM2 in glioblastoma.



1. INTRODUCTION

Gliomas represent the most frequently occurring primary brain tumors that arise due to the abnormality in the glial cells such as ependymal cells, oligodendrocytes, astrocytes, etc.¹ Based on the cells of origin, these gliomas are classified as anaplastic astrocytoma, oligodendrogliomas, and glioblastoma.² Glioblastoma represents the most lethal and malignant form of brain tumor and accounts for 80% of the cases as recognized by the World Health Organization (WHO).³ However, the overall median survival of the patient remains only 9–15 months following the standard therapeutic regimens such as surgery, radiotherapy, and chemotherapy.^{4,5} This lack of precise therapeutic targeting of these tumors is due to the undefined etiology and incomplete knowledge of the underlying mechanism behind this disease. Recent data published concedes that there is 91% involvement of p53 pathway downregulation in a variety of carcinomas.⁶ As the treatment options are very limited, there is an urgent need to explore more options.⁷ In that case, ubiquitin E3 ligase remains an untouched area of discussion as the inhibitors targeting these ligases are very few in count. Ubiquitylation represents a reversible post-translational modification that is regulated by ubiquitin E3 ligases.⁸ Ubiquitin E3 ligases are known to target a broad spectrum of substrates that are involved in processes like DNA repair, apoptosis, and metabolism.⁹ Ubiquitin E3 ligases are the pinnacle of ubiquitination with a high frequency

of selectivity against the substrate, therefore, making them an attractive drug target.¹⁰

Various ubiquitin E3 ligases are known to play an important role in commanding several activities of cells. Ubiquitin E3 ligases such as MDM2 (mouse double minute 2),¹¹ BRCA1 (breast and ovarian cancer susceptibility protein 1),¹² neural precursor cell-expressed developmentally downregulated 4 (NEDD4),¹³ tripartite motif-containing 21 (TRIM21),¹⁴ ring finger 41 (RNF41),¹⁵ ubiquitin-protein E3 ligase (UBE3A),¹⁶ and various other E3 ligases impart an important role. Although very few inhibitors are currently available that can target these ligases and can cause suppression in GBM proliferation,^{17–19} our study aimed to identify a ubiquitin E3 ligase whose expression was higher in glioblastoma and plays a prominent role in GBM signaling. For this, we performed expressional and mutational studies to predict the most suitable E3 ligase for therapeutics. Through our observations, MDM2 was found to be the most suitable ubiquitin E3 ligase as it shows higher mutational frequencies in GBM and is also involved in the activation of p53.²⁰ MDM2 acts as a ubiquitin

Received: December 12, 2022

Accepted: January 17, 2023

Published: January 26, 2023



E3 ligase and functions by binding to p53 (tumor suppressor protein).²¹ The binding of MDM2 to p53 causes the inactivation of p53, leading to the functional loss in p53 activity.²² The functions mediated by p53 are DNA repair, senescence, apoptosis, arrest in cellular growth, and cell growth.²³ Whenever there is cellular stress like genotoxicity, damage to the DNA, oncogene activation, and hyperproliferative stress, there is upregulation of an enzyme p14 alternate reading frame protein (ARF).²⁴ This enzyme remains upstream to MDM2, promotes escape of p53 from MDM2 degradation and therefore, the tumor-suppressing functions of p53 are not lost.²⁵ Studies have shown that mutation in MDM2 during cancerous conditions causes gene amplification in glioblastomas and on the side, p53 remains wild type.²⁶ This amplification causes an overexpression in MDM2 that causes p53 inactivation and increased cancer progression. Hence, breaking the MDM2-p53 interactions seems to be a promising therapeutic approach to treating glioblastomas.²⁷ Studies have been done to identify inhibitors that can potentially target MDM2 but are still in the pipeline. Inhibitors such as RG7112 (analogous to nutlin) cause MDM2 inactivation leading to increased cellular apoptosis and cell cycle arrest showing a reduction in tumor growth in xenografts.²⁸ Nutlin-3a is known to inhibit the MDM2-p53 interactions and enhance p53-mediated apoptosis in osteosarcoma.²⁹ Other inhibitors of MDM2 such as CGM097, MK8242, MI77301, and RG7388 are known to be used in various cancers although only a few are known to play an important role in the therapeutics of GBM.^{30–33} Studies have also shown that inhibiting MDM2 can also be a therapeutic option in treating GBMs possessing wild-type p53.^{34,35} These studies prove that MDM2 can be an effective target in tumorigenicity and breaking the p53-MDM2 interactions can be significant in GBM treatment. However, computational and *in silico* analysis by inculcating a combined approach of docking at a molecular level and dynamics simulation studies at the initial screening and analysis can help us to identify potential inhibitors against these ligases as they are very limited in count.^{36,37}

Researchers have focused on identifying synthetic inhibitors as therapeutic options but these chemical inhibitors possess enhanced cytotoxicity. Studies concerning the use of natural alkaloids in GBM therapeutics are very few in number.³⁸ Natural alkaloids can be of great value as they show very less or no side effects. Alkaloids represent an important class of natural compounds and are shown to induce cell death in GBM as they are potent antioxidants.³⁹ Alkaloids such as melatonin (monoamine alkaloid) are able to inhibit MDM2 in the MCF7 breast cancer cell line.⁴⁰ Melatonin is also known to inhibit phosphorylation of MDM2, enhancing acetylation of p53 thereby leading to p53-MDM2 disruption and gain of functions of p53.⁴¹ Another study found that papaverine (non-narcotic opium alkaloid) was able to induce suppression in GBM activity.⁴² Evodiamine is a natural alkaloid derived from the fruit of *Evodia rutaecarpa* (medicinal plant) mostly used by the Chinese in medicine.⁴³ This alkaloid is known to exhibit the property of anti-inflammation and is known to be reported in reducing the proliferation of cancerous cells by the process of apoptosis and cell cycle arrest.⁴⁴ Evodiamine was found to induce calcium/JNK-mediated autophagy and mitochondrial-mediated apoptosis in GBM.^{45,46} However, the role of evodiamine in targeting MDM2 as a ubiquitin E3 ligase remains unclear. Another alkaloid sanguinarine, which is a benzophenanthridine alkaloid, was able to induce apoptosis in

human breast carcinoma cells.⁴⁷ A recent study shows that evodiamine can inhibit liver carcinoma via Met/EGFR signaling.⁴⁸ Evodiamine was found to induce apoptosis in lung carcinoma.⁴⁹ Evodiamine has been shown to target the cancer stem-like cells through the p55-p21-Rb pathway in breast cancer.⁵⁰ Sanguinarine, a benzophenanthridine, is a nitrogen-containing alkaloid isolated from the roots of *Sanguinaria canadensis*.⁵¹ This alkaloid is known to possess antibacterial and anti-inflammatory properties. Sanguinarine is found to induce apoptosis in a p53-dependent manner in hepatocellular carcinoma.⁵² Sanguinarine was also able to induce apoptosis in C6 rat glioblastoma cells.⁵³ Sanguinarine was also able to induce metastasis in breast cancer.⁵⁴ Sanguinarine is known to induce ROS-dependent activation of autophagy and possesses an anti-glioma effect.⁵⁵

However, the role of sanguinarine in targeting MDM2 is not understood and how these alkaloids can be the potential inhibitors of ubiquitin E3 ligase is also unknown.⁵⁶ Studies have shown that alkaloids can induce self-ubiquitination and degradation in MDM2 by targeting MDM2-DAXX-HAUSP interactions.⁵⁷ Alkaloids such as berberine, matrine, and melatonin are reported to be effective in reducing the expression of MDM2 or decreasing the stability in acute lymphoblastic leukemia, liver carcinoma, and breast cancer.^{41,58} Other studies in which alkaloids can be seen in altering the MDM2-p53 signaling are indole-3-carbinol⁵⁹ and fluspirilene⁶⁰ targeting breast and colon cancer. Since alkaloids can target a variety of cancers, very few or no studies are available on the therapeutic targeting of GBM using alkaloids. In our study, we screened two natural alkaloids, i.e., evodiamine and sanguinarine based on the literature, docking, and simulation studies. Also, we checked how these compounds interact with MDM2 and used nutlin-3a as the reference against MDM2.³⁶

Our study was focused on the identification of a potent ubiquitin E3 ligase and how these ubiquitin E3 ligases can be targeted using natural inhibitors. Our approach was based on using mutational analysis, pathway studies, and expressional analysis to explore the role of various ubiquitin E3 ligases in GBM. In the end, we were able to identify MDM2 as a targetable E3 ligase and we also tried to target this ligase with evodiamine and sanguinarine. These alkaloids were screened from the compound library, and the various physicochemical properties of these compounds were also accessed. Further, molecular docking and dynamics simulation studies were also performed to predict whether these inhibitors can target MDM2 and could be a new therapeutic avenue in targeting GBMs.

2. MATERIALS AND METHODOLOGY

2.1. Collection of Raw Data. Datasets that are used in the current study have been extracted from the National Centre for Biotechnology Information (NCBI) gene expression omnibus (GEO) (<https://www.ncbi.nlm.nih.gov/geo/>).⁶¹ The microarray gene expression profiles were obtained from GSE 4290, GSE 104291, and GSE 50161 datasets. The platform used in GSE 104291, GSE 50161, and GSE 4290 is GPL570 [HG-U133_Plus_2] Affymetrix human genome.

2.2. Identification of Differentially Expressed Genes. The present study utilized GEO2R (<https://www.ncbi.nlm.nih.gov/geo/geo2r>), a web-based interactive tool that works on the R language limma package. GEO2R can be used as a comparative tool for two or more sets of samples and is helpful

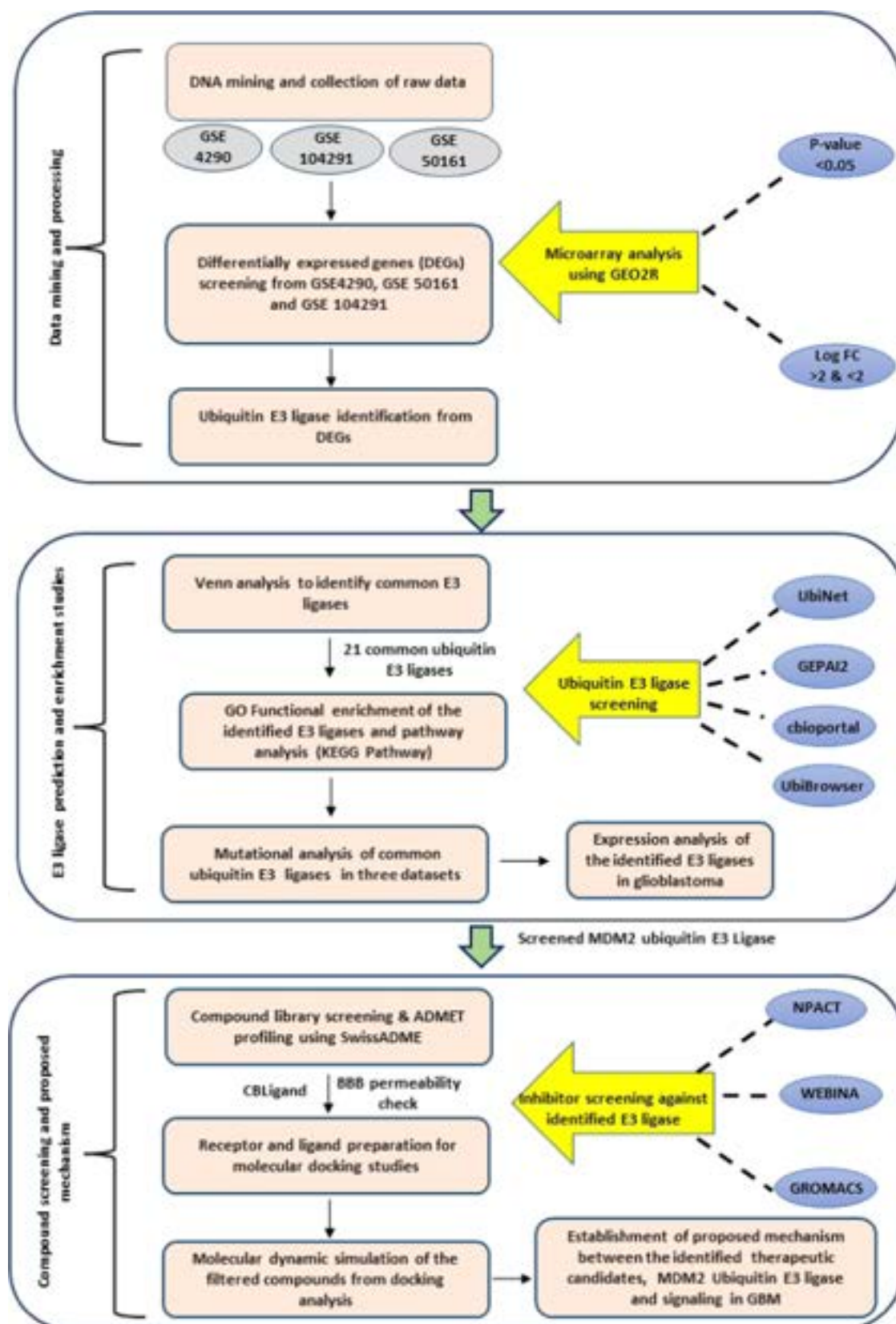


Figure 1. Workflow overview: data extraction was performed from the National Centre for Biotechnology Information (NCBI) gene expression omnibus (GEO). Data analysis and processing were performed using GEO2R. After data processing, the differentially expressed genes (DEGs) were filtered out from the datasets GSE 4290, GSE 104291, and GSE 50161. These DEGs were then filtered using parameters such as P -value and the fold change (log FC) values. Prediction of potential ubiquitin E3 ligases present within these three datasets was done using UbiNet and the confirmation of the DEGs acting as ubiquitin E3 ligases was done using UbiBrowser. Post E3 ligase prediction, Venn analysis was done to identify the common ubiquitin E3 ligases present within the three datasets. GO functional enrichment and pathway analyses were done using SHINYGO

Figure 1. continued

7.16 to identify the functions of each of the 21 common ubiquitin E3 ligases and the pathways associated with them. After the enrichment and pathway analysis, mutational frequencies of the 21 common E3 ligases were checked using cBioportal to predict the most suitable and targetable ubiquitin E3 ligase for our study focusing on glioblastomas (GBMs). Using gene expression profiling interactive analysis 2 (GEPiA2), the expressions were checked for the ligases filtered after mutational analysis. Selection of the most appropriate E3 ligase for our study was preceded by exploring the compound libraries and we selected the naturally occurring plant-based anticancer compound activity-target (NPACT) library and alkaloids class for this study. The blood–brain permeability (BBB) scores were checked to identify the compounds that can cross the BBB using SwissADME. ADMET analysis was then applied to the filtered compound passing the BBB to check the parameters such as absorption, distribution, metabolism, excretion, and toxicity of the alkaloids. The protein structure of mouse double minute (MDM2) that was identified as the most suitable target based on mutational frequencies was downloaded using a protein database (PDB). Ligand structures were downloaded using PubChem along with their canonical SMILES. After the preparation of the receptor and ligand, docking was carried out to check for the most suitable ligand binding with the receptor (MDM2), showing the highest binding affinity and rate of inhibition. Compounds showing the best interaction and inhibition then proceeded for molecular dynamics simulations (MDS) studies till 50 ns to validate the interactions and the stability of the complex (protein–ligand). Based on all the analyses performed, a mechanism was proposed for how the identified inhibitors can target the MDM2 that might be able to suppress GBMs.

in the prediction of differential expression in the GEO series.⁶¹ We used GEO2R to filter out the genes that were differentially expressed in these three datasets. To study the biological prospects, biological functions were annotated for differentially expressed genes. P -value < 0.05 and the \log FCI > 2 and \log FCI < 2 were used as cut-off criteria to filter out the differentially expressed genes (DEGs).

2.3. Screening of Ubiquitin E3 Ligases and Venn Analysis. The DEGs from the above three datasets were screened for the presence of any ubiquitin E3 ligases. UbiBrowser2.0 (<http://ubibrowser.bio-it.cn/>), an integrated bioinformatics platform was used as an identification tool for ubiquitin E3 ligases in these DEGs. Final confirmation of these DEGs as ubiquitin E3 ligases was done using UbiNet2.0 (<https://awi.cuhk.edu.cn/~ubinet/index.php>). DEGs that were identified as ubiquitin E3 ligases were then analyzed by VENN analysis to filter out common E3 ligases in these three datasets.

2.4. Functional Enrichment Analysis of Identified Ubiquitin E3 Ligases. To scrutinize the biological, cellular, and molecular functions and the various pathways involved in these ubiquitin E3 ligases, Gene Ontology (GO) terms and pathway prediction were done using SHINYGO 7.16 (<http://bioinformatics.sdstate.edu/go/>). Parameters such as a P -value < 0.05 and count > 3 were set as the threshold for significantly enriched terms. Eventually, the functional enrichment network was constructed.

2.5. Mutational Analysis and Expression Analysis of Common Ubiquitin E3 Ligases. To predict the mutational signatures of the identified ubiquitin E3 ligases, we used the cBio cancer genomic portal (<https://www.cbioportal.org/>). This platform can analyze the molecular data retrieved from cancerous tissues and cytogenetics and is useful in the determination of epigenetics and genetic levels. Expression analysis followed by mutational analysis was done using gene expression profiling interactive analysis 2 (<http://gepia2.cancer-pku.cn/>) to predict the rate of expression of identified E3 ligases in glioblastoma and to check whether the data is statistically significant or not. Here, n represents the value of normal patient count, whereas t represents the number of patients affected and suffering from glioblastoma. This data was obtained from TCGA and the expression analysis was performed using GEPiA2.

2.6. Compound Library Screening. In the present study, 70 alkaloids were taken from the naturally occurring plant-based anticancer compound activity-target (NPACT) database. The 3D chemical structure and canonical SMILES of

these alkaloids were downloaded using PubChem.⁶² Ligand confirmations were downloaded in the 2D SDF format and visualization was done using Avogadro (<https://avogadro.cc/>) and then converted to the PDB format. These structures were checked for the presence of any H-bond or any other bound group apart from our ligand of interest.

2.7. Analysis of ADMET Descriptors and the Blood–Brain Barrier (BBB). ADMET profiling (i.e., absorption, distribution, metabolism, excretion, and toxicity) of selected compounds was conducted using SwissADME.⁶³ Both the physical and pharmaceutical properties were screened using SwissADME. CBligand (<https://www.cbligand.org/CCGS/>) was used as a platform to check the BBB permeability of the compounds used in the study. On the basis of the results obtained from SwissADME and CBligand analysis, filtered compounds were considered further for molecular docking and simulations with the filtered ubiquitin E3 ligase.

2.8. Molecular Docking Studies. The PDB structure of MDM2 (PDB id: 3JZK) was downloaded from the RCSB PDB database. Molecular docking was performed against the MDM2 receptor protein with filtered alkaloids. Docking analysis was performed using WEBINA (<https://durrantlab.pitt.edu/webina/>), a JavaScript that runs Auto Dock Vina entirely in a web browser.⁶⁴ Molecular docking of MDM2 was performed with different alkaloids. Heteroatoms that were present within the PDB structure of MDM2 were removed and hydrogen was added using WEBINA. Structural visualization of MDM2 was done using Avogadro and UCSF Chimera (<https://www.cgl.ucsf.edu/chimera/>). Docking was performed by employing a grid size of x -axis = 40, y -axis = 45, and z -axis = 40. Prediction of docking results was based on the best interactions between the receptor and the ligand and on the binding affinity. The 3D and 2D confirmations were generated using Discovery Studio 2020.⁶⁵ The complex that showed the best binding affinity as compared to the reference then proceeded for MD simulation studies.

2.9. Molecular Dynamics Simulations of Protein–Ligand Complexes. MD simulation of the identified compounds with MDM2 was performed individually using the GROMACS 2019.3 package (<https://bioexcel.eu/gromacs-2019-6-is-available/>). The top 14 ligand–protein complexes were first simulated at 20 ns to check the stability of the complexes. Complexes that were found to be stable at 20 ns were then considered for simulation on a 50 ns timescale to provide an insight into how stable they are and to see how they behave dynamically. Complex preparation was done using the CHARMM36 all-atom force field. The charge topology of the

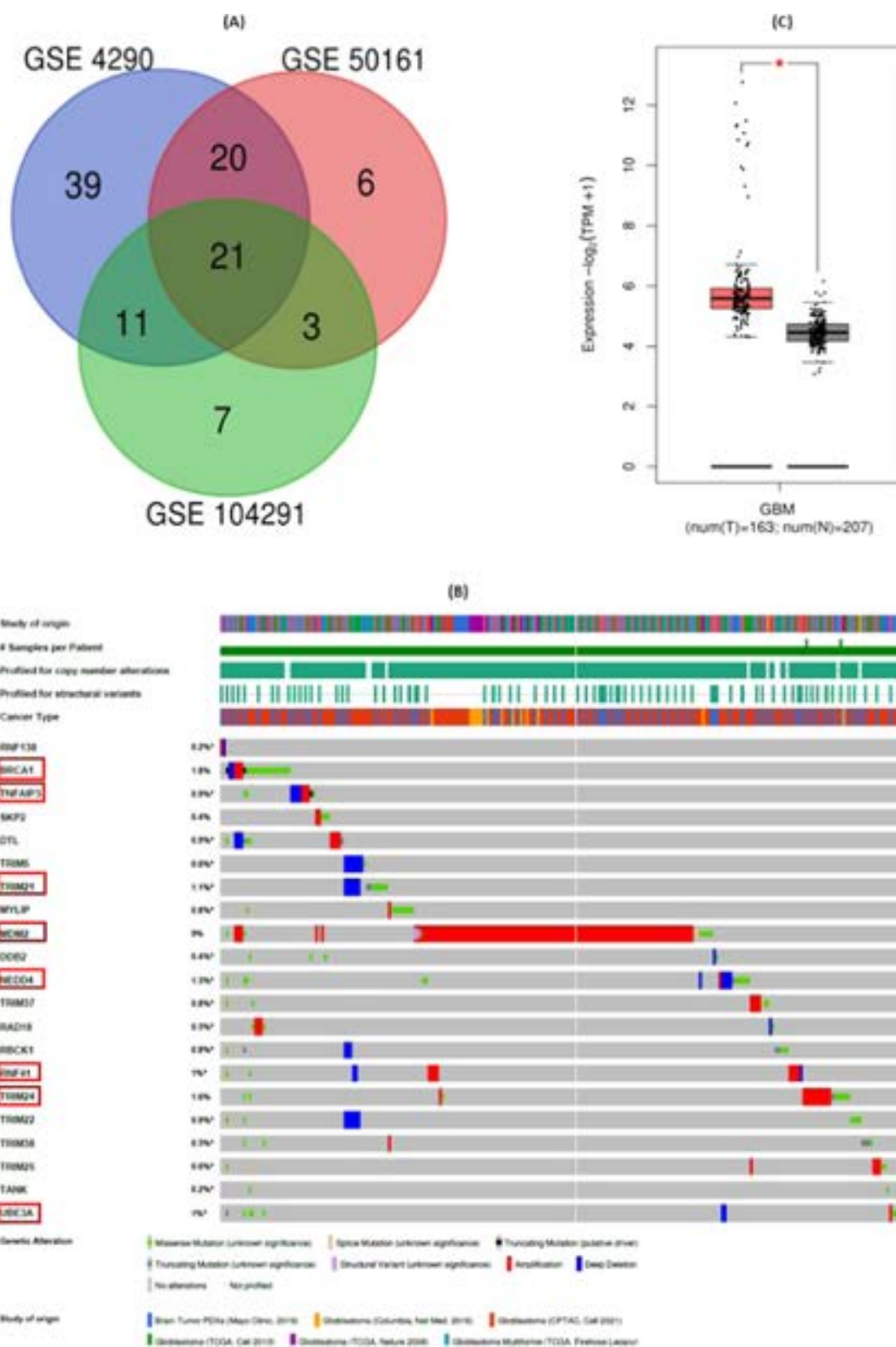


Figure 2. (A) Venn diagram and tabular description of the overlap between ubiquitin E3 ligases obtained from the datasets GSE 104291, GSE 4290, and GSE 50161. Significant overlaps show that 21 ubiquitin E3 ligases were commonly shared in these datasets. (B) Mutational analysis of the 21 common ubiquitin E3 ligases revealed that MDM2 showed the highest frequency among all of the other ligases in GBM. The percentages of mutations in the top 8 ubiquitin E3 ligases were MDM2 (9%), BRCA1 (1.8%), TRIM24 (1.6%), NEDD4 (1.3%), TRIM21 (1.1%), RNF41 (1%), UBE3A (1%), and TNFAIP3 (0.9%). MDM2 was found to be the most favorable ubiquitin E3 ligase that can be targeted in countering GBM. (C) Expression levels of MDM2. The expressional rate was defined between the GBM and normal samples from the TCGA database. Plots with an asterisk (*) on the top suggest that the data is statistically significant.

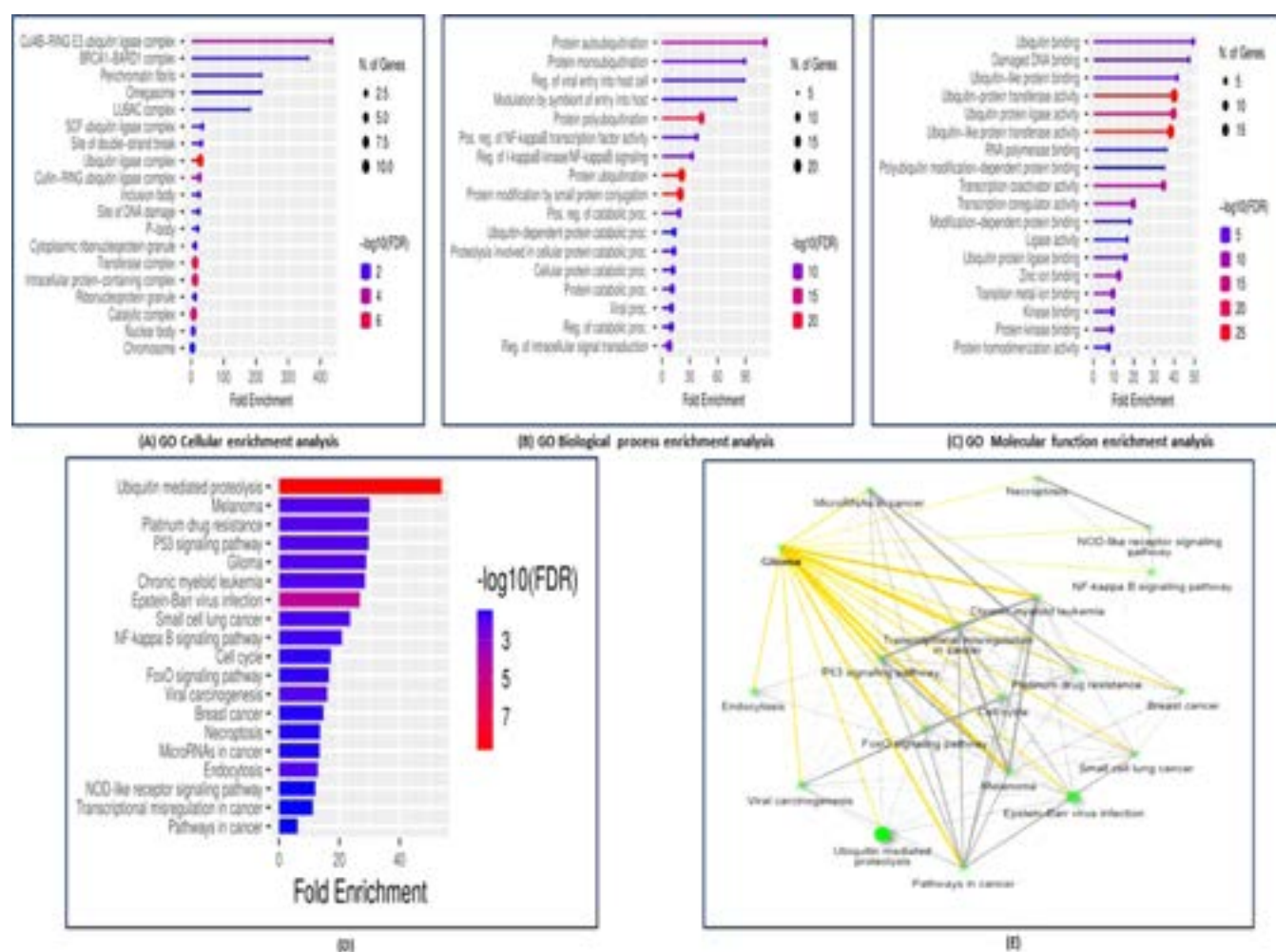


Figure 3. (A–C) Gene ontology (GO) functional enrichment analysis of 21 common ubiquitin E3 ligases and (D, E) schematic representation of the KEGG pathway enrichment. (A) GO cellular Enrichment analysis revealed that the top processes in which most of the ligases are involved were the ubiquitin ligase complex, transferases complex, intracellular protein-containing complex, and catalytic complex. The color and the size of the dots indicate if the false discovery rate (FDR) is significant or not. The bigger the dots, the more is the intensity of the red color, showing the greater significance and number of genes involved in that process. (B) GO biological process enrichment showed that the majority of ubiquitin E3 ligases were involved in processes like protein ubiquitination, protein modification by small protein conjugation, protein polyubiquitination, and proteolysis involved in the cellular protein catabolic process. (C) GO molecular function enrichment identified that most of the ligases were involved in ubiquitin-protein transferase activity, ubiquitin-like protein transferase activity, ubiquitin-protein ligase activity, and transcription coactivator activity. The more the red color of the dots, the more significant the FDR and the processes in which these ligases are involved. (D) Depicts the bar plot images of the various pathways for 21 ubiquitin E3 ligases and how they are enriched. The red bars here represent the most enriched and significant pathway and the blue bars represent less significance. Ubiquitin-mediated proteolysis is composed of most of the significant and overlapped genes followed by the Epstein–Barr virus infection, platinum drug resistance, p53 signaling, endocytosis, and glioma. (E) KEGG pathway network based on nodes and edges. The bigger the nodes present, the greater the number of genes involved, and thicker edges here represent significance. Edges for glioma have been highlighted in yellow.

compounds was generated using CGenFF and then solvated in a cubical boundary box with a dimensional separation of 1.0 nm using a TIP3 water model. Charge neutralization was done via the addition of precise concentrations of chloride [Cl⁻] ions and sodium [Na⁺] ions. Energy minimization was performed at 10 kJ/mol/nm using the long steepest descent algorithm for 10,000 steps followed by 10,000 steps of a conjugate gradient to avoid any steric clashes. The system was then subjected to equilibration with position-restrained (NVT and NPT) dynamics simulations at a constant temperature and pressure of 300 K and 1 bar for a duration of 50 ns. The plots for the root-mean-square deviation (RMSD), root-mean-square fluctuation (RMSF), the radius of gyration (Rg), and

the number of hydrogen bonds were then plotted. Complete methodology and workflow are shown in Figure 1.

3. RESULTS

3.1. Raw Data Collection and DEG Screening. The raw data from three gene expression profiles (GSE 4290, GSE 104291, and GSE 50161) were downloaded from NCBI GEO databases. Of these, GSE 4290 datasets comprised 81 glioblastoma samples and 23 nontumor samples, 4 glioblastoma and 2 nontumor samples existed in the 104291 dataset, and 34 glioblastoma and 13 normal brain samples were present in the GSE 50161 dataset. DEGs between the GBM samples and normal control samples were obtained from these three datasets.

3.2. Ubiquitin E3 Ligase Identification and Venn Analysis. After the identification of DEGs, screening of ubiquitin E3 ligases was done within these DEGs. These DEGs were individually picked up to check whether they showed the activity of an E3 ligase or not. DEGs that functioned as a substrate for a particular ligase were omitted from the study. A total of 181 ligases were predicted out of which 89 were present in GSE 4290, 50 in GSE 50161, and 42 in GSE 104291 and are shown in the [Supporting Information File, Table 1](#). Venn analysis was then conducted to deduce the common ligases among all of the ligases that were present in these three datasets. Furthermore, 21 overlapping ubiquitin E3 ligases were procured using the Venn diagram and are represented in [Figure 2A](#). The number of overlapping ubiquitin E3 ligases present in these datasets are shown in the [Supporting Information File 1, Table 2](#).

3.3. Expression Profiling and Mutational Analysis. To further substantiate the study, mutational signatures were predicted for 21 E3 ligases. Each gene acting as ubiquitin E3 ligase was checked for the rate of mutational frequencies and the kind of mutations they carry. MDM2 (9%) showed the highest percentage among the 21 ubiquitin E3 ligases. For ligases other than MDM2, the frequency of mutations was BRCA1 (1.8%), TRIM24 (1.6%), NEDD4 (1.3%), TRIM21 (1.1%), RNF41 (1%), and UBE3A (1%) and the mutational signatures that were carried in most of the ligases were of amplification and missense type. An overview of the mutational analysis performed for all of the ubiquitin E3 ligases has been shown in [Figure 2B](#). Out of these 21 E3 ligases, the expressional analysis was performed only for those ligases that showed higher mutational frequencies using TGCA GBM data. The expressional analysis was carried out using GEPAL2. Noteworthy, when compared with control samples, the expression levels of MDM2, BRCA1, TRIM24, NEDD4, and TRIM21 were higher in GBM samples and showed statistical significance and the expressional analysis can be derived from [Figure 2C](#). On the other hand, expressional levels in the case of UBE3A and RNF41 were also higher but the data was not significant statistically. On the other hand, expressional levels in the case of UBE3A and RNF41 were also higher but the data was not significant statistically, and the expressions can be seen in the [Supporting Information File, Figure 1](#).

3.4. Functional Enrichment and Pathway Analysis. On the basis of the results mentioned above, a functional enrichment analysis of 21 ubiquitin E3 ligases was performed. Three types of enrichment analysis were done, comprising biological process (BP), molecular function (MF), and cellular component (CC). All these enrichments are shown in [Figure 3A–C](#). The majority of ligases were mainly associated with GO_BP terms such as ubiquitin-protein transferase activity, protein polyubiquitination, ubiquitin-protein ligase activity, and protein autoubiquitination. In the case with GO_CC terms, these genes were involved in the formation of the ubiquitin ligase complex, transferase complex, Cul4B-RING E3 ubiquitin ligase complexes, and BRCA1-BARD1 complexes. As for GO_MF, most of the genes were related to ubiquitin binding, ubiquitin-protein transferase activity, ubiquitin-protein ligase activity, ubiquitin-like protein transferase activity, and damaged DNA binding. A detailed overview of the ligases and the process with which they are associated have been summarized in [Table 1](#).

In addition, the KEGG pathway analysis showed that these ubiquitin E3 ligases were significantly involved in ubiquitin-

Table 1. Tabular Representation of GO Functionally Enriched Ubiquitin E3 Ligases with the Associated Biological Processes and Molecular Functions

GO	category	description	log P	enrichment	Z-score	hits	hits list
GO:0016567	GO biological processes	protein ubiquitination	-31.79	42.48	28.79	20	BRCA1 DD2 MDM2 TRIM37 NEDD4 SKP2 TRIM21 TNFAIP3 UBE3A TRIM25 TRIM24 RNF41 TRIM22 TRIM38 RBCK1 MYLIP RNF138 ID TL RAD18 TRIM5
GO:0032446	GO biological processes	protein modification by small protein conjugation	-30.96	38.65	27.43	20	BRCA1 DD2 MDM2 TRIM37 NEDD4 SKP2 TRIM21 TNFAIP3 UBE3A TRIM25 TRIM24 RNF41 TRIM22 TRIM38 RBCK1 MYLIP RNF138 ID TL RAD18 TRIM5
GO:0000209	GO biological processes	protein polyubiquitination	-24.92	89.47	35.14	14	BRCA1 DD2 MDM2 NEDD4 SKP2 TRIM21 TNFAIP3 UBE3A RNF41 TRIM22 TRIM38 RBCK1 DTL TRIM5
GO:0030163	GO biological processes	protein catabolic process	-14.19	24.27	16.56	12	MDM2 NEDD4 SKP2 TNFAIP3 UBE3A TRIM25 TRIM24 RNF41 TRIM38 RBCK1 MYLIP DTL
GO:0051603	GO biological processes	proteolysis is involved in the cellular protein catabolic process	-13.08	25.22	16.17	11	MDM2 NEDD4 SKP2 TNFAIP3 UBE3A TRIM25 RNF41 TRIM38 RBCK1 MYLIP DTL
GO:0004842	GO molecular functions	ubiquitin-protein transferase activity	-32.88	63.09	34.33	19	BRCA1 DD2 MDM2 TRIM37 NEDD4 TRIM21 TNFAIP3 UBE3A TRIM25 TRIM24 RNF41 TRIM22 TRIM38 RBCK1 MYLIP RNF138 ID TL RAD18 TRIM5
GO:0019787	GO molecular functions	ubiquitin-like protein transferase activity	-32.41	59.65	33.36	19	BRCA1 DD2 MDM2 TRIM37 NEDD4 TRIM21 TNFAIP3 UBE3A TRIM25 TRIM24 RNF41 TRIM22 TRIM38 RBCK1 MYLIP RNF138 ID TL RAD18 TRIM5
GO:0061630	GO molecular functions	ubiquitin-protein ligase activity	-22.81	63.70	29.56	14	MDM2 TRIM37 NEDD4 TRIM21 UBE3A TRIM25 TRIM24 RNF41 TRIM22 TRIM38 MYLIP RNF138 RAD18 TRIM5
GO:0061659	GO molecular functions	ubiquitin-like protein ligase activity	-22.56	61.19	28.95	14	MDM2 TRIM37 NEDD4 TRIM21 UBE3A TRIM25 TRIM24 RNF41 TRIM22 TRIM38 MYLIP RNF138 RAD18 TRIM5
GO:0003713	GO molecular functions	transcription coactivator activity	-13.12	48.65	20.59	9	BRCA1 TRIM37 TRIM21 UBE3A TRIM25 TRIM24 TRIM22 TRIM38 TRIM5

Table 2. Tabular Representation of the KEGG Pathway Analysis of the Predicted Ubiquitin E3 Ligases along with Their Fold Change and Enrichment False Discovery Rate (FDR)

enrichment FDR	hits	fold enrichment	pathway	hit list
1.74×10^{-09}	7	53.89125296	ubiquitin-mediated proteolysis	BRCA1, NEDD4, TRIM37, UBE3A, DDB2, MDM2, SKP2
2.55×10^{-05}	5	26.86940123	Epstein–Barr virus infection	NEDD4, TNFAIP3, DDB2, MDM2 SKP2
0.013265001	2	29.74037834	platinum drug resistance	BRCA1, MDM2
0.013265001	2	29.74037834	P53 signaling pathway	DDB2, MDM2
0.013265001	3	12.92290249	endocytosis	NEDD4, MDM2, RNF41
0.013265001	3	16.04222379	viral carcinogenesis	UBE3A, MDM2, SKP2
0.013265001	2	28.94730159	glioma	DDB2, MDM2
0.013265001	2	30.15343915	melanoma	DDB2, MDM2
0.013265001	2	28.56641604	chronic myeloid leukemia	DDB2, MDM2
0.017380146	2	23.59834369	small-cell lung cancer	DDB2, SKP2
0.020082398	2	20.87545788	NF-kappa B signaling pathway	TNFAIP3, TRIM25
0.026614554	2	16.57288259	FoxO signaling pathway	MDM2, SKP2

Table 3. Tabular Representation of the Various Alkaloids Docked against MDM2 and Their ADMET Profiling^a

alkaloid	BBB predictor	BBB SwissADME	affinity (kcal/mol)	molecular mass (<500 Da)	docking coordinates	H-bond donor (<5)	H-bond acceptor (<10)	octal water partition coefficient (log < 5)	molar refractivity (40–130)
brucine	yes	yes	−8.2	394.46 g/mol	40–40–40	0	5	1.84	114.04
chelerythrine	yes	yes	−8.1	348.37 g/mol	40–40–40	0	4	3.02	101.6
isostrychnine	yes	yes	−8.2	334.41 g/mol	40–40–40	1	3	1.85	102.77
sanguinarine	yes	yes	−8.6	334.41 g/mol	40–40–40	0	3	2.09	101.05
tomatidine	yes	yes	−8.6	354.44 g/mol	40–40–40	1	4	2.61	103.74
(R)-cryptopleurine	yes	yes	−7.9	393.48 g/mol	40–40–40	0	5	4.04	119.16
cepharanthine	yes	yes	−9	369.45 g/mol	40–40–40	0	5	3.33	108.8
ellipticine	yes	yes	−8.6	303.36 g/mol	40–40–40	1	1	2.7	97.67
evodiamine	yes	yes	−8.6	315.49 g/mol	40–40–40	1	2	3.88	96.52
isotetrandrine	yes	no	−8.2	275.26 g/mol	40–40–40	0	4	2.88	76.67
liriodenine	yes	yes	−8.3	478.62 g/mol	40–40–40	0	6	4.43	147.34
tylophoridicine C	yes	no	−8.1	381.42 g/mol	40–40–40	2	5	0.78	112.73
tylophoridicine F	yes	yes	−8.6	395.45 g/mol	40–40–40	1	5	1.11	117.2
6-O-desmethylandofine	yes	yes	−8.2	349.42 g/mol	40–40–40	1	4	3.67	108.2

^aAlkaloids highlighted in red represent evodiamine and sanguinarine with their binding energies highlighted in yellow.

mediated proteolysis, Epstein–Barr virus infection, p53 signaling, and endocytosis. Figure 3D,E tries to give an overview of KEGG pathways in which these ligases were involved. Further, all of the terms were merged into clusters based on similarities and the top pathways that were enriched with most of the overlapping ligases are represented in Table 2.

3.5. Compound Prediction, BBB, and ADMET Parameters. On the basis of literature mining, we identified NPACT, a database comprising different classes of natural compounds and selected the alkaloid class from the compound library; 70 compounds were selected from the database and the BBB permeability and the BBB score were checked using the SVM algorithm in CBligand. On the basis of BBB prediction, initially, 54 compounds were filtered. ADMET profiling for these 70 compounds was done to check whether the compounds fall under the prescribed limits of ADMET analysis. Properties such as molecular mass (<500 Da), number of H-bond donors (<5), number of H-bond acceptors (<10), octal water partition coefficient (log < 5), and molar refractivity (40–130) were considered for our study. The number of violations of the Lipinski rule of five was also taken into consideration for these 70 compounds. Only 54 compounds showed zero violation of the Lipinski rule and also satisfied the ADMET threshold and were further assessed for docking and simulation studies. The parameters of the

alkaloid can be seen in the Supporting Information File, Table 3.

3.6. MDM2-Alkaloids' Interaction Profiling. Molecular docking was carried out for the screened ubiquitin E3 ligase (MDM2) with different alkaloid compounds. Any extra residue attached to the ligand was removed along with any heteroatom. Any hydrogen or water attached to either the ligand or the receptor was also omitted before proceeding with docking. The reference study conducted before using nutlin-3a as a reference compound with MDM2 shows a binding affinity of −7.9 kcal/mol. However, we used a more stringent threshold of −8.0 kcal/mol in our study to shortlist the compounds, showing specific and nonspecific bindings. Docking was performed for 54 compounds and out of these only 14 compounds showed a binding energy of above −8.0 kcal/mol. These binding energies demonstrate the high binding affinity of these compounds against MDM2. The higher the binding in negative terms indicates the more the inhibition capability of these compounds for MDM2. During MDM2 docking, the maximum number of compounds along with the reference ligand showed common interactions with the receptor residues at Ile61, His96, Ile99, Leu54, Val93, and Tyr100. A binding potential of above −8.5 kcal/mol was seen in cepharanthine (−9 kcal/mol), sanguinarine (−8.6 kcal/mol), evodiamine (−8.6 kcal/mol), tomatidine (−8.6 kcal/

Table 4. Tabular Representation of Binding Energies and the Interaction of Evodiamine, Sanguinarine, and Nutlin with MDM2

compounds	binding energy (kJ/mol)	interacting residues
evodiamine	−8.6	Val93, Ile61, His96, Ile99, Leu54 and Leu57
sanguinarine	−8.6	Val93, Ile61, His96, Tyr100, Leu64
reference (nutlin)	−7.9	Val93, Ile61, His96, Ile99, Leu54, Phe55, Phe91, Phe86, Leu57 and Lys51.

mol), ellipticine (−8.6 kcal/mol), and tylophoridicine F (−8.6 kcal/mol). The binding energies of various alkaloids with the best affinity and the docking coordinates along with other properties can be interpreted in Table 3.

After the successful completion of docking, these 14 compounds then proceeded with molecular simulation studies. Evodiamine and sanguinarine showed the best possible interactions as compared to the reference used in our study, and the binding energies along with the interactions can be observed in Table 4.

The 2D and 3D confirmations of evodiamine, sanguinarine, and the reference after binding with MDM2 can be observed in Figure 4A–C.

3.7. MDM2-Alkaloid Complexes' Dynamic Stability.

All of the 14 compounds having binding energy above −8.0 kcal/mol were subjected to MD simulations for 50 ns, which helped us to understand the pattern of interaction and the dynamic behavior. The stability of these compounds with MDM2 was analyzed using RMSD obtained from MD simulations. The RMSD of different protein–ligand complexes along with the RMSD of ligands alone were considered. The backbone of the complexes (MDM2-sanguinarine and MDM2-evodiamine) were found to be stable when compared with the MDM2-reference complex or with the protein alone. The RMSD showed a fluctuation in the beginning and reached 0.30 nm but gradually decreased and was stable in the range of 0.15–0.25 nm when compared with the reference complex. Till 20 ns there was a slight deviation in the stability of complexes (MDM2-sanguinarine and MDM2-evodiamine) from the MDM2-reference complex. After 25 ns of simulation, the complexes started stabilizing themselves and after 35 ns both the complexes achieved better stability and were interactive till 50 ns, which can be seen in Figure 5A. Similarly, the RMSD of all of the ligands is given in Figure 5B, and it clearly shows that sanguinarine and evodiamine are both stable when compared with the reference compound; however, the RMSD of the ligand sanguinarine fluctuated in the beginning and reached 0.7 nm, but after 32 ns, it started to stabilize and was in the range of 0.2–0.4 nm.

The RMSF of both the complexes along with the MDM2-reference is depicted in Figure 5C. It can be seen that the RMSF values of the two complexes are in the range with the MDM2-reference complex and are found to be stable in the range of 0.1–0.2 nm. The Rg is generally identified to check the compactness of the protein structure, and if the structure is stably folded, it will remain stable over time. It can be seen that the Rg values for both MDM2-evodiamine and MDM2-sanguinarine were found to be stable and compact for 50 ns, holding an average Rg of 1.6 nm (Figure 6A) when compared with MDM2-reference. The Coulomb's interaction energy of each of the complexes was calculated and from the analysis it was seen that as compared to the reference, the interaction energy was more negative in the case of the other two complexes, suggesting a higher binding potential of the MDM2 receptors with ligands sanguinarine and evodiamine. The

overall interaction can be seen in Figure 6B. The plots for H-bonds and pairing within 0.35 nm in Figure 6C,D shows the interactions of the amino acid residue of MDM2 with evodiamine, sanguinarine, and reference compounds during the 50 ns simulations. The formation of different types of bonds between various complexes suggests important evidence for the inhibitory potential of evodiamine and sanguinarine.

4. DISCUSSION

GBM is highly aggressive and metastatic among other tumors of the central nervous system (CNS) with very complicated biology and carries a poor prognosis. The molecular mechanism and the signaling pathways underlying these tumors are of great significance and therefore in-depth studies are needed to counter these tumors. The overall survival in patients is very less and the therapeutic angles are also fewer. When talking about chemotherapeutics, temozolomide acts as a gold standard against these solid tumors. Surgery followed by concurrent radiotherapy remains an option. As ubiquitin E3 ligases target a large number of substrates that are regulators of the majority of cellular functions such as apoptosis, DNA repair, and metabolism, hence, they can be the therapeutic drug targets in GBMs.¹⁵ This study has tried to identify the various ubiquitin E3 ligases whose expressions are comparatively higher in GBMs, their involvement in functions operating at molecular and cellular levels, and mutational frequencies of the identified ubiquitin E3 ligase in GBMs. After the identification of targetable E3 ligases, we also tried to predict substantial inhibitors that could inhibit the expression of these identified ubiquitin E3 ligases.

Using high-throughput studies and a bioinformatics approach, DEGs were first extracted from three GBM datasets using the GEO database. These DEGs were analyzed using UbiNet and Ubibrowser (tools to predict whether the DEG is ubiquitin E3 ligase or just the substrate of any ligase). Only 21 ubiquitin E3 ligases were retrieved that were shared equally among the three datasets for GBM. Functional enrichment and KEGG analysis were carried out to see how these ubiquitin E3 ligases play an intricate role in glioblastoma at molecular, cellular, and biological levels along with the pathways on which they act. It was seen that at biological levels, out of 21 ligases, 20 were involved in the process of protein ubiquitination, protein modification by small protein conjugation, and 14 hits were involved in protein polyubiquitination. At molecular levels, most of the hits were associated with ubiquitin-protein transferase activity and ubiquitin-protein ligase activity. It was conferred from these functional enrichments that most of the hits that were common in these processes were MDM2, BRCA1, RNF41, TRIM21, NEDD4, and TRIM24. Similarly, the KEGG pathway analysis also revealed that out of these ligases, MDM2 was majorly involved in the pathways like endocytosis, ubiquitin-mediated proteolysis, and various pathways in cancer. Researchers have shown that MDM2 plays a prominent role in mediating the activation of p53 during various signaling cascades,⁶⁶ and therefore, they can be better

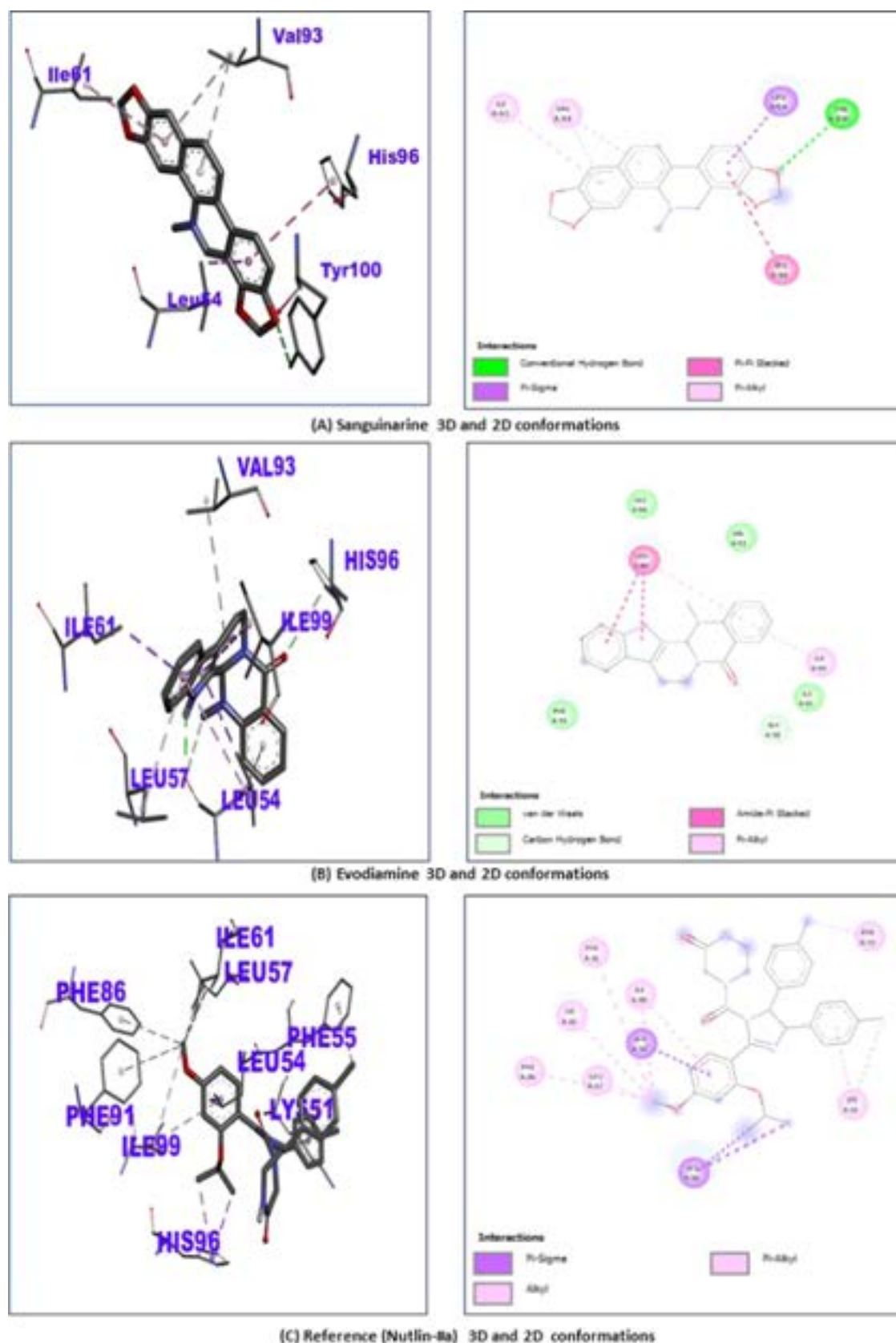


Figure 4. (A–C) Molecular docking confirmations: Representation of 2D and 3D confirmation of MDM2 binding with (A) sanguinarine shows binding at the residues Val93, Ile61, His96, Tyr100, and Leu64 of the MDM2 protein. (B) Evodiamine represents the interactions at the sites Val93, Ile61, His96, Ile99, Leu54, and Leu57 of MDM2. (C) Reference ligand (nutlin-3a) showing interactions with MDM2 at the residues sites Val93, Ile61, His96, Ile99, Leu54, Phe55, Phe91, Phe86, Leu57, and Lys51.

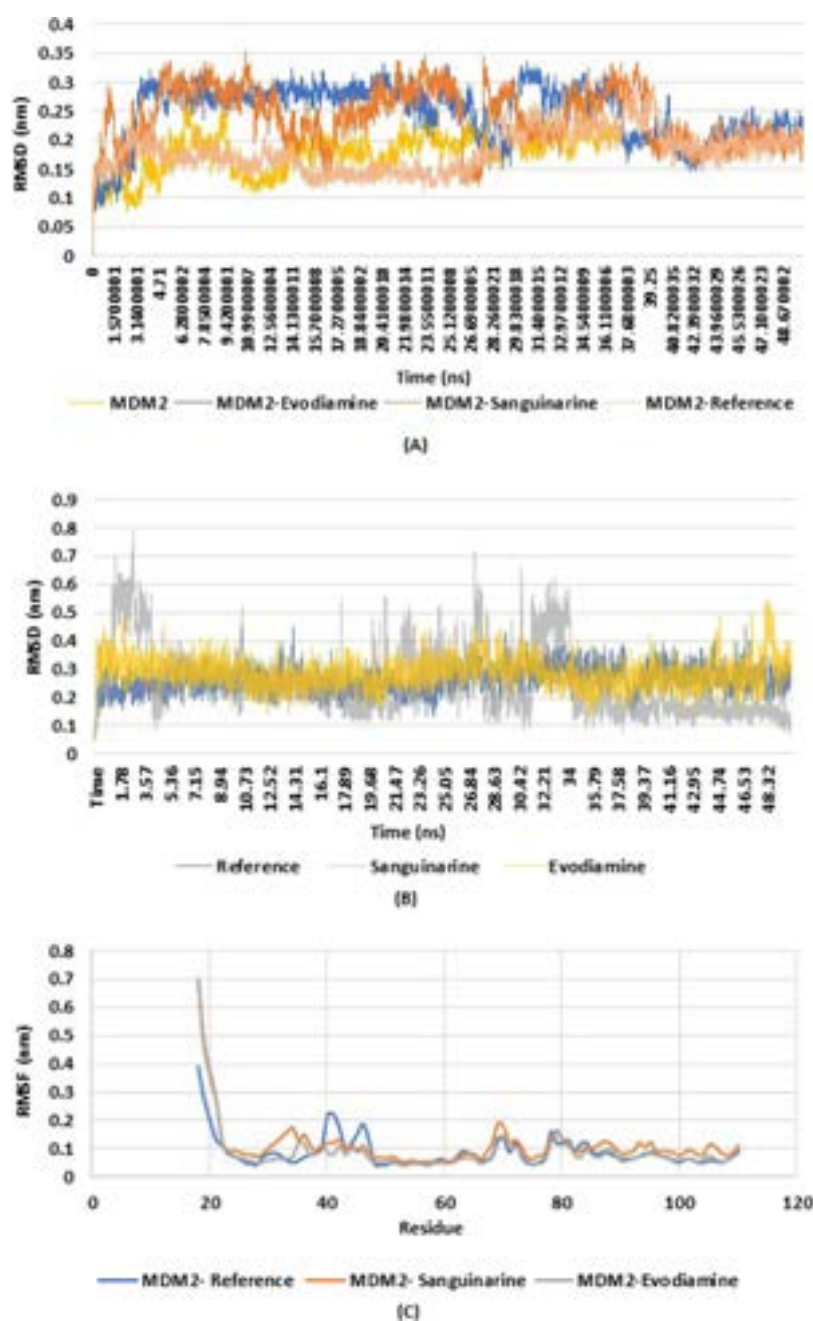


Figure 5. (A–C) Plots depicting variations in the root-mean-square deviation (RMSD) and root-mean-square fluctuations (RMSF) in protein alone, ligand alone, and protein–ligand complexes. (A) RMSD of MDM2, MDM2-evodiamine, MDM2-sanguinarine, and MDM2-reference complexes were calculated and plotted on the graph. The Y-axis represents the RMSD in nanometers (nm), and the X-axis represents the time in nanoseconds (ns). The RMSD of each of these was calculated at a timescale of 50 ns. Highlighted in gold represents the RMSD peak of the MDM2 protein itself. The MDM2-evodiamine RMSD peak can be seen in blue. The RMSD peak of the MDM2-sanguinarine complex is represented in orange and the peak for the MDM2-reference complex is represented in blue. This graph clearly shows that when the overall RMSD was compared, MDM2-evodiamine and MDM2-sanguinarine complexes were found to be stable against the MDM2-reference complex till 50 ns. RMSD of these complexes can be seen as stable in the range of 0.15–0.25 nm and showed stability after 35 ns. (B) Overall RMSD peak of the reference ligand, sanguinarine, and evodiamine are highlighted in blue, gray, and gold. The RMSD of the sanguinarine and evodiamine was found in the range of 0.2–0.4 nm and was stable till 50 ns. (C) RMSF peaks of MDM2-reference, MDM2-sanguinarine, and MDM2-evodiamine are represented in blue, orange, and gray, respectively. The RMSF of MDM2-sanguinarine and MDM2-evodiamine can be seen in the range with the MDM2-reference complex.

targets as ubiquitin E3 ligases. The mutational frequencies of these ubiquitin ligases were checked using data from TGCA and Mayo clinic and it was found that MDM2 carried a mutational frequency of 9% and the mutations were of the amplification type. Expression analysis of MDM2 along with other ubiquitin E3 ligases in GBM revealed that in most of the

cases, the data showed statistical significance. This tells us that the expression of MDM2 was comparatively higher in patients with GBM as compared to the normal group of people according to TGCA. As very few studies are available on how ubiquitin E3 ligases can be therapeutically important and therefore, by predicting the expression of every ligase, selective

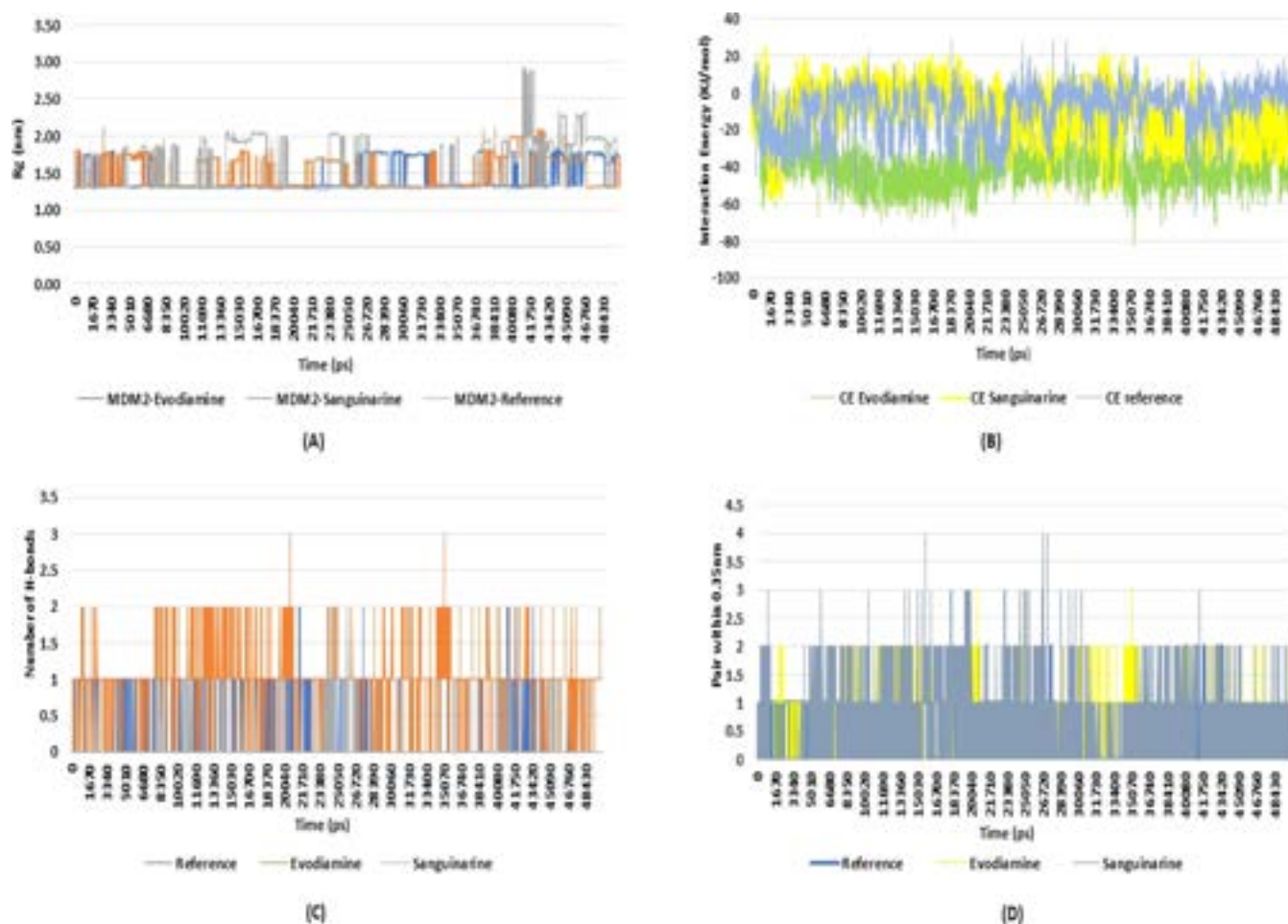


Figure 6. (A–D) Plots representing the radius of gyration (R_g), interaction energy, number of H-bonds, and H-bond pairs within 0.35 nm. (A) R_g of all of the complexes (MDM2-evodiamine, MDM2-sanguinarine, and MDM2-reference) plotted against time with the Y-axis representing R_g in nanometers (nm), while the X-axis shows time interval in picoseconds (ps). Peak showing the interaction R_g of MDM2-evodiamine is highlighted in blue, orange in the case of MDM2-sanguinarine, and gray in MDM2-reference. The R_g of MDM2-reference showed fluctuations from the other two complexes but in the case of MDM2-evodiamine and MDM2-sanguinarine, the peaks were in the range when compared with the MDM2-reference complex, (B) Coulomb's interaction energy in kJ/mol plotted against time in ps. The Coulomb's interaction energy peaks in the case of MDM2-evodiamine are shown in light green, MDM2-sanguinarine in yellow, and MDM2-reference in blue. The interaction was more toward the negative and reached -70 kJ/mol in the case of MDM2-evodiamine and reached -60 kJ/mol in MDM2-sanguinarine as compared to MDM2-reference (-40 kJ/mol) suggesting a more stable interaction in the case of evodiamine and sanguinarine. (C) Plot for the number of H-bonds on each residue against time in ps. The overall H-bonds in the case of reference per residue were comparatively lower and the peak is displayed in blue. The peak for H-bonds in the case of evodiamine is shown in orange and for sanguinarine in gray. The number of H-bonds in the case of evodiamine was higher, followed by sanguinarine and reference. (D) H-bond pairing within a radius of 0.35 nm can be seen in the reference (blue), evodiamine (yellow), and sanguinarine (gray). These pairings with MDM2 suggest that the pairs per residue formed in the case of sanguinarine and the pair formation were almost equal in the reference and evodiamine suggesting greater stability of sanguinarine and evodiamine with MDM2 till 50,000 ps (50 ns).

targeting using either siRNA or any drug or natural compound can somehow reduce the expression of these ubiquitin E3 ligases.

Molecular docking studies showed that binding energies of evodiamine (-8.6 kJ/mol) and sanguinarine (-8.6 kJ/mol) were comparatively higher than that of the reference compound (-7.6 kJ/mol), suggesting a more sustained inhibitory effect of these alkaloids against MDM2. Sanguinarine was able to bind at the residues Val93, Ile61, His96, Tyr100, and Leu64 of the MDM2 protein while evodiamine represents interactions at the sites Val93, Ile61, His96, Ile99, Leu54, and Leu57 of MDM2. The reference showed interaction with MDM2 at the residue sites Val93, Ile61, His96, Ile99, Leu54, Phe55, Phe91, Phe86, Leu57, and Lys51. Although evodiamine and sanguinarine predicted fewer

interactions as compared to the reference, based on the affinity score, these compounds were checked for stability with MD simulations. From the results obtained from simulation studies, the fluctuation and stability of the system during the simulation and the outcome trajectories for all of the complexes were inspected using different simulation parameters. These parameters included the backbone RMSDs for all of the atoms and ligands, RMSF of individual amino acid residues, formation of H-bonds, and R_g . RMSD plots when compared showed that the hits bounded to MDM2, evodiamine, and sanguinarine possessed lower fluctuations in RMSD and greater stability at the active site during the simulation at 50 ns. The RMSDs were calculated between the initial conformations and final conformations throughout 50 ns in dynamics simulations. This showed us that evodiamine and

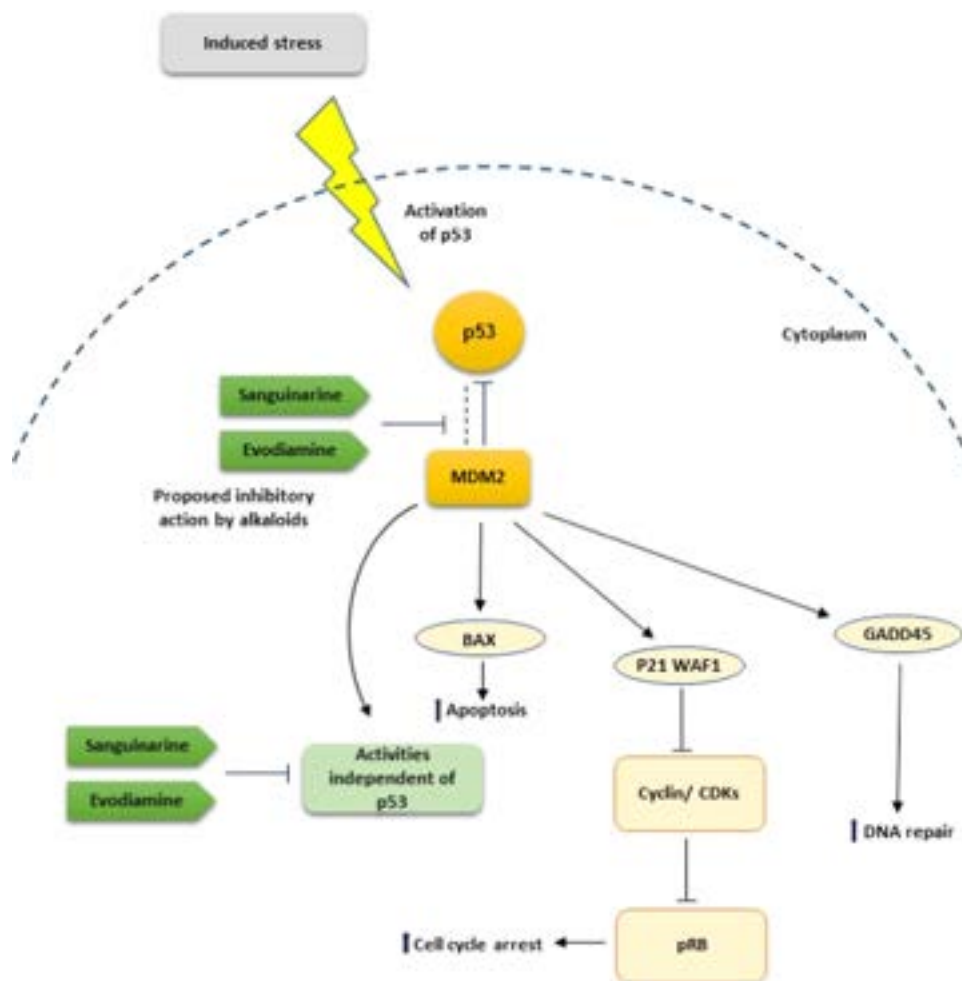


Figure 7. Proposed mechanism of action of evodiamine and sanguinarine in MDM2 inhibition. Stress-induced due to genotoxicity, DNA damage, ionizing radiations, and other factors cause the activation of p53 (tumor suppressor gene) bound to MDM2. Overexpressed MDM2 causes the degradation of p53 and is not able to function properly. We hypothesized that breaking the MDM2-p53 interaction by either evodiamine or sanguinarine can prevent the degradation of p53. Upon preventing degradation of p53, activation of downstream targets associated with p53-MDM2 interactions such as the Bcl2-associated protein (BAX) causing apoptosis, growth arrest, and DNA-damage inducible gene (GADD45), and the P21 WAF causes an increase in apoptosis, DNA repair, and cell cycle arrest, therefore, restoring the normal cellular mechanism and can suppress glioblastoma.

sanguinarine showed more stable binding when compared with the reference. RMSF on the other hand represented the important residues that were involved in strong interactions with specific ligands. The pattern of RMSF peaks suggests that the fluctuations in the values of evodiamine and sanguinarine were close to the reference and exhibited almost similar patterns. Coming to the Rg, it was seen that Rg values of the backbone atoms of MDM2 when bound to evodiamine and sanguinarine were nearly the same when compared with the reference bound to MDM2 and were maintained thoroughly till 50 ns. The results were generated from interaction energy peaks, and it can be conferred that the interactions between evodiamine, sanguinarine, and MDM2 were more stable and stronger as compared to the reference. These findings somewhere reinforced the credibility of docking results, suggesting the potential role of evodiamine and sanguinarine as potent inhibitors of MDM2.

Previous studies have shown that MDM2 acts as ubiquitin E3 ligases and also promotes the ubiquitination of p53.⁶⁷ This process mediated by MDM2 leads to the identification and interaction of the proteasome by p53 thereby causing increased

degradation of p53. However, the mechanism by which evodiamine and sanguinarine target the MDM2 and hence p53 remains unclear. We, therefore, proposed a mechanism of how both of these compounds could potentially target MDM2 and can induce a therapeutic response in GBM, and the proposed mechanism can be seen in Figure 7.

5. CONCLUSIONS

In summary, the role of MDM2 as a potential ubiquitin E3 ligase was identified, and how it can be the game changer in the therapeutic targeting of GBM. Through our studies, it was assumed that targeting this ligase using a natural class of inhibitors instead of synthetic compounds can be more fruitful. Also, our study tried to give a proposed mechanism of how evodiamine and sanguinarine disrupt MDM2-p53 interactions and target the p53 signaling in GBM. As very few studies are available concerning therapeutics in GBM, there is an urgent need to explore other opportunities so that survival can be enhanced in patients suffering from this cancer. However, more concrete studies are still needed to display how

evodiamine and sanguinarine can exploit this cancer for better therapeutics.

■ ASSOCIATED CONTENT

SI Supporting Information

The Supporting Information is available free of charge at <https://pubs.acs.org/doi/10.1021/acsomega.2c07904>.

Ubiquitin E3 ligases (Table 2); common interacting ligases (Table 2); BBB scores and ADMET profiling (Table 3); and expressional analysis (Figure 1) (PDF)

■ AUTHOR INFORMATION

Corresponding Author

Pravir Kumar – Molecular Neuroscience and Functional Genomics Laboratory, Delhi Technological University, Delhi 110042, India; orcid.org/0000-0001-7444-2344; Phone: +91- 9818898622; Email: pravirkumar@dtu.ac.in, kpravir@gmail.com

Author

Sudhanshu Sharma – Molecular Neuroscience and Functional Genomics Laboratory, Delhi Technological University, Delhi 110042, India

Complete contact information is available at:

<https://pubs.acs.org/10.1021/acsomega.2c07904>

Author Contributions

P.K. conceived and designed the manuscript; S.S. collected and analyzed the data; and S.S. and P.K. wrote the manuscript, discussed the results, and analyzed the entire data.

Notes

The authors declare no competing financial interest.

■ ACKNOWLEDGMENTS

The authors would like to thank the senior management of Delhi Technological University (DTU) and the Department of Science and Technology (DST), India, for their constant support and financial assistance to Senior Research Fellowship (SRF) Sudhanshu Sharma (Fellow ID: IF190188).

■ ABBREVIATIONS

GBM:glioblastomas; BRCA1:breast and ovarian cancer susceptibility protein 1; NEDD4:neural precursor cell-expressed developmentally downregulated 4; TRIM 21:tripartite motif-containing 21; RNF41:ring finger41; UBE3A:ubiquitin-protein E3 ligase; MDM2:mouse double minute 2; ARF:alternate reading frame; EGFR:epidermal growth factor receptor; GEPAI2:gene expression profiling interactive analysis 2; GEO:gene expression omnibus; PDB:protein database; RMSD:root-mean-square deviation; RMSF:root-mean-square fluctuation; Rg:radius of gyration; MD simulation:molecular dynamics simulations; NPT:constant temperature, constant pressure; NVT:constant temperature, constant volume; BAX:Bcl2-associated protein; GADD45:growth arrest and DNA-damage inducible gene; KEGG:Kyoto Encyclopedia of Genes and Genomics; ADMET:chemical absorption, distribution, metabolism, excretion, and toxicity; GO:gene ontology

■ REFERENCES

- (1) Komori, T. Grading of Adult Diffuse Gliomas According to the 2021 WHO Classification of Tumors of the Central Nervous System. *Lab. Invest.* **2022**, *102*, 126–133.
- (2) Masui, K.; Mischel, P. S.; Reifenberger, G. Molecular Classification of Gliomas. In *Handbook of Clinical Neurology*; Elsevier, 2016; Vol. 134, pp 97–120. DOI: 10.1016/B978-0-12-802997-8.00006-2.
- (3) Gupta, A.; Dwivedi, T. A Simplified Overview of World Health Organization Classification Update of Central Nervous System Tumors 2016. *J. Neurosci. Rural Pract.* **2017**, *08*, 629–641.
- (4) Di Carlo, D. T.; Cagnazzo, F.; Benedetto, N.; Morganti, R.; Perrini, P. Multiple High-Grade Gliomas: Epidemiology, Management, and Outcome. A Systematic Review and Meta-Analysis. *Neurosurg. Rev.* **2019**, *42*, 263–275.
- (5) Krex, D.; Klink, B.; Hartmann, C.; Von Deimling, A.; Pietsch, T.; Simon, M.; Sabel, M.; Steinbach, J. P.; Heese, O.; Reifenberger, G.; Weller, M.; Schackert, G. Long-Term Survival with Glioblastoma Multiforme. *Brain* **2007**, *130*, 2596–2606.
- (6) Donehower, L. A.; Soussi, T.; Korkut, A.; Liu, Y.; Schultz, A.; Cardenas, M.; Li, X.; Babur, O.; Hsu, T. K.; Lichtarge, O.; Weinstein, J. N.; Akbani, R.; Wheeler, D. A. Integrated Analysis of TP53 Gene and Pathway Alterations in The Cancer Genome Atlas. *Cell Rep.* **2019**, *28*, 1370–1384.
- (7) Frosina, G. Limited Advances in Therapy of Glioblastoma Trigger Re-Consideration of Research Policy. *Crit. Rev. Oncol./Hematol.* **2015**, *96*, 257–261.
- (8) Brooks, C. L.; Gu, W. Dynamics in the P53-Mdm2 Ubiquitination Pathway. *Cell Cycle* **2006**, *3*, 893–897.
- (9) Zheng, N.; Shabek, N. Ubiquitin Ligases: Structure, Function, and Regulation. *Annu. Rev. Biochem.* **2017**, *86*, 129–157.
- (10) Huang, X.; Dixit, V. M. Drugging the Undruggables: Exploring the Ubiquitin System for Drug Development. *Cell Res.* **2016**, *26*, 484–498.
- (11) Clegg, H. V.; Itahana, K.; Zhang, Y. Unlocking the Mdm2-P53 Loop: Ubiquitin Is the Key. *Cell Cycle* **2008**, *7*, 287–292.
- (12) Umphlett, M.; Shea, S.; Tome-Garcia, J.; Zhang, Y.; Hormigo, A.; Fowkes, M.; Tsankova, N. M.; Yong, R. L. Widely Metastatic Glioblastoma with BRCA1 and ARID1A Mutations: A Case Report. *BMC Cancer* **2020**, *20*, No. 47.
- (13) Huang, X.; Chen, J.; Cao, W.; Yang, L.; Chen, Q.; et al. The many substrates and functions of NEDD4-1. *Cell Death Dis.* **2019**, *10*, No. 904.
- (14) Alomari, M. TRIM21 – A Potential Novel Therapeutic Target in Cancer. *Pharmacol. Res.* **2021**, *165*, No. 105443.
- (15) Humphreys, L.; Smith, P.; Chen, Z.; et al. The role of E3 ubiquitin ligases in the development and progression of glioblastoma. *Cell Death Differ.* **2021**, *28*, 522–537.
- (16) Simchi, L.; Panov, J.; Morsy, O.; et al. Novel Insights into the Role of UBE3A in Regulating Apoptosis and Proliferation. *J. Clin. Med.* **2020**, *9*, No. 1573.
- (17) Zhang, S.; Peng, X.; Li, X.; Liu, H.; Zhao, B. BKM120 Sensitizes Glioblastoma to the PARP Inhibitor Rucaparib by Suppressing Homologous Recombination Repair. *Cell Death Dis.* **2021**, *12*, No. 546.
- (18) Lian, Y.; Huang, Y.; Zhang, Y.; Chen, D. CACYBP Enhances Cytoplasmic Retention of P27Kip1 to Promote Hepatocellular Carcinoma Progression in the Absence of RNF41 Mediated Degradation. *Theranostics* **2019**, *26*, 8392–8408.
- (19) Zhao, Z.; Wang, Y.; Yun, D.; Huang, Q. TRIM21 Overexpression Promotes Tumor Progression by Regulating Cell Proliferation, Cell Migration and Cell Senescence in Human Glioma. *Cell Death Dis.* **2021**, *12*, No. 14.
- (20) Haupt, Y.; Maya, R.; Kazaz, A.; Oren, M. Mdm2 Promotes the Rapid Degradation of P53. *Nature* **1997**, *387*, 296–299.
- (21) England, B.; Huang, T.; Karsy, M. Current Understanding of the Role and Targeting of Tumor Suppressor P53 in Glioblastoma Multiforme. *Tumor Biol.* **2013**, *34*, 2063–2074.
- (22) Zhao, Y.; Aguilar, A.; Bernard, D.; Wang, S. Small-Molecule Inhibitors of the MDM2–P53 Protein–Protein Interaction (MDM2 Inhibitors) in Clinical Trials for Cancer Treatment: Miniperspective. *J. Med. Chem.* **2015**, *58*, 1038–1052.

- (23) Mello, S. S.; Attardi, L. D. Deciphering P53 Signaling in Tumor Suppression. *Curr. Opin. Cell Biol.* **2018**, *51*, 65–72.
- (24) Kurki, S.; Latonen, L.; Laiho, M. Cellular Stress and DNA Damage Invoke Temporally Distinct Mdm2, P53 and PML Complexes and Damage-Specific Nuclear Relocalization. *J. Cell Sci.* **2003**, *116*, 3917–3925.
- (25) Jin, Y.; Xiao, W.; Song, T.; Feng, G.; Dai, Z. Expression and Prognostic Significance of P53 in Glioma Patients: A Meta-Analysis. *Neurochem. Res.* **2016**, *41*, 1723–1731.
- (26) Schiebe, M.; Ohneseit, P.; Hoffmann, W.; Meyermann, R.; Rodemann, H. P.; Bamberg, M. Analysis of Mdm2 and P53 Gene Alterations in Glioblastomas and Its Correlation with Clinical Factors. *J. Neuro-Oncol.* **2000**, *49*, 197–203.
- (27) Nag, S.; Zhang, X.; Srivenugopal, K. S.; Wang, M.-H.; Wang, W.; Zhang, R. Targeting MDM2-P53 Interaction for Cancer Therapy: Are We There Yet? *Curr. Med. Chem.* **2014**, *21*, 553–574.
- (28) Her, N. G.; Oh, J. W.; Oh, Y. J.; Han, S.; Cho, H. J.; Lee, Y.; Ryu, G. H.; Nam, D. H. Potent Effect of the MDM2 Inhibitor AMG232 on Suppression of Glioblastoma Stem Cells. *Cell Death Dis.* **2018**, *9*, No. 792.
- (29) Wang, B.; Fang, L.; Zhao, H.; Xiang, T.; Wang, D. MDM2 Inhibitor Nutlin-3a Suppresses Proliferation and Promotes Apoptosis in Osteosarcoma Cells. *Acta Biochim. Biophys. Sin.* **2012**, *44*, 685–691.
- (30) Ding, Q.; Zhang, Z.; Liu, J. J.; Jiang, N.; Zhang, J.; Ross, T. M.; Chu, X. J.; Bartkovitz, D.; Podlaski, F.; Janson, C.; Tovar, C.; Filipovic, Z. M.; Higgins, B.; Glenn, K.; Packman, K.; Vassilev, L. T.; Graves, B. Discovery of RG7388, a Potent and Selective P53-MDM2 Inhibitor in Clinical Development. *J. Med. Chem.* **2013**, *56*, 5979–5983.
- (31) Wang, Y.; Hoi, P.; Chan, J.; Lee, S. New Perspective on the Dual Functions of Indirubins in Cancer Therapy and Neuroprotection. *Anti-Cancer Agents Med. Chem.* **2014**, *14*, 1213–1219.
- (32) Holzer, P.; Masuya, K.; Furet, P.; Kallen, J.; Valat-Stachyra, T.; Ferretti, S. S.; Berghausen, J.; Le Bouisset-Leonard, M.; Buschmann, N.; Pissot-Soldermann, C.; Rynn, C.; Ruetz, S.; Stutz, S.; Chè Ne, P.; Jeay, S.; Gessier, F. Discovery of a Dihydroisoquinolinone Derivative (NVP-CGM097): A Highly Potent and Selective MDM2 Inhibitor Undergoing Phase 1 Clinical Trials in P53wt Tumors. *J. Med. Chem.* **2015**, *58*, 6348–6358.
- (33) Sun, D.; Li, Z.; Rew, Y.; Gribble, M.; Bartberger, M. D.; Beck, H. P.; Canon, J.; Chen, A.; Chen, X.; Chow, D.; Deignan, J.; Duquette, J.; Eksterowicz, J.; Fisher, B.; Fox, B. M.; Fu, J.; Gonzalez, A. Z.; Gonzalez-Lopez De Turiso, F.; Houze, J. B.; Huang, X.; Jiang, M.; Jin, L.; Kayser, F.; Liu, J.; Lo, M. C.; Long, A. M.; Lucas, B.; McGee, L. R.; McIntosh, J.; Mihalic, J.; Oliner, J. D.; Osgood, T.; Peterson, M. L.; Roveto, P.; Saiki, A. Y.; Shaffer, P.; Toteva, M.; Wang, Y.; Wang, Y. C.; Wortman, S.; Yakowec, P.; Yan, X.; Ye, Q.; Yu, D.; Yu, M.; Zhao, X.; Zhou, J.; Zhu, J.; Olson, S. H.; Medina, J. C. Discovery of AMG 232, a Potent, Selective, and Orally Bioavailable MDM2-P53 Inhibitor in Clinical Development. *J. Med. Chem.* **2014**, *57*, 1454–1472.
- (34) Canon, J.; Osgood, T.; Olson, S. H.; Saiki, A. Y.; Robertson, R.; Yu, D.; Eksterowicz, J.; Ye, Q.; Jin, L.; Chen, A.; Zhou, J.; Cordover, D.; Kaufman, S.; Kendall, R.; Oliner, J. D.; Coxon, A.; Radinsky, R. The MDM2 Inhibitor AMG 232 Demonstrates Robust Antitumor Efficacy and Potentiates the Activity of P53-Inducing Cytotoxic Agents AMG 232 Regresses Tumors. *Mol. Cancer Ther.* **2015**, *14*, 649–658.
- (35) Al-Ghabkari, A.; Narendran, A. In Vitro Characterization of a Potent P53-MDM2 Inhibitor, RG7112 in Neuroblastoma Cancer Cell Lines. *Cancer Biother. Radiopharm.* **2019**, *34*, 252–257.
- (36) Sirous, H.; Chemi, G.; Campiani, G.; Brogi, S. An Integrated in Silico Screening Strategy for Identifying Promising Disruptors of P53-MDM2 Interaction. *Comput. Biol. Chem.* **2019**, *83*, No. 107105.
- (37) Lemos, A.; Gomes, A. S.; Loureiro, J. B.; et al. Synthesis, Biological Evaluation, and in Silico Studies of Novel Aminated Xanthenes as Potential P53-Activating Agents. *Molecules* **2019**, *24*, No. 1975.
- (38) Zhai, K.; Siddiqui, M.; Abdellatif, B.; Liskova, A.; Kubatka, P.; Büsselberg, D. Natural Compounds in Glioblastoma Therapy: Preclinical Insights, Mechanistic Pathways, and Outlook. *Cancers* **2021**, *13*, No. 2317.
- (39) Rehman, S.; Khan, H. Advances in Antioxidant Potential of Natural Alkaloids. *Curr. Bioact. Compd.* **2017**, *13*, 101–108.
- (40) Cos, S.; Sánchez-Barceló, E. J. Melatonin Inhibition of MCF-7 Human Breast-Cancer Cells Growth: Influence of Cell Proliferation Rate. *Cancer Lett.* **1995**, *93*, 207–212.
- (41) Proietti, S.; Cucina, A.; Dobrowolny, G.; D'Anselmi, F.; Dinicola, S.; Masiello, M. G.; Pasqualato, A.; Palombo, A.; Morini, V.; Reiter, R. J.; Bizzarri, M. Melatonin Down-Regulates MDM2 Gene Expression and Enhances P53 Acetylation in MCF-7 Cells. *J. Pineal Res.* **2014**, *57*, 120–129.
- (42) Inada, M.; Shindo, M.; Kobayashi, K.; Sato, A.; Yamamoto, Y.; Akasaki, Y.; Ichimura, K.; Tanuma, S. I. Anticancer Effects of a Non-Narcotic Opium Alkaloid Medicine, Papaverine, in Human Glioblastoma Cells. *PLoS One* **2019**, *14*, No. e0216358.
- (43) Gavaraskar, K.; Dhulap, S.; Hirwani, R. R. Therapeutic and Cosmetic Applications of Evodiamine and Its Derivatives—A Patent Review. *Fitoterapia* **2015**, *106*, 22–35.
- (44) Jiang, J.; Hu, C. Evodiamine: A Novel Anti-Cancer Alkaloid from *Evodia Rutaecarpa*. *Molecules* **2009**, *14*, 1852–1859.
- (45) Liu, A. J.; Wang, S. H.; Chen, K. C.; Kuei, H. P.; Shih, Y. L.; Hou, S. Y.; Chiu, W. T.; Hsiao, S. H.; Shih, C. M. Evodiamine, a Plant Alkaloid, Induces Calcium/JNK-Mediated Autophagy and Calcium/Mitochondria-Mediated Apoptosis in Human Glioblastoma Cells. *Chem. Biol. Interact.* **2013**, *205*, 20–28.
- (46) Liang, Z.; Wang, Y.; Zhang, H.; Deng, J.; Lei, F.; Li, J.; Shi, T.; Wang, S.; Li, R.; Wang, Z. Design, Synthesis and Bioactivity Evaluation of Favorable Evodiamine Derivative Scaffold for Developing Cancer Therapy. *Eur. J. Med. Chem.* **2022**, *239*, No. 114530.
- (47) Choi, W. Y.; Kim, G. Y.; Lee, W. H.; Choi, Y. H. Sanguinarine, a Benzophenanthridine Alkaloid, Induces Apoptosis in MDA-MB-231 Human Breast Carcinoma Cells through a Reactive Oxygen Species-Mediated Mitochondrial Pathway. *Chemotherapy* **2008**, *54*, 279–287.
- (48) Du, H.; Peng, Q.; Gu, J.; Qiu, P.; Liu, L.; Du, B.; Jiang, Y.; Tan, Y. Effect of Evodiamine on Cancer Metabolism of Liver Tumor Through Met/EGFR and HIF Pathways. *SSRN Electron. J.* **2022**, *0*, No. 29.
- (49) Mohan, V.; Agarwal, R.; Singh, R. P. A Novel Alkaloid, Evodiamine Causes Nuclear Localization of Cytochrome-c and Induces Apoptosis Independent of P53 in Human Lung Cancer Cells. *Biochem. Biophys. Res. Commun.* **2016**, *477*, 1065–1071.
- (50) Han, S.; Woo, J. K.; Jung, Y.; Jeong, D.; Kang, M.; Yoo, Y. J.; Lee, H.; Oh, S. H.; Ryu, J. H.; Kim, W. Y. Evodiamine Selectively Targets Cancer Stem-like Cells through the P53-P21-Rb Pathway. *Biochem. Biophys. Res. Commun.* **2016**, *469*, 1153–1158.
- (51) Basu, P.; Kumar, G. S. Sanguinarine and Its Role in Chronic Diseases. In *Anti-inflammatory Nutraceuticals and Chronic Diseases*; Springer, 2016; pp 155–172.
- (52) Zhang, B.; Wang, X.; Deng, J.; Zheng, H.; Liu, W.; Chen, S.; Tian, J.; Wang, F. P53-Dependent Upregulation of miR-16-2 by Sanguinarine Induces Cell Cycle Arrest and Apoptosis in Hepatocellular Carcinoma. *Cancer Lett.* **2019**, *459*, 50–58.
- (53) Han, M. H.; Kim, S. O.; Kim, G. Y.; Kwon, T. K.; Choi, B. T.; Lee, W. H.; Choi, Y. H. Induction of Apoptosis by Sanguinarine in C6 Rat Glioblastoma Cells Is Associated with the Modulation of the Bcl-2 Family and Activation of Caspases through Downregulation of Extracellular Signal-Regulated Kinase and Akt. *Anticancer Drugs* **2007**, *18*, 913–921.
- (54) Ghauri, M. A.; Su, Q.; Ullah, A.; Wang, J.; Sarwar, A.; Wu, Q.; Zhang, D.; Zhang, Y. Sanguinarine Impedes Metastasis and Causes Inversion of Epithelial to Mesenchymal Transition in Breast Cancer. *Phytomedicine* **2021**, *84*, No. 153500.
- (55) Pallichankandy, S.; Rahman, A. ROS-dependent activation of autophagy is a critical mechanism for the induction of anti-glioma effect of sanguinarine. *Free Radical Biol. Med.* **2015**, *89*, 708–720.

- (56) Kulikov, R.; Letienne, J.; Kaur, M.; Grossman, S. R.; Arts, J.; Blattner, C. Mdm2 Facilitates the Association of P53 with the Proteasome. *Proc. Natl. Acad. Sci. U.S.A.* **2010**, *107*, 10038–10043.
- (57) Zhang, X.; Gu, L.; Li, J.; Shah, N.; He, J.; Yang, L. Degradation of MDM2 by the Interaction between Berberine and DAXX Leads to Potent Apoptosis in MDM2-Overexpressing Cancer Cells. *Cancer Res.* **2010**, *73*, 9895–9904.
- (58) Zhou, N.; Li, J.; Li, T. Matrine-induced Apoptosis in Hep3B Cells via the Inhibition of MDM2. *Mol. Med. Rep.* **2017**, *15*, 442–450.
- (59) Brew, C. T.; Aronchik, I.; Hsu, J. C.; Sheen, J.-H.; Dickson, R. B.; Bjeldanes, L. F.; Firestone, G. L. Indole-3-carbinol activates the ATM signaling pathway independent of DNA damage to stabilize p53 and induce G1 arrest of human mammary epithelial cells. *Int. J. Cancer* **2006**, *118*, 857–868.
- (60) Patil, S. P.; Pacitti, M. F.; Gilroy, K. S.; Ruggiero, J. C.; Griffin, J. D.; Butera, J. J.; Notarfrancesco, J. M.; Tran, S.; Stoddart, J. W. Identification of Antipsychotic Drug Fluspirilene as a Potential P53-MDM2 Inhibitor: A Combined Computational and Experimental Study. *J. Comput. Aided. Mol. Des.* **2015**, *29*, 155–163.
- (61) Clough, E.; Barrett, T. The Gene Expression Omnibus Database. *Methods Mol. Biol.* **2016**, *1418*, 93–110.
- (62) Kim, S.; Thiessen, P. A.; Bolton, E. E.; Chen, J.; Fu, G.; Gindulyte, A.; Han, L.; He, J.; He, S.; Shoemaker, B. A.; Wang, J.; Yu, B.; Zhang, J.; Bryant, S. H. PubChem Substance and Compound Databases. *Nucleic Acids Res.* **2016**, *44*, D1202–D1213.
- (63) Daina, A.; Michielin, O.; Zoete, V. SwissADME: A Free Web Tool to Evaluate Pharmacokinetics, Drug-Likeness and Medicinal Chemistry Friendliness of Small Molecules. *Sci. Rep.* **2017**, *7*, No. 42717.
- (64) Kochnev, Y.; Hellemann, E.; Cassidy, K. C.; Durrant, J. D. Webina: An Open-Source Library and Web App That Runs AutoDock Vina Entirely in the Web Browser. *Bioinformatics* **2020**, *36*, 4513–4515.
- (65) Pawar, S. S.; Rohane, S. H. Review on Discovery Studio: An Important Tool for Molecular Docking. *Asian J. Res. Chem.* **2021**, *14*, 1–3.
- (66) Daniele, S.; Costa, B.; Zappelli, E.; da Pozzo, E.; et al. Combined Inhibition of AKT/MTOR and MDM2 Enhances Glioblastoma Multiforme Cell Apoptosis and Differentiation of Cancer Stem Cells. *Sci. Rep.* **2015**, *5*, No. 9956.
- (67) Kubbutat, M. H. G.; Jones, S. N.; Vousden, K. H. Regulation of P53 Stability by Mdm2. *Nature* **1997**, *387*, 299–303.

Recommended by ACS

Kuwanon H Inhibits Melanoma Growth through Cytotoxic Endoplasmic Reticulum Stress and Impaired Autophagy Flux

Xin Hu, Hongjuan Cui, *et al.*

SEPTEMBER 06, 2023

JOURNAL OF AGRICULTURAL AND FOOD CHEMISTRY

READ 

Therapeutic Targeting of Regulated Signaling Pathways of Non-Small Cell Lung Carcinoma

Gulam Mustafa Hasan, Manzar Alam, *et al.*

JULY 17, 2023

ACS OMEGA

READ 

Design and Computational Analysis of an MMP9 Inhibitor in Hypoxia-Induced Glioblastoma Multiforme

Smita Kumari and Pravir Kumar

MARCH 12, 2023

ACS OMEGA

READ 

p53-Bad* Fusion Gene Therapy Induces Apoptosis In Vitro and Reduces Zebrafish Tumor Burden in Hepatocellular Carcinoma

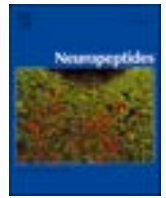
Katherine E. Redd Bowman, Carol S. Lim, *et al.*

DECEMBER 09, 2022

MOLECULAR PHARMACEUTICS

READ 

Get More Suggestions >



Dissecting the functional significance of HSP90AB1 and other heat shock proteins in countering glioblastomas and ependymomas using omics analysis and drug prediction using virtual screening

Sudhanshu Sharma, Pravir Kumar^{*}

Molecular Neuroscience and Functional Genomics Laboratory, Delhi Technological University, Shahabad Daultapur, Bawana Road, Delhi 110042, India

ARTICLE INFO

Keywords:

Heat shock proteins
Glioblastoma
Ependymomas
Omics
Brain tumors, Cancer, Crosstalk, *In-silico*

ABSTRACT

Heat shock proteins (HSPs) are the evolutionary family of proteins that are highly conserved and present widely in various organisms and play an array of important roles and cellular functions. Currently, very few or no studies are based on the systematic analysis of the HSPs in Glioblastoma (GBMs) and ependymomas. We performed an integrated omics analysis to predict the mutual regulatory differential HSP signatures that were associated with both glioblastoma and ependymomas. Further, we explored the various common dysregulated biological processes operating in both the tumors, and were analyzed using functional enrichment, gene ontology along with the pathway analysis of the predicted HSPs. We established an interactome network of protein-protein interaction (PPIN) to identify the hub HSPs that were commonly associated with GBMs and ependymoma. To understand the mutual molecular mechanism of the HSPs in both malignancies, transcription factors, and miRNAs overlapping with both diseases were explored. Moreover, a transcription factor-miRNAs-HSPs coregulatory network was constructed along with the prediction of potential candidate drugs that were based on perturbation-induced gene expression analysis. Based on the RNA-sequencing data, HSP90AB1 was identified as the most promising target among other predicted HSPs. Finally, the ranking of the drugs was arranged based on various drug scores. In conclusion, this study gave a spotlight on the mutual targetable HSPs, biological pathways, and regulatory signatures associated with GBMs and ependymoma with an improved understanding of crosstalk involved. Additionally, the role of therapeutics was also explored against HSP90AB1. These findings could potentially be able to explain the interplay of HSP90AB1 and other HSPs within these two malignancies.

1. Introduction

Heat shock proteins (HSPs) also known as stress proteins are an important class of proteins that are activated by the cells in response to heat shock or in response to stimuli (external or internal) such as unavailability of nutrition, heat, and cold, hypoxia and so on (Bond and Schlesinger, 1987). These classes of proteins are involved in the presentation of antigens, assembly of hormonal receptors, protein folding, and cell trafficking (Lianos et al., 2015). Due to the various roles that

HSPs play in maintaining cellular integrity, a disruption in their machinery causes a depletion in cellular proteostasis leading to cell death (Saibil, 2013). Due to this malfunction, their levels are significantly increased in cancerous cells as compared to the normal tissue (Hu et al., 2022). Therefore, their mechanism is taken up by the malignant cells for their proliferation and survival (Sherman et al., 2007). As HSPs play an intricate role in the origin of these cancerous cells, increased cellular growth and the maintenance of tumor cells show their importance in cancer biology and therefore, can be employed as potential therapeutic

Abbreviations: GBM, Glioblastomas; HSPs, Heat shock proteins; PPIN, Protein-Protein interaction network; EGFR, Epidermal growth factor receptor; HSPMdb, Heat shock protein modulatory database; TRANSFAC, Transcription factor database; EMT, epithelial-to-mesenchymal transitions; GEPAL2, Gene expression profiling interactive analysis 2; GEO, Gene expression; KEGG, Kyoto encyclopedia of genes and genomics; GO, Gene ontology; GATA2, GATA-binding factor 2; FOXC1, Fork head box C1; USF2, Upstream transcription factor 2; PDGFR- β , Platelet derived growth factor receptors; β RTKs, Receptor tyrosine kinases; IDH1, Isocitrate dehydrogenase 1; CREEDS, Crowd extracted expressions of differential signatures; RMSD, Root mean square deviations; RMSF, Root mean square fluctuations; Rg, Radius of gyration; TFs, Transcription factors; WNT, Wingless-type murine mammary tumor virus integration sites; BBB, Blood brain barrier; PDB, Protein databank; ADMET, absorption, distribution, metabolism, excretion and toxicity..

^{*} Corresponding author at: Room# FW4TF3, Mechanical Engineering Building, Shahabad Daultapur, Bawana Road, Delhi 110042, India.

E-mail address: pravirkumar@dtu.ac.in (P. Kumar).

<https://doi.org/10.1016/j.npep.2023.102383>

Received 3 July 2023; Received in revised form 7 September 2023; Accepted 10 September 2023

Available online 14 September 2023

0143-4179/© 2023 Elsevier Ltd. All rights reserved.

targets. HSPs also play an important role in cancer cell evasion, tumor cellular division, mechanism of DNA repair, metastasis, and invasion into the surrounding normal cells (Hasan et al., 2022). These HSPs are classified based on the molecular weights comprising different families—HSP90, HSP110, DNAJ, and smaller HSPs (Kampinga et al., 2009).

Malignant tumors that originate from the brain are hard to treat due to their location of origin as they are deeply embedded within the brain, their ability to metastasize rapidly, and aggressive behavior thereby, leading to poor prognosis in patients and decreased overall survival. Glioblastomas (GBMs) and ependymomas are Grade IV tumors that originate from the glial cells and are the most aggressive tumors of the central nervous system (CNS) (Han et al., 2018). Ependymomas are tumors of the neuroectodermal region (Oppenheim et al., 1994) and arise from the glial cells and are present in the parenchyma of the brain due to the migration of the ependymal cells of the fetus from the periventricular areas (Centeno et al., 1986). The prevalence of ependymoma is higher in males as compared to females and can happen in age groups (De Angelis et al., 2013). Overall survival of the patients suffering from ependymoma remains around 40% (Gatta et al., 2002). Glioblastoma on the other hand is the most commonly occurring brain tumor and can arise from oligodendrocytes, astrocytes, or ependymal cells. Their classification is based on the site of the origin and can be defined as either oligodendrogliomas, astrocytomas, or glioblastomas (Masui et al., 2016). These tumors are more aggressive than ependymomas as they are more lethal and account for almost 75% of the cases recognized by the World Health Organization (WHO) (Komori, 2022). Standard therapy in glioblastoma remains temozolomide followed by radiotherapy, which causes short survival and poor prognosis in patients. The median survival in patients suffering from glioblastoma remains only 10–16 months after treatment (Krex et al., 2007). In both the tumors described there is a lack in therapeutically targeting these tumors as these tumors have unpredictable etiologies and the complex mechanism of these tumors is still unknown. The availability of information regarding the role of chemotherapy in the case of ependymoma (Bouffet and Foreman, 1999) is very limited, and only surgery remains an option. Although the potency to counter the primary tumors in both the high-grade and low-grade ependymomas is not upon the mark more aggressive therapies are being employed in the clinics to find some better therapeutics in countering ependymomas. Here HSPs come into counterplay as they mediate several cellular processes and could be a potential therapeutic avenue in countering both GBMs and ependymomas.

HSP90 is the most studied class and its inhibitors are found to be effective in the treatment of cancer. One study investigated the role of 17-allylamino-17-demethoxygeldanamycin (17-AAG) or Tanespimycin as a therapeutic agent in GBM (Sauvageot et al., 2009). This inhibitor was found to be effective in combination with Olaparib and also caused the inhibition of Poly ADP-ribose polymerase (PARP) in the case of glioblastoma. However, no study claims its role in the inhibition of ependymomas. Another study used ZD1839 (Iressa), which is an inhibitor of epidermal growth factor receptor (EGFR) against glioma cells (Premkumar et al., 2006). Inhibitors of HSP70 such as VER-155008, and MAL3-101 also showed promising results against various brain tumors (Braunstein et al., 2011). Studies have also shown that cannabinoid agonist such as WIN55-212-2 was found to be efficient in human glioblastoma cell line U-251MG and also showed to alter the expression levels of HSP70, cathepsin, and p53 (Silva et al., 2019). These studies suggest that targeting HSPs can be more fruitful and hence, more studies are needed to be done against HSPs to understand the role of HSPs in countering both tumors. Therefore, our findings may provide a better understanding of the pathways of the HSPs that are mutually dysregulated in both GBMs and ependymomas, and this opens new opportunities in the therapeutic options in both brain malignancies.

2. Material and methodology

2.1. Retrieval of raw data

The dataset employed in the study was extracted from the National Centre of Biotechnology Information (NCBI) gene expression omnibus (GEO) (<https://www.ncbi.nlm.nih.gov/geo/>) (Clough and Barrett, 2016). The microarray gene expression profiles were obtained from the GSE 50161 dataset. The dataset used for the study was based on the criteria as discussed. The first criterion was to use only those datasets that contained the array expression analysis data of human brain tissue samples from GBM patients, ependymoma, and healthy patients. Second, the dataset must possess the ependymoma, GBM, and control samples in one dataset itself. Third, all the patient samples present within the dataset whether healthy or tumor are not previously exposed to any kind of prior treatment (chemotherapy or radiotherapy). Fourthly, the number of human patient samples either healthy, GBM, or ependymoma-affected should not be <10 in number within the dataset respectively (Yao et al., 2019). The platform that is used in GSE 50161 is GPL570 [HG-U133_Plus_2] Affymetrix human genome.

2.2. Data processing, analysis of DEGs, and prediction of HSPs

Raw read counts for input data were obtained from the TCGA or GEO dataset. R package DESeq2 was also used for data extraction. The analysis was further nurtured using GEO2R (<https://www.ncbi.nlm.nih.gov/geo/geo2r>) a web-based interactive tool that works on the R language limma package. GEO2R acts as a tool for the comparative establishment of two or more sets of gene samples in the GEO series (Clough and Barrett, 2016). To study the underlying biological prospects, biological functions were annotated for the differentially expressed genes. Parameters such as P -value < 0.05 and the $|\text{Log FC}| > 2$ and $|\text{Log FC}| < 2$ were used as cut-off criteria to filter the differentially expressed genes. Identification of HSPs from the screened DEGs, commonly regulating in both tumors was done using the HSPMdb (Singh et al., 2020) database and by literature survey.

2.3. Protein-protein functional interaction and network analysis

Interaction of proteins was committed using Network Analyst (Advani and Kumar, 2022) which is an online bioinformatic tool (Zhou et al., 2019). All the common heat shock proteins were used as input in network preparation. Network Analyst is used as a network construction and visualization tool that incorporates various databases for analysis. Topological parameters such as Degree centrality and distribution of betweenness were done using a network analyzer using Cytoscape. Degree centrality refers to the number of connections in the network and also the impact of a node on the network. The betweenness centrality of the nodes represents the shortest distance between the nodes passing through the query node. In addition to this, a module explorer panel was also used for the identification of interlinked proteins in the network. Based on the number of proteins involved in the interaction these modules were ranked. First-order network analysis was done to reduce the hairball effect. For the analysis of large and complicated biological networks, nodes are considered significant and are hampered by this hairball effect.

2.4. Functional enrichment and pathway analysis

To determine the functional aspects of the predicted overlapping HSPs, the functional annotation map module of the database for visualization, annotation, and integration we used the DAVID bioinformatics database. This database was used for the analysis and to give annotation to the identified overlapping HSPs. We also used another tool for the Gene Ontology (GO) term and the pathway prediction was done using SHINY GO 7.16 (<http://bioinformatics.sdstate.edu/go/>). Parameters

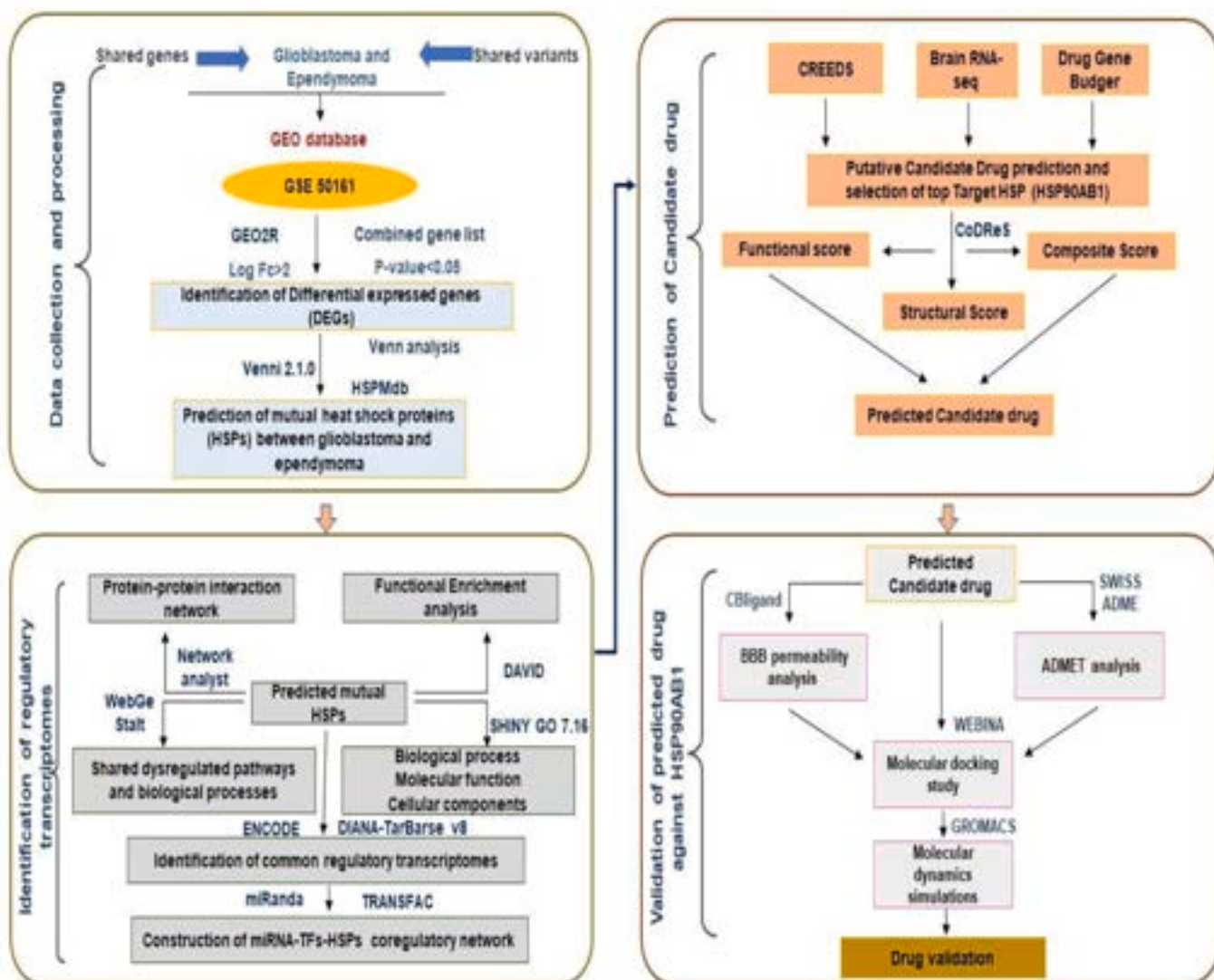
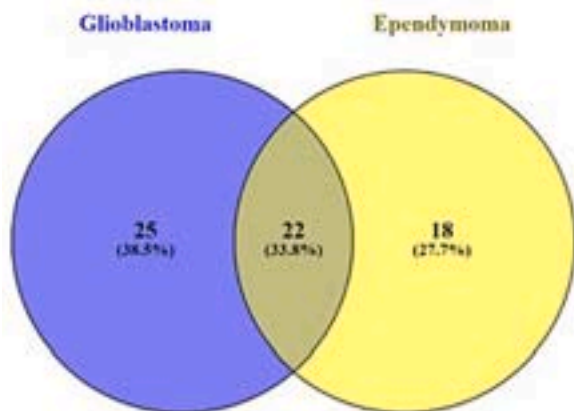


Fig. 1. Workflow pipeline: Data was retrieved from the Gene Expression Omnibus (GEO) database for transcriptomics studies. Data processing was done using Gene expression profiling interactive analysis 2 (GEPAl2) After data processing the identification of putative Heat shock proteins (HSPs) was carried out using a literature survey and the HSPMdb database. Following the prediction, the intersection of common HSPs in Glioblastoma (GBMs) and ependymoma was done using Venn diagrams. Protein-protein interaction (PPI) analysis extracted common hub genes to search for disease-disease similarity. These hub genes were further subjected to enrichment analysis and pathway analysis to obtain significant pathways and common GO terms. The common regulation of the two indications was further confirmed by identifying common transcription factors (TFs) and microRNAs (miRNA). CREEDs analysis and LINC1000 Drug Gene Budger were used to identify potential candidate drugs targeting HSPs mutually in GBMs and ependymoma. Finally, the ranking of the candidate drugs was done using CoDRes giving the functional, structural, and composite scores of the candidate drugs.

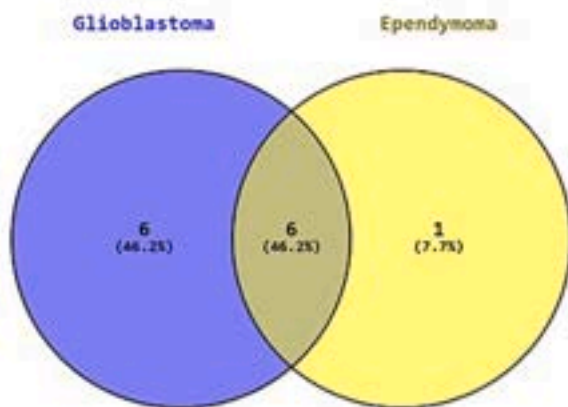
such as $|P\text{-value} < 0.05|$, $|\text{Log Fc} > 2|$ and $|\text{Log Fc} < 2|$ were used as thresholds for significantly enriched terms. Eventually, the functional enrichment network was constructed (Sharma and Kumar, 2023). Enrichment analysis was done to understand the biological process, molecular function, and cellular components using GO term analysis. Kyoto Encyclopedia of Genes and Genomes (KEGG) pathway analysis was conducted for the common predicted HSPs in glioblastoma and ependymoma. The analysis was performed using Web-Gestalt (WEB-based Gene Set Analysis Toolkit). Web-Gestalt which is a web-based functional enrichment tool can identify the KEGG pathway that is associated with the genes required to be studied. Also helps to identify the genes interacting in each pathway along with their Entrez ID (Liao et al., 2019) (Zhang et al., 2005). A P -value of < 0.05 was used as the cutoff criterion in KEGG analysis. Further, the dot plot for the enriched KEGG pathways was plotted using cluster Profiler package 4.0 (Wu et al., 2021).

2.5. Identification of common regulatory transcriptomes

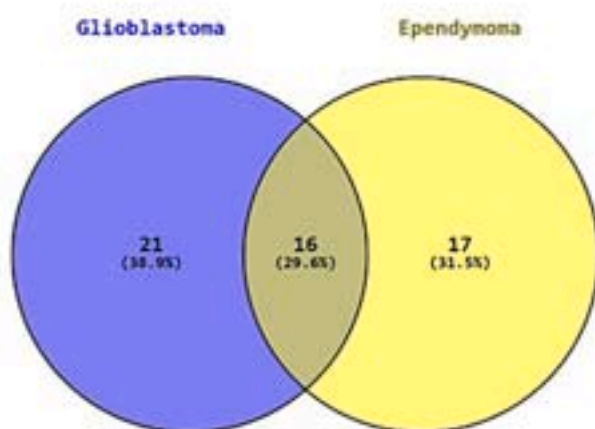
For the identification of common HSP transcriptomes, the coinciding genes were targeted in different databases. This analysis was done to identify the common transcription factors (TFs) and miRNAs that were regulatory at both translational and post-translational levels in GBM and ependymoma. The prediction of common regulatory transcriptional factors (Falktoft et al., 2009) was done using ENCODE database (Auerbach et al., 2013) (Goi et al., 2013), which is a ChIP sequencing data that is based on the BETA Minus algorithm (Bisht et al., 2020). The signals with peak intensity < 500 and potential regulatory score < 1 , are used as thresholds in the BETA algorithm used by this database. Potential prediction of miRNA was done using the DIANA-TarBase v8 database (Karagkouni et al., 2018), which encompasses experimentally validated miRNA targets of genes of different species.



(A) Common Differential HSPs in Glioblastoma and ependymoma



(B) Common Upregulated HSPs in Glioblastoma and ependymoma



(C) Common Downregulated HSPs in Glioblastoma and ependymoma

Glioblastoma	Ependymoma
HSPBAP1	DNAJC10
HSPBP1	DNAJB11
CRYBB3	DNAJB14
CRYZL1	DNAJC11
CRYZ	DNAJC4
HSPA1A	DNAJB13
HSPA6	DNAJC3
HSPAS	DNAJB12
HSPA4	DNAJB5
HSPH1	DNAJC2
HSP90AB1	DNAJA3
HSP90B1	DNAJC1
HSP90AA1	DNAJB8
HSPD1	DNAJC16
DNAJC11	DNAJC15
DNAJC13	HSCB
DNAJB2	SEC63
DNAJA1	HSPA1A
DNAJB12	HSPA1L
DNAJC19	HSPH1
HSPA1A	HSCB
DNAJB11	HSPB1
DNAJC2	TRAP1
DNAJC10	HSP90B1
HSPE1	HSP90AA1
DNAJB6	HSP90AB1
DNAJB14	MKKS
TCP10L	HSPE1
TCP11L1	MOB4
BBS10	HSPD1
BBS7	CCT6B
BBS1	CCT3
CCT6A	CCT2
CCT2	BBS12
CCT6B	
CCT5	
CCT3	
CCT8	
HSPD1	
HSPE1	

*Commonly downregulated HSPs in glioblastoma and ependymoma

Glioblastoma	Ependymoma
DNAJC6	DNAJC6
DNAJB2	DNAJC5
HSPB8	DNAJC12
HSPA2	DNAJC27
HSPA12A	DNAJA4
DNAJA4	HSPA12A
DNAJC27	HSPB3
DNAJB4	
HSPA1A	
HSPB3	
DNAJC12	
CRYAB	

*Commonly upregulated HSPs in glioblastoma and ependymoma

Fig. 2. Representation of the various heat shock proteins (HSPs) identified to be common in both Glioblastoma and ependymoma. (A) 22 out of 65 HSPs predicted using a literature survey were found to be overlapping in Glioblastomas and ependymomas. (B) 6 out of 7 predicted HSPs identified to be upregulated in both glioblastoma and ependymomas. (C) 16 out of 38 HSPs predicted to be mutually occurring in both glioblastoma and ependymomas.

2.6. Transcriptional and post-transcriptional regulation of TF-HSP, TF-miRNA, miRNA-HSPs and HSPs-TF

The prediction of TF-HSPs and TF-miRNA interactions was done using the Transcription factor (TRANSFAC) database. TRANSFAC (Matys et al., 2006; Wingender et al., 2019) is a comprehensive database of transcription factor-target gene interactions. We selected only those TF-HSP pairs that were found to be conserved in humans. To study the post-transcriptional regulation at miRNA and TF levels, we used three reliable databases for miRNA-target prediction. The three databases that were used are Miranda (Betel et al., 2008), TargetScan (Agarwal et al., 2015), and PITA (Kertesz et al., 2007). The data in these databases is obtained from low and high-throughput experimental procedures. Only those pairs were selected that were present in at least two databases. Further, the construction of the miRNA-TF-HSPs coregulatory network was done using Network Analyst.

2.7. Drug screening and target HSP confirmation

The common regulatory HSPs and key drivers that were screened from DEGs obtained were then used for CREEDS (Wang et al., 2016). The database can be accessed using (<https://maayanlab.cloud/CREEDS/>) After the prediction from CREEDS the results obtained were then subjected to Drug Gene Budger (<https://maayanlab.cloud/DGB/>). Confirmation of the best HSP that could be targeted from the list of identified HSPs was done using Brain-RNA seq (<https://www.brainrnaseq.org/>). Brain-RNA seq is a web-based database containing the RNA sequence information of the cells of the glial and neuronal origin.

2.8. Ranking and scoring of predicted drugs

Drugs predicted using CREEDS and Drug Gene Budger analysis were then used as input to the computational drug repositioning score (CoDRES) tool. CoDRES (Karatzas et al., 2019) is a computational analysis tool that allows a functional score (FS) and structural score (STS) for independent drugs based on the disease of interest. This tool gives the best repositioning score to the identified drugs based on their similarity and functions.

2.9. Molecular docking, ADMET, and blood-brain barrier (BBB) analysis

Molecular docking studies were performed for the confirmation of the identification of candidate drugs. The PDB confirmation of HSP90AB1 (PDB ID: 3NMQ) was retrieved from the RCSB PDB database. WEBINA (<https://durrantlab.pitt.edu/webina/>) which is a web-based interaction that works on JavaScript and runs AUTODOCK Vina on the web. Heteroatoms within the HSP90AB1 structure were omitted and the addition of hydrogen was done using UCSF chimera and Avogadro. The grid size was set with the following coordinates (X-axis = 30, Y-axis = 30, and Z-axis = 30). The 2D and 3D interactions of the complexes were visualized using Discovery Studio (<https://biovia-discovery-studio-2022-client.software.informer.com/>). The ADMET (absorption, distribution, metabolism, excretion, and toxicity) of the predicted candidate drugs was done using SWISSADME. The BBB permeability (Masoumi et al., 2018) of the predicted candidate drugs was checked using Cbligand (<https://www.cbligand.org/BBB/mainpage.php>).

2.10. Molecular dynamic (MD) simulation studies

Dynamic simulation studies were performed using the GROMACS 2019.3 package (<https://bioexcel.eu/software/gromacs/>) following docking analysis for final validation. Preparation of the complexes was done using Charmm37 all-atom forcefield. The generation of the charge topology was conducted using CGenFF along with solvation in a cubical boundary box with a dimensional gap of 1.0 nm (applying the TIP3 water model). The addition of Na⁺ and Cl⁻ ions was done to perform

charge neutralization. Minimization of energy carried out at 20KJ/mol/mm by implementing a descent-long algorithm of 10,000 steps proceeded by 10,000 steps of the conjugate gradient to remove any steric hindrance. The calculation for the root mean square fluctuation (RMSF), root mean square deviations (RMSD), Interaction energy, and radius of gyration was done and then plots were constructed.

The detailed pipeline of the study is represented in Fig. 1.

3. Results

3.1. Collection of raw data

Microarray data from the gene expression profile GSE 50161 was downloaded from NCBI GEO databases. A total of 130 human surgical samples of the brain were present in the dataset. Out of these the count of the diseased ependymoma samples present in this dataset was 46, the count for diseased glioblastoma samples was 33 and the number of normal brain samples that were present in this dataset was 13. The rest of the samples were not employed for analysis as those were astrocytoma and medulloblastoma samples and our study was focused on GBM and ependymoma only.

3.2. Differential expression of HSPs in ependymoma and GBM samples

Identification of the DEGs of which the expression levels were highly correlated may highlight the pathological and biological events occurring between GBMs, ependymoma, and the potential signature genes. The DEGs were picked by comparing the genes between the normal and the diseased samples. In the case of glioblastoma based on the *P*-value out of 20,713 genes, 9261 genes were filtered out. A total of 6107 genes were identified to be differentially expressed and downregulated after applying a fold change of less than or equal to 2 and 1736 genes were found to be upregulated when the fold change was above or equal to 2. When talking about ependymoma, out of 21,051 genes, 9222 genes were filtered out based on the *P*-value. From these 7214 genes were identified to be downregulated based on Log Fc < 2 and 1919 genes were found to be upregulated when we applied a Log Fc > 2. After the prediction of DEGs in both the diseased states, evaluation of the heat shock proteins in both GBM and ependymoma was done. Based on the data available from HSPMdb and literature mining, HSPs were selected from these DEGs. A total of 52 HSPs were identified from the DEGs obtained from GBM samples and 41 HSPs were obtained from DEGs of ependymoma samples. Following Venn analysis, a total of 22 HSPs was predicted, commonly regulating in both tumors. The summarization of the overlapping HSPs can be seen in Fig. 2. These 22 HSPs were preceded for further analysis. The list of all HSPs can be seen in the Supporting Information File, Table 1.

3.3. Construction of HSPs PPIN identifies dysregulated genes linking GBM and ependymoma

HSPs are known to possess many important biological functions and a vast biological significance. 22 regulatory HSPs obtained after Venn analysis were used to construct a panorama of the protein-protein interaction network. This interaction network was plotted to predict the biological interactions that were significant commonly in glioblastoma and ependymoma. These 22 differentially expressed HSPs were used for mapping to the parental network as the hub nodes which later formed a subnetwork comprising of all the interactions. The resultant PPI network showed 8 different subnetworks with several nodes and intercalating edges. To further reduce the 'hairball effect' PPI network mapping of the first order was done that only contained the seed nodes and other interconnecting nodes. From these 8 different subnetworks only the largest subnetwork comprising of 669 nodes and 1247 edges, which are known to be differential HSPs interaction and were used for further analysis. The assessment of the subnetwork was based on

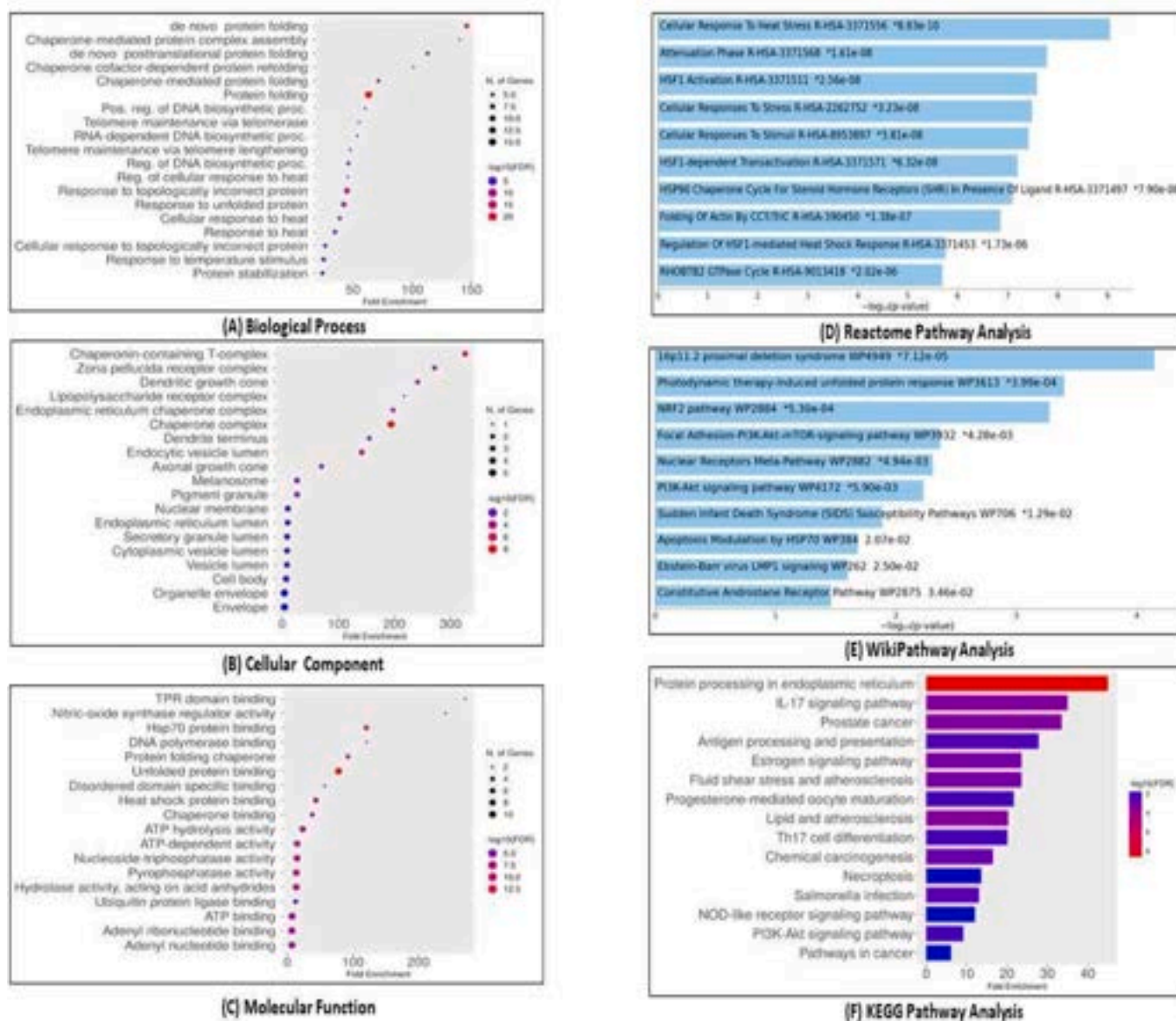


Fig. 3. (A–C) Gene ontology (GO) functional enrichment analysis of 22 common ubiquitin E3 ligases. (A) GO Biological Enrichment analysis involved in protein folding, chaperone-mediated protein complex assembly, and chaperone-mediated protein folding requiring cofactors. The bigger the dots, the greater the color is red, showing the greater significance and number of genes involved in that process. (B) GO Cellular process enrichment showed that the majority of HSPs were associated with extracellular exosomes, endoplasmic reticulum, membrane formation, endoplasmic reticulum chaperone complexes, and endocytic vesicle lumens. (C) GO Molecular function enrichment identified that the majority of the HSPs can be seen in processes such as unfolded protein binding, ATP binding, ATPase activity, RNA binding, and ubiquitin protein ligase binding. (D–F) Depicts the images of the various pathways for 22 Heat Shock proteins (HSPs) and how they are enriched in Reactome, WikiPathway, and KEGG analysis. Most overlapping HSPs can be visualized in pathways such as ‘protein processing in endoplasmic reticulum (Enrichment FDR: 2.43E-09)’, ‘IL-signaling pathway reticulum (Enrichment FDR: 0.000493)’, ‘Pathway involved in Glioma reticulum (Enrichment FDR: 0.000498)’, ‘Antigen processing and presentation reticulum (Enrichment FDR: 0.000543)’, ‘Estrogen signaling pathways reticulum (Enrichment FDR: 0.000933)’, ‘Lipid and atherosclerosis pathway reticulum (Enrichment FDR: 0.000419)’, and ‘Pathways in cancer (Enrichment FDR: 0.017039)’. HSP90AB1, HSP90B1, and HSP90B1 were found to be involved in most of the intersecting pathways in both glioblastoma and ependymoma. Other HSPs that were identified in other pathways were DNAJC10, DNAJB11, HSPH1, and DNAJB12. The bigger the nodes represent a greater number of genes involved and thicker edges here represent significance.

different topological parameters consisting of betweenness and degree centrality. We found that degrees ranging from 1 to 371 and betweenness ranging from 0 to 137,466.1 in the largest subnetwork. Nodes with higher values were predicted to be the hub nodes while those with higher betweenness values were known to be bottleneck nodes. Through our observations we predicted that HSP90AA1 (Degree:371; Betweenness: 137466.1), HSPD1 (Degree:103; Betweenness: 41658.09), CCT2 (Degree:103; Betweenness: 31247.69), HSP90AB1 (Degree:172; Betweenness: 29831.8), HSPA1A (Degree:106; Betweenness: 26204.73) as the top five hub nodes with the highest values of degrees. These hub

nodes can be seen as the possible therapeutic targets in both glioblastoma and ependymoma as they show the largest involvement with the interacting signaling cascades. To further give a better illustration of the network we performed module analysis to identify modules possessing identical biological functions. Out of the different modules, we only selected the top 3 modules based on the P -value ≥ 0.05 and the size of the module ranging from 5 to 70 genes, and are shown in the Supporting Information File, Fig. 2(A–D). Module 0 (p -value 6.34E-11) consisted of HSP90AB1, DNAJC2, DNAJC4, HSPA1A, HSPA12A and HSPH1 as hub nodes, module 1 (p -value 7.66E-19) had CCT2, CCT6B and CCT3 hub

Table 1

Tabular representation of GO functionally enriched heat shock proteins (HSPs) with associated biological processes, molecular functions, and cellular components in glioblastoma and ependymoma.

Category	Term	Hit Count	GO	P-Value	Genes Hit list	List Total	Fold Enrichment	Benjamin	FDR
GO Biological Processes	Protein folding	15	GO:0006457	2.04E-16	DNAJC10, HSP90AA1, DNAJB11, HSP90AB1, DNAJC2, HSPE1, HSPH1, CCT6B, DNAJA4, HSPD1, DNAJB12, CCT3, DNAJB14, CCT2, HSP90B1	22	61.82063953	3.67667E-14	3.28858E-14
GO Biological Processes	Chaperone-mediated protein complex assembly	5	GO:0051131	4.82E-09	CCT2, HSP90AA1, HSP90AB1, HSPD1, HSPA1A	22	219.6931818	2.89097E-07	2.58581E-07
GO Biological Processes	Chaperone mediated protein folding requiring cofactor	5	GO:0051085	3.03E-08	HSPH1, DNAJB12, DNAJB14, HSPE1, HSPA1A	22	142.1544118	1.36441E-06	1.22039E-06
GO Biological Processes	Protein refolding	4	GO:0042026	1.83E-06	HSP90AA1, DNAJA4, HSPD1, HSPA1A	22	154.664	5.58535E-05	4.99579E-05
GO Biological Processes	Protein stabilization	6	GO:0050821	1.86E-06	CCT3, CCT2, HSP90AA1, HSP90AB1, HSPD1, HSPA1A	22	26.36318182	5.58535E-05	4.99579E-05
GO Biological Processes	Cellular response to heat	4	GO:0034605	1.93E-05	HSP90AA1, HSP90AB1, HSPD1, HSPA1A	22	71.6037037	0.000497264	0.000444775
GO Biological Processes	Ubiquitin-dependent ERAD pathway	4	GO:0030433	6.54E-05	DNAJC10, DNAJB12, DNAJB14, HSP90B1	22	47.73580247	0.001471778	0.001316424
GO Biological Processes	Regulation of protein ubiquitination	3	GO:0031396	0.000139	HSP90AA1, HSP90AB1, HSPA1A	22	161.1083333	0.002773943	0.002481138
GO Biological Processes	Positive regulation of telomerase activity	3	GO:0051973	0.000504	CCT2, HSP90AA1, HSP90AB1	22	85.29264706	0.009068588	0.008111348
GO Biological Processes	Regulation of cellular protein localization	2	GO:1903827	0.014646	HSP90AA1, HSP90AB1	20	128.8866667	0.125536434	0.112285366
GO Molecular Functions	Unfolded protein binding	11	GO:0051082	3.11E-17	CCT3, CCT2, HSP90AA1, HSP90AB1, DNAJA4, DNAJB11, HSPE1, HSP90B1, HSPD1, CCT6B, HSPA1A, CCT3, CCT2, HSP90AA1, HSP90AB1, HSPD1, HSPA1A	21	75.60450745	2.30298E-15	1.8984E-15
GO Molecular Functions	ATPase activity	8	GO:0016887	4.78E-08	HSP90AB1, HSP90B1, HSPD1, CCT6B, HSPA1A	21	20.34759214	1.76753E-06	1.45702E-06
GO Molecular Functions	ATP binding	12	GO:0005524	8.57E-08	CCT3, CCT2, HSP90AA1, HSPH1, HSP90AB1, DNAJA4, HSPA12A, HSPE1, HSP90B1, HSPD1, CCT6B, HSPA1A	21	7.011402614	2.11353E-06	1.74224E-06
GO Molecular Functions	Hsp70 protein binding	5	GO:0030544	1.58E-07	DNAJC2, DNAJA4, DNAJC10, DNAJB12, DNAJB14	21	95.7852077	2.76797E-06	2.28171E-06
GO Molecular Functions	Protein binding involved in protein folding	5	GO:0044183	1.87E-07	CCT3, CCT2, HSP90AB1, CCT6B, HSPA1A	21	91.87560739	2.76797E-06	2.28171E-06
GO Molecular Functions	Chaperone binding	4	GO:0051087	0.000203	DNAJA4, DNAJC10, HSPE1, HSPD1	21	32.74112554	0.002506195	0.002065917
GO Molecular Functions	Ubiquitin protein ligase binding	5	GO:0031625	0.000269	CCT2, HSP90AA1, HSP90AB1, HSPD1, HSPA1A	21	14.66418489	0.00284237	0.002343035
GO Molecular Functions	RNA binding	8	GO:0003723	0.000533	CCT3, DNAJC2, HSP90AA1, HSP90AB1, HSPE1, HSP90B1, HSPD1, HSPA1A	21	4.896701305	0.004386134	0.003615597
GO Molecular Functions	Disordered domain specific binding	3	GO:0097718	0.000692	HSP90AA1, HSP90AB1, HSPA1A	21	73.003861	0.00512362	0.004223524
GO Molecular Functions	TPR domain binding	2	GO:0030911	0.008432	HSP90AA1, HSP90AB1	21	225.0952381	0.052958379	0.04365488
GO Cellular component	Endoplasmic reticulum chaperone complex	3	GO:0034663	5.42E-05	DNAJB11, DNAJC10, HSP90B1	22	255.1239669	0.002088319	0.001627261
GO Cellular component	Chaperonin-containing T-complex	3	GO:0005832	5.42E-05	CCT3, CCT2, CCT6B	22	255.1239669	0.002088319	0.001627261
GO Cellular component	Endocytic vesicle lumen	3	GO:0071682	0.00015	HSP90AA1, HSPH1, HSP90B1	22	155.9090909	0.003267354	0.00254599

(continued on next page)

Table 1 (continued)

Category	Term	Hit Count	GO	P-Value	Genes Hit list	List Total	Fold Enrichment	Benjamin	FDR
GO Cellular component	Extracellular exosome	10	GO:0070062	0.00017	CCT3, CCT2, HSP90AA1, HSPH1, HSP90AB1, HSPA12A, HSPE1, HSP90B1, HSPD1, HSPA1A	22	4.215658159	0.003267354	0.00254599
GO Cellular component	Melanosome	3	GO:0042470	0.004989	HSP90AA1, HSP90AB1, HSP90B1	22	26.98426573	0.055795764	0.043477219
GO Cellular component	Endoplasmic reticulum	6	GO:0005783	0.005072	DNAJB11, DNAJC10, DNAJB12, DNAJB14, HSP90B1, HSPA1A	22	4.906230134	0.055795764	0.043477219
GO Cellular component	Ficolin-1-rich granule lumen	3	GO:1904813	0.007017	HSP90AA1, HSP90AB1, HSPA1A	22	22.63196481	0.058322387	0.045446016
GO Cellular component	Sperm plasma membrane	2	GO:0097524	0.007122	HSP90B1, HSPD1	22	267.2727273	0.058322387	0.045446016
GO Cellular component	Zona pellucida receptor complex	2	GO:0002199	0.008136	CCT3, CCT2	22	233.8636364	0.058322387	0.045446016
GO Cellular component	Membrane	10	GO:0016020	0.008332	HSP90AA1, HSP90AB1, DNAJA4, DNAJB11, DNAJC10, DNAJB12, DNAJB14, HSPE1, HSP90B1, HSPD1	22	2.468869215	0.058322387	0.045446016

nodes while module 2 (p-value 3.04E-03) had HSPD1 and HSPE1 hub nodes.

3.4. Functional enrichment and pathway analysis of the predicted HSPs

Gene ontology (GO) enrichment analysis of 22 HSPs was performed using the DAVID database and with the SHINY GO enrichment tool. Based on the above-mentioned results, three types of functional enrichment analysis were performed. This analysis was done to look at the biological process (BP), cellular component (CC), and molecular functions (MF). These enrichments can be seen in Fig. 3.

Most of the HSPs in GO_BP were involved in protein folding, chaperone-mediated protein complex assembly, and chaperone-mediated protein folding requiring cofactors. When taking about the GO_CC, these HSPs were associated with extracellular exosomes, endoplasmic reticulum, membrane formation, endoplasmic reticulum chaperone complexes, and endocytic vesicle lumens. Coming to the GO_MF, the majority of the HSPs can be seen in processes such as unfolded protein binding, ATP binding, ATPase activity, RNA binding, and ubiquitin protein ligase binding. A comprehensive overview of these heat shock proteins commanding various processes in GBMs and ependymoma can be visualized in Table 1. To enumerate the various common regulatory pathways that are deregulated mutually in GBMs and ependymoma, we conducted pathway enrichment of the hub HSPs using Reactome, wiki, and KEGG analysis. The 22 differentially expressed HSPs were used as an input for enrichment. A distinct count of 15 pathways had been enriched for this study. These are represented in Fig. 3 (D–F).

Pathways having high enrichment FDR values were selected for the study. Most overlapping HSPs can be visualized in pathways such as 'protein processing in endoplasmic reticulum (Enrichment FDR: 2.43E-09)', 'IL-signaling pathway reticulum (Enrichment FDR: 0.000493)', 'Pathway involved in Glioma reticulum (Enrichment FDR: 0.000498)', 'Antigen processing and presentation reticulum (Enrichment FDR: 0.000543)', 'Estrogen signaling pathways reticulum (Enrichment FDR: 0.000933)', 'Lipid and atherosclerosis pathway reticulum (Enrichment FDR: 0.000419)', and 'Pathways in cancer (Enrichment FDR: 0.017039)'. HSP90AB1, HSP90B1, and HSP90B1 were found to be involved in most of the intersecting pathways in both glioblastoma and ependymoma. Other HSPs that were identified in other pathways were DNAJC10, DNAJB11, HSPH1, and DNAJB12. These results suggest that

HSP90AB1, HSP90b1, and HSP90B1 have multiple metabolic functions and are involved in various processes in the human body. The detailed information on all the pathways is summarized in Table 2.

3.5. Identification of mutual regulatory transcriptomes linking HSPs in GBMs and ependymoma

To study the mutualistic role of each of the predicted HSPs and to establish a link between glioblastoma and ependymoma at transcriptional and post-transcriptional levels, we tried to decipher a connection of the hub genes with the miRNAs and TFs. GATA2, FOXC1, USF2,

NFIC, FOXL1, RELA, YY1, CREB1, NFKB1, and E2F1 were disclosed to be the top 10 interacting transcription factors with the hub HSPs and are summarized in Table 3. The link can be visualized in Fig. 4.

Likewise, hsa-miR-16-5p, hsa-miR-26b-5p, hsa-miR-92a-3p, hsa-miR-335-5p and hsa-miR-92a-3p, hsa-miR-15a-5p, hsa-miR-193b-3p, hsa-miR-218-5p, hsa-miR-501-5p, hsa-miR-1-3p/has-miR-206/has-miR-613 were selected as the top interacting miRNAs with hub HSPs and can be visualized in Fig. 5A.

All of these interacting miRNAs are summarized in Table 4. The list of all HSPs showing interactions with TFs can also be seen in Supporting Information File, Table 2, and Fig. 2.

3.6. Establishment of miRNA-TFs- target HSPs coregulatory network

To understand the regulatory relationship between miRNAs and TFs, the miRNA-TFs-HSPs regulation network was constructed as shown in Fig. 5B. hsa-miR-181d and has-miR-23a had the rate of connectivity with the target HSPs and TFs. Whereas, several miRNAs were identified to have mutual targets such as has-miR-30C and has-miR-30b showed interactions with HSPH1 and CCT2., various TFs were also found to be interconnected with different HSPs like GABA, MYC, RFX1, and EGFR1. These regulatory TFs interacted with DNAJC2, DNAJC10, HSPH1, and CCT2. We also visualized different modules to develop a better relationship between the transcriptomes and the target HSPs.

Module 0 shows the interaction of CCT3 with E2F1 that was interacting with DNAJC10. hsa-miR-141 was found to be interacting with HSPD1 and with E2F1. Other miRNA has-miR-206 showed interlink with HSPD1 and HSF2. Similarly, hsa-miR-217 interacted with CCT2 and with transcription factor E2F7. From module 1 we predicted that HSP90B1 was interacting with has-miR-522 which in turn was regulated

Table 2

Tabular representation of KEGG pathway analysis of the predicted HSPs along with their fold change and enrichment false discovery rate (FDR) in glioblastoma and ependymoma.

Enrichment FDR	Hits	Pathway Genes	Fold Enrichment	Pathway	Genes Hit list
2.43E-09	7	169	44.96252	Protein processing in the endoplasmic reticulum	[DNAJC10 HSP90AA1 DNAJB11 HSP90AB1 HSPH1 DNAJB12 HSP90B1
0.000493	3	93	35.0169	IL-17 signaling pathway	HSP90AA1 HSP90AB1 HSP90B1
0.000498	3	97	33.5729	Glioma	HSP90AA1 HSP90AB1 HSP90B1
0.00543	2	78	27.83394	Antigen processing and presentation	HSP90AA1 HSP90AB1
0.000933	3	138	23.59834	Estrogen signaling pathway	HSP90AA1 HSP90AB1 HSP90B1
0.000933	3	138	23.59834	Fluid shear stress and atherosclerosis	HSP90AA1 HSP90AB1 HSP90B1
0.00766	2	100	21.71048	Progesterone-mediated oocyte maturation	HSP90AA1 HSP90AB1
0.000419	4	214	20.29016	Lipid and atherosclerosis	HSP90AA1 HSP90AB1 HSPD1 HSP90B1
0.007706	2	108	20.10229	Th17 cell differentiation	HSP90AA1 HSP90AB1
0.002261	3	197	16.53082	Chemical carcinogenesis	HSP90AA1 HSP90AB1 HSP90B1
0.015034	2	159	13.65439	Necroptosis	HSP90AA1 HSP90AB1
0.003886	3	249	13.0786	Salmonella infection	HSP90AA1 HSP90AB1 HSP90B1
0.017039	2	180	12.06138	NOD-like receptor signaling pathway	HSP90AA1 HSP90AB1
0.00766	3	354	9.199354	PI3K-Akt signaling pathway	HSP90AA1 HSP90AB1 HSP90B1
0.017039	3	530	6.144474	Pathways in cancer	HSP90AA1 HSP90AB1 HSP90B1

by ZEB1. HSP90B1 was also interacting with NFYA, SREBF1 and BPTF along with has-miR-99a, hsa-miR-148 and has-miR-624. Module 2 revealed the interaction of DNAJC6 with FOXO3B, FOXO1, and NFIL3 which in turn also showed interactions with has-miR-323-3p, hsa-miR-876-3p, and hsa-miR-501-5p. Modules can be seen in the Supporting Information File, Fig. 3.

Table 3

Tabular summarization of top transcription factors and their associated heat shock proteins (HSPs) common both in glioblastoma and ependymoma.

Id	Transcription factor (TFs)	Associated HSPs	Degree	Betweenness
2624	GATA2	CCT2, DNAJC12, HSP90AB1, HSP90AA1, HSPH1, CCT3, DNAJC11, DNAJC2, HSP90B1, DNAJA4, HSPA12A, DNAJB14, HSPD1	14	188.62
2296	FOXC1	CCT2, DNAJC12, DNAJC6, HSPB3, HSP90AA1, HSPH1, DNAJC2, DNAJC10, DNAJC27, DNAJA4, DNAJB14, HSPD1, HSPE1	13	171.09
7392	USF2	HSPA1A, HSPH1, CCT3, HSP90B1, DNAJC27, HSPE1, DNAJB11, DNAJB12	8	66.85
4782	NFIC	HSPA1A, DNAJC12, HSP90AB1, DNAJC10, HSP90B1, HSPD1, CCT6B, DNAJB11	8	54.68
2300	FOXL1	CCT2, HSPB3, HSP90AA1, HSPH1, DNAJB14, HSPD1, HSPE1, CCT6B	8	51.5
5970	RELA	HSP90AB1, HSP90AA1, DNAJC11, HSP90B1, DNAJA4, HSPA12A, DNAJB11	7	48.25
7528	YY1	CCT2, HSPH1, CCT3, DNAJA4, DNAJB14, DNAJB11	7	31.86
1385	CREB1	DNAJC6, HSP90AB1, HSP90B1, DNAJC27, DNAJA4, HSPA12A	6	23.18
4790	NFKB1	HSP90AB1, DNAJC2, HSP90B1, HSPA12A, DNAJB11	5	14.14
1869	E2F1	DNAJC12, HSP90B1, DNAJA4, DNAJB14, HSPE1	5	12.81

3.7. Prediction of potential drug candidates and putative targetable HSP validation

To identify therapeutic candidates that could potentially target HSPs in GBMs and ependymoma, we performed the CREEDS analysis followed by Drug Gene Budger from LINCl000. As the CREEDS dataset comprises thousands of single-drug induced gene expression signatures obtained from GEO, these drugs could be used as therapeutics in the reversal of GBMs and ependymoma. To nurture our study, we used those gene set-drug pairs that carried significant *p*-values. In the initial screening, we identified 26 drugs when we fed the upregulated hub HSPs into CREEDS with a *P*-value <10⁻¹⁰ as a threshold. Similarly, 148 drugs were obtained when downregulated hub HSPs were screened against the CREEDS database with the same filters. From further analysis, we predicted 5 drugs that could reverse the expression of the upregulated hub HSPs and 30 drugs that could reverse the expressional signature of the downregulated hub HSPs by checking the drug profiles. To crosscheck our results, we used Drug Gene Budger to explore our predicted drugs in the L1000 database. Only the drugs that caused the differential gene expression of important HSPs, followed by Log Fc higher than 2 for upregulated HSPs and Log Fc lower than 2 for downregulated HSPs were considered for analysis using Drug Gene Budger. We found that only 2 drugs could reverse the expression pattern of upregulated HSPs in glioblastoma and ependymoma and 11 drugs for the expression reversal in downregulated HSPs. Resveratrol and cycloheximide were found to be changing the expression patterns of the upregulated HSPs. Similarly, Gefitinib, trovafloxacin, bortezomib, doxorubicin, imatinib, cytarabine,

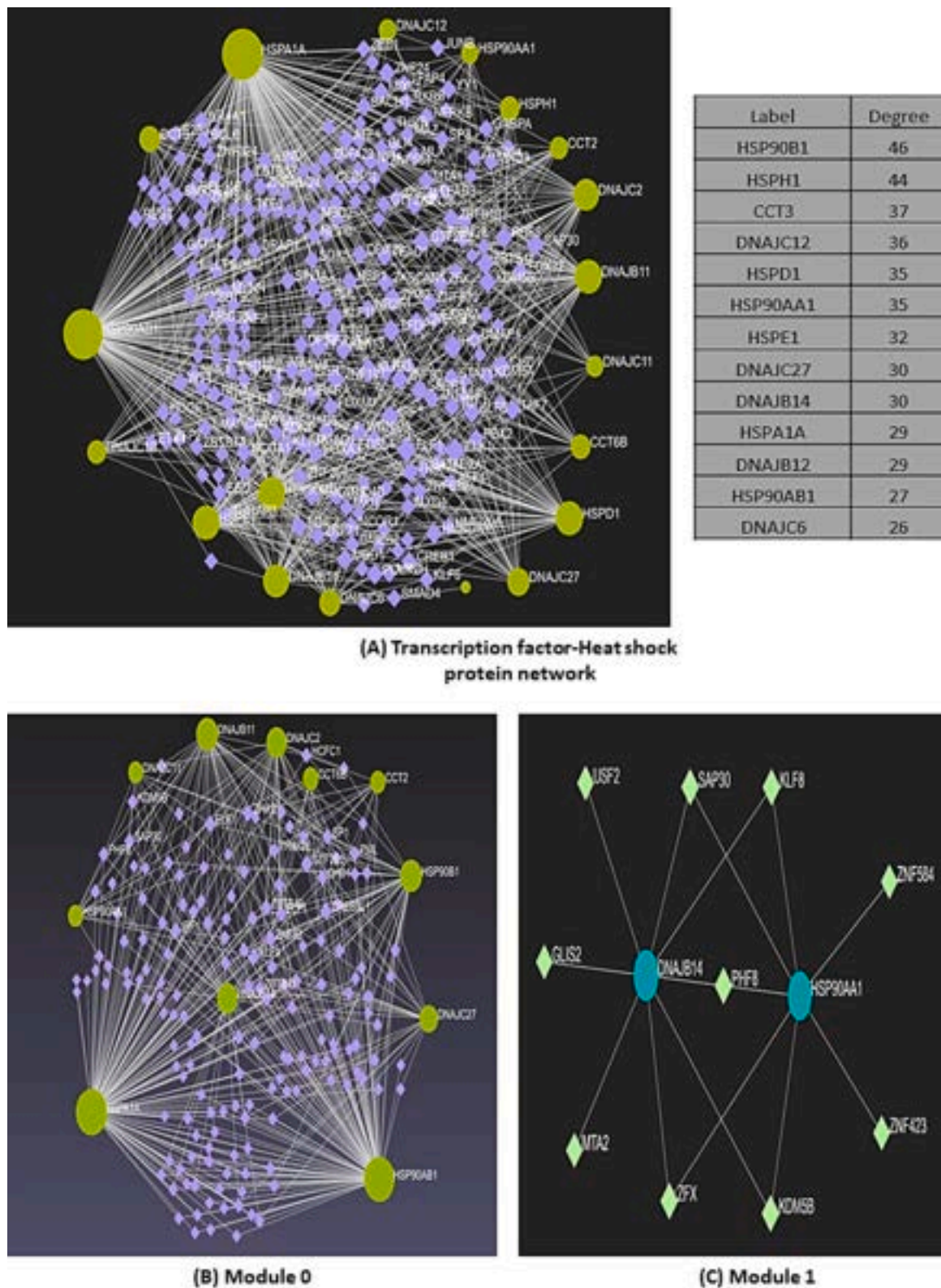
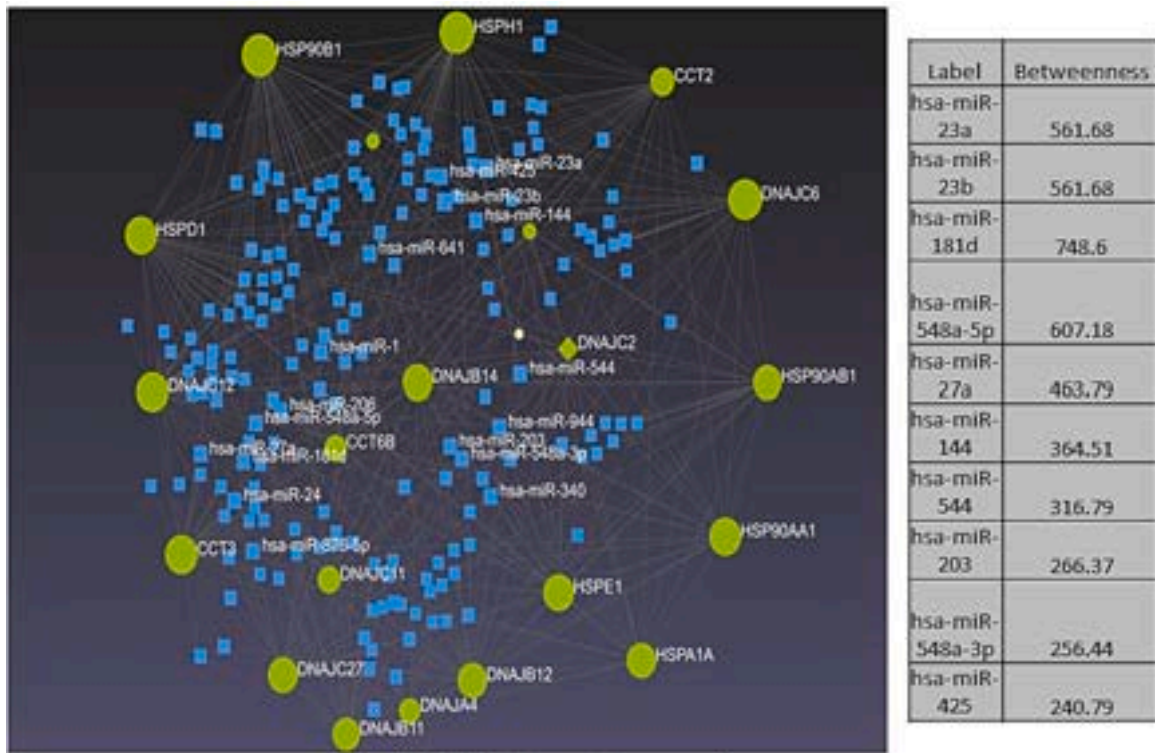
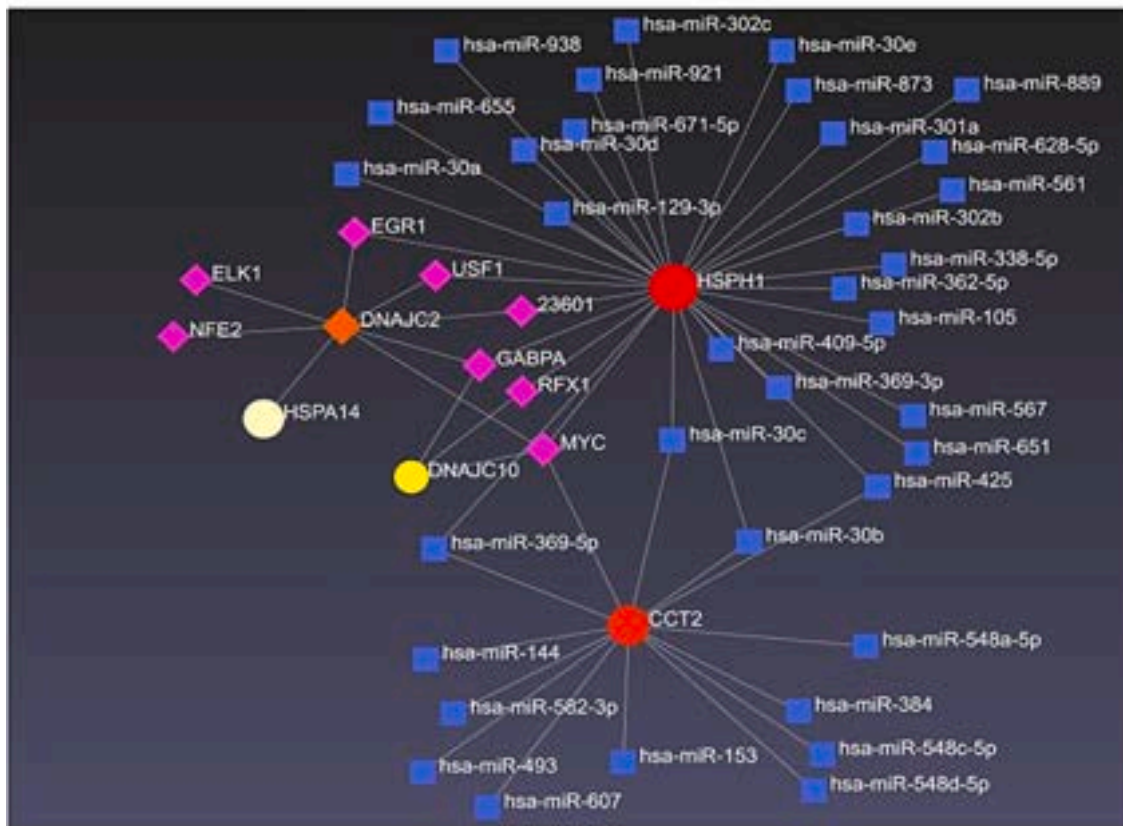


Fig. 4. (A) Transcription Factor-Heat shock protein networks showing the interaction between the hub HSPs and associated transcription factors (TFs). The red circles represent the hub genes and the blue diamond represents the associated TFs. (B) Module 0 represents 11 query nodes, HSP90AB1, HSPA1A, HSP90B1, CCT2, DNAJC2, DNAJB11, and CCT6B. (C) Module 1 represents 2 query nodes DNAJb14 and HSP90AA1. The yellow diamond in the module represents interacting TFs common in Glioblastoma (GBMs) and Ependymoma.



(A) miRNA-HSPs interaction network



(B) TF-miRNA-HSPs coregulatory network

Fig. 5. (A): Representation of the miRNAs showing interacting with Heat shock proteins (HSPs) common in GBMs and ependymoma. The green circles represent the HSPs and the blue squares represent the associated. (B) The regulatory relationship between miRNAs and TFs, the miRNA-TFs-HSPs regulation network was constructed highlighting HSP90B1 interacting with various miRNAs that are mutually associated in both the tumors. Similarly, hsa-miR-217 interacted with CCT2 and with transcription factor E2F7. HSP90B1 was interacting with has-miR-522 which in turn was regulated by ZEB1. HSP90B1 was also interacting with NFYA, SREBF1, and BPTF along with has-miR-99a, hsa-miR-148, and has-miR-624.

Table 4

Tabular representation of common regulatory miRNAs targeting various heat shock proteins (HSPs) in glioblastoma and ependymoma.

microRNA	p-value	FDR	Odd ratio	Number of interactions	Target Genes
hsa-miR-16-5p	1.63361E-05	0.008462105	0.217053903	10	HSPA1A, HSP90B1, DNAJC2, DNAJA4, CCT6B, CCT3, HSPD1, HSPH1, HSP90AA1, DNAJC10
hsa-miR-26b-5p	0.038242532	0.354424512	0.435408922	6	DNAJC2, DNAJC12, HSPA12A, DNAJC11, DNAJC6, HSPD1
hsa-miR-92a-3p	0.040501731	0.354424512	0.392286245	5	HSP90B1, HSP90AB1, HSPH1, DNAJB12, DNAJC27
hsa-miR-335-5p	0.298229545	0.392050052	0.732434944	5	HSPB3, DNAJB14, HSP90B1, HSPA1A, HSP90AB1
hsa-miR-92a-3p	0.040501731	0.354424512	0.392286245	5	HSP90B1, HSP90AB1, HSPH1, DNAJB12, DNAJC27
hsa-miR-15a-5p	0.015947705	0.354424512	0.249883829	4	HSPA1A, HSP90B1, CCT6B, DNAJC10
hsa-miR-193b-3p	0.02825663	0.354424512	0.297281599	4	HSP90AB1, DNAJC11, CCT2, HSPH1
hsa-miR-218-5p	0.02446857	0.354424512	0.284386617	4	HSP90B1, DNAJC2, DNAJC11, DNAJA4
hsa-miR-501-5p	0.001310597	0.339444689	0.073420074	3	HSP90AB1, HSP90AA1, DNAJB14
hsa-miR-1-3p/ hsa-miR-206/ hsa-miR-613	0.133738208	0.354424512	0.427973978	3	HSPD1, HSP90B1, DNAJC10

estradiol, luteolin, nilotinib, and dasatinib were able to reverse the activity in downregulation hub HSPs. Out of 22 HSPs, only 9 were found targetable based on the analysis made from CREEDS and Drug Gene Budger. These HSPs were HSP90AB1, HSPH1, CCT2, HSP90B1, DNAJA4, DNAJC6, HSPAA1, DNAJC10 and HSPA1A. We further proceeded to identify the most suitable HSP among all as a target against all the predicted drugs. Based on the RNA sequencing data and expression pattern of these HSPs, HSP90AB1 was found to be the most prominent HSP against the identified ones. The expression rate in the microglial cells was 227.30 in the case of HSP90AB1, 92.03 in the case of HSPH1, 18.67 in DNAJC10, 15.93 in CCT2, 0.33 in DNAJC6, and 120.37 in case of HSP90B1. Therefore, HSP90AB1 was used to target for further analysis. The plots of the expression pattern of all the predicted HSPs can be visualized in the Supporting Information File, Fig. 5.

3.8. Drug prioritization based on ranking scores using CoDReS

The results obtained from CREEDS and LINC 1000 Drug Gene Budger analysis were then checked for functional and structural properties. The comprehensive comparative scores representing the structural, functional, and composite scores are shown in Fig. 6.

From the analysis, we predicted that four drugs- imatinib, cytarabine, estradiol, and resveratrol have functional and structural score values of 1 while three drugs- Nilotinib, gefitinib, doxorubicin have a functional score of 1 but structural score was less than one. On the other hand, bortezomib, cycloheximide, luteolin, and dasatinib had a structural score of 1 but the functional score was <1. These drugs were repositioned based on their composite CoDReS scores and imatinib, cytarabine, estradiol, resveratrol, and cycloheximide were identified as the top drugs. With these observations, we considered resveratrol, cycloheximide, gefitinib, and imatinib as the most promising candidates for this study. The details of the individual scores are summarized in Table 5.

3.9. Docking, ADMET, and BBB studies against HSP90AB1

Drugs that were prioritized based on the drug ranking and various scores were then proceeded for docking analysis. Docking analysis of HSP90AB1 was done against a reference drug (cepharanthine) to compare the binding scores with imatinib, gefitinib, cycloheximide, and resveratrol. All these four drugs along with the reference were checked for the presence of any extra residue or any heteroatom. Any extra water atoms were removed before docking analysis. The reference drug (Cepharanthine) to compare the binding affinity of HSP90AB1 shows a score of -9.1 Kcal/mol. Binding energy here shows the overall affinity of the drugs for HSP90AB1. The greater the binding scores in negative terms display more inhibition capacity of all these four prioritized drugs against HSP90AB1. The common residues identified during the docking analysis of all these targets along with reference were Met98, Gly135,

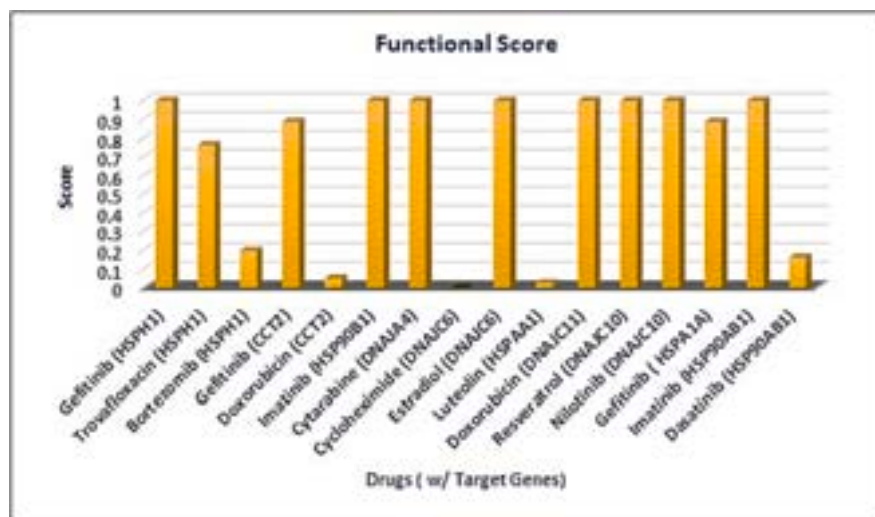
and Val186. The binding energies calculated post-docking analysis were -9.1 Kcal/mol for the reference drug, -9.3 Kcal/mol for resveratrol, -9.2 Kcal/mol in case of cycloheximide, -9.7 Kcal/mol for gefitinib and -10.9 in case of imatinib. The results obtained after docking analysis can be visualized in Fig. 7.

After docking analysis, these drugs were targeted for the ADMET to check for any violation of the Lipinski rule of five for better results and whether they could cross the BBB parameter. Our results demonstrated that all the drugs fitted to the ADMET scores and all of them were able to cross the BBB permeability filter that was done using CBligand. All the docking scores along with the ADMET and BBB scores can be visualized in Table 6.

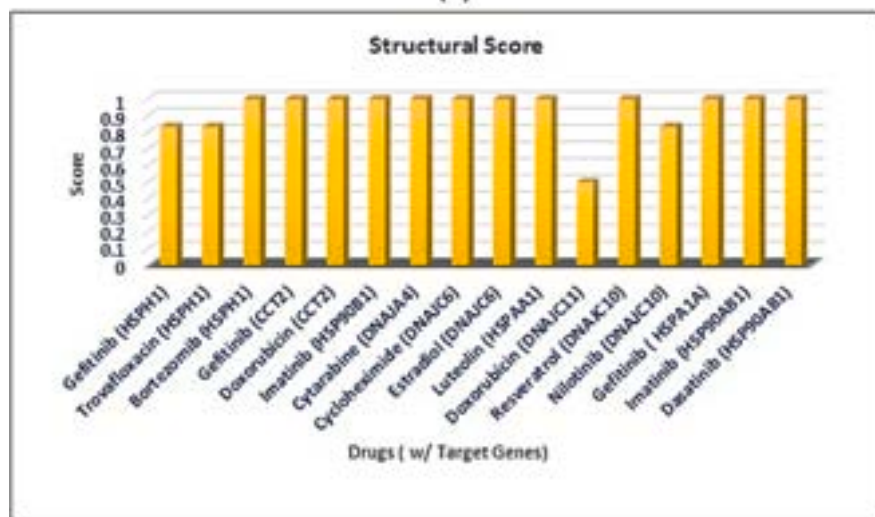
3.10. MD simulations

After the docking analysis for the final confirmational studies, drugs were subjected to MD simulations for 50 ns to check whether the complexes were stable or not. These simulations will help to identify the expression patterns and their dynamic nature. The pattern of stability was checked by calculating the RMSD plot of all the complexes with HSP90AB1.

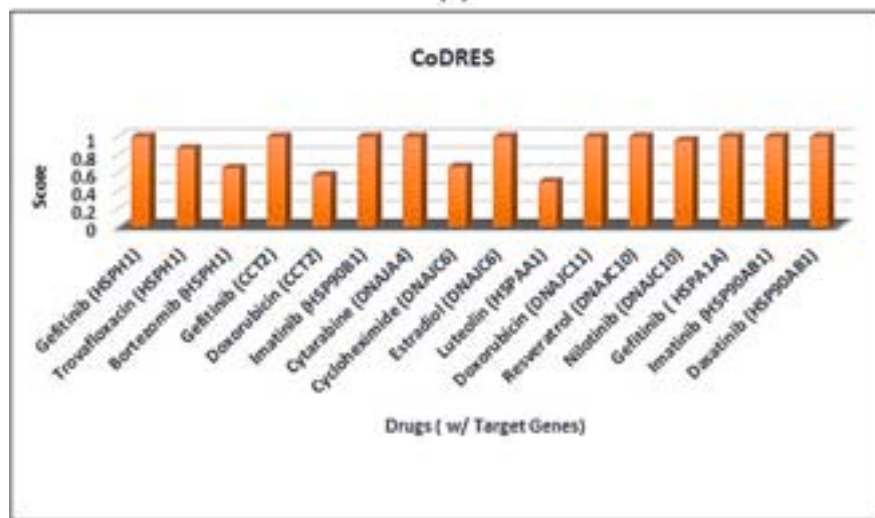
The RMSD of all the ligands complexed with protein and the ligands alone was calculated. The comparison of all the complexes with the reference (HSP90AB1-Cepharanthine) revealed that the backbone of complexes (HSP90AB1-resveratrol, HSP90AB1-gefitinib, HSP90AB1-imatinib, HSP90AB1-Cycloheximide) was stable and integrated. There was a slight fluctuation in the starting and the peak intensity reached between 0.30 nm and 0.33 nm for all the complexes but it decreased eventually thereby showing a stability ranging from 0.15 nm to 0.25 nm as compared to the reference. A deviation was observed in the beginning up to 20 ns but as the simulation time increased the complexes started to stabilize themselves and all the complexes achieved defined stability till 50 ns can be visualized in Fig. 8(A). The compactness in the protein-ligand complex and the folding capacity of protein over time were calculated using the Rg of 1.7 nm. However, an increase in the Rg in the case of HSP90AB1-Geftinib was observed and the peak intensity of 2.70 nm was observed at around 43 ns but the compactness was maintained in all the structures at an average Rg of 1.8 nm and can be seen in Fig. 8 (B). The interaction energy of every complex was measured and it can be preferred from the observations that the binding potential of all four complexes was more as compared to the reference complex Fig. 8(C). The greater the values in negative terms suggest a stronger binding and more stability. Coming to the RMSF which measures the rate of displacement of atoms around the reference, the stability in the peaks of all the complexes (HSP90AB1-cycloheximide, HSP90AB1-resveratrol, HSP90AB1-imatinib, HSP90AB1-gefitinib) was more as compared to the reference complex and can be observed from Fig. 8(D).



(A)



(B)



(C)

Fig. 6. Representation of the scores of the candidate drugs obtained using CoDRES (A) Function scores of the candidate drugs. We predicted that four drugs- imatinib, cytarabine, estradiol, and resveratrol have a functional score value of 1 (B) Structural score value of 1 while three drugs- Nilotinib, gefitinib, doxorubicin have a functional score of 1 but the structural score was less than one (C) Composite CoDRES scores of various candidate drugs. With these observations, we considered resveratrol, cycloheximide, and gefitinib as the most promising candidates.

Table 5

Tabular representation of the comparative scores of different drug-targeting heat shock proteins (HSPs).

Drug name	Targetable Heat shock proteins (HSPs)	Expression Pattern	Drug Bank ID	Functional Score	Structural Score	CoDRS
Gefitinib	HSPH1	Downregulate	DB00137	1	0.833333	1
Trovafloxacin	HSPH1	Downregulate	DB00685	0.762656	0.833333	0.87054
Bortezomib	HSPH1	Downregulate	DB00188	0.199532	1	0.65429
Gefitinib	CCT2	Downregulate	DB00317	0.887728	1	1
Doxorubicin	CCT2	Downregulate	DB00997	0.050992	1	0.573268
Imatinib	HSP90B1	Downregulate	DB00619	1	1	1
Cytarabine	DNAJA4	Downregulate	DB00987	1	1	1
Cycloheximide	HSP90AB1	Upregulate	N/A	0	1	0.666667
Estradiol	DNAJC6	Downregulate	DB00783	1	1	1
Luteolin	HSPAA1	Downregulate	DB15584	0.024504	1	0.5
Doxorubicin	DNAJC11	Downregulate	DB00997	1	0.5	1
Resveratrol	HSP90AB1	Upregulate	DB02709	1	1	1
Nilotinib	DNAJC10	Downregulate	DB04868	1	0.833333	0.959982
Gefitinib	HSPA1A	Downregulate	DB00317	0.887728	1	1
Imatinib	HSP90AB1	Upregulate	DB00619	1	1	1
Dasatinib	HSP90AB1	Upregulate	DB01254	0.161974	1	1

4. Discussion

HSPs comprise a family of proteins that are conserved in both the eukaryotes and prokaryotes and play a significant role in the regulation of apoptosis and autophagy, proteostasis, and the regulation of polypeptides. They also act to protect the cells from various stresses like ionizing radiations, heat shock, and hypoxia. Coming from the class of molecular chaperones they are involved in protein folding under normal metabolic conditions and thus, are the enhancers in protein repair during molecular stress. When talking about tumor cells the expression of HSPs is highly elevated as compared to the normal cells. We retrieved the data for both GBM and ependymoma from GEO and also studied the transcriptomic data and further analyzed the integrated pathways, biological processes, and therapeutic targets. Starting with the analysis we first identified the overlapping differentially expressed genes in both the tumors. From the list of filtered DEGs, identification of potential HSPs was done using literature mining and from HSPMdb database. Based on Venn analysis, 22 overlapping HSPs were obtained that were called differentially expressed HSPs.

We constructed a protein-protein interaction network with all the predicted 22 differentially expressed HSPs based on different topological parameters. The hub HSPs obtained after network analysis are known to be mediators in a variety of biological processes in both glioblastoma and ependymoma. HSP90AA1 one of the hub proteins is found to be overexpressed in IDH-wild type GBMs (Zuehlke et al., 2015) although the role of HSP90AA1 in ependymoma is still unclear. HSP90AA1 plays a significant role in maintaining the integrity of various signaling pathways and resistance to stress-induced apoptosis in normal cells. Another hub protein HSPD1 is known to play an important role in the folding of proteins imported from mitochondria or their refolding under mitochondrial stress (Gomez-Llorente et al., 2020). Studies have also shown that HSPD1 is involved in many diseases such as neurodegenerative diseases and cardiovascular diseases (Teng et al., 2019). They are also reported to play an important role in cancer development. Very few studies are available on their role in brain tumors, however, their expression was seen elevated in meningiomas. Ependymomas do not show any positive immunohistochemical reaction and show lower expression levels of HSPD1 (Rappa et al., 2013). CCT2 (Chaperonin containing tailless complex, TCP) are the members of the HSP60 family and their expression is found to be elevated in cancerous brain tissues as compared to normal brain tissues. Studies have shown that the expression of these proteins is elevated in Grade IV glioblastomas and can be used as a diagnostic marker (Hallal et al., 2019). The role of CCT2 in ependymoma remains still unexplored. HSP90AB1 comes under the class of HSP90 superfamily and is known to be overexpressed in tumors of glial origin (Hermisson et al., 2000). HSP90AB1 levels are seen to be elevated in recurrent GBMs (Zhang et al., 2005).

Expression levels of HSP90AB1 were found to be highly elevated in carcinomas of the head and neck and showed poor prognosis along with a high mortality rate. Researchers have shown that HSP90AB1 can be a better prognostic factor and therapeutic option in both malignancies (Zhang et al., 2022). Gefitinib is also known to induce cell death and decreased cell proliferation in non-small cell lung carcinomas (Zhou et al., 2023). Imatinib on the other hand is known to be an effective treatment in case of stromal tumors of gastrointestinal origin and a variety of malignancies (Venkataraman et al., 2023). HSPA1A another class coming from the HSP70 family was found to be interacting with endoplasmic reticulum-alpha causing its increased expression and leading to an increase in cellular proliferation in MCF-7 breast cancer (Yano et al., 1996). A higher expression level of HSPA1A is observed in ependymoma (Liu et al., 2020) suggesting better therapeutic targets in combating these lethal tumors.

To better understand the functional aspects of the identified HSPs and what are the mutual role they play in GBMs and ependymoma, different enrichments have been done to predict a relationship between the interconnected dysregulated pathways between these two tumors. Functional enrichment and KEGG pathway analysis revealed the role of these 22 HSPs and how they play an intricate role at biological, molecular, and cellular levels along with the pathways on which they act. From the enrichment done at biological levels, out of 22 HSPs, 15 differentially expressed HSPs were involved in protein folding, 6 HSPs were involved in protein stabilization and 5 were involved in chaperone-mediated protein complex assembly and chaperone-mediated protein folding requiring cofactors. Out of these HSP90AA1, HSP90AB1, HSPD1, HSPA1A, and CCT2 were commonly present in every biological process. Studies suggest that HSP90AA1 is exploited by the tumor cells to enhance and support their activation of oncoproteins, comprising several kinases and TFs (Xu et al., 2012). Researchers have seen that the product of the HSP90AA1 protein is known to act as a key player in tumor invasion and proliferation (Sims et al., 2011). At molecular levels, 11 of the counts were associated with unfolded protein binding, 12 were involved in ATP binding and 8 were involved in ATPase activity. Here the prevalence of HSP90AB1, HSPA1A, CCT2, HSPD1, and HSP90AA1 was the most even at molecular levels. Coming to the cellular counterpart, out of 22 hub HSPs, 10 were present in extracellular exosomes, 6 were in the endoplasmic reticulum and 10 HSPs were present in the membrane. HSP90AA1 was present in almost all the cellular counterparts suggesting its major role in GBMs and ependymoma. The expression of HSP90AA1 is found to be elevated in various cancers and studies have predicted that the therapeutic inhibition of HSP90AA1 results in good prognosis and increased overall survival of lung cancer patients (Niu et al., 2022). When we performed the KEGG pathway analysis, we observed that most of the HSPs were involved in protein processing in the endoplasmic reticulum, pathways in cancer, and glioma signaling.

Table 6
Tabular representation of scores for binding affinity, ADMET, and BBB permeability.

Compound	Affinity (kcal/mol)	Grid Size	Interacting residues	Canonical smiles	BBB CBligand	CBligand Score	Molecular Mass (g/mol)	H-bond donor (<5)	H-bond donor (<10)	Octal partition coefficient (Log <5)	Molar Refractivity
Reference (Cepharanthine)	-9.1	30-30-30	Asp54; Ala55; Met98; Leu107; Gly135; Val186	CN1CCC2 = CC3 = C(C4 = C2C1CC5 = CC=C(C=C5) OC6 = C(C=CC(=O)C7C8 = CC(C=C(C8CCN7C) OC) O4) OC) OCO3	Yes	0.076	493.6	2	6	3.49	154.5
Resveratrol	-9.3	30-30-30	Met98; Val150; Leu107; Phe138; Val186; Trp162; Asp93	Cl = CC(=CC=C1C=CC2 = CC(=CC(=C2) O) O) O	Yes	0.041	228.24	3	3	2.48	67.88
Cycloheximide	-9.2	30-30-30	Phe138; Gly135; Asn51; Gly137	CC1CC(C(=O) C(C1) C(C2CC(C(=O) NC(=O) C2) O) C	Yes	0.05	281.35	2	4	1.3	78.47
Gefitinib	-9.7	30-30-30	Leu107; Phe138; Leu48; Asp93; Val150; Trp162; Leu103; Asn51; Gly135	COCl = C(C=C2C(C=C1) N=CN=C2NC3 = CC(C=C(C=C3) F) Cl) OCCCN4CCOCC4	Yes	0.027	446.9	7	1	3.92	121.66
Imatinib	-10.9	30-30-30	Ala55; Met98; Leu103; Phe170; Phe138; Leu107; Asn51; Ile104	CC1 = C(C=C(C=C1) NC(=O) C2 = CC=C(C=C2) CN3CCN(CC3) C) NC4 = NC=CC(=N4) C5 = CN=CC=C5	Yes	0.03	606.71	0	8	3.96	179.18

as an important prognostic marker (Weiner et al., 1996). Therefore, it can be conferred that the therapeutic side of these 5 HSPs can be explored to counter these malignant brain tumors as they have major involvement in their pathology and occurrence.

To further nurture our study and to establish a more concrete connection between the identified HSPs with GBMs and ependymomas, we explored the regulatory signatures of the transcriptomes (TFs and miRNAs). Among the top identified TFs, GATA2 (GATA-binding factor 2) was found to be the most interactive in both pathologies. GATA2 is known to be the regulator of constitutive PD-L1 and PD-L2 expression in most of the brain tumors(Fu et al., 2020). Another interacting TF Forkhead box C1 (FOXC1) is a known conserved TF and plays an important role in tumorigenesis and is also involved in epithelial-to-mesenchymal transitions (EMT) in gliomas(Cao et al., 2019). Upstream transcription factor 2 (USF2) is known to be a modulator of cellular proliferation and its silencing can reduce the tumor load in glioblastomas(Cox et al., 2013). Among the top interacting miRNAs, hsa-miR-16-5p is known to be involved in the pathogenesis of glioblastoma and astrocytoma however, no study claims the involvement of hsa-miR-26b-5p in ependymomas and glioblastoma, hsa-miR-16-5p are reported to be the regulators of signaling cascades along with WEE1, CHEK1, and MCL1. Here the increased expression of this miRNA, reduced cellular proliferation, increased cell viability, increased cell cycle arrest, and increased response to irradiation and chemotherapy (Krell et al., 2019). Another miRNA hsa-miR-26b-5p is known to inhibit cellular proliferation and EMT in triple-negative breast cancer(Ma et al., 2021). Also, miR-26b-5p is found to be an important regulator in Burkitt lymphoma cellular growth(Niu et al., 2020). We also established a miRNA-TFs-HSPs coregulatory network to understand how these TFs and miRNAs are commanding the HSPs in both of these morbidities. Using an integrative miRNA-TF- HSPs target network we identified several dysregulated miRNAs that were connective to the various HSPs and the associate TFs. GABA, MYC, RFX1, and EGFR were the major TFs that were interconnected with the HSPs along with the miRNAs. MYC is an important TFs family and is composed of TFs c-myc, Mycn, and Mycl. These regulatory TFs are required for the development of the brain and its overexpression induces cellular proliferation in gliomas(Perry et al., 2009) and medulloblastomas(Haberler et al., 2006; Shrestha et al., 2021). Regulatory factor X1 (RFX1) is known to play an intricate role in causing chemoresistance and recurrence in glioblastoma(Issac et al., 2021). However, their role is unknown in ependymomas. From the modules prepared from the network, it was found that CCT3 was interacting with E2F1 and DNAJC10. Another module showed the interaction of HSP90B1 with BPTF, SREBF1, and NFYA. Through these interactions, we can conclude that these HSPs are interacting commonly with regulatory miRNAs and TFs.

To understand the potential role of different drugs and to identify putative candidates that can reverse the effect of both GBMs and ependymomas, we analyzed the CREEDS database and the LINC1000 Drug Gene Budger. From the drug screening, it was found that 2 drugs were able to reverse the effects of the HSPs whose expressions were upregulated while 11 drugs were able to reverse the effect of the downregulated HSPs. Resveratrol a polyphenol present in plants such as grapes and peanuts is known to possess properties of antioxidants(Shankar et al., 2007). Studies have shown that resveratrol has been found to show suppression activity in various neurological disorders like Alzheimer's disease(Ma et al., 2020) and Parkinson's disease(Öztürk et al., 2019). Cycloheximide is known to induce paraptosis which is induced by the inhibition of cyclophilins in GBMs(Wang et al., 2017). However, the role of cycloheximide in ependymoma remains unclear. Various inhibitors like the ganetespib and cycloheximide is known to induce apoptotic arrest and reduced tumorigenicity targeting HSP90 class in various cancers(Youssef et al., 2023). Cycloheximide is also known to cause differential effects in neuronal and glioma cells that are treated with chemotherapy and radiotherapy(Chao et al., 1999). To further validate our results and the drugs obtained we performed the drug ranking and

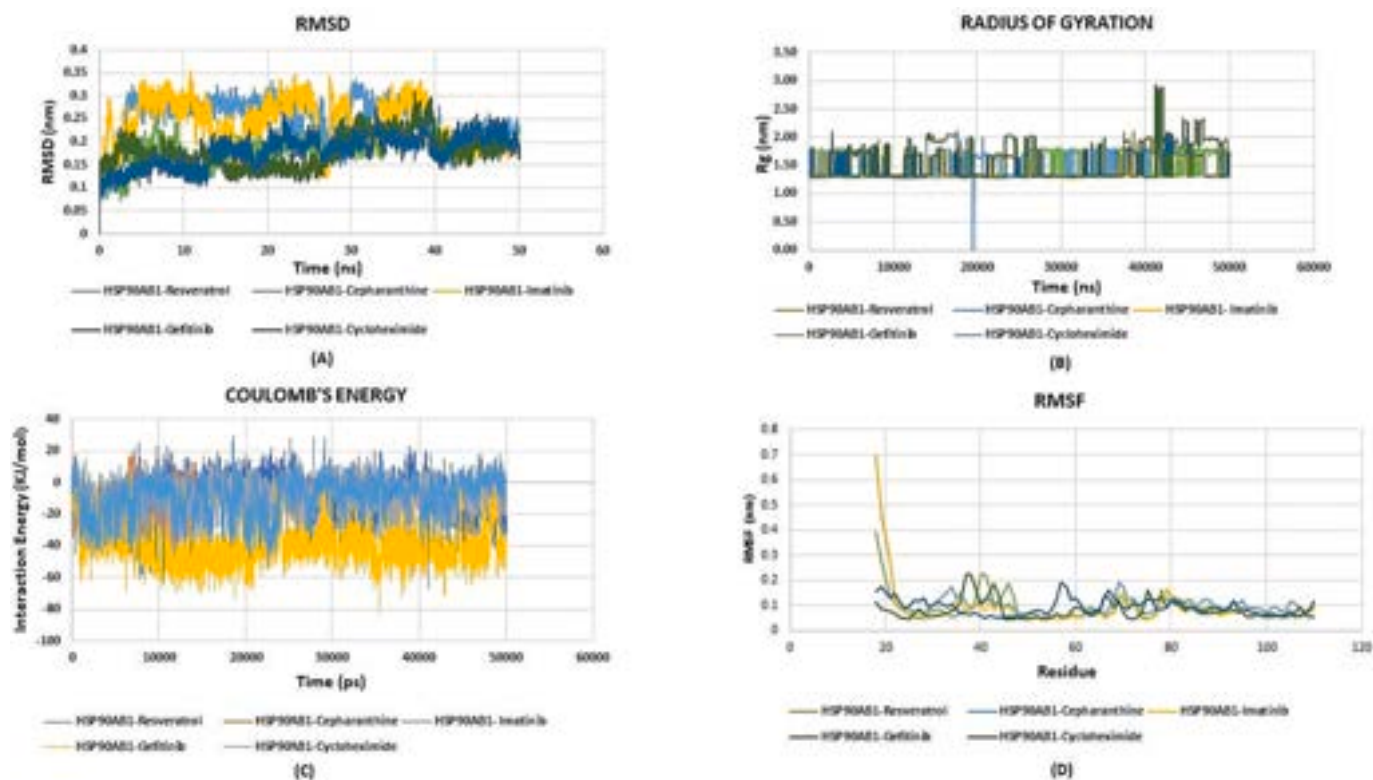


Fig. 8. (A-D) Plot representing the root mean square deviation (RMSD), Radius of gyration (Rg) of all the complexes, interaction energies, and the root mean square fluctuations (RMSF) till 50 ns. (A) Represent the various RMSD of different complexes. RMSD values of the complexes when compared with the reference complex (HSP90AB1-Cepharanthine) showed that the backbone of complexes (HSP90AB1-resveratrol, HSP90AB1-gefitinib, HSP90AB1-imatinib, HSP90AB1-Cycloheximide) was more stable and integrated. (B) The radius of gyration of all the complexes showed the folding capacity of the protein over some time and the peak intensity showed a slight deviation of peak value 2.70 nm. Rest all the complexes were under the limit and better peaks were observed. (C) Coulomb's energy represents the interaction energy of the complexes. The binding affinities of all four complexes were better than the reference complex. (D) RMSF represents the rate of displacement of atoms around the target atom. Stability can be seen to be more in all four complexes when compared with the reference complex.

predicted the structural, functional, and composite scores of the drugs obtained after the analysis from CREEDS and Drug gene Budger. Imatinib, cytarabine, gefitinib, estradiol, resveratrol, and cycloheximide were predicted as the top 5 drugs. With these observations, we considered resveratrol, cycloheximide, gefitinib, and imatinib as the most promising candidates for this study and the hub HSPs that were found targetable with these drugs were HSP90AB1, CCT2, HSPH1, DNAJC10. We further proceeded with the study by identifying the most suitable HSP candidate among all the top HSPs. Using Brain-RNA sequencing data, the expression patterns of the individual HSPs were checked whether the expression levels were higher in glial cells or not as both these tumors originate from microglial cells within the brain. From our results discussed above, HSP90AB1 was found to be the most promising HSP, and the expression levels were elevated in both the GBM and ependymoma. Studies have shown that inhibition of HSP90AB1 significantly reduced the activity of adenylate cyclase post-chronic morphine treatment (Koshimizu et al., 2010). Another study identified the role of gallic acid as an inhibitory effect on skin squamous cell carcinomas and reduced expression of HSP90AB1 (de Jesus et al., 2023). Expression levels of HSP90AB1 in recurrent glioblastomas. Inhibitor NW457 is known to suppress glioblastoma when given in combination with radiotherapy (Orth et al., 2021). This shows that the effective targeting of HSP90AB1 could ideally suppress the activity of both of these tumors.

To validate the drugs identified from CREEDS and DrugGene Budger we performed molecular docking and MD simulations of all the four predicted drugs (gefitinib, imatinib, cycloheximide, and resveratrol) against HSP90AB1. Cepharanthine was used as a reference drug to compare to docking scores of our predicted drugs against HSP90AB1 (Liu et al., 2022). From docking analysis, it was identified that the binding

affinities for resveratrol (−9.3 Kcal/mol), cycloheximide (−9.2 Kcal/mol), gefitinib (−9.7 Kcal/mol), imatinib (−10.9 Kcal/mol) were comparatively higher when checked with the reference drug (−9.1 Kcal/mol), suggesting an inhibitory effect of these drugs against HSP90AB1. As the docking results were favorable, we further validated our study using MD simulations at 50 ns. The stability index the fluctuations in the system and the probable result trajectories of all the complexes were seen by applying different parameters during simulations. The parameters used while conducting the analysis were RMSD for all the complexes, RMSF of all the amino acid residues, Rg, and the interaction energies of each of the individual complexes. The RMSD of all the complexes was measured between the initial and the final confirmations of the protein-ligand complexes till 50 ns. A stable binding was observed in all the complexes when compared with the reference complex. The peak pattern of RMSF showed us that all four complexes were nearby during fluctuations in amino acid residue when compared with the reference complex suggesting a much stronger bonding. When talking about the Rg and the coulombs interaction energy, all the findings showed a much better interaction pattern of HP90AB1 with resveratrol, gefitinib, imatinib, and cycloheximide. Overall, these findings were able to nurture the credibility of the results obtained using CREEDS, Drug-Gene Budger, and docking analysis, suggesting the potential therapeutic efficiency of these drugs in the therapeutics suppression of GBMs and ependymomas. We also proposed an inhibitory mechanism of how these drugs are acting in the signaling cascades in both diseases and how targeting HSP90AB1 can mutually suppress both tumors. A proposed mechanism of these inhibitors that can target the HSP machinery has been shown in Fig. 9.

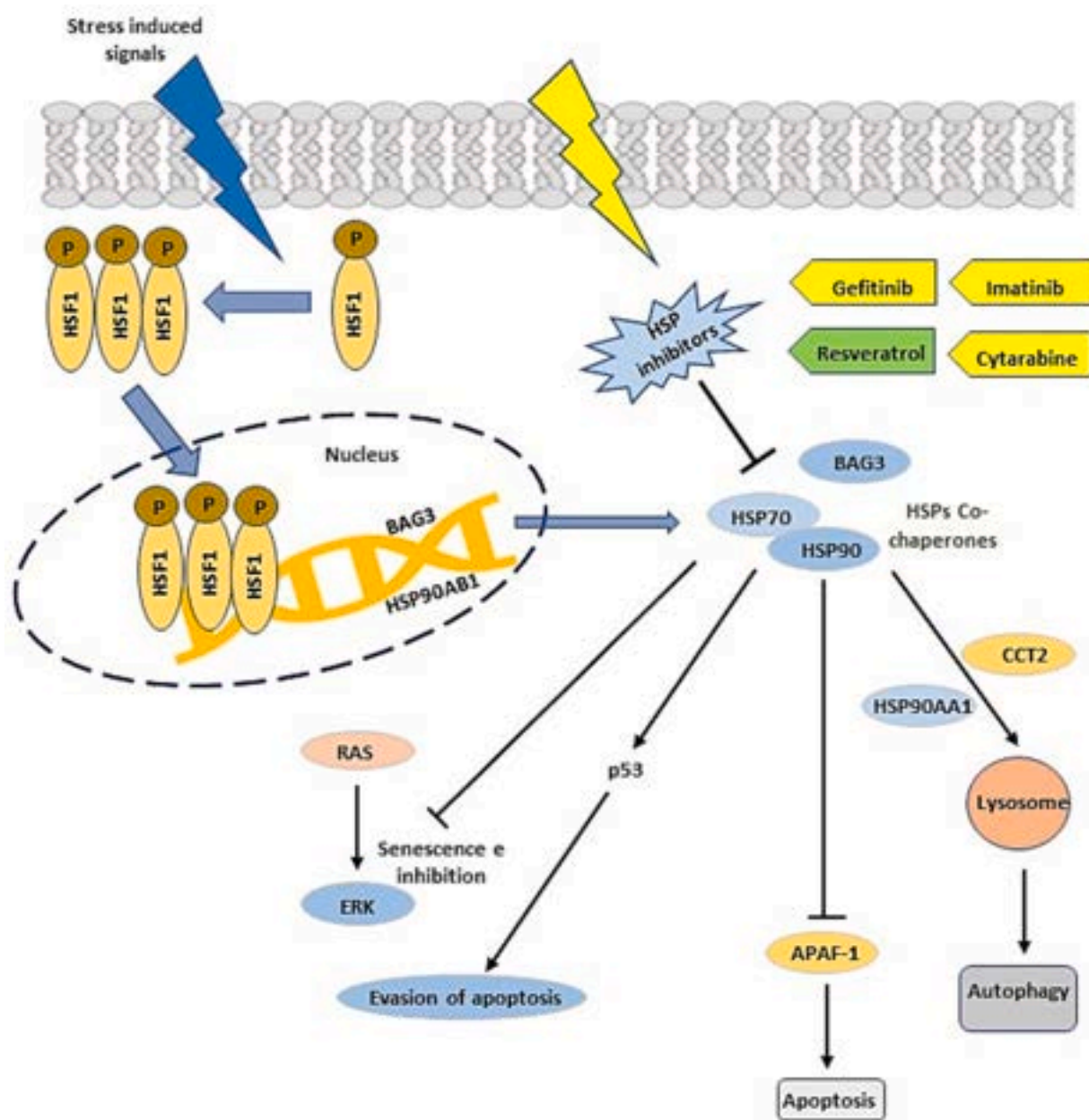


Fig. 9. Diagrammatic representation of the proposed mechanism of inhibitory action of HSPs inhibitors in Heat Shock Protein (HSPs) mediated pathway. The binding of the HSPs inhibitors to HSP70 and HSP90 cochaperone machinery can cause an increase in the level of the apoptotic protease activating factor-1 (APAF-1) which is suppressed under normal conditions. This activation can cause an increase in the levels of the apoptotic machinery. We also hypothesized that gefitinib, imatinib, cytarabine, and cycloheximide directly could prevent the binding of cochaperones that are induced in response to stress and hence, promote autophagy. Gefitinib, imatinib, cytarabine, and resveratrol binding to the target HSP causes inhibition of the downstream targets and prevents the binding of HSPs co-chaperones with HSP70 and HSP90 assembly causing cell cycle arrest, increased apoptosis, and other cellular processes finally, causing death of tumor cells. Also, these inhibitors could induce senescence and inhibition in the progression of ependyomas and glioblastomas.

5. Conclusion

Herein, we tried to identify the molecular mechanism and the common regulatory pathway of HSPs and how they share various transcriptomes and regulatory signatures mutually in GBMs and ependyomas. With our findings, we have explored a mechanistic approach to understanding the interlink of HSPs between GBMs and ependyoma. We identified HSP90AB1, HSPA1A, CCT2, HSPD1, and HSP90AA1 as the key candidate of HSPs that can be used as therapeutic targets in countering GBMs and ependyomas. With this study, we identified HSP90AB1 as a promising candidate in the therapeutic targeting of GBM and ependyomas. We proposed that gefitinib, imatinib,

resveratrol, and cytarabine could potentially target HSP90AB1 and can promote cell death in both glioblastoma and ependyomas. This study will provide a more mechanistic link to how these two malignancies can be targeted mutually and the interlinked molecular mechanisms. However, more concrete studies are needed on how these drugs are working against HSP90AB1 in both of the morbidities through *in vitro* and *in vivo* studies.

Supplementary data to this article can be found online at <https://doi.org/10.1016/j.npep.2023.102383>.

Funding

None.

Author's contribution

PK conceived and designed the manuscript. SS collected and analyzed data. SS and PK wrote the manuscript, discussed the results, and analyzed the entire data.

Conflict of interest

Both authors read the manuscript and declared no conflict or competing interests.

Data availability

Data will be made available on request.

Acknowledgment

We would like to thank the senior management of Delhi Technological University (DTU) and the Department of Science and Technology (DST), India, for their constant support and financial assistance to Senior Research Fellowship (SRF) to Sudhanshu Sharma (Fellow ID: IF190188).

References

- Abounader, R., Neuro-oncology, J.L., 2005. Scatter factor/hepatocyte growth factor in brain tumor growth and angiogenesis. *J. Neuro-oncol.* <https://doi.org/10.1215/S1152851705000050>, 2005. academic.oup.com. undefined, 2005.
- Advani, D., Kumar, P., 2022. Deciphering the molecular mechanism and crosstalk between Parkinson's disease and breast cancer through multi-omics and drug repurposing approach. *Neuropeptides* 96, 102283. <https://doi.org/10.1016/j.npep.2022.102283>.
- Agarwal, V., Bell, G.W., Nam, J.W., Bartel, D.P., 2015. Predicting effective microRNA target sites in mammalian mRNAs. *Elife* 4. <https://doi.org/10.7554/ELIFE.05005>.
- Amini-Khoei, H., Saghaei, E., Mobini, G.-R., Sabzevary-Ghahfarokhi, M., Ahmadi, R., Bagheri, N., Mokhtari, T., 1942. Possible involvement of PI3K/AKT/mTOR signaling pathway in the protective effect of selegiline (deprenyl) against memory impairment following ischemia reperfusion. *Elsevier* 101942. <https://doi.org/10.1016/j.npep.2019.101942>.
- Auerbach, R.K., Chen, B., Butte, A.J., 2013. Relating genes to function: identifying enriched transcription factors using the ENCODE ChIP-Seq significance tool. *Bioinformatics* 29, 1922–1924. <https://doi.org/10.1093/BIOINFORMATICS/BTT316>.
- Betel, D., Wilson, M., Gabow, A., Marks, D.S., Sander, C., 2008. The microRNA.org resource: targets and expression. *Nucleic Acids Res.* 36, D149. <https://doi.org/10.1093/NAR/GKM995>.
- Bisht, I., Ambasta, R.K., Kumar, P., 2020. An integrated approach to unravel a putative cross-talk network in Alzheimer's disease and Parkinson's disease. *Neuropeptides* 83, 102078. <https://doi.org/10.1016/j.npep.2020.102078>.
- Bond, U., Schlesinger, M.J., 1987. Heat-shock proteins and development. *Adv. Genet.* 24, 1–29. [https://doi.org/10.1016/S0065-2660\(08\)60005-X](https://doi.org/10.1016/S0065-2660(08)60005-X).
- Bouffet, E., Foreman, N., 1999. Chemotherapy for intracranial ependymomas. *Childs Nerv. Syst.* 15, 563–570. <https://doi.org/10.1007/S003810050544>.
- Braunstein, M.J., Scott, S.S., Scott, C.M., Behrman, S., Walter, P., Wipf, P., Coplan, J.D., Chrigo, W., Joseph, D., Brodsky, J.L., Batuman, O., 2011. Antimyeloma effects of the heat shock protein 70 molecular chaperone inhibitor MAL3-101. *J. Oncol.* 2011. <https://doi.org/10.1155/2011/232037>.
- Cao, Q., Wang, X., Shi, Y., Zhang, M., Yang, J., Dong, M., Mi, Y., Zhang, Z., Liu, K., Jiang, L., Wang, N., Wang, P., 2019. FOXC1 silencing inhibits the epithelial-to-mesenchymal transition of glioma cells: involvement of [beta]-catenin signaling. *Mol. Med. Rep.* 19, 251–262. <https://doi.org/10.3892/mmr.2018.9650>.
- Carballo, G.B., Honorato, J.R., De Lopes, G.P.F., Spohr, T.C.L.D.S.E., 2018. A highlight on sonic hedgehog pathway. *Cell Commun. Signal* 16. <https://doi.org/10.1186/S12964-018-0220-7>.
- Centeno, R.S., Lee, A.A., Winter, J., Barba, D., 1986. Supratentorial ependymomas: neuroimaging and clinicopathological correlation. *J. Neurosurg.* 64 (2), 209–215. <https://doi.org/10.3171/jns.1986.64.2.0209>.
- Chao, K.S.C., Hsu, J.S.J., Xu, J., Ezekiel, U.R., Eves, E., Rosner, M., Hsu, C.Y., 1999. Differential effect of cycloheximide on neuronal and glioma cells treated with chemotherapy and radiation. *J. Neuro-Oncol.* 45, 19–26. <https://doi.org/10.1023/A:1006342006836/METRICS>.
- Clough, E., Barrett, T., 2016. The gene expression omnibus database. *Methods Mol. Biol.* 1418, 93–110. https://doi.org/10.1007/978-1-4939-3578-9_5.
- Cox, J.L., Wilder, P.J., Gilmore, J.M., Wuebben, E.L., Washburn, M.P., Rizzino, A., 2013. The SOX2-interactome in brain cancer cells identifies the requirement of MSI2 and USP9X for the growth of brain tumor cells. *PLoS One* 8, 62857. <https://doi.org/10.1371/JOURNAL.PONE.0062857>.
- De Angelis, R., Sant, M., Coleman, M.P., Francisci, S., Baili, P., Pierannunzio, D., Trama, A., Visser, O., Brenner, H., Ardanaz, E., Bielska-Lasota, M., Engholm, G., Nennecke, A., Siesling, S., Berrino, F., Capocaccia, R., 2013. Cancer survival in Europe 1999–2007 by country and age: results of EURO-CARE-5—a population-based study. *thelancet.com*. [https://doi.org/10.1016/S1470-2045\(13\)70546-1](https://doi.org/10.1016/S1470-2045(13)70546-1).
- de Jesus, S.F., de Souza, M.G., dos Queiroz, L.R.P., de Paula, D.P.S., Tabosa, A.T.L., Alves, W.S.M., da Silveira, L.H., da Ferreira, A.T.S., Martuscelli, O.J.D., Farias, L.C., de Paula, A.M.B., Santos, S.H.S., Guimaraes, A.L.S., 2023. Gallic acid has an inhibitory effect on skin squamous cell carcinoma and acts on the heat shock protein HSP90AB1. *Gene* 851, 147041. <https://doi.org/10.1016/J.GENE.2022.147041>.
- Falktoft, B., Georg, B., Fahrnkruug, J., 2009. Calmodulin interacts with PAC1 and VPAC2 receptors and regulates PACAP-induced FOS expression in human neuroblastoma cells. *Neuropeptides* 43, 53–61. <https://doi.org/10.1016/J.NPEP.2009.02.001>.
- Fu, Y., Liu, C.J., Kobayashi, D.K., Johanns, T.M., Bowman-Kirigin, J.A., Schaeffler, M.O., Mao, D.D., Bender, D., Kelley, D.G., Uppaluri, R., Bi, W.L., Dunn, I.F., Tao, Y., Luo, J., Kim, A.H., Dunn, G.P., 2020. GATA2 regulates constitutive PD-L1 and PD-L2 expression in brain tumors. *Sci. Rep.* 10. <https://doi.org/10.1038/S41598-020-65915-Z>.
- Gatta, G., Capocaccia, R., Coleman, M.P., Gloeckler Ries, L.A., Berrino, F., 2002. Childhood cancer survival in Europe and the United States. *Wiley Online Libr.* 95, 1767–1772. <https://doi.org/10.1002/cncr.10833>.
- Goi, C.L., Little, P., Xie, C., 2013. Cell-type and transcription factor specific enrichment of transcriptional cofactor motifs in ENCODE ChIP-seq data. *BMC Genomics* 14, 1–11. <https://doi.org/10.1186/1471-2164-14-S5-S2/FIGURES/4>.
- Gomez-Llorente, Y., Jebara, F., Patra, M., Malik, R., Nisemblat, S., Chomsky-Hecht, O., Parnas, A., Azem, A., Hirsch, J.A., Ubarretxena-Belandia, I., 2020. Structural basis for active single and double ring complexes in human mitochondrial Hsp60-Hsp10 chaperonin. *Nat. Commun.* 11 (1), 1916. <https://doi.org/10.1038/s41467-020-15698-8>.
- Haberler, C., Slavc, I., Czech, T., Gelpi, E., Heinzl, H., Budka, H., Urban, C., Scarpatetti, M., Ebetsberger-Dachs, G., Schindler, C., Jones, N., Klein-Franke, A., Maier, H., Jauk, B., Kiefer, A., Hainfellner, J.A., 2006. Histopathological prognostic factors in medulloblastoma: high expression of survivin is related to unfavourable outcome. *Eur. J. Cancer* 42, 2996–3003. <https://doi.org/10.1016/j.ejca.2006.05.038>.
- Hallal, Susannah, Russell, B.P., Wei, Heng, Yuk Lee, M.T., Toon, C.W., Sy, Joanne, Shivalingam, Brindha, Buckland, Michael E., Kaufman, Kimberley L., Hallal, S., Wei, H., T Lee, M.Y., Sy, J., Shivalingam, B., Buckland, M.E., Kaufman, K.L., 2019. Extracellular vesicles from neurosurgical aspirates identifies chaperonin containing TCP1 subunit 6A as a potential glioblastoma biomarker with prognostic. *Wiley Online Libr.* 19. <https://doi.org/10.1002/PMC.201800157>.
- Han, L., Tang, L., Jiang, Z., Jiang, Y., 2018. Enhanced radiosensitization of human glioblastoma multiforme cells with phosphorylated peptides derived from Gli2. *Neuropeptides* 70, 87–92. <https://doi.org/10.1016/J.NPEP.2018.05.009>.
- Hasan, A., Rizvi, S.F., Parveen, S., Mir, S.S., 2022. Molecular chaperones in DNA repair mechanisms: role in genomic instability and proteostasis in cancer. *Life Sci.* 120852. <https://doi.org/10.1016/j.lfs.2022.120852>.
- Henaou-Restrepo, J., Caro-Urrego, Y.A., Barrera-Arenas, L.M., Arango-Viana, J.C., Bermudez-Munoz, M., 2021. Expression of activator proteins of SHH/GLI and PI3K/Akt/mTORC1 signaling pathways in human gliomas is associated with high grade tumors. *Exp. Mol. Pathol.* 122, 104673. <https://doi.org/10.1016/J.YEXMP.2021.104673>.
- Hermisson, M., Strik, H., Rieger, J., Dichgans, J., Meyermann, R., Weller, M., 2000. Expression and functional activity of heat shock proteins in human glioblastoma multiforme. *Neurology*. <https://doi.org/10.1212/WNL.54.6.1357>.
- Hu, C., Yang, J., Qi, Z., Wu, H., Wang, B., Zou, F., Mei, H., Liu, J., Wang, W., Liu, Q., Key, A.P., 2022. Heat shock proteins: biological functions, pathological roles, and therapeutic opportunities. *Wiley Online Libr.* 3. <https://doi.org/10.1002/mco2.161>.
- Issac, J., Raveendran, P.S., Das, A.V., 2021. RFX1: a promising therapeutic arsenal against cancer. *Cancer Cell Int.* 21, 1–19. <https://doi.org/10.1186/S12935-021-01952-6/FIGURES/5>.
- Kampinga, H.H., Hageman, J., Vos, M.J., Kubota, H., Tanguay, R.M., Bruford, E.A., Cheetham, M.E., Chen, B., Hightower, L.E., 2009. Guidelines for the nomenclature of the human heat shock proteins. *Cell Stress Chaperones*. <https://doi.org/10.1007/s12192-008-0068-7>.
- Karagkouni, D., Paraskevopoulou, M.D., Chatzopoulos, S., Vlachos, I.S., Tastsoglou, S., Kanellou, I., Papadimitriou, D., Kavakiotis, I., Maniou, S., Skoufos, G., Vergoulis, T., 2018. DIANA-TarBase v8: a decade-long collection of experimentally supported miRNA–gene interactions. *Nucleic Acids Res.* 46 (D1), D239–D245. <https://doi.org/10.1093/nar/gkx1141>.
- Karatzas, E., Minadakis, G., Kolios, G., Delis, A., Spyrou, G.M., 2019. A web tool for ranking candidate drugs against a selected disease based on a combination of functional and structural criteria. *Comput. Struct. Biotechnol. J.* 17, 939–945. <https://doi.org/10.1016/J.CSBJ.2019.05.010>.
- Kertesz, M., Iovino, N., Unnerstall, U., Gaul, U., Segal, E., 2007. The role of site accessibility in microRNA target recognition. *Nat. Genet.* 39 (10), 1278–1284. <https://doi.org/10.1038/ng2135>.
- Komori, T., 2022. Grading of adult diffuse gliomas according to the 2021 WHO classification of tumors of the central nervous system. *Lab. Invest.* 102 (2), 126–133. <https://doi.org/10.1038/s41374-021-00667-6>.
- Koshimizu, T., Aki, Tsuchiya, H., Tsuda, H., Fujiwara, Y., Shibata, K., Hirasawa, A., Tsujimoto, G., Fujimura, A., 2010. Inhibition of heat shock protein 90 attenuates

- adenylate cyclase sensitization after chronic morphine treatment. *Biochem. Biophys. Res. Commun.* 392, 603–607. <https://doi.org/10.1016/J.BBRC.2010.01.089>.
- Krell, A., Wolter, M., Stojcheva, N., Hertler, C., Liesenberger, F., Zapotka, M., Weller, M., Malzkorn, B., Reifemberger, G., 2019. MiR-16-5p is frequently down-regulated in astrocytic gliomas and modulates glioma cell proliferation, apoptosis and response to cytotoxic therapy. *Neuropathol. Appl. Neurobiol.* 45, 441–458. <https://doi.org/10.1111/NAN.12532>.
- Krex, D., Klink, B., Hartmann, C., Von Deimling, A., Pietsch, T., Simon, M., Sabel, M., Steinbach, J.P., Heese, O., Reifemberger, G., Weller, M., Schackert, G., 2007. Long-term survival with glioblastoma multiforme. *Brain* 130, 2596–2606. <https://doi.org/10.1093/BRAIN/AWM204>.
- Li, H., Bath, I.S., Qu, X., Xu, L., Song, N., Wang, R., Liu, Y., 2017. IGF-IR signaling in epithelial to mesenchymal transition and targeting IGF-IR therapy: overview and new insights. *Mol. Cancer* 16(1), 1–15. <https://doi.org/10.1186/S12943-016-0576-5>.
- Lianos, G.D., Alexiou, G.A., Mangano, Alberto, Mangano, Alessandro, Rauseri, S., Boni, L., Dionigi, G., Roukos, D.H., 2015. The role of heat shock proteins in cancer. *Cancer Lett.* <https://doi.org/10.1016/j.canlet.2015.02.026>.
- Liao, Y., Wang, J., Jaehnig, E.J., Shi, Z., Zhang, B., 2019. WebGestalt 2019: gene set analysis toolkit with revamped UIs and APIs. *Nucleic Acids Res.* 47, W199–W205. <https://doi.org/10.1093/NAR/GKZ401>.
- Liu, S.J., Magill, S.T., Vasudevan, H.N., Hilz, S., Villanueva-Meyer, J.E., Lastella, S., Daggubati, V., Spatz, J., Choudhury, A., Orr, B.A., Demaree, B., Seo, K., Ferris, S.P., Abate, A.R., Oberheim Bush, N.A., Bollen, A.W., McDermott, M.W., Costello, J.F., Raleigh, D.R., 2020. Multiplexed molecular profiling reveals epigenomic intratumor heterogeneity in ependymoma. *Cell Rep.* 30, 1300. <https://doi.org/10.1016/J.CELREP.2020.01.018>.
- Liu, Jiaqin, Sun, T., Liu, S., Liu, Jian, Fang, S., Tan, S., Zeng, Y., Zhang, B., Li, W., 2022. Dissecting the molecular mechanism of cepharanthine against COVID-19, based on a network pharmacology strategy combined with RNA-sequencing analysis, molecular docking, and molecular dynamics simulation. *Comput. Biol. Med.* 151 <https://doi.org/10.1016/J.COMPBIOMED.2022.106298>.
- Ma, X.R., Sun, Z.K., Han, X., Li, S., Jiang, X., Chen, S., Zhang, J., Lu, H., 2020. Neuroprotective effect of resveratrol via activation of Sirt1 signaling in a rat model of combined diabetes and Alzheimer's disease. *Front. Neurosci.* 13 <https://doi.org/10.3389/FNINS.2019.01400/FULL>.
- Ma, S., Wei, H., Wang, C., Han, J., Chen, X., Li, Y., 2021. MiR-26b-5p inhibits cell proliferation and EMT by targeting MYCBP in triple-negative breast cancer. *Cell. Mol. Biol. Lett.* 26 <https://doi.org/10.1186/S11658-021-00288-3>.
- Manfreda, L., Rampazzo, E., Biology, L.P., 2023. Wnt Signaling in Brain Tumors: A Challenging Therapeutic Target. <https://doi.org/10.3390/biology.undefined.2023>.
- Masoumi, J., Abbasloui, M., Parvan, R., Mohammadnejad, D., Pavon-Djavid, G., Barzegari, A., Abdolalizadeh, J., 2018. ne. *Neuropeptides* 70, 76–86. <https://doi.org/10.1016/J.NPEP.2018.05.008>.
- Masui, K., Mischel, P.S., Reifemberger, G., 2016. Molecular classification of gliomas. *Handb. Clin. Neurol.* 134, 97–120. <https://doi.org/10.1016/B978-0-12-802997-8.00006-2>.
- Matys, V., Kel-Margoulis, O.V., Fricke, E., Liebich, I., Land, S., Barre-Dirrie, A., Reuter, I., Chekmenev, D., Krull, M., Hornischer, K., Voss, N., Stegmaier, P., Lewicki-Potapov, B., Saxel, H., Kel, A.E., Wingender, E., 2006. TRANSFAC and its module TRANSCompel: transcriptional gene regulation in eukaryotes. *Nucleic Acids Res.* 34 <https://doi.org/10.1093/NAR/GKJ143>.
- Misawa-Omori, E., Okihara, H., Ogawa, T., Abe, Y., Kato, C., Ishidori, H., Fujita, A., Kokai, S., Ono, T., 2023. Reduced mastication during growth inhibits cognitive function by affecting trigeminal ganglia and modulating Wnt signaling pathway and ARHGAP33 molecular transmission. *Neuropeptides* 102370. <https://doi.org/10.1016/j.npep.2023.102370>.
- Niu, F., Kazimierska, M., Nolte, I.M., Terpstra, M.M., de Jong, D., Koerts, J., van der Sluis, T., Rutgers, B., O'connell, R.M., Kok, K., van den Berg, A., Dzikiewicz-Krawczyk, A., Kluiver, J., 2020. The miR-26b-5p/KPNA2 axis is an important regulator of Burkitt lymphoma cell growth. *Cancers* 12, 1464. <https://doi.org/10.3390/CANCERS12061464>.
- Niu, M., Zhang, B., Li, L., Su, Z., Pu, W., Zhao, C., Wei, L., Lian, P., Lu, R., Wang, R., Wazir, J., Gao, Q., Song, S., Wang, H., 2022. Targeting HSP90 inhibits proliferation and induces apoptosis through AKT1/ERK pathway in lung cancer. *Front. Pharmacol.* 12 <https://doi.org/10.3389/FPHAR.2021.724192/FULL>.
- Obacz, J., Avril, T., Le Reste, P.J., Urra, H., Quillien, V., Hetz, C., Chevret, E., 2017. Endoplasmic reticulum proteostasis in glioblastoma—from molecular mechanisms to therapeutic perspectives. *Sci. Signal.* 10 <https://doi.org/10.1126/SCISIGNAL.AAL2323>.
- Oppenheim, J.S., Strauss, R.C., Mormino, J., Sachdev, V.P., Rothman, A.S., 1994. Ependymomas of the third ventricle. *Neurosurgery* 34(2), 350–353. <https://doi.org/10.1227/00006123-199402000-00020>.
- Orth, M., Albrecht, V., Seidl, K., Kinzel, L., Unger, K., Hess, J., Kreutzer, L., Sun, N., Stegen, B., Nieto, A., Maas, J., Winssinger, N., Friedl, A.A., Walch, A.K., Belka, C., Zitzelsberger, H., Niyazi, M., Lauber, K., 2021. Inhibition of HSP90 as a strategy to radiosensitize glioblastoma: targeting the DNA damage response and beyond. *Front. Oncol.* 11 <https://doi.org/10.3389/FONC.2021.612354/FULL>.
- Öztürk, Y., Günaydin, C., Yalçın, F., Nazroğlu, M., Braidı, N., 2019. Resveratrol enhances apoptotic and oxidant effects of paclitaxel through TRPM2 channel activation in DBTRG glioblastoma cells. *Oxidative Med. Cell. Longev.* 2019 <https://doi.org/10.1155/2019/4619865>.
- Perry, A., Miller, C.R., Gujrati, M., Scheithauer, B.W., Zambrano, S.C., Jost, S.C., Raghavan, R., Qian, J., Cochran, E.J., Huse, J.T., Holland, E.C., Burger, P.C., Rosenblum, M.K., 2009. Malignant gliomas with primitive neuroectodermal tumor-like components: a clinicopathologic and genetic study of 53 cases. *Brain Pathol.* 19, 81–90. <https://doi.org/10.1111/J.1750-3639.2008.00167.X>.
- Premkumar, D.R., Arnold, B., Pollack, I.F., 2006. Cooperative inhibitory effect of ZD1839 (Iressa) in combination with 17-AAG on glioma cell growth. *Mol. Carcinog.* 45, 288–301. <https://doi.org/10.1002/MC.20141>.
- Rappa, F., Unti, E., Baiamonte, P., Cappello, F., Scibetta, N., 2013. Different immunohistochemical levels of Hsp60 and Hsp70 in a subset of brain tumors and putative role of Hsp60 in neuroepithelial tumorigenesis. *Eur. J. Histochem.* 57(2) <https://doi.org/10.4081/Fejh.2013.e20>.
- Saibil, H., 2013. Chaperone machines for protein folding, unfolding and disaggregation. *Nat. Rev. Mol. Cell Biol.* 14(10), 630–642. <https://doi.org/10.1038/nrm3658>.
- Sauvageot, C.M.E., Weatherbee, J.L., Kesari, S., Winters, S.E., Barnes, J., Dellagatta, J., Ramakrishna, N.R., Stiles, C.D., Kung, A.L.J., Kieran, M.W., Wen, P.Y.C., 2009. Efficacy of the HSP90 inhibitor 17-AAG in human glioma cell lines and tumorigenic glioma stem cells. *Neuro-oncology* 11(2). <https://doi.org/10.1215/15228517-2008-060>.
- Shankar, S., Singh, G., Srivastava, R.K., 2007. Chemoprevention by resveratrol: molecular mechanisms and therapeutic potential. *Front. Biosci.* 12, 4839–4854. <https://doi.org/10.2741/2432>.
- Sharma, S., Kumar, P., 2023. Decoding the role of MDM2 as a potential ubiquitin E3 ligase and identifying the therapeutic efficiency of alkaloids against MDM2 in combating glioblastoma. *ACS Omega* 8(5). <https://doi.org/10.1021/acsomega.2c07904>.
- Sherman, M., of, G.M.-A. of the N.Y.A., 2007. Heat shock proteins in cancer. *Wiley Online Libr.* 1113, 192–201. <https://doi.org/10.1196/annals.1391.030> undefined, 2007.
- Shrestha, S., Morcavallo, A., Gorrini, C., Chesler, L., 2021. Biological role of MYCN in medulloblastoma: novel therapeutic opportunities and challenges ahead. *Front. Oncol.* 11 <https://doi.org/10.3389/FONC.2021.694320/FULL>.
- Sie, M., Den Dunnen, W.F.A., Lourens, H.J., Meeuwissen-De Boer, T.G.J., Scherpen, F.J.G., Zommerman, W.W., Kampen, K.R., Hoving, E.W., De Bont, E.S.J.M., 2015. Growth-factor-driven rescue to receptor tyrosine kinase (RTK) inhibitors through Akt and Erk phosphorylation in pediatric low grade astrocytoma and ependymoma. *PLoS One* 10. <https://doi.org/10.1371/JOURNAL.PONE.0122555>.
- Silva, A.G., Lopes, C.F.B., Júnior, C.G.C., Thomé, R.G., Dos Santos, H.B., Reis, R., de Azambuja Ribeiro, R.L.M., 2019. WIN55, 212-2 induces caspase-independent apoptosis on human glioblastoma cells by regulating HSP70, p53 and Cathepsin D. *Toxicol. in Vitro* 57, 233–243. <https://doi.org/10.1016/j.tiv.2019.02.009>.
- Sims, J.D., McCreedy, J., Jay, D.G., 2011. Extracellular heat shock protein (Hsp)70 and Hsp90 α assist in matrix metalloproteinase-2 activation and breast cancer cell migration and invasion. *PLoS One* 6. <https://doi.org/10.1371/JOURNAL.PONE.0018848>.
- Singh, P., Unik, B., Puri, A., Nagpal, G., Singh, B., Gautam, A., Sharma, D., 2020. HSPMdb: a computational repository of heat shock protein modulators. *Database* 2020, 3. <https://doi.org/10.1093/DATABASE/BAAA003>.
- Teng, R., Liu, Z., Tang, H., Zhang, W., Chen, Y., Xu, R., Chen, L., Song, J., Liu, X., Deng, H., 2019. HSP60 silencing promotes Warburg-like phenotypes and switches the mitochondrial function from ATP production to biosynthesis in ccRCC cells. *Redox Biol.* 24, 101218. <https://doi.org/10.1016/j.redox.2019.101218>.
- Venkataraman, V., George, S., Cote, G.M., 2023. Molecular advances in the treatment of advanced gastrointestinal stromal tumor. *Oncologist*. <https://doi.org/10.1093/oncolo/oyad167> p. oyad167.
- Wang, Z., Monteiro, C.D., Jagodnik, K.M., Fernandez, N.F., Gundersen, G.W., Rouillard, A.D., Jenkins, S.L., Feldmann, A.S., Hu, K.S., McDermott, M.G., Duan, Q., Clark, N.R., Jones, M.R., Kou, Y., Goff, T., Woodland, H., Amaral, F.M.R., Szteto, G.L., Fuchs, O., Schüssler-Florenz Rose, S.M., Sharma, S., Schwartz, U., Bausela, X.B., Szymkiewicz, M., Maroulis, V., Salykin, A., Barra, C.M., Kruth, C.D., Bongio, N.J., Mathur, V., Todoric, R.D., Rubin, U.E., Malatras, F., Fulp, C.T., Galindo, J.A., Motiejunaite, R., Juschke, C., Dishuck, P.C., Lahl, K., Jafari, M., Aibar, S., Zaravinos, A., Steenhuizen, L.H., Allison, L.R., Gamallo, P., De Andres Segura, F., Dae Devlin, T., Pérez-García, V., Ma'ayan, A., 2016. Extraction and analysis of signatures from the gene expression omnibus by the crowd. *Nat. Commun.* 7(1), 1–11. <https://doi.org/10.1038/ncomms12846>.
- Wang, L., Gundelach, J.H., Bram, R.J., 2017. Cycloheximide promotes paraptosis induced by inhibition of cyclophilins in glioblastoma multiforme. *Cell Death Dis.* 8(8) <https://doi.org/10.1038/cddis.2017.217> e2807–e2807.
- Weiner, H.L., Rothman, M., Miller, D.C., Ziff, E.B., 1996. Pediatric brain tumors express multiple receptor tyrosine kinases including novel cell adhesion kinases. *Pediatr. Neurosurg.* 25(2), 64–72. <https://doi.org/10.1159/000121099>.
- Wingender, E., Kel, A., Krull, M., 2019. Transcription factor databases. *Encycl. Bioinform. Comput. Biol. ABC Bioinform.* 1–3, 134–141. <https://doi.org/10.1016/B978-0-12-809633-8.20216-1>.
- Wu, T., Hu, E., Xu, S., Chen, M., Guo, P., Dai, Z., Feng, T., Zhou, L., Tang, W., Zhang, L., Fu, X., Liu, S., Bo, X., Yu, G., 2021. clusterProfiler 4.0: a universal enrichment tool for interpreting omics data. *Innov* 2, 100141. <https://doi.org/10.1016/J.XINN.2021.100141>.
- Xu, W., Mollapour, M., Prodromou, C., Wang, S., Scroggins, B.T., Palchick, Z., Beebe, K., Siderius, M., Lee, M.J., Couvillon, A., Trepel, J.B., Miyata, Y., Matts, R., Neckers, L., 2012. Dynamic tyrosine phosphorylation modulates cycling of the HSP90-P50 CDC37-AHA1 chaperone machine. *Mol. Cell* 47, 434–443. <https://doi.org/10.1016/j.molcel.2012.05.015>.
- Yano, M., Naito, Z., Tanaka, S., Asano, G., 1996. Expression and roles of heat shock proteins in human breast cancer. *Jpn. J. Cancer Res.* 87, 908–915. <https://doi.org/10.1111/J.1349-7006.1996.TB02119.X>.
- Yao, F., Zhang, K., Zhang, Y., Guo, Y., Li, A., Xiao, S., Liu, Q., Shen, L., Ni, J., 2019. Identification of blood biomarkers for Alzheimer's disease through computational

- prediction and experimental validation. *Front. Neurol.* 9 <https://doi.org/10.3389/FNEUR.2018.011158>.
- Youssef, M.E., Cavalu, S., Hasan, A.M., Yahya, G., Abd-Eldayem, M.A., Saber, S., 2023. Role of Ganetespib, an HSP90 inhibitor, in cancer therapy: from molecular mechanisms to clinical practice. *Int. J. Mol. Sci.* 24 (5), 5014. <https://doi.org/10.3390/ijms24055014>.
- Zhang, B., Kirov, S., Snoddy, J., 2005. WebGestalt: an integrated system for exploring gene sets in various biological contexts. *Nucleic Acids Res.* 33. <https://doi.org/10.1093/NAR/GK1475>.
- Zhang, M., Pan, Y., Qi, X., Liu, Y., Dong, R., Zheng, D., Chang, Q., Zhang, J., Fang, W., Zhong, Y., 2018. Identification of new biomarkers associated with IDH mutation and prognosis in astrocytic tumors using NanoString nCounter analysis system. *Appl. Immunohistochem. Mol. Morphol.* 26 (2), 101–107. <https://doi.org/10.1097/PAL.0000000000000396>.
- Zhang, H., Yin, X., Zhang, X., Zhou, M., Xu, W., Wei, Z., Song, C., Han, S., Han, W., 2022. HSP90AB1 promotes the proliferation, migration, and glycolysis of head and neck squamous cell carcinoma. *Technol. Cancer Res. Treat.* 21 <https://doi.org/10.1177/15330338221118202>.
- Zhou, G., Soufan, O., Ewald, J., Hancock, R.E., Basu, N., Xia, J., 2019. NetworkAnalyst 3.0: a visual analytics platform for comprehensive gene expression profiling and meta-analysis. *Nucleic Acids Res.* 47 (W1), W234–W241. <https://doi.org/10.1093/nar/gkz240>.
- Zhou, G., Pu, Y., Zhao, K., Chen, Y., Zhang, G., 2023. Heat shock proteins in non-small-cell lung cancer-functional mechanism. *Front. Biosci. - Landmark* 28. <https://doi.org/10.31083/J.FBL2803056/HTM>.
- Zuehlke, A.D., Beebe, K., Neckers, L., Prince, T., 2015. Regulation and function of the human HSP90AA1 gene. *Gene* 570, 8–16. <https://doi.org/10.1016/J.GENE.2015.06.018>.